Università di Pisa
Dipartimento di Ingegneria dell'Energia,
dei Sistemi, del Territorio e delle Costruzioni
DESTeC

Scuola di Dottorato in Ingegneria "L. da Vinci"
Programma di Energetica Elettrica e Termica
XXVII ciclo

Tesi di Dottorato di Ricerca
PhD thesis
SSD: ING-IND/11 - Fisica Tecnica Ambientale

Sustainable design of ground-source heat pump systems: optimization of operative life performances

Progettazione sostenibile di sistemi a pompa di calore geotermica: ottimizzazione delle prestazioni operative

Candidato:

Paolo Conti
Matricola 487342

Relatori:

Prof. Ing. Walter Grassi

Prof. Ing. Daniele Testi

Anno 2015

. . . Καὶ ἠγάπησαν οἱ ἄνθρωποι μᾶλλον τὸ σκότος ἢ τὸ φῶς.

— Giacomo Leopardi, "La Ginestra"
— Giovanni, III, 19

. . . Handle so, als ob die Maxime deiner Handlung durch deinen Willen zum allgemeinen Naturgesetze werden sollte.

— Immanuel Kant, Grounding for the Metaphysics of Morals

Preface

Traditional engineering design process is based on a sequential approach starting from the definition of the project objectives, the identification of a main technological solution to address the set goals, the identification of technical and economical constraints, and the application of the "precautionary principle" to ensure the meeting of project specifications. The latter point is obtained by oversizing the main equipment, on the basis of the worse operative situation, and the installation of additional back-up devices.

With regard to energy systems, the ever-increasing demand of high-efficiency solutions, low production cost and strict environmental regulation have prompted operators to look for alternative sizing and control approaches in order to ensure the technical efficiency, the economic profitability, and the sustainability of the project. Modern engineering design approach is not aimed only at sizing system components to meet project specifications and constraints, but it seeks the optimal design and management strategies in terms of energetic and economic performances. The latter looks for rigorous methods of decision making, such as optimization methods, which are based on the predictions of the operative performances of the future project. Indeed, an accurate evaluation of the energy fluxes during the operative period is a mandatory input for any cost-benefit analysis. In addition, we note that modern systems are generally made of coupled subsystems, in which different technologies (each of one with its own characteristics) cooperate for concurrent objectives. The optimal design configuration can be achieved through a holistic simulation of the overall equipment on the basis of a proper modeling of the physical mechanisms involved and including mutual interactions among different components.

The design of ground-source heat pump systems is a paradigmatic case to apply the above-mentioned considerations. Independently from the specific configuration adopted, these systems always require a proper synergy among ground-coupled unit and back-up generators in order to limit installation costs and ensure appropriate economic and energy savings, together with the sustainable exploitation of the ground source.

Abstract

This Thesis deals with an innovative approach to the design of ground-source heat pump systems (GSHP), based on performance optimization during the entire operational life. Both design and management strategies are taken into account in order to find the optimal level of exploitation of the ground source, minimizing a proper performance index. The proposed method takes into account all the macro-systems governing the energy balance of the GSHP, namely: building thermal energy loads, efficiencies of the heat pump unit and back-up systems, and thermal response of the ground source. For each of them, suitable simulation models are presented and discussed.

A rigorous mathematical formulation of the optimal design problem is provided, together with a specific resolution technique. In this regard, we also propose a statistically based evaluation methodology in order to analyze the soundness of the results of the optimization procedure.

The main results of the proposed design and optimization methodology are: thermal capacities of heat pump and back-up generators, length and number of ground heat exchangers and the optimal load share between GSHP and back-up systems (control strategy). If installation costs and energy prices are taken into account, investment figures are also an output. We show how a proper synergy among GSHP and back-up generators leads to notable energetic and economic benefits, ensuring higher energetic performances, lower installation costs, and a sustainable exploitation of the ground-source.

The proposed methodology can be conveniently applied to numerous professional, political, economic, and research activities. In this Thesis, we present two case studies. The first one refers to a typical professional design case, showing both the energetic and economic benefits achievable through the illustrated procedure with respect to traditional design methods. The second one illustrates as the proposed methodology can be applied to investigate the technological room for improvement of GSHP technology: in other words, we figure out the subsystem on which technological development should be focused, the expected benefits and some hints about a possible strategy for research activities.

Sommario

L'obiettivo di questa tesi è quello di proporre una metodologia di progettazione innovativa per i sistemi a pompa di calore geotermica (GSHP), basata sull'ottimizzazione delle prestazioni operative dell'impianto. Vengono analizzati sia il dimensionamento che la strategia di controllo del sistema in modo da ottenere il livello di sfruttamento ottimale del terreno come sorgente termica. La suddetta metodologia prende in considerazione tutti i sottosistemi che concorrono al bilancio energetico dell'impianto GSHP: il fabbisogno termico dell'edificio, le prestazioni dell'unità pompa di calore e dei generatori di integrazione ed il terreno. Per ognuno di questi sottosistemi, vengono proposti e discussi diversi modelli di simulazione. Viene inoltre proposta una formulazione matematica del problema di ottimizzazione e una specifica strategia risolutiva. A questo proposito, è stata elaborata una specifica metodologia statistica per valutare la qualità della soluzione ottenuta tramite gli algoritmi di ottimizzazione.

I principali risultati ottenibili dalla suddetta metodologia progettuale sono: il dimensionamento della pompa di calore geotermica e dei generatori di integrazione, la lunghezza ed il numero delle sonde geotermiche e la strategia di controllo ottimale in termini di suddivisione del carico tra il sistema geotermico e le tecnologie di integrazione. Introducendo nell'analisi i costi di installazione e i prezzi dell'energia è possibile valutare anche l'opportunità economica dell'investimento. Illustreremo come un'opportuna sinergia tra il sistema geotermico e i generatori di integrazione comporti notevoli vantaggi energetici ed economici, migliorando le prestazioni operative, riducendo i costi di installazione e contribuendo allo sfruttamento sostenibile del terreno.

La metodologia proposta è applicabile in diversi ambiti professionali, politici, economici e di ricerca. A tal proposito, presenteremo due casi studio. Il primo si riferisce ad un tipico problema di dimensionamento di un impianto: verranno quindi evidenziati i vantaggi energetici ed economici conseguibili attraverso l'applicazione della suddetta metodologia rispetto a quelle tradizionali. Nel secondo caso studio, illustreremo come sia possibile analizzare i margini di miglioramento della tecnologia GSHP tramite le stesse procedure di simulazione ed ottimizzazione. Quest'ultime verranno utilizzate per valutare l'influenza dei diversi sottosistemi sulle prestazioni finali dell'impianto GSHP, quantificando i possibili benefici di un eventuale sviluppo tecnologico e fornendo alcuni suggerimenti riguardo quali sottosistemi necessitano una maggiore attività di ricerca.

Contents

Nomenclature

Symbols

$\dot{m}$	Flow rate	$\mathrm{kg\,s^{-1}}$
$\dot{Q}$	Thermal power	W
$\dot{q}$	Heat flux per unit length	$\mathrm{W\,m^{-1}}$
$\dot{W}$	Electrical power	W
$\mathbf{g}$	Body acceleration vector	$\mathrm{m\,s^{-2}}$
$\mathbf{V}$	Volume-average velocity with respect to fluid volume only	$\mathrm{m\,s^{-1}}$
$\mathbf{v}$	Seepage or Darcy velocity	$\mathrm{m\,s^{-1}}$
c	Specific heat	$\mathrm{J\,kg^{-1}\,K^{-1}}$
c_p	Specific heat at constant pressure	$\mathrm{J\,kg^{-1}\,K^{-1}}$
CR	Capacity Ratio	
D	Dimensionless borehole installation depth	
d	Borehole installation depth	m
F_J	Cumulative distribution function	
F_J	Probability distribution function	
f_T	Penalization faction due to the actual sources temperature	
f_{CR}	Penalization faction due to the actual capacity ratio	
Fo	Fourier number	

H	Depth	m
h	Hydraulic head	m
J	Performance Index	
K	Hydraulic conductivity	$\mathrm{m\,s^{-1}}$
N_{BHE}	Boreholes number	
N_U	U-pipes number in a single borehole	
p	Pressure	Pa
Pe	Péclet number	
Q	Thermal energy	J or kWh
R	Dimensionless radial distance	
r	Radial coordinate	m
R_b	Borehole thermal resistance	
R_g	Effective thermal resistance of ground	$\mathrm{m\,K\,W^{-1}}$
R_{BHE}	Borehole aspect ratio	
s_w	Water well drawdown	m
T	Temperature	K or °C
t	Time	s or h
W	Electrical energy	J or kWh
Z	Dimensionless axial distance	
z	Axial coordinate	m

Superscripts

b	Generic borehole
BHE	Borehole heat exchanger
C	Cooling mode
$cond$	Condenser
DC	Declared capacity conditions

e	External	
eff	Effective	
eva	Evaporator	
f	Fluid phase	
g	Ground	
$grout$	Borehole grouting material	
H	Heating mode	
i	Inner	
in	Inlet/Supply conditions	
l	End-user loop, thermal load	
m	Overall thermo-physical property in porous media	
nom	Nominal/Rating operative conditions	
out	Outlet/Return conditions	
s	Steady-state condition	
w	Fluid circulating within the ground-coupled loop	

Subscripts

0	Initial time	
i	Generic time step	
N	Total time steps number	
n	Current time step	

Greek Letters

α	Thermal diffusivity	$\mathrm{m^2\,s^{-1}}$
γ	Euler–Mascheroni constant	
κ	Permeability	$\mathrm{m^2}$
λ	Thermal conductivity	$\mathrm{W\,m^{-1}\,K^{-1}}$
μ	Mean value	

ϕ	Porosity	
π	Pi	
σ	Standard deviation	
τ	Reference time period	s or h
Θ	Dimensionless temperature	
θ	Angular coordinate	rad

Mathematical functions

cos	Cosine function
exp	Exponential function
Γ	Generalized incomplete gamma function
ln	Natural logarithm
$\log_{10}$	Base-10 logarithm
Ei	Exponential integral function
erf	Gauss error function
$erfc$	Complementary error function
I_0	Modified Bessel function of the first kind, zero order
J_0	Bessel function of the first kind, zero order
J_1	Bessel function of the first kind, first order
K_0	Modified Bessel function of second kind, zero order
Y_0	Bessel function of the second kind, zero order
Y_1	Bessel function of the second kind, first order

List of acronyms

AHP Absorption Heat Pump system

ASHP Air-source Heat Pump system

ASHRAE American Society of Heating, Refrigerating, and Air-Conditioning Engineers

BHE Borehole Heat Exchanger

CBA Cost-benefit Analysis

AHP Absorption heat pump system

CDF Cumulative Distribution Function

COP Coefficient of Performance in heating mode

DP Dynamic Programming

DX Direct-expansion system

EER Energy Efficiency Ratio in cooling mode

EP Energy Pile

FCS Finite Cylindrical Source

FEM Finite Element Method

FLS Finite Line Source

FUE Fuel Utilization Efficiency

GA Genetic Algorithm

GHE Ground Heat Exchanger

GHP Ground-coupled Heat Pump

GCHP Ground-coupled Heat Pump system

GSHP Ground-source Heat Pump system

GUE Gas Utilization Efficiency

GWHP Groundwater Heat Pump system

HDPE High-density Polyethylene

HP Heat Pump system

HVAC Heating, Ventilating and Air Conditioning system

HGSHP Hybrid GSHP system

IAQ Indoor Air Quality

ICS Infinite Cylindrical Source

IGSHPA International Ground Source Heat Pump Association

ILS Infinite Line Source

IRR Internal Rate of Return

MILS Moving Infinite Line Source model

MFLS Moving Finite Line Source model

NPV Net Present Value

PDF Probability Distribution Function

PI Profitability Index

PWL Pumping Water Level

RES Renewable Energy Source

REV Representative Elementary Volume for porous media analysis

SAHPS Solar thermal Assisted Heat Pump System

SPP Simple Payback Period

SWHP Surface-water Heat Pump system

SWL Static Water Level

TC Total Cost

TRT Thermal Response Test

TRCM Thermal Resistance and Capacity Model

UNI Ente Nazionale Italiano di Unificazione

1 Introduction

The aim of this Thesis is to define an innovative design approach for ground-source heat pump systems (GSHP) based on the optimization of its operative performances. The latter are evaluated through a proper simulation model taking into account the behavior and the interactions among each GSHP subsystem (viz. ground reservoir, ground heat exchangers, ground-coupled loop and connecting ductwork, ground-coupled heat pump unit, back-up generators, and building end-user system). Components size and overall control strategy are investigated according to energetic and/or economic performance indexes in order to ensure a sustainable, efficient, and profitable exploitation of the ground source.

Heat pumps (HPs) are a widely used technology for thermal energy generation in buildings, capable of efficiently supplying heating, cooling, and sanitary hot water. Particularly, GSHPs are globally recognized as one of the most promising technologies in terms of economic and energy savings. Drivers promoting the use of ground energy systems are summarized in Table 1.1. However, despite the aroused interest, operative performances can result below expectations. This uncertainty on final performances and the relevant installation cost limit the attractiveness of GSHPs with respect to other solutions (e.g. air heat pumps, condensing boilers, solar technologies).

Current design methodologies derive from the traditional approach to heating and cooling (H&C) system design: the first step concerns the analysis of building needs to identify a reference thermal power (typically the peak load) and select the heat pump capacity. The second step deals with the characterization of the ground source in terms of thermo-physical properties and undisturbed temperature level. Finally, ground heat exchangers (GHEs) are sized to match the thermal requirements of the heat pump unit. In this perspective, each subsystem aims to meet the demands of the previous one according to a sequential and hierarchical logic. Coupling effects due to components interaction are not explicitly considered.

Another critical issue of current design methodologies is the choice of the heat pump capacity. As above-mentioned, usually, the reference value for HP design coincides with the peak load. This approach aims to maximize the ground-source contribution presuming that GSHPs have higher efficiency with respect to back-up generators. Actually, there is

Table 1.1. Drivers for the use of ground-source energy systems (after [1]).

Driver	Specification	Notes
Energy	Modern buildings design are required to consider several active and passive energy saving measures. GSHPs are one of the main technologies for potential energy savings.	Heat pump systems (including ground-source ones) require input energy (heat or work) to operate. Typical modern *vapor-compression* HPs can provide $3-5$ of useful heat units for every unit of supplied electrical energy. Absorption systems can provide $1.3-1.7$ of useful heat units for every unit of supplied thermal energy[1]. We stress that energy savings should be evaluated in terms of *primary energy*.
Environment	Due to the potential energy savings, GSHP systems might notably contribute to lowering the environmental impact of energy conversions. However, they need specific environmental precautions, especially during the installation phases.	As ground energy systems are becoming more popular, it will become increasingly necessary to consider the impact of heat extraction/injection on local underground environment and possible interactions among nearby systems. This topic refers to *sustainability* issues.
Economics	GSHP can offer significant reduction of operative costs of heating&cooling services	Special attention shall be payed to installation costs in order to ensure the investment profitability.
Regulation	National and international authorities recognize the importance of energy efficiency and energy saving measures, imposing minimal levels of performance and encouraging high efficiency solutions via tailored incentives.	The potential contribution of HP technologies in energy savings and environmental objectives is globally accepted.

[1] Absorption systems are mainly used for heating purposes because of their low efficiency in cooling mode.

no guarantee that this is the best design strategy.

As a matter of fact, heat pump performances depend on actual operative conditions, i.e. the temperature of the sources and HP unit capacity ratio. System operation alters the initial state of the ground source; in fact, due to its huge thermal capacity, the ground temperature evolution is the result of the entire history of heat exchanges. High capacity GSHPs result in higher heat extraction/injection of heat from/to the soil: Consequently, large exchange surfaces are required to avoid the temperature drift of the source. A peak-based approach results in high installation costs without ensuring adequate system performances.

Significant improvements can be achieved by redefining the objectives of the project phase. The final goal of the design method is not to guarantee that a certain peak thermal power is delivered by the GSHP, but that the energetic and economic performances of the overall system (back-up generators included) are maximized. In particular, we stress that the use of any H&C technology is convenient only when it delivers useful thermal energy

with higher efficiency than alternative solutions. This rationale of maximum performances does not necessary coincide with the maximization of the ground source exploitation.

In order to obtain a thorough and efficient design, it is necessary to consider each one of the following aspects:

- *Sustainability* of the thermal performance of the ground source over multi-year operation;
- *Estimation of the operative energy efficiencies* of the heat pump, as opposed to "*reference design conditions*";
- *Optimization* of the share of the required thermal load between GSHP and backup generators, instead of designing for peak-load coverage by means of the GSHP alone;
- Efficient *control* of the system, in order to match variable energy demands of the building users;
- *Optimal sizing* of ground-coupled heat pump unit (GHP) and ground heat exchangers, based on a cost-benefit analysis (CBA) among energetic performances, operational & maintenance costs, and initial investment.

GSHPs design process includes sources selection, equipment sizing, and apparatus arrangement. Traditional design methodologies aim to match a reference thermal power demand under nominal conditions, but do not consider the behavior and the actual performance of system components during the operational life. On the contrary, the proposed holistic approach conceives the design process as a 4 in 1 activity, including feasibility study, sizing process, performance analysis, and optimization. Furthermore, the control strategy shall be included in the list of design variables because of its relevance in ground temperature evolution.

The development of simple and effective methods for the simulation and optimization has already been identified as one of the main research priorities in GSHP subjects [2]. In this perspective, the design process becomes a "simulation-based" optimization procedure in which alternative design solutions are optimized and rated according to proper energetic/economical performance indexes. We stress that the term "optimization" does not refer to any technological development of GSHP equipment. In this work, we propose a novel methodological approach to GSHP design in order to maximize the operative performances of the overall system at the current status of components efficiencies. In other words, we aim at identifying the optimal design solution and management strategies among current suitable alternatives.

This Thesis deals with all of the above mentioned research topics. In Chapter 2, we will analyze current ground-source heat pump technology with a particular focus on heat source characteristics and current design methodologies. Possible issues and room for improvement are investigated. In Chapter 3, we will review the main models for GSHP performance simulation. This work is focused on closed-loop ground-coupled systems, but some features of groundwater technology and water wells are also presented. Chapter 4 will be dedicated to the description of the proposed simulation model (set of equations), optimization algorithm and resolution strategies. Two case studies are presented in Chapter 5 to show favorable applications of the proposed methodology.

2 Ground-source heat pump technology: an overview

2.1 *Heat pump systems: terminology and basic concepts*

As stated in every thermodynamics textbook, *heat pumps* are devices able to transfer heat from a cold source to a hot one (heat sink), in contrast with the natural direction of the heat flow [3]. To do that, a given amount of driven energy is required: i.e. heat or work. In the first case, we refer to *absorption systems* (AHP); in the second case, we refer to *vapor-compression systems*.

According to this definition, all pieces of refrigeration equipment are heat pumps. However, in common engineering terminology, the term "heat pump" is generally referred to devices with prevailing heating purposes, while the terms *air conditioners* and *chillers* are referred to refrigeration tasks. Anyway, there are no conceptual differences between the two modes of operation, aside from our definition of the useful effect (Fig. 2.1). *Dual-mode* units are those heat pumps that alternately provide heating or cooling [4].

Applied heat pump systems include a large variety of applications (e.g. heating and cooling, domestic and service water heating, industrial and agricultural processes), driven equipment (absorption devices, electric and endothermic engines), heat sources and sinks (air, water, ground, solar energy, process heat or exhaust streams) [4], [5].

A large number of publications, books, articles, and reports have reviewed heat pump technology and its potential in energy savings and environmental protection has been globally reconsigned (see, for instance, [4]–[9]). HPs are currently arousing the interest of political institutions and legal authorities: for instance, European Directive 2009/28/EC has recognized HPs as a RES technology, also setting a method to evaluate the renewable share of the delivered heat [10].

In the following sections, we will describe the main features of HP technology, paying particular attention to possible heat source/sink alternatives and traditional design strategies.

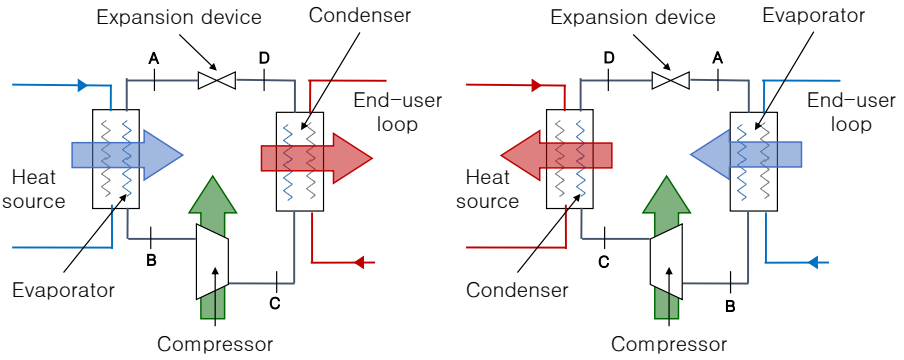

(a) *Heating mode.* (b) *Cooling mode.*

Figure 2.1. Scheme of a vapor-compression HP unit. The arrows represent the energy fluxes.

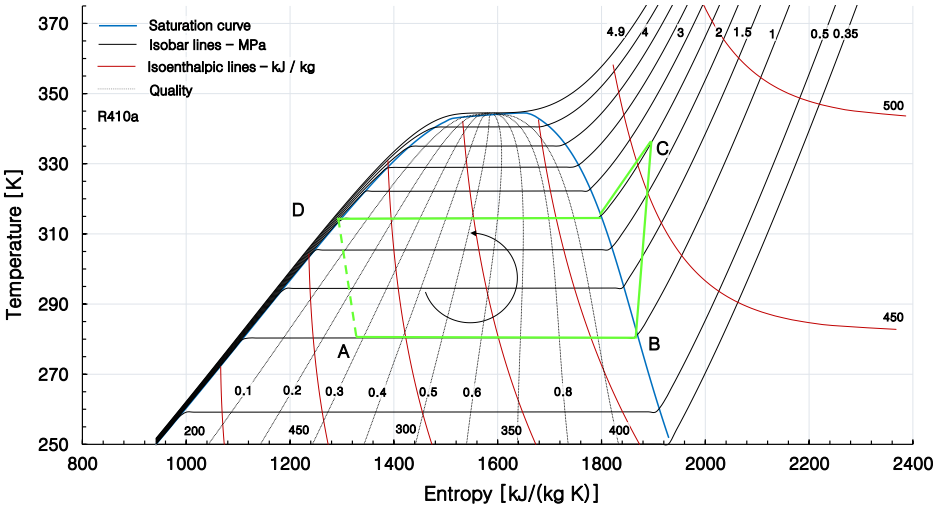

Figure 2.2. Reference thermodynamic cycle of a real heat pump. Working fluid: R410A.

Fig. 2.2 shows the physical model of a classical vapor-compression HP unit: it consists of a reverse thermodynamic cycle, in which the working fluid follows four main processes: evaporation (A – B), compression (B – C), desuperheating and condensation (C – D), and lamination (D - A).

Heat pumps operation is characterized by its *coefficient of performance* (COP) defined as the useful effect produced (i.e. delivered thermal energy) divided by total energy input (i.e. energy supply at compressor and auxiliaries). Analogously, in cooling mode, we traditionally refer to the *energy efficiency ratio* (EER[1]). The two coefficient read:

$$COP = \frac{\dot{Q}_{cond}}{\dot{W}} \tag{2.1a}$$

$$EER = \frac{\dot{Q}_{eva}}{\dot{W}} \tag{2.1b}$$

where $\dot{Q}_{cond}$ and $\dot{Q}_{eva}$ are the thermal power exchanges at the condenser and evaporator, respectively, and $\dot{W}$ is the total power input of the system (auxiliaries included).

To date, a universal standardization for HPs terminology does not exist; consequently, different authors use the same generic acronym COP/EER to evaluate different quantities. For example, COP values are used by manufacturers to express the ratio of the instantaneous thermal power delivered by HP unit and the instantaneous electrical input at the compressor; likewise, the same acronyms COP are used by designers to indicate the integral energetic performance of overall HP systems (auxiliaries included).

For the sake of clarity, Table 2.1 gives a list of the main energetic indexes and terms that will be used in this Thesis (reference can also be made to the acronyms list on page XXI). In particular, we want to highlight the differences among power, energy, and primary energy terms.

This Thesis deals mainly with vapor-compression systems, thus we are not going to provide a specific term list for absorption heat pumps; however, all previous considerations about terminology can be easily extended to AHPs. For example, the so-called *fuel utilization efficiency* (FUE)or *gas utilization efficiency* (GUE) are the reference indexes for AHPs heating performances[2]: however, their physical meaning coincides with COP one.

According to thermodynamic principles, real cycles (Fig. 2.2) can be converted to an equivalent Carnot cycle exchanging the same energy amounts between two equivalent temperatures, $\overline{T}_{cond}$ and $\overline{T}_{eva}$. With reference to Fig. 2.2, the definitions of $\overline{T}_{cond}$ and $\overline{T}_{eva}$

1 Anglo-American manufacturers are used to indicate the cooling power of heat pumps in British thermal unit per hour (Btu/h), whereas energy input is expressed in kW. A 3.413 reducing factor has to be used to make EER dimensionless.

2 Absorption systems are mainly used for heating purposes because of their low efficiency in cooling mode

Table 2.1. Energetic indexes for vapor-compression heat pump systems.

Acronym	Name	Definition
COP/EER	Heat pump COP/EER	Useful **thermal power** divided by **total power input** (auxiliaries included).
COP'/EER'	Thermodynamic cycle COP/EER	Useful **thermal power** divided by **compressor power input** (auxiliaries excluded).
$\langle COP \rangle$ / $\langle EER \rangle$	Average COP/EER	Delivered/removed **thermal energy** divided by **total energy input** (auxiliaries included). The coefficient refers to a **specified time period** during the heating/cooling season.
$SCOP/SEER$	Seasonal COP/EER	Delivered/removed **thermal energy** divided by **total energy input** (auxiliaries included). The coefficient refers to the **entire heating/cooling season**.
SPF	Seasonal Performance Factor	As $SCOP$ or $SEER$
PER	Primary Energy Ratio	Useful **thermal energy** during a season divided by **total primary energy input** (auxiliaries included)

read:

$$\overline{T}_{cond} = \frac{1}{s_C - s_D} \int_D^C T ds = \frac{\dot{Q}_{cond}}{s_C - s_D} \tag{2.2a}$$

$$\overline{T}_{eva} = \frac{1}{s_C - s_D} \int_A^B T ds = \frac{\dot{Q}_{eva}}{s_C - s_D} \tag{2.2b}$$

The COP and EER of the equivalent Carnot cycle correspond to the actual coefficients of performance of the reference HP cycle:

$$COP' = \frac{\dot{Q}_{cond}}{\dot{Q}_{cond} - \dot{Q}_{eva}} = \frac{\overline{T}_{cond}}{\overline{T}_{cond} - \overline{T}_{eva}} \tag{2.3a}$$

$$EER' = \frac{\dot{Q}_{eva}}{\dot{Q}_{cond} - \dot{Q}_{eva}} = \frac{\overline{T}_{eva}}{\overline{T}_{cond} - \overline{T}_{eva}} \tag{2.3b}$$

$$\tag{2.3c}$$

As well-known, COP and EER values increase when $\overline{T}_{cond}$ and $\overline{T}_{eva}$ are close [3]. Therefore, at least in theory, temperature level is the main criterion for rating suitable heat sources alternatives [11]. This principle is the one that has stimulated the interest in ground and water source applications: indeed, theoretically, the latter media have more favorable and stable temperature with respect to the outdoor air. Practically, design of real HP systems cannot neglect many other typical engineering issues (see section 2.2).

In this regard, it is worth recalling that the equivalent condensing/evaporating temperatures are necessarily higher/lower than those of cold/hot sources; otherwise, the heat transfer process does not occur. Using the sources temperature to estimate COP/EER values results in an optimistic overestimation of HP efficiency; on the contrary, real performances are notably affected by the effectiveness of the heat transfer apparatus and HP components. Consequently, the coupling among thermal sources and HP unit always needs a proper equipment design.

These basic considerations about thermodynamic mechanisms of heat pumps operation are sufficient to hint us one of the main issues of HP design. High performances can be obtained only with a reduced temperature difference among HP working fluid and heat sources, therefore, large heat transfer surfaces, large components, and high installation costs are needed. We can conclude that one of the main goals of HP designers is to investigate the best tradeoff between system efficiency and initial costs.

Another useful parameter to evaluate HP performances is the so-called *second-law-efficiency*, η^{II}. It is defined in Eqs. (2.4) for heating and cooling mode, respectively.

$$\eta_H^{II} = \frac{COP}{COP_{id}} \tag{2.4a}$$

$$\eta_C^{II} = \frac{EER}{EER_{id}} \tag{2.4b}$$

where COP and EER are the actual coefficients of performance of a given HP unit, whereas COP_{id} and EER_{id} are the theoretical Carnot efficiencies under the same sources temperature.

Heat pump manufacturers refer their data-sheets to the outlet temperature of secondary fluids from evaporator $T_{eva,out}$ and condenser $T_{cond,out}$ (see fig 2.3), in accordance with current technical standards for HPs rating (see, for instance, [12]–[16]).

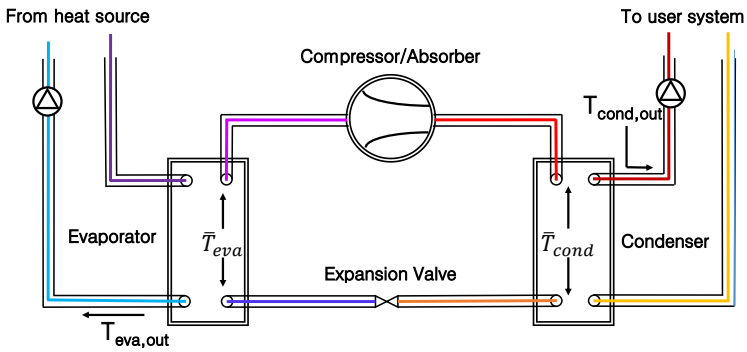

Figure 2.3. Generic heat pump scheme. We highlighted the different points of evaluation of $T_{cond,out}$, $T_{eva,out}$, $\overline{T}_{cond}$, and $\overline{T}_{eva}$.

If we are interested in heat pump analysis, we can consider $T_{eva,out}$ and $T_{cond,out}$ as the source and sink temperatures: therefore, we can use these values to define COP_{id} and EER_{id} as in equations (2.5).

$$COP_{id} = \frac{T_{cond,out}}{T_{cond,out} - T_{eva,out}} \tag{2.5a}$$

$$EER_{id} = \frac{T_{eva,out}}{T_{cond,out} - T_{eva,out}} \tag{2.5b}$$

then:

$$\eta_H^{II} = COP \left(\frac{T_{cond,out} - T_{eva,out}}{T_{cond,out}} \right) \tag{2.6a}$$

$$\eta_C^{II} = EER \left(\frac{T_{cond,out} - T_{eva,out}}{T_{eva,out}} \right) \tag{2.6b}$$

Similarly to other second-law-efficiency indexes (see for instance [17], [18]), η^{II} represents the deviation among the performance of a real device and the theoretical/maximum performance achievable under the same operative conditions (i.e. heat source temperature). In other words, it quantifies the loss of efficiency due to the employment of real technological components. Consequently, the ratios η_H^{II} and η_C^{II} are necessary lower than one [9], [11], [17], [18]. Second-law efficiency is a useful concept for heat pumps analysis, as it allow us to investigate the thermodynamic mechanisms of HPs operation apart from technological drawbacks.

Fig. 2.4 shows η_H^{II} (red markers) and η_C^{II} (blue markers) values of several real HPs as a function of the supply temperature to the external and internal heat sources: T_{int} and T_{out} correspond to $T_{cond,out}$ and $T_{eva,out}$ in heating mode, respectively, and *vice versa* in cooling mode. We collected data on units within a 20-100 kW capacity range from different manufacturers. η^{II} values are shown in Table 2.2 and Fig. 2.4.

	Heating mode	Cooling mode
Water-to-water units	$0.48 - 0.55$	$0.37 - 0.47$
Air-to-water units	$0.30 - 0.38$	$0.15 - 0.25$

Table 2.2. Typical ranges of the second-law efficiency of modern HPs in heating (η_H^{II}) and cooling mode (η_C^{II}).

We note that that water-to-water units have higher second-law efficiencies than air ones, irrespective of sources temperature. This is mainly related to the intrinsic efficiency of HP components (evaporator, condenser, compressor...): in this work, we do not deal with

specific analysis of HP units, therefore the above-mentioned values are taken as reference without performing specific studies.

Besides, there are no significant differences among different firms, hinting a specific level of development for current HP technology (see again fig. 2.4). For further details on this subject and on thermodynamic analysis of heat pump units, the reader can refer, among others, to [8], [18]–[30]. We will discuss again this topic in section 5.2, where we will investigate the benefits of a technological development, i.e. by increasing η^{II} values.

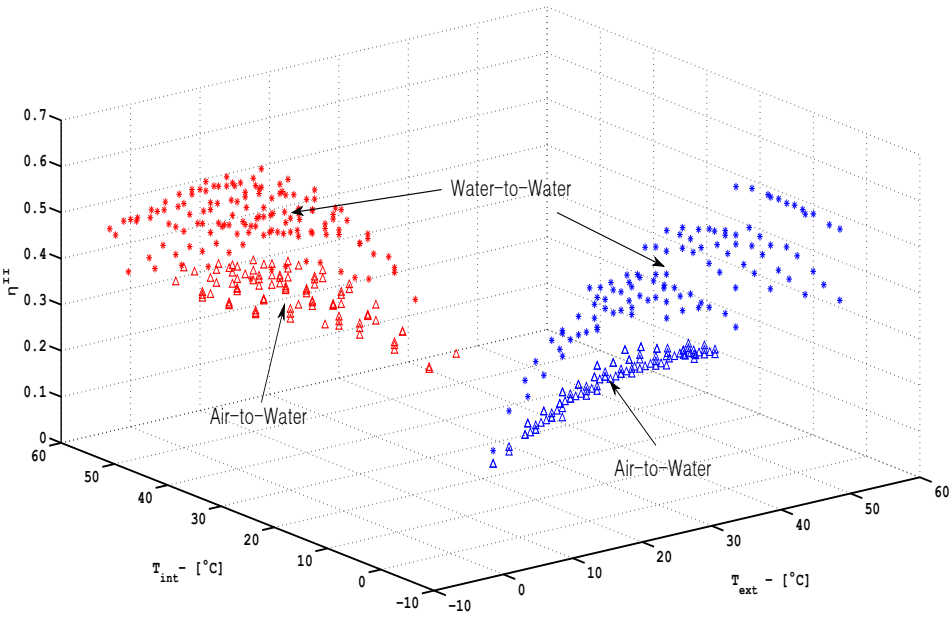

Figure 2.4. Typical values of second-law efficiencies, η^{II}, of modern HP unit. Asterisk markers refer to water-to-water units and triangle markers refer to air-to-water units.

2.2 *Heat sources and sinks*

In common HP terminology, the term *heat source* refers to the medium from which heat is removed. Analogously, *heat sink* refers to the source toward heat is delivered. Selecting the best heat source and technology for any specific heat pump application is influenced by many technical and economic factors: e.g. geographic location, climate, thermo-physical properties of the source medium, service provided, building characteristics, thermal load evolution, available budget, economical, legal and environmental contexts. However, it is possible to outline some general features of the most common heat sources/sinks.

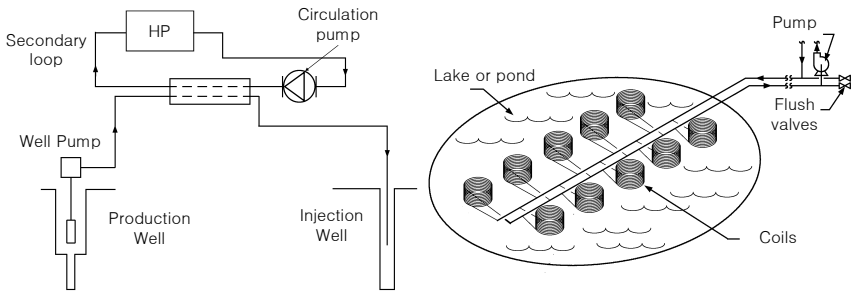

(a) *Open-loop configuration*. (b) *Closed-loop configuration*.

Figure 2.5. Scheme of a water-source heat pump system.

Air

Outdoor air is an universal heat source/sink and it is widely used both in residential, office, commercial, and services buildings. Air-source heat pump systems (ASHP) have greater ease of installation and lower costs than water- and ground-source heat pumps, however their heating capacity and efficiency are strongly affected by outdoor temperature variation. Moreover, frost may form on the external coil when outdoor air temperature is lower than 5 °C [4]. Consequently, defrosting cycles have to be performed periodically.

Under very humid climate conditions, heat pumps may require defrosting after as little as 20 minutes of operation [4]. Frost formation and defrosting cycles affect ASHPs viability because of loss of available heating power and overall efficiency reduction.

An interesting application of air-source systems is the one that exploits the exhausted air from large and commercial buildings. This is an ideal operative configuration for heat pump units as the exhaust air has a constant advantageous temperature level in both heating and cooling period. In these conditions HPs act as heat recovery devices increasing the overall energy efficiency of the building [4].

Water

Water is a very attractive heat source/sink because of its natural temperature and heat transfer aptitude. Water source can be exploited by means of both open- and closed-loop systems. The former solution employs traditional water wells to obtain groundwater (Fig. 2.5- a), the latter uses submerged heat exchangers in open ponds, lakes, or streams in a similar manner to the ground-coupled heat pumps (Fig. 2.5- b).

However, water use is strongly subjected to legal and environmental judgment by com-

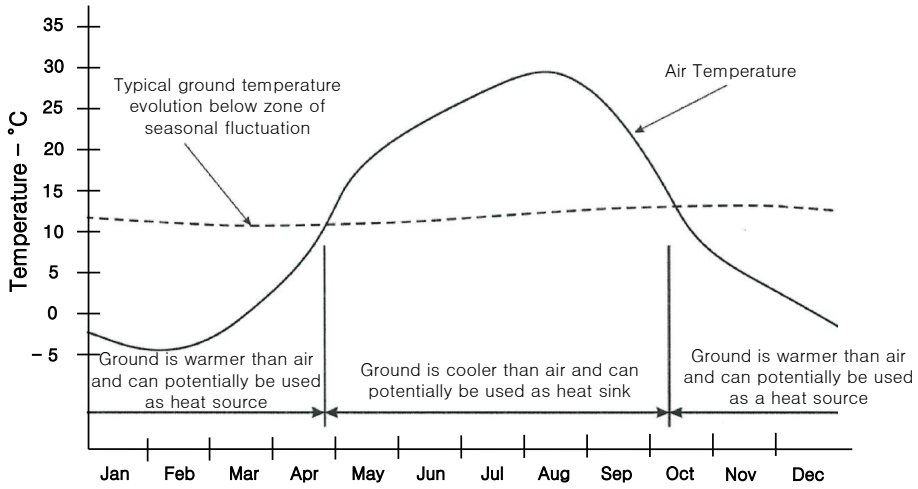

Figure 2.6. Typical annual air and ground temperature evolution. At depths more than few meters (e.g. $1-3$) the annual fluctuation of ground temperature is much less than air one. Theoretically, this results in a most advantageous heat source (or sink).

petent authorities. Moreover, water quality have to be analyzed to evaluate the possibility of clogging, fouling, scaling or corrosion. A secondary loop could be necessary to separate the well fluid from HP equipment (Fig. 2.5- a).

A proper system design is needed to ensure a nonconsumpitive (i.e. sustainable) use of the water: injection systems can be used, too. When water is pumped back into the aquifer (or to a pond or lake), special attention must be payed to the water temperature drop across the HP unit in order to prevent an excessive temperature alteration of the water body [6], [31].

Here, we want to cite also an interesting application of waste industrial water (e.g., spent warm water in laundries, plant effluent, warm condenser water) as heat source for heat pumps systems. According to [4] sewage waters from industrial processes offers numerous opportunities for applied heat pump systems. Industrial streams often have temperatures higher than surface body or groundwater, therefore, they are particularly appropriate for heating purposes. Sanitary water from buildings, hotels, spas can be exploited in a similar way. The viability, the selection, the design of those kind of systems are affected by economic factors, legal constraints, and desired levels of output capacity and temperature.

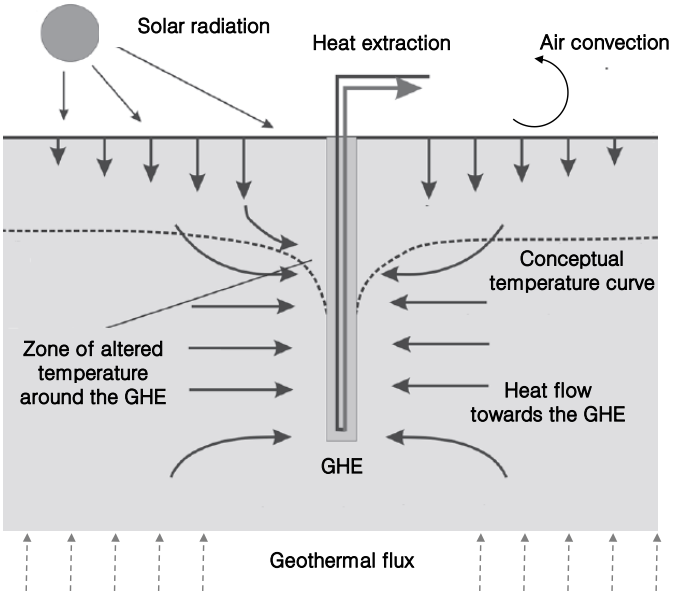

Figure 2.7. Conceptual model, with upper and lower boundary conditions of ground source (after [31]).

Ground

The ground is a very common heat source and sink [2], [4], [7]–[9], [32]. The so-called *ground heat exchanger* (GHE) is the technical device that enables the heat exchange between the heat pump and soil medium. It consists in one or more buried coils where a cold/hot carrier fluid circulates. The main attractiveness of the ground source is its rather constant temperature at a certain depth that should ensure, at least in theory, higher performances with respect to the air (Fig 2.6). Actually, the ground temperature evolution is not affected only by "natural" phenomena (i.e. outdoor air, solar radiation, soil moisture, mass transfer phenomena, ...), but the heat exchange at the GHE surface is a relevant term of the energy balance. A qualitative overview of the main energy exchanges determining the ground temperature is given in Fig. 2.7 [1], [31].

he relevance of each term varies according to the specific technical, environmental, and operational contexts. The energy transfer within the soil occurs mainly by conduction, with additional advective effects in case of relevant groundwater movement. Due to its high thermal capacity, ground temperature is slightly affected by surface phenomena. In undisturbed conditions (no GHEs operation) the depth of thermal penetration from the ground surface is about $d_p = \sqrt{2\alpha/\omega}$, where ω is the angular frequency of the surface temperature evolution. Typical values of d_p vary from 1-3 m for annual oscillations.

Regarding depth strata, the effects of natural ground gradient can be considered negligible in depths less than 100 - 150 m, therefore it has no relevant influence on typical GHEs operation.

GHEs operation alters the natural thermal evolution of the ground source: indeed, the history of the heat exchanges causes a thermal-affected zone around each GHE. The relevance of the alteration is a function of the composition, humidity, groundwater movement and GHEs installation depth [33]. For vertical BHEs, the heat exchange with the circulating fluid is the predominant term in the ground energy balance [34], [35].

The resulting fluctuation of the ground temperature affects the HP performances, therefore, a proper GSHP design cannot neglect this reciprocal interference between system operation and ground source temperature. The thermal diffusivity and seepage velocity of the soil are the dominant physical quantities governing the heat transfer process: their values vary widely from wet clay to dry sandy soil [33], therefore, an accurate characterization of the site is a necessary step of GSHP design process (see sections 2.1 and 2.2). Typical values of hydraulic and thermal properties of soils and rocks are reported in Appendix 1.

There are two main GHE configurations: horizontal and vertical arrangement. Pros and cons of the latter configurations will be discussed in section 2.3, together with current design methodologies.

Hybrid systems: solar-source heat pumps and cooling towers

As above-mentioned, the energy exchange between the ground/water and GSHP equipment alters the initial state of the source. Depending on the specific project and context, different preventative measures can be applied to ensure an advantageous and sustainable exploitation of the ground source. In particular, buildings with severe imbalances in cooling and heating load could result in excessive ground temperature alteration: therefore, large GHEs dimension and high installation costs would be required to maintain a favorable ground temperature. Additional heat rejecters or absorber (e.g. *cooling towers* or *solar technologies*) are commonly employed to reduce the GHEs size and project investment [1], [6], [9], [36].

These kinds of systems are named *hybrid ground-source heat pump systems* (HGSHP). They split the evaporation/condensation process among more heat sources in order to reduce or balance the annual heat load at the ground [6], [9], [37]–[40]. In this work, we just touch on the main characteristics and principles of those systems, without providing specific analyses.

Solar thermal assisted heat pump systems (SAHPS) are widespread solutions for heating-dominated applications. Solar collectors can be used as an additional thermal source (Fig. 2.8) to reduce the heat extraction from the ground. The principal advantage of using solar energy as thermal source is that, when available, it provides heat at higher temperature than water and ground sources, increasing the overall efficiency of the system. Compared

to solar heating solutions (without heat pumps), the collector efficiency and capacity are increased because a lower collector temperature is required. Further details on SAHPS systems can be found in [41]

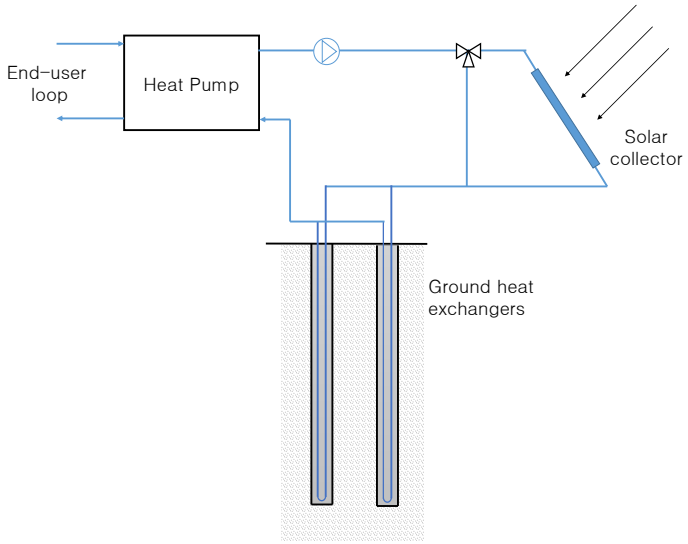

Figure 2.8. Schematic diagram of a HGCHP system with solar collector.

For cooling-dominated loads, a *cooling tower* can can be connected in series with the GHEs (see Fig. 2.9). This situation occurs in many large buildings with air-handle unit and/or de-humidification service; therefore, installing additional fluid coolers reduces the required GHEs length and project costs. According to ASHRAE handbook, the ground system should be designed to meet heating needs, then, one or more cooling towers are used to cover the residual load. For further details, the reader can refer to [6], [9], [42].

For the sake of clarity, we note that in common engineering vocabulary, the term "hybrid" refers also to those configurations in which alternative technologies are used to reduce the building load at the heat pump. In other words, when additional generators act like back-up units. In this Thesis, we use the term "hybrid" when additional technologies operate as heat sources, on the contrary, the term "back-up" is referred to those generators that assist the HP unit in delivering the end-user thermal load.

2.2.1 Criteria and methods for heat sources evaluation

Tables 2.3, 2.4, and 2.5 show a qualitative comparison among the three most common source media (i.e. air, water, and ground) according to the following properties:

- **Suitability**, seen as the potentiality of the medium to be used as a thermal source;

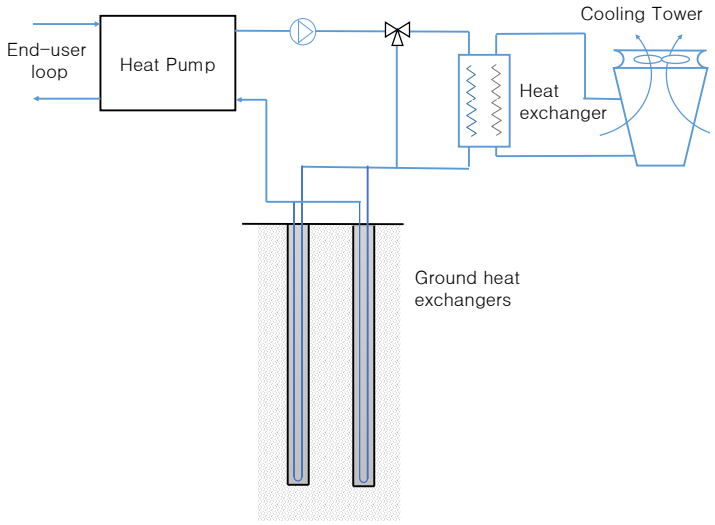

Figure 2.9. Schematics diagram of a HGCHP with cooling tower.

- **Sustainability**, seen as the aptitude of the medium to maintain advantageous conditions for exploitation during all the operational life of the coupled HP system;
- **Availability**, seen as the level of accessibility and technical feasibility with current technologies;
- **Installation costs**, seen as the total expenditure to purchase equipment and installation works;
- **Operation & Maintenance** , seen as the estimation of operative performance and maintenance required;
- **Temperature**, seen as the typical temperature level of the source at its undisturbed/initial state;
- **Technical features**, i.e. some general considerations on the main technical pros and cons for medium exploitation.

Two steps seems necessary in order to properly evaluate the opportunity of exploiting a given source:

1. The characterization of the *initial/undisturbed state of the source*. Typical analyses concern: annual outdoor temperature and humidity for ASHPs; aquifer temperature and volume, permeability, and depth for open-loop systems; ground temperature, thermal diffusivity, groundwater moment for closed-loop systems. The two main site-investigation techniques are:

- The *thermal response test* (TRT): which is able to determine the effective thermal conductivity

Table 2.3. Qualitative evaluations of air as thermal source [4]

AIR Medium		Suitability		Sustainability	Availability		Costs		Temperature		Technical features	
		Heat Source	Heat Sink		Location relative to need	Coincidence with need	Installation	O&M	Level	Variation	Pros	Cons
Outdoor	Ambient air	Good, but efficiency decrease at low air temperature	Good, but efficiency decrease at high air temperature	Excellent, HP operation does not affect source temperature	Everywhere	Always available	Low	Moderate	Depend on geographical zone	Generally elevate	Most common	Defrosting and supplementary heat usually required
Exhaust air from building ventilation	Building ventilation	Excellent	Fair	Excellent, HP operation does not affect source temperature	Good, if planned during building design	Generally available	Low to moderate	Low with "clean" air	Excellent	Very Low	Excellent energy-conservation strategy	Insufficient for typical loads: back-up needed

Table 2.4. Qualitative evaluations of water as thermal source [4]

WATER Medium		Suitability		Sustainability	Availability		Costs		Temperature		Technical features	
		Heat Source	Heat Sink		Location relative to need	Coincidence with need	Installation	O&M	Level	Variation	Pros	Cons
Ground-water	Wells	Excellent	Excellent	Good for large aquifers and high flow rates	Vary by locations	Always available	Depending on aquifer depth	Moderate, possible fouling or scaling	Good	Stable	Established know-how in wells drilling	Legal and environmental limits
Surface	Lakes, rivers, seas	Excellent	Excellent	Excellent for large body, HP operation does not affect source temperature	Limited, depend on proximity	Usually continuous	Depend on proximity	Low, scaling and fouling depend on water quality	Good	Low		Legal and environmental limits
Processing waters	Condensing tower, industrial processes	Excellent	Poor	Good	Varies	Varies	Low	Moderate, depending on water quality	Generally high	Depend on process, generally low	Excellent energy conservation strategy	Suitable only where heating need is coincident with heat disposal
Waste waters	Raw or treated sewage, gray water	Good to excellent	Good	Good	Varies	Varies	Depend on proximity and sewage composition	Varies, high for raw sewage	Excellent	Usually low	Excellent energy conservation strategy	Uncommon, may clog, foul, scale or, corrode

Table 2.5. Qualitative evaluations of ground as thermal source [4]

GROUND Medium		Suitability		Sustainability	Availability		Costs		Temperature		Technical features	
		Heat Source	Heat Sink		Location relative to need	Coincidence with need	Installation	O&M	Level	Variation	Pros	Cons
Ground-coupled	Closed geothermal-coupled loops	Varies with soil condition, good if ground is moist	Varies with soil condition, good if ground is moist	Poor, an accurate design and control are required to avoid temperature drift	Depends on soil suitability and GHEs configuration	Always available	High to moderate, depending on GHEs dimensions	Low to moderate, depends on design and control quality	Good	Depends on exploitation strategy	Favorable and constant temperature of the ground source, especially for moist soils.	Precautions are required to avoid temperature drift of the source
Direct expansion	Refrigerant circulated in ground loop	Varies with soil condition, good if ground is moist	Varies with soil condition, good if ground is moist	Poor, an accurate design and control are required to avoid temperature drift	Depends on soil suitability and GHEs configuration	Always available	High to moderate, depending on GHEs dimensions	Low to moderate, depends on design and control quality	Good	Depends on exploitation strategy	Favorable and constant temperature of the ground source, especially for moist soils	Precautions are required to avoid temperature drift of the source and refrigerant leaks

and diffusivity of the soil, together with the so-called “borehole thermal resistance" (see section 3.2). These parameters are needed to closed-loop systems design.

- The *pumping test*: which is able to determine the hydraulic conductivity, aquifer specific storage, and well efficiency. These parameters are needed to groundwater system design.

A brief review of the above-mentioned site-investigation techniques can be found in Appendix 2.

2. The *evaluation of medium potential in terms of energy/economic performances* of the HP system. This step involves typical matters of HVAC design: we aims to evaluate technical and economic suitability of the source medium in terms of overall GSHP system performance, in other words, we need to evaluate the energy amount that could be extracted/developed from/to the heat source in a sustainable and advantageous way. A given medium is a proper thermal source only if it is able to ensure an adequate heat transfer at the coupled exploitation system with a profitable efficiency. Therefore, the final decision on a project does not depend only on soil characteristics, but is based on the evaluation of system operative behavior.

TRT and/or pumping test represent the fundamental starting step of any ground-source system design as they provide an accurate evaluation of the thermo-physical properties of the local ground source. However, they are not sufficient to complete the assessment of project viability. Indeed, as stated in the second point of the above list, a cost-benefit analysis is needed to investigate the opportunity of employing a ground-source system rather than other heat sources or technologies. In particular, the achievable energy and/or economic savings have to be adequate to repay installation expenditures.

The evaluation and the optimization of GSHPs performances is the main topic of this Thesis: we will extensively discuss it in Chapter 4.

2.3 *Possible configurations and equipment layout*

Heat pump systems are classified not only by heat sources (sinks), other classification criteria regard heating and cooling distribution fluid, thermodynamic cycle (i.e. vapour-compression or absorption devices), size and configuration. In section 2.2 we discussed the main features of common heat source media (i.e. air, ground, and water), together with a proper evaluation criteria based on the deviation between initial/undisturbed state and operative behavior (see section 2.2.1). In this section, we will describe the technical layout and typical configurations of common HP systems. Furthermore, we will introduce some features of classical design procedures in order to highlight their basis and assumptions.

Terminology

According to ASHRAE [6], the term *ground-source heat pump* (GSHP) refers to those systems that use ground or water as heat sources or sinks. Both technical and scientific literature include groundwater and surface-waters (lakes, rivers, ponds...) within the GSHP

set (see for instance, [6], [9]). Many parallel terminologies are currently used: e.g. "*open-loop*" refers to *groundwater heat pump systems* (GWHPs), "*closed loop*" is manly used to indicate *ground-coupled heat pump systems* (GCHPs). *Surface-water heat pump systems* (SWHPs) could be both open- and closed-loop solutions depending on whether fluid is pumped from the water body or closed coils are employed without water abstraction (Fig. 2.5-b). Another terminology is used by HP manufacturers to classify the secondary fluids circulating in the evaporator/condenser: i.e. *air-to-air*, *air-to-water*, *water-to-water*, *water-to-air* systems.

In this work, we refer to ASHRAE terminology as illustrated in Fig. 2.10. The *horizontal GCHPs* set has been renamed in *shallow GCHPs* in order to include the so-called *thermo-active ground structures* (e.g. energy piles) and other shallow configurations (e.g. geothermal baskets).

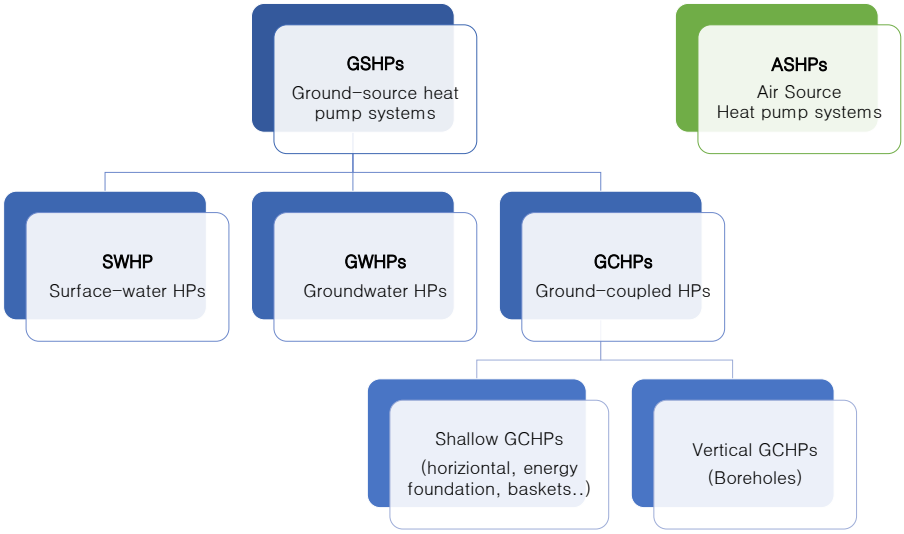

Figure 2.10. Ground-source heat pump systems (GSHPs) classification and terminology.

2.3.1 Air-source heat pump systems - ASHPs

ASHPs can be considered as one of the main "competitor" of ground-source systems. Indeed, despite the elevate variability of performances due to the fluctuation of the outdoor climate, air-source systems present several technical and economical advantages that make this kind of solutions more attractive than ground-coupled ones. Moreover, ASHPs have an established and straightforward design methodology that facilitates designers evaluations.

In regions with average climate, air-to-air and heat pumps (also named "split systems"', see Fig. 2.11) are particularly widespread in low-capacity and residential applications because of their low cost and ease of installation [4], [43]. These systems are mainly used

for cooling tasks, but dual-mode units have become very common in the market. HPs sales are almost totally made of air source units (95%) [43], especially in Mediterranean areas where they are mainly used for summer cooling. The reasons are quite simply: ASHPs are cheap and easy to install, also in existing buildings. Besides, cooling service few technology alternatives, while building heat needs are too low to justify expensive investments. Moreover, traditional heating technologies (e.g. condensing boiler) have already reached a notable level of reliability and do not require high-qualified designers and installers. Mixed boiler-ASHP systems are still the most attractive solution, especially in low capacity applications as residential dwellings.

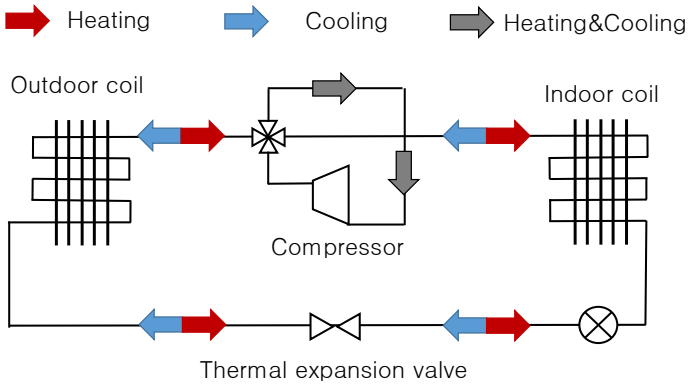

Figure 2.11. Dual-mode air-to-air heat pumps scheme. The flow of the refrigerant causes the change from heating to cooling service.

Air-to-water units (Fig. 2.12) are very common in medium-large capacity applications (e.g. large dwellings, tertiary sectors, offices and commercial buildings). They are commonly employed as generation device(s) in air-handling systems [5] or in low-medium temperature hydronics systems (e.g. fan coils).

We shortly mention other two particular applications of air-to-water HPs: the so-called "*internal-source heat pumps*"', which use indoor conditioned air as heat source for sanitary hot water production, and the so-called *exhaust-air systems* which recover heat from exhaust air channels to heat the incoming air. Both systems take advantage of the high temperature of indoor climate with respect to outdoor one.

ASHP design

In this Thesis, we do not deal with ASHP design, therefore, in this section, we shortly describe the typical sizing procedure for air-source systems just to highlight the main deviations and similarities between air- and ground-coupled sizing approaches.

As above-mentioned, heat pump systems are generally used both in heating and cooling

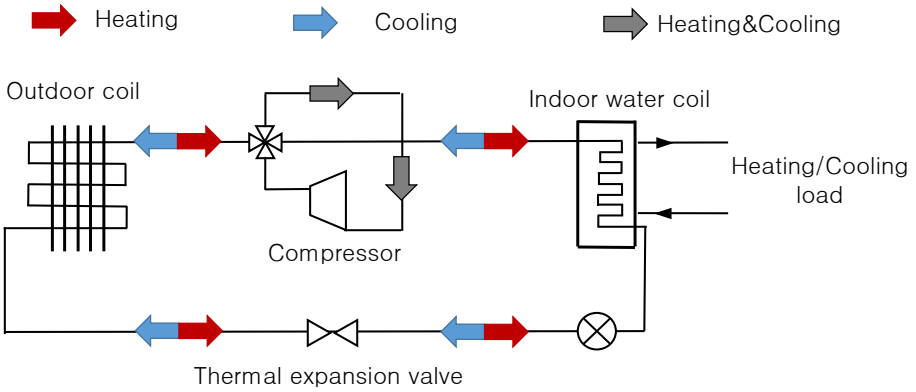

Figure 2.12. Dual-mode air-to-water heat pumps scheme. The flow of the refrigerant causes the change from heating to cooling service.

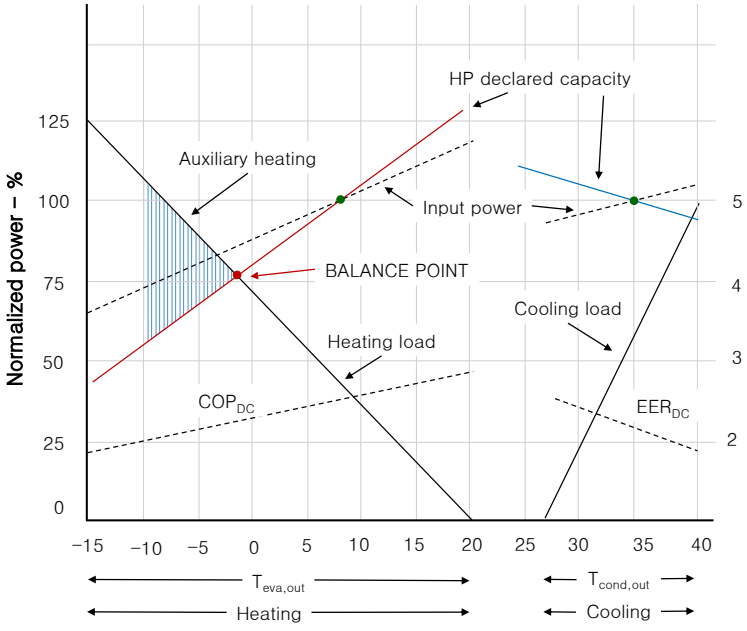

Figure 2.13. Operative characteristics of a air-source heat Pump (after [5], [44]). Power values are normalized according to the reference value in standard rating conditions (green markers) [12].

period, thus we have to ensure a proper system efficiency in both operational modes. All these factors make ASHPs sizing more critical with respect to traditional generators: unlike boilers, that have a single capacity value that identify the maximum thermal output in any operative conditions, HPs maximum capacity is strongly dependent on the temperature of heat sources (see the red and the blue lines in Fig. 2.13).

The nominal values declared by manufacturers are referred to standard rating conditions [12], therefore, HP's technical documentation always includes tables and/or charts showing the maximum thermal output (i.e. *"declared capacity"*') and corresponding efficiency (COP_{DC},EER_{DC})[3] as a function of outlet temperature from evaporator ($T_{eva,out}$) and condenser ($T_{cond,out}$).

The standard design process for ASHPs is based on the chart shown in Fig. 2.13. In the latter, thermal power values have been normalized according to the reference output of HP unit (green markers). Thermal needs of the buildings are assumed as a function of the outdoor temperature both in heating and cooling period. We note that also the the *building load* curves are normalized according to the nominal capacities of the HP.

The so-called *balance point* (or bivalent temperature) is the outdoor temperature at which heat pump output equals the building load [4], [5], [13]. The thermal capacity of the selected air-source heat pump unit determines the balance point value. The higher the bivalent temperature (i.e. low ASHP capacity), the higher back-up heating occurs. On the other hand, an elevate capacity HP unit results in a continuous modulation of its thermal output, causing the so-called "cycling losses" [45].

The optimal selection of the balance point (i.e. heat pump thermal capacity) is an ongoing-research topic [44], [46]. The current European standard EN 14825:2012 [13] assumes the following values of the bivalent temperature: -7 °C or lower for colder climates, 2 °C or lower for average climates, and 7 °C or lower for warmer climates. Naldi *et al.* [46] has developed an optimization algorithm to investigate the optimal balance point of air-to-water heat pump systems in heating mode. ASHRAE handbooks [4], [5] suggest sizing air-source heat pump units seeking the lowest balance point in heating mode that avoid an excessive oversize in cooling period. This approach aims to minimize the need of supplemental heat, however it does not seem the most advantageous strategy. Indeed, high capacity HP units result in higher installation costs and longest modulation periods. Depending on unit control capability, cycling losses reduce heat pumps efficiency.

Several studies have demonstrated the benefits of multi-generation systems (see, for instance, [41]) made of HPs and one or more back-up generators. The latter can be used to support the heat pump when its capacity is insufficient to deliver the total building load; analogously, back-ups can replace heat pump unit during low thermal load period, avoiding cycling losses. This issue affects also GSHPs and will be deeply discussed in section 3.3.

3 In this work, quantities with *DC* subscripts are always referred to the maximum thermal output at given operative conditions (i.e. the temperature of the thermal sources).

2.3.2 Ground coupled heat pump systems - GCHPs

As well-known, the ground temperature below a certain depth remains nearly constant due to the large heat capacity of the soil that limits the influence of surface heat exchange phenomena (see section 2.2). These favorable thermal conditions have aroused the interest in ground exploitation as heat source (see Fig. 2.6).

The first known record of the concept of using the ground as heat source for a heat pump was found in a Swiss patent issued in 1912. Since then, GSHP systems have experienced a continuous growth in terms of installations number and related research activity. In particular, two periods of intense development can be identified: the first began in both North America and Europe after World War Two and lasted until the early 1950s, the second has started during the first oil crisis in 1970 and it is still ongoing [1], [2], [36], [47]. In Italy, the diffusion of GSHP technologies has started during the 2000s, following the great deal of legislative activity on energy efficiency and renewable energy sources. Recent statistics estimate that global GSHPs installed capacity have grown continuously during the last 20 years with an average rate of 20−30% annually [36], [48].

Usually, the term "*ground-source system*" is related to the ground heat exchanger apparatus. However, we stress that GSHP operation depends on numerous other components. The typical layout of GSHP systems is show in Fig. 2.14. We have four main subsystems: the *ground source*, the *ground-coupled loop* (including the ground heat exchangers or water wells), the *ground-coupled heat pump unit* GHP, *peaking/back-up* generator(s), and the *end-user system*. All those subsystems shall be considered to assess a proper analysis of the system.

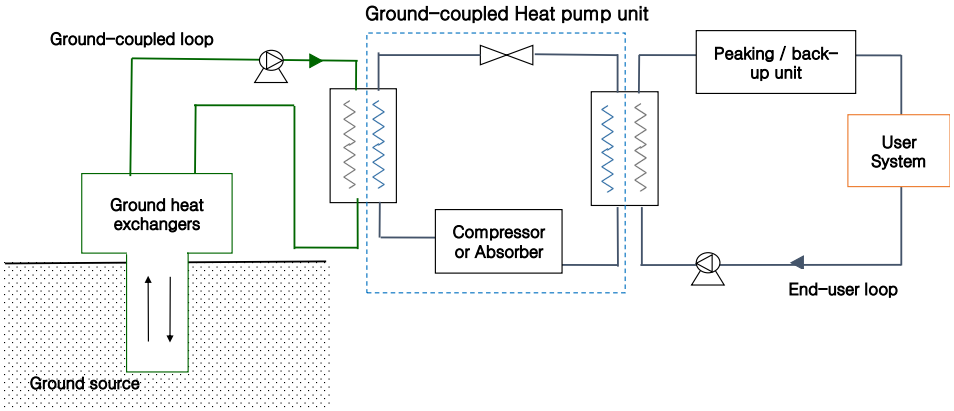

Figure 2.14. Scheme of GSHP subsystems.

With regard to GHP configurations, all the GSHP systems can be considered as a water-to-water system (figs. 2.15 and 2.16), with the only exception of the so called *direct-expansion systems* (fig. 2.17). The latter uses flooded or ground-embedded ducts as

evaporator/condenser, without using a secondary loop. However, their use is strongly limited because of the great quantity of refrigerant fluid needed and environmental restrictions. Heating/cooling changeover can be obtained changing the flow direction of the refrigerant (Fig. 2.15); another common solution is the one that switches the water circuits (Fig. 2.16) [4].

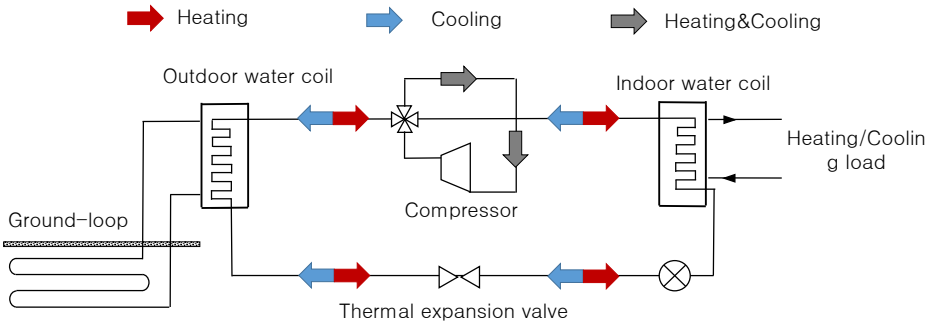

Figure 2.15. Ground-coupled heat pump scheme

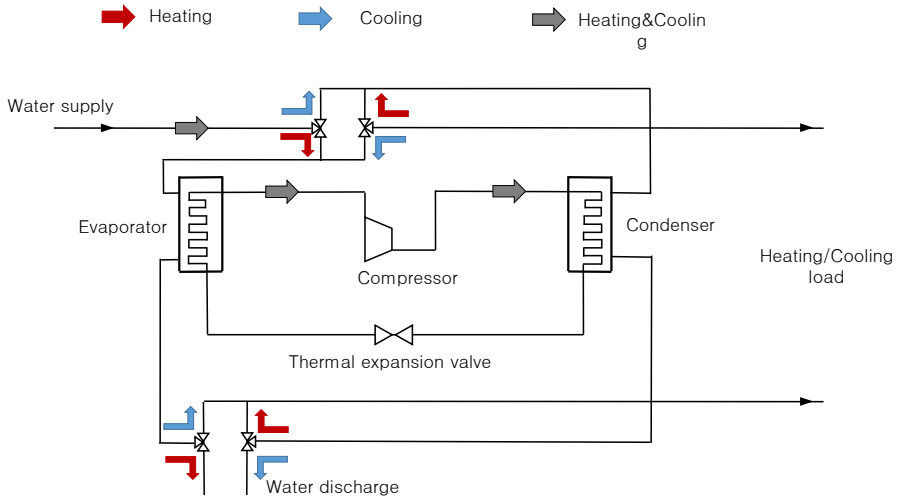

Figure 2.16. Water-to-water sytsems with seondary fluid changeover.

GCHP systems consist of one or more heat pump units that is coupled to a closed heat exchanger buried in the soil (Figs. 2.15, 2.18, and 2.20). Heat is extracted from or rejected to the ground through a circulating fluid: pure water or antifreeze mixtures can be used [9], [49]. This kind of systems have experienced a large development both in research and professional fields as demonstrated by the notable increasing of the energetic performances

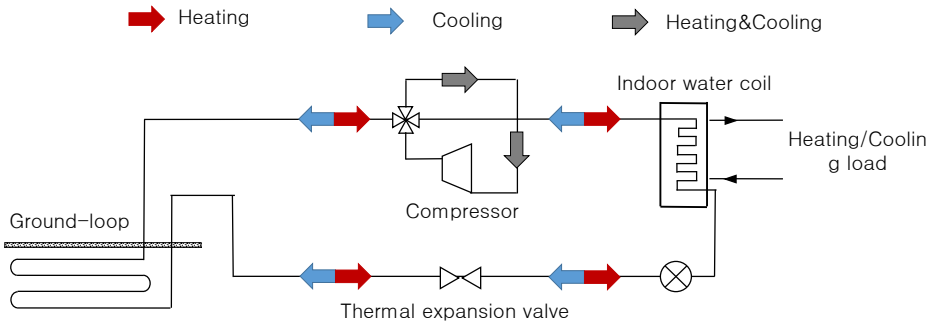

Figure 2.17. Direct expansion DX system scheme with refrigerant changeover.

since 1970s [2], [8]. Today, GCHPs have become the most widespread configuration among GSHP systems [9], [32], [50].

The GCHP set is further subdivided according to ground heat exchanger design: vertical and horizontal. *Vertical GCHPs* make use of several boreholes (BHEs) in which two or four HDPE ducts are placed. Subsequently, the bore is filled with a solid medium (i.e. the grout material) to ensure a good "thermal contact" among the ground and U-pipes. Typical ducts diameter varies from 20 to 40 mm. One or two close return U-bends are placed at the bottom of the BHE, hence the names *"1-U and 2-U configurations"*. Boreholes are typically 100 to 150 mm in diameter with a depth range from 20 to 180 m [9], [49], [50].

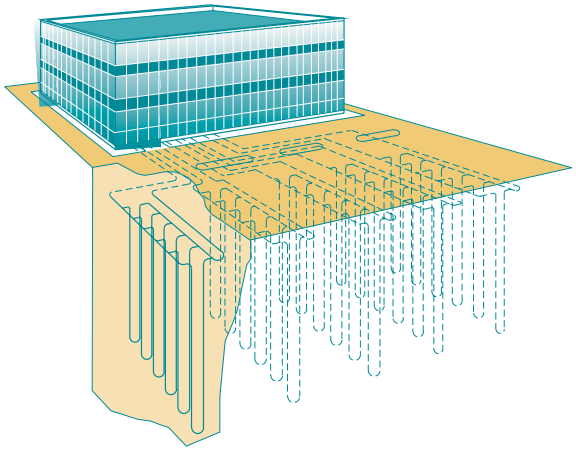

Figure 2.18. Vertical ground-coupled heat pump piping (after [51]).

Generally, we need to install more BHEs to match the required GHEs length (see section 2.4.1): thus, we are used to refer to a *"BHE field*" to indicate the overall ground heat

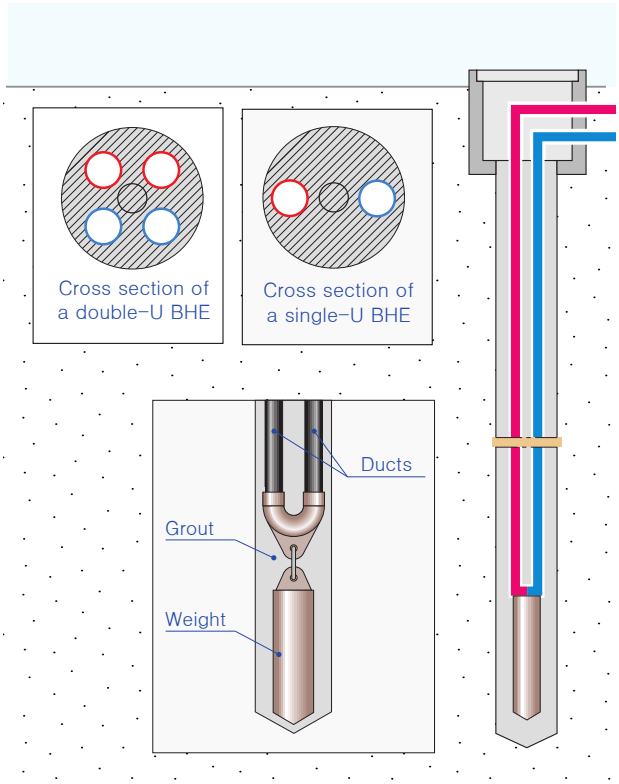

Figure 2.19. Scheme of a typical borehole heat exchanger.

exchanger apparatus. The boreholes can be placed in a single row or in a grid pattern according to the space availability. Typical separation distance among two consecutive BHEs varies from 6 to 10 m: this range is considered as a proper tradeoff among space requirement and thermal interference [6]. This distance can be optimized according to the annual ground energy balance, groundwater movement, or any other phenomenon that mitigates the temperature drift within the BHE field. Employing a supplemental heat rejecter or heat absorber could be necessary to reduce the required BHEs number decreasing initial costs (i.e. hybrid systems, see section 2.2).

Advantages of the vertical GCHPs are [6], [9], [52]:

1. relative small plots of ground required;
2. limited variation of soil temperature and thermal properties during the system operation (if properly designed and managed);
3. reduced pipework and pumping energy required (BHEs are generally in parallel).

4. fair heat transfer performances.

Disadvantages are:

1. higher installation costs because of expensive equipment needed to drill the boreholes;
2. limited availability of skilled contractors to design and perform installation works;
3. a high level of system design and management is needed to avoid operational fails [1].

The reference design method for vertical GSHP is the ASHRAE one [6]: we will describe it in section 2.4.1. Also several "rules of thumb" are currently available: European technical standards [53], [54] indicate the specific heat transfer rate per unit depth ($W\,m^{-1}$) as a function of the ground type and operation period. However, these values seem too approximate with respect to actual operative conditions.

Horizontal GCHPs (Fig. 2.20) consist of a series of pipe arrangements laid out in dug trenches approximately 1–2 m below the ground surface [9], [50], [55]. Pipes can be connected together either in series or in parallel: possible configurations can be divided into several subgroups [6], [9], [50], [52]: e.g. single-pipe, multi-pipe, spira (Figs. 2.21,2.22,2.23).

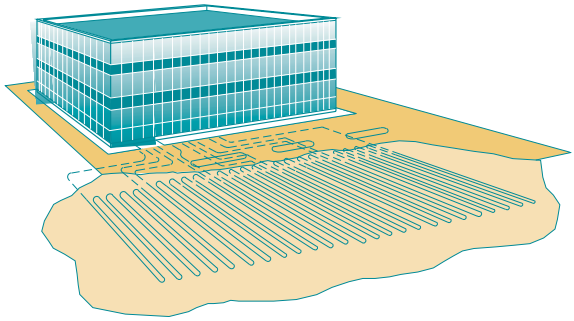

Figure 2.20. Horizontal ground-coupled heat pump piping (after [51]).

Horizontal configurations are characterized by large ground areas required, pipes length, and the influence of surface phenomena. For example, in exclusive heating-mode systems, the main thermal recharge is provided by the solar radiation on the earth surface [50]. Other factor affecting GHEs performances are the convective heat exchange with the outdoor air, soil moisture and mass transfer phenomena: e.g. freezing,thawing,drying, rewetting... [55]. Due to the number and complexity of the cited physical mechanisms, the modeling of the energy exchanges in the shallow strata of the soil is an ongoing research topic.

With respect to vertical configurations, the advantages of horizontal GCHPs are [6], [9], [52]:

1. lower installation costs with respect to vertical GCHPs because relatively simple installation procedure;

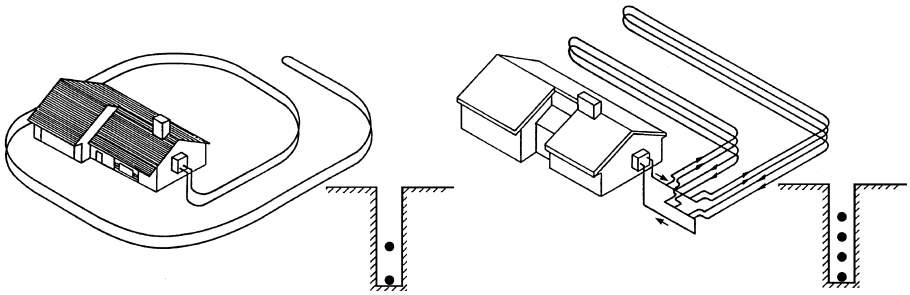

(a) *Series ground loop.* (b) *Parallel ground loop.*

Figure 2.21. Parallel and series horizontal ground heat exchanger configurations.

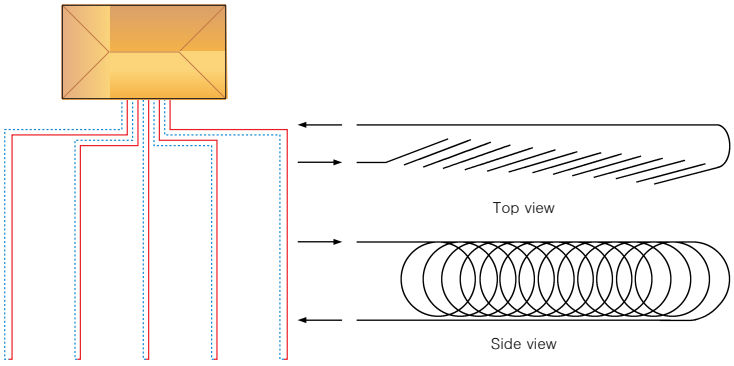

(a) *Top global view.* (b) *Spiral coil.*

Figure 2.22. Vertical layout of spiral earth coil.

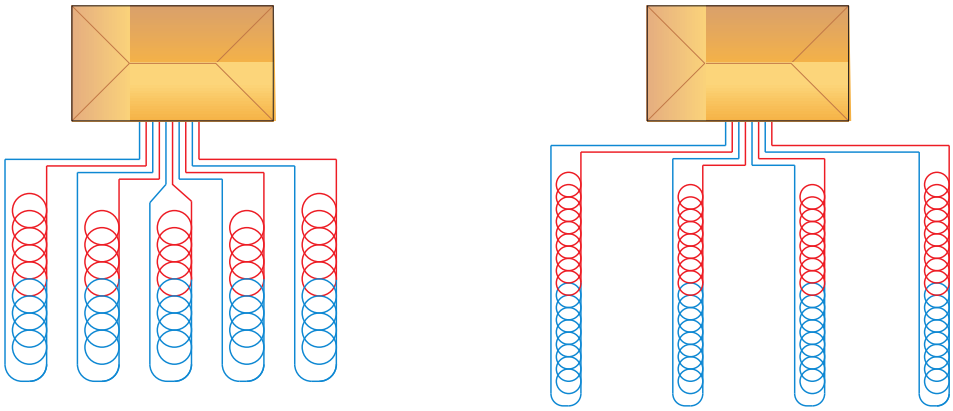

Figure 2.23. Horizontal layout of spiral earth coil.

2. ease of installation (if adequate ground area is available);
3. usually, there is no potential for aquifer contamination because of the shallow depth of the trench;
4. there is minimal residual temperature drift due to unbalanced annual loads on the ground loop, as the heat transfer to or from the ground loop is generally small compared to heat transfer occurring at the ground surface [6].

Disadvantages are:

1. larger ground area requirement: horizontal systems are not feasible in most urban and sub-urban zones;
2. greater variations in performance because ground temperatures and thermal properties fluctuate with season, rainfall, and burial depth;
3. lower system efficiencies with respect to vertical GSHPs [6];
4. slightly higher pumping-energy requirement.

Due to the lack of established physical models, the design of horizontal GSHPs is mainly based on rough "rules of thumb" given by engineering handbooks and manufacturers guidelines [6], [9], [56]. Florides and Kalogirou [50] suggest installing 35–60 m long per kW of heating or cooling capacity. Scientific reviews [9] and European technical standards (e.g. EN 15,450:2007 [53], [57]) propose some reference values of the specific power of extraction/absorption per ground area (see, for instance, Table 2.6).

Table 2.6. Specific extraction power for horizontal ground heat exchangers (after [9]).

Type of ground	$\dot{q} - \mathrm{W/m^2}$
Dry sandy ground	10÷15
Moist sandy ground	15÷20
Dry clay ground	20÷25
Moist clay ground	25÷30
Ground with ground-water	30÷35

Thermo-active foundations

Both vertical and horizontal GCHP systems involve several series of ground heat exchangers and ground-coupled loops. Independently from the adopted configuration, GHEs installation results in a significant investment costs. One way to reduce these costs is to use building foundations (e.g. piles) of new constructions as ground heat exchangers (Fig. 2.24) [58]–[60].

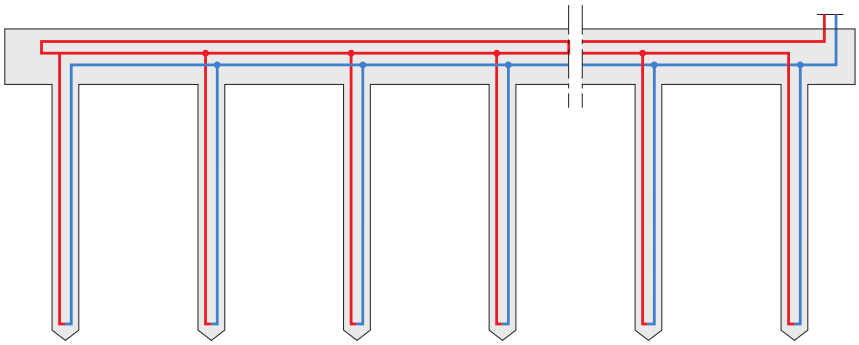

Figure 2.24. Schematic diagramm of thermoactive foundations. Coils are embedded within foundaton piles.

Energy piles (EPs) are dual-purpose heat exchangers with structural and thermal aims. Using building foundations will not require additional costs as the piles have to be necessary installed to have an adequate bearing capacity. This design solution has not yet reached an established level of technological maturity, however, the installations number is steady increasing (see for instance [58], [61], [62]).

Piles can be precast or cast-in-place element. In the case of a hollow precast pile, the pipes are placed within the hollow part in contact with the inner wall of the concrete. In the case of cast-in-place piles, the pipes are fixed to the inner side of the metallic reinforcement of the concrete. Pipes may be embedded in configurations of U-tubes or spiral coil (see Fig. 2.25). Spiral coil configuration has the advantage of a greater heat transfer area per unit depth, however, due to the limited dimension of typical foundations (10-30 m) excessive

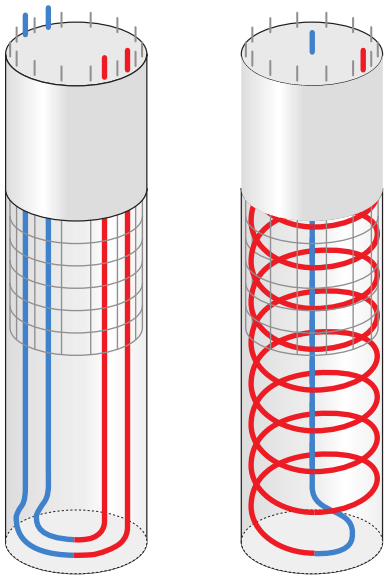

Figure 2.25. Examples of possible configurations of an energy pile (i.e. double-U and spiral).

linear heat fluxes should be avoided to limit the temperature alteration of the ground and pile body.

To now, no specific design methodologies have been issued: therefore, the required energy piles number is estimated through the very same methodology of vertical GHEs [57]. The latter represents a critical assumption as both geometry and heat transfer mechanism are notably different in the two configurations. EPs are high-massive and chunky bodies, with a lower aspect-ratio than standard BHEs. Consequently, both axial heat fluxes and heat capacity inertia affect final heat transfer performances [58]. Furthermore, they are installed in proximity of the building structure and ground surface: the related thermal interactions should be taken into account.

The analysis of EPs thermal performances is an ongoing research topic. In particular, several numerical and analytical studies have dealt with thermal modeling in order to improve current design methodology [63]–[69]. Other authors have investigated the interaction between heat transfer process, bearing capacity of the building structure, and surrounding soil [70]–[73]. Further research topics concern the analysis of the thermal interactions between thermal piles and slab-on-grade building foundations [74].

2.3.3 Groundwater heat pump systems - GWHPs

Open-loop systems use local groundwater as heat source (or sink). In these systems, the fluid enters the evaporator/condenser exchanging heat with the heat pump unit (Fig. 2.26). A secondary loop could be required depending on water quality to avoid fouling, scaling, and clocking of the evaporator/condenser. Aquifers temperature is typically advantageous for heat pump applications as it is very close to the undisturbed ground temperature.

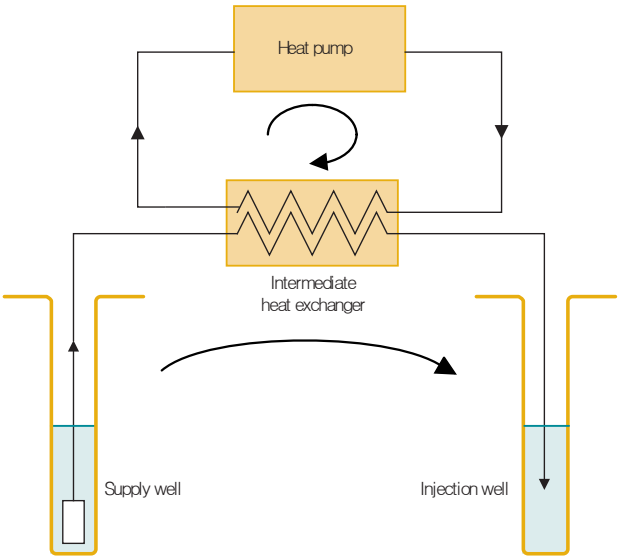

Figure 2.26. Open loop (groundwater) configuration with intermediate heat exchanger (after [51]).

The feasibility and the sustainability of GWHP projects depend on the availability of an adequate flow rate from wells and aquifer volume. The required flow at the GHP is typically 100 - 200 $\mathrm{L\,h^{-1}\,kW^{-1}}$ [52], corresponding to a temperature drop of $5-10$ K between the inlet and outlet sections of the evaporator/condenser.

Depending on local hydrological context, rejection systems can be necessary, otherwise, water can be discharged to surface bodies (local regulation shall be taken into account). Rejection aims to maintain groundwater availability, but runs the risk of hydraulic and "*thermal feedback*" among wells. Moreover, the migration of a thermal plume of warm or cold groundwater down the hydraulic gradient should be avoided to limit the impact on other users (Fig. 2.27) [31], [75]–[78].

A proper GWHP design is based on the tradeoff among well pumping power and heat pump performances. The higher the groundwater flow , the higher GSHP capacity and efficiency is, because of a more favorable average temperature within HP evaporator/con-

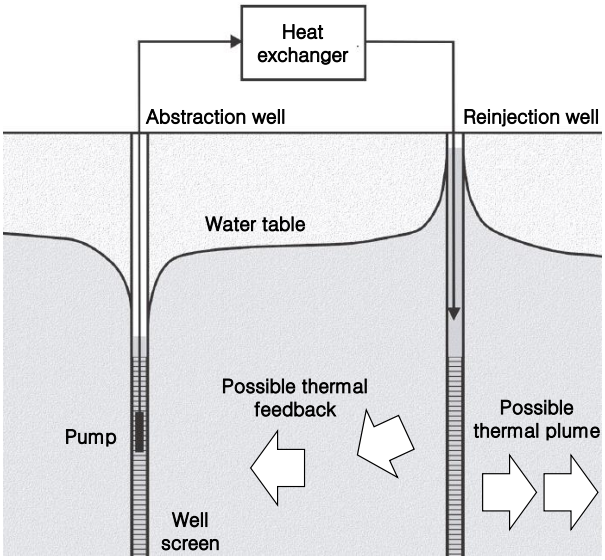

Figure 2.27. Scheme of the "*thermal feedback*" between injection and abstraction wells.

denser ($\overline{T}_{eva/cond}$). However, at some point, higher groundwater flows result in excessive pumping powers with respect to the corresponding increase of ground-coupled heat pump performances [6]. The key-step in any open-loop system design is the identification of the maximum COP over a suitable range of groundwater flows.

This optimization process involves the evaluation of heat pumps and well(s) performances. In particular, we need the so-called "*well productivity curve*" (i.e. the hydraulic head at various groundwater flows) and the GHP performances versus entering water temperature and flow rate. The former is generally derived from well pump test (see section 2.2), the latter is obtained by manufacturers data-sheets.

The main advantages of GWHPs with respect to GCHPs are [1], [52]:

1. reduced installation costs because of simple design and lower drilling requirements;
2. higher capacity availability because of the direct employment of the heat source (i.e. the water) and its heat transfer aptitude;
3. possible direct-use of the groundwater for cooling;
4. possible coupling with water uses: e.g. potable water supply, irrigation...

Disadvantages are:

1. high level of bureaucracy and environmental regulations on extraction and disposal

phases;
2. depending on water quality, pumps and heat exchangers are subject to corrosion, fouling, scaling, and clocking;
3. an accurate design of pumping devices is required to avoid overall GWHPs efficiency reduction.

2.4 *Traditional design methodologies*

Nowadays, only GCHP systems have specific design procedures to calculate the required borehole dimension to match a given thermal load. Other GSHP configurations, as above mentioned, are sized according to several suggested values of GHE length per unit of kW output (see, for instance, [6], [54], [56], [79]–[81]. These values can be considered as "rules of thumb" for preliminary considerations, but do not seem adequate for an accurate design. In the next section we will analyze current design methods, highlighting their assumptions and criteria, in order to show issues and room for improvement.

2.4.1 ASHRAE method

ASHRAE method is the worldwide reference methodology for BHEs sizing [6], [82]. The procedure is based on the work by Kavanaugh and Rafferty [42] that has rearranged the steady-state method of Ingersoll *et al.* [83].

As above mentioned, the heat exchange between the soil and the GSHP system alters the temperature of the ground source reducing the available thermal capacity of the system. The time-dependent heat transfer occurring at the ground heat exchanger surface is modeled by using a series of three constant heat-rate "pulses" corresponding to daily, monthly, and annual time scale, respectively. The effective ground thermal resistance is calculated as a function of time in order to take into account the temperature drift of the soil. A term is also included to consider the thermal resistance among circulating fluid and BHE surface (i.e. the so-called "*borehole thermal resistance*", R_b). Finally, the so-called *temperature penalty* quantifies the thermal interference among adjacent boreholes.

ASHRAE method uses two similar equations (Eqs. (2.7) and (2.8)) to evaluate the necessary BHE depth in heating and cooling mode [6]. The final borehole size corresponds to the larger one.

$$H_{BHE,H} = \frac{\dot{Q}_a R_{g,a} + \left(\dot{Q}_{lh} - \dot{W}_h\right)\left(R_b + PLF_m R_{g,m} + R_{g,d} F_{sc}\right)}{T_g^0 - \frac{T_{w,in}+T_{w,out}}{2} - T_p} \tag{2.7}$$

$$H_{BHE,C} = \frac{\dot{Q}_a R_{g,a} + \left(\dot{Q}_{lc} - \dot{W}_c\right)\left(R_b + PLF_m R_{g,m} + R_{g,d} F_{sc}\right)}{T_g^0 - \frac{T_{w,in}+T_{w,out}}{2} - T_p} \tag{2.8}$$

where (in alphabetic order):

- F_{sc} is the short-circuit heat loss factor;
- $H_{BHE,C}$ is the required bore depth for cooling, m;
- $H_{BHE,H}$ is the required bore depth for heating, m;
- PLF_m is the part-load factor during the reference design month;
- $\dot{Q}_a$ is the net annual average power to the ground, kW;
- $\dot{Q}_{lc}$ is the building design cooling load, kW;
- $\dot{Q}_{lh}$ is the building design heating load, kW;
- $R_{g,a}$ is the effective thermal resistance of ground (annual pulse), $\mathrm{m\,K\,W^{-1}}$;
- $R_{g,d}$ is the effective thermal resistance of ground (peak daily pulse), $\mathrm{m\,K\,W^{-1}}$;
- $R_{g,m}$ is the effective thermal resistance of ground (monthly pulse), $\mathrm{m\,K\,W^{-1}}$;
- R_b is the thermal resistance of the borehole, $\mathrm{m\,K\,W^{-1}}$;
- T_g^0 is the undisturbed ground temperature, °C;
- T_p is the temperature penalty for interference among adjacent bores, K or °C;
- $T_{w,in}$ is the liquid temperature at the BHE inlet section, K or °C;
- $T_{w,out}$ is the liquid temperature at the BHE outlet section, K or °C;
- $\dot{W}_h$ is the system power input at design heating load, W;
- $\dot{W}_c$ is the system power input at design cooling load, W.

Depending on thermal load profile, a notable deviation can occur between $H_{BHE,C}$ and $H_{BHE,H}$. As above-mentioned, according to the specific technical and economical constraints, the shallow depth can be drilled and a back-up system have to be used to compensate the undersized mode (see section 2.2)

Effective ground thermal resistances - $R_{g,a}$,$R_{g,m}$,$R_{g,d}$

The effective ground thermal resistances $R_{g,d,m,a}$ depend on ground properties, boreholes dimension, and reference "heat pulse" duration. The ground is conservatively assumed as a pure-conductive medium, neglecting groundwater effects. Under this assumption, the heat transfer process is related only to Fourier number (i.e. $Fo_{BHE} = \alpha_g \tau / r_{BHE}^2$). ASHRAE method is based on three effective thermal resistances that correspond to three heat pulses: a 10 years pulse of $\dot{Q}_a$, a 1 month pulse of $\dot{Q}_m$ and a 6 h pulse of $\dot{Q}_d$. Therefore, an equal number of $Fo_{r_{BHE}}$ values are calculated, one for each reference period of time.

$$\tau_1 = 3650 \quad \text{days} \qquad \tau_2 = 3650 + 30 \quad \text{days} \qquad \tau_f = 3650 + 30 + 0.25 \quad \text{days}$$

$$Fo_{g,1} = \frac{\alpha_g \left(\tau_f - \tau_1\right)}{r_{BHE}^2} \qquad Fo_{g,2} = \frac{\alpha_g \left(\tau_f - \tau_2\right)}{r_{BHE}^2} \qquad Fo_{g,f} = \frac{\alpha_g \tau_f}{r_{BHE}^2}$$

$R_{g,a}$, $R_{g,m}$, $R_{g,d}$ read:

$$R_{g,a} = \left(G_f - G_1\right) / \lambda_g \tag{2.9a}$$

$$R_{g,m} = \left(G_1 - G_2\right) / \lambda_g \tag{2.9b}$$

$$R_{g,d} = G_2 / \lambda_g \tag{2.9c}$$

G-values is obtained through the *infinite cylindrical heat source* model (ICS) by Carslaw and Jaeger (ICS) [83], [84] (Fig. 2.28). For better details on infinite cylindrical heat source model, the reader can refer to section 3.1.1.

Borehole thermal resistance - R_b

The borehole thermal resistance, R_b, is a stationary parameter that relates the mean fluid temperature in the BHE to the average temperature of the borehole-ground interface. The borehole thermal resistance (R_b) is a function of BHE radius and depth, thermo-physical properties of grout material, characteristics and disposition of embedded ducts. We will discuss these topics, the physical modeling and several evaluation formulas of BHEs in section 3.2.

Degradation coefficient - F_{sc}

The degradation coefficient F_{sc} takes into account the short-circuit heat losses among the upward- and downward-flowing ducts of the BHE. ASHRAE method relates F_{sc} values to the flow rate circulating within the BHEs and overall system capacity (see Fig. 2.7). If one or more boreholes are arranged in series, short-circuit losses decrease as a consequence of the greater distance between supply and return sections.

Table 2.7. F_{sc} values (after [6]).

BHEs number in series	F_{sc}	
	36 mL s^{-1} kW^{-1}	54 mL s^{-1} kW^{-1}
1	1.06	1.04
2	1.03	1.02
3	1.02	1.01

Fluid temperatures - $T_{w,in}$ and $T_{w,out}$

Selecting the operative temperature of the ground-coupled loop is one of the more critical steps of the design process. Values close to ground temperature result in higher system efficiency, but require deeper BHEs, thus unreasonable costs. Values far from T_g^0 reduce

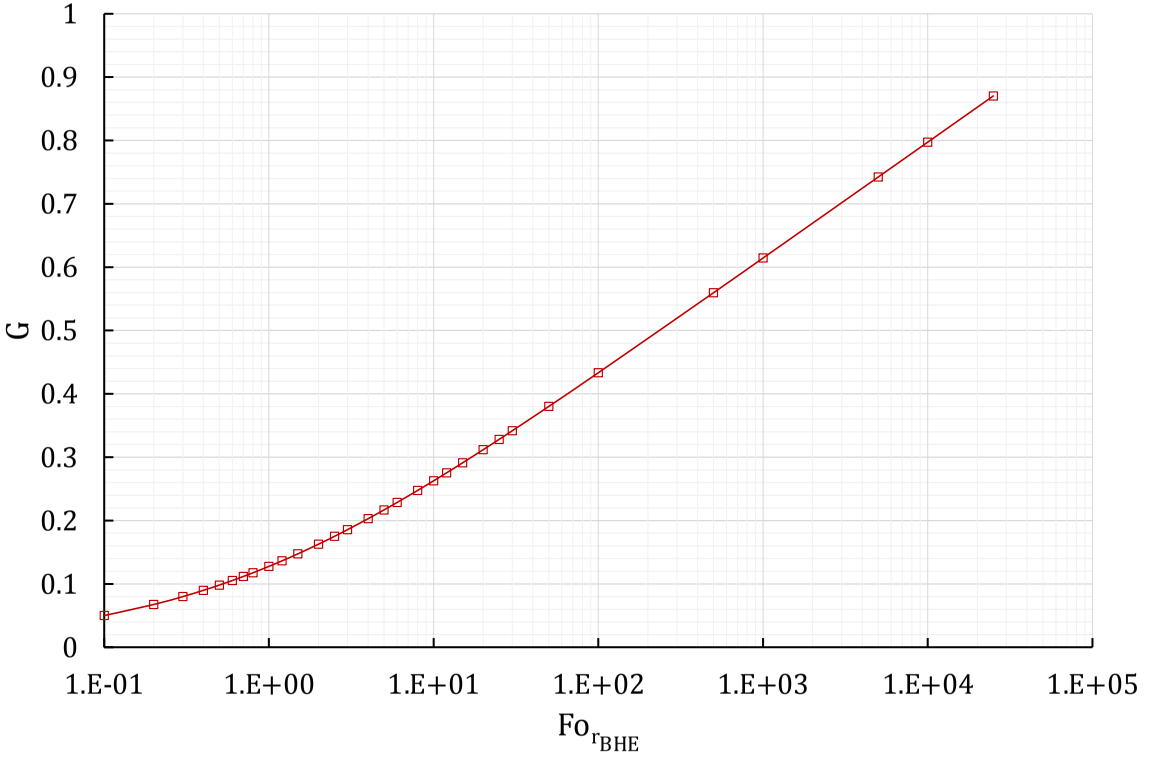

Figure 2.28. *G* factor as a function of Fourier number (ICS model).

boreholes size, but HP capacity and efficiency get worse. ASHRAE suggests considering a return temperature $T_{w,out}$ $6 - 11$ K lower than undisturbed ground temperature in heating mode, and $11 - 17$ K higher in cooling mode.

Temperature penalty factor -T_p

The temperature penalty T_p takes into account the thermal interferences among adjacent boreholes. Designers should aim to select a reasonable separation distance to minimize required land area without increasing T_p. ASHRAE handbook [6] presents some T_p values for a $10x10$ BHEs grid, however these values are just an exemplification without actual design intentions [6]. Several studies have dealt with temperature penalty evaluation (see for instance [85]–[87]). However, as stated also by [88], the thermal interaction among BHEs can be evaluated through traditional ground models, together with space and time superposition techniques. We will discuss this topic in section 3.1.3.

ASHRAE design procedure for vertical GCHP systems can be outlined through the following steps ([6], [89]).

1. Calculate reference cooling and heating loads, and estimate off-peak loads;
2. Evaluate annual heat extraction from and rejection to the ground through an estimation of seasonal COP, seasonal EER, and equivalent full load hour in cooling and heating mode;
3. Select operative temperatures of the circulating fluid within the BHEs;
4. Select ground-coupled heat pump(s) to match cooling and heating loads;
5. Design pipework apparatus aiming at minimizing duct costs and hydraulic losses;
6. Conduct site survey to determine ground thermal properties and drilling conditions;
7. Determine and evaluate possible BHE field arrangements that are likely to be optimum for the specific building and site (bore depth, separation distance, completion methods, annulus grout/fill, and header arrangements);
8. Determine ground heat exchanger dimensions with Eqs. (2.7) and (2.8);
9. Iterate to evaluate alternative operative temperatures, flow rates, BHEs arrangement, etc;
10. Design end user-loop;
11. Select auxiliaries (e.g. pumps). If pumping energy exceeds 8 % of the total system demand, different loop layouts should be investigated.

The reader has probably noted the qualitative form of the suggested steps. The only quantitative formula of ASHRAE method are Eqs. (2.7) and (2.8). This is the main issue of ASHRAE method: many operative parameters (e.g. ground-coupled loop temperatures and flow rate, piping arrangements, BHEs position...) shall be selected *a priori*. Moreover, there is no explicit indications on the optimization phase mentioned in step #9. In short, an high level of experience seems necessary for a proper employment of the method. However, there is no guarantee that the final design is the most cost-effective [82].

2.4.2 The Italian technical standard UNI 11466 : 2012

The *"Ente Nazionale Italiano di Unificazione"'* - UNI has recently implemented the ASHRAE method. Consequently, in Italy, BHEs design procedure is currently regulated by the UNI 11466:2012. The proposed approach is very similar to the original one, but some minor specifications have been included. In this section we describe these further contents that we consider particularly useful for a proper employment of the ASHRAE method.

The two base equations, Eqs. (2.7) and (2.8), remain the same, but additional indications on the evaluation of operative temperature and iterative optimization (steps # 3 and # 9) are provided.

In particular, the UNI 11466:2012 includes the simulation of the heat pump performance within the BHEs design procedure, proposing an iterative algorithm that couples the HP unit efficiency to the total depth of borehole heat exchangers (see Fig. 2.29). The initial COP/EER, $T_{w,in}$, and $T_{w,out}$ values correspond to the rating conditions of the selected HP unit [12]. Then, a first sizing of ground heat exchanger depth is performed through Eqs. (2.7) and (2.8).

Depending on the largest value between $H_{BHE,H}$ and $H_{BHE,C}$, the circulating fluid is going to be closer to the ground temperature T_g^0 during the cooling or heating season. Consequently, HP efficiency have to be recalculated. The UNI 11466:2012 proposes to evaluate the new operative fluid temperatures through Eqs. (2.10) and (2.11).

$$\frac{T_{w,in}+T_{w,out}}{2} = T_g^0 - -T_p - \frac{\dot{Q}_a R_{ga} + \left(\dot{Q}_{l,h} - \dot{W}_h\right)\left(R_b + PLF_m R_{gm} + R_{gd} F_{sc}\right)}{\max\left(H_{BHE,H}; H_{BHE,C}\right)} \tag{2.10}$$

$$\frac{T_{w,in}+T_{w,out}}{2} = T_g^0 - -T_p - \frac{\dot{Q}_a R_{ga} + \left(\dot{Q}_{l,c} - \dot{W}_c\right)\left(R_b + PLF_m R_{gm} + R_{gd} F_{sc}\right)}{\max\left(H_{BHE,H}; H_{BHE,C}\right)} \tag{2.11}$$

Eqs. (2.10) and (2.11) are modified expressions of Eqs. (2.7) and (2.8), but a different BHE depth is considered. Thus, the new COP/EER of the GHP unit is evaluated according to the new mean temperature of the fluid by means of the manufacturers data-sheets or specific technical standards (i.e. [90]). The calculation of $H_{BHE,C}$ and $H_{BHE,H}$ is now iterated till convergence. For better details on Italian standard methodology, the reader can refer to [57].

UNI 11466:2012 algorithm (Fig. 2.29) is based on the same criteria of the original ASHRAE method. However, designers might take benefits by using a a more straightforward procedure.

The main drawback of Italian procedure (similarity to the original ASHRAE one) is the absence of specification about the optimal share of the building thermal load that will

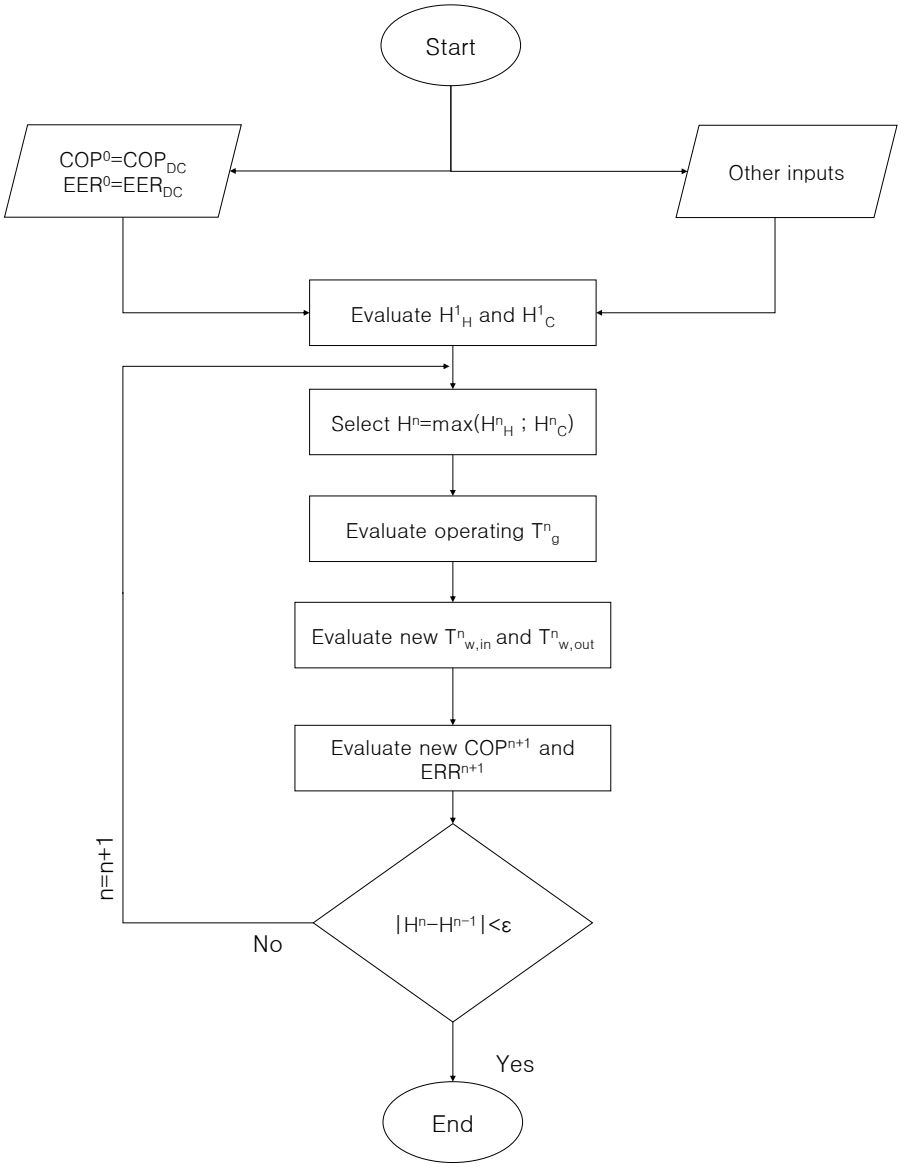

Figure 2.29. Flow chart of the UNI 11466:2012 method.

be delivered thanks to the ground source. Moreover, the actual evolution of the ground temperature is not evaluated, as well as its impact on system performances and final design [4]. We think that considering a complete operative life simulation might improve the whole design process, leading to more cost-effective solutions. These topics will be discussed in the following section 2.4.3.

2.4.3 Remarks on traditional design methods

Traditional design methodologies of HVAC systems (i.e. boiler and air condition systems) are based on two sequential steps, namely: the evaluation of end-user thermal needs and heat generators sizing. As usual in engineering practice, the "precautionary principle" is often adopted: in other words, the generation unit(s) is selected on the basis of the building peak load. In this perspective, back-up systems are designed to operate only in particular conditions or to match unforeseen needs.

This approach has been partially modified for ASHP systems since heat pump units do not have a unique value of nominal capacity. As above-mentioned, the maximum thermal output depends on actual operative conditions. In section 2.3.1 we illustrated as the ASHPs design is based on the so-called "*balance-point*"; however, for cooling or dual-mode systems, the summer peak load remains the reference value for selecting the HP unit. As a matter of fact, the ASHP design strategy cannot be applied to GSHP as the source temperature is not a given input, but it results from project design and actual operation (see section 3.1.3).

Though current GSHP design methods differ from peak-based approaches, ASHRAE method requires a "design heating load"(kW) without specifying if it coincides with the maximum thermal need of the building [91]; however, the latter is a very common interpretation. Also the other "rules of thumb" (e.g. meters of borehole per kW of heating/cooling output) can be applied with every reference thermal power: therefore, the decision on the share of the building load (heating and/or cooling) that will rely on the ground source remains up to designers.

This is the main issue of traditional design methodologies. Despite their valuable and practical usefulness, as stressed in [82], most of these standards are based on several design parameters decided *a priori* (e.g. operative temperatures and flow rates, generators capacity, heating/cooling load at the ground source, reference design period...). Only designers with a great experience and competence are able to make this kind of choices properly during the initial phases of the project. Usually, especially for small/medium capacity systems, the above-mentioned "precautionary principle" is adopted, aiming at maximizing the load share delivered by the GSHP. In other words, the only constraint to the BHEs number is the available economical budget. Canadian Standard Association [92] suggests that GSHP should meet the 70% of residential buildings peak heating or cooling demand, whichever is greater. No actual indications are provided for large commercial or office buildings [91]. Moreover, the use of a single reference does not seem ubiquitously

4 The two methods use three effective thermal resistances depending on time and penalty factor T_p to take into account the thermal alteration of the ground source.

applicable. For example, Ni *et al.* [93] tested different heat pump capacity as a portion of peak demand: for the particular building in their study, they found that optimal design (in terms of economic savings) is reached if the GSHP system delivers the 60% of the building peak load, leaving the residual 40% to the gas boiler.

Another issue of traditional methods is the hierarchical and sequential logic that characterizes the sizing of subsystem components. The following list summarizes the main steps of classical procedures:

1. The building needs are evaluated and analyzed, both in terms of energy and power;
2. The ground source is characterized through reference data or site-investigation techniques (TRT or pumping test, see Appendix 2);
3. A share of the building load is attributed to the GSHP system (generally the peak load is chosen as reference);
4. The nominal capacity of the ground-coupled heat pump unit is chosen equal to the previous-step reference power;
5. Several operative parameters are decided *a priori* (e.g. operative temperature, flow rates, control strategy, components layout. . .);
6. Ground-coupled loop and ground heat exchangers (or wells) are designed according to previous steps results;
7. An iterative calculation of steps #5 and #6 is performed in order to refine the overall design results.

This sequential logic characterizes also current engineering handbooks and technical guidelines. Some standards are focused on building needs (e.g. [57], [94]–[98]), others deal with generators nominal capacity (e.g. [53], [95], [96]), others evaluated the necessary depth of GHEs (e.g. [6], [54], [57]). At the moment, an holistic established procedure does not exist.

Currently, the experimentally monitored seasonal performance factors (SPF) of GSHPs vary significantly (see Table 2.8) [24], [81], [99]–[110]. This wide range of variation can be ascribed to the different assumptions made by designers in applying available methods [6], [54], [57], [79], [82], [91], [92]. Therefore, despite their theoretical potential in energy and economic savings, high installation costs and operative performances uncertainty limit the GSHP attractiveness with respect to alternative technologies.

In our opinion, a novel design approach is one of the possible drivers to overcome current GSHPs drawbacks and stimulate the diffusion of this technology. In particular, four steps seem priority:

1. Overcome the idea that maximizing the ground exploitation leads to the most efficient design solution. Indeed, together with sustainability issues, this approach leads to large size components (i.e. high costs) without ensuring appropriate energy/economic savings. In other words, each GSHP design should investigate the optimal share of the building load delivered by the ground-coupled system on the basis of a proper cost-benefit analysis.

Table 2.8. Example of monitored performances of real GSHP systems.

Author(s)	Type of system	Results	Supply water at the user system
[99] Bakirci, K	Vertical - GCHP (Residential building)	SCOP = 2.7	50 °C
[100] Capozza, A	Vertical - GCHP (Residential building)	SCOP = 2.77	≈ 30 °C
[100] Capozza, A	Vertical - GCHP (Office building)	SCOP ≈ 3.5 / SEER ≈ 3.7	
[110] Franco *et al.*	Vertical - GCHP	SCOP ≈ 2.4	35 °C
[81] Grattieri, W	Vertical - GCHP	SCOP =2.5	38 °C
[81] Grattieri, W	Vertical - GCHP	SCOP =3.1	54 °C
[81] Grattieri, W	GWHP	SCOP =2.1	45 °C
[81] Grattieri, W	GWHP	SCOP =2.5	45 °C
[81] Grattieri, W	GWHP	SCOP =3.5	35 °C
[81] Grattieri, W	SWHP	SCOP =2.3	35 °C
[101] Hepbasli *et al.*	Vertical - GCHP	SCOP =1.4	41 °C
[102] Hwang *et al.*	Vertical - GCHP (University)	SEER ≈ 5.9	7 °C
[103] Karabacak *et al.*	Vertical - GCHP (University)	SEER ≈ 2.6	9 °C
[104] Michopoulos *et al.*	Vertical - GCHP (Municipality Hall)	SCOP≈ 5.5 / SEER ≈ 5	45 °C / 7 °C
[105] Montagud *et al.*	Vertical - GCHP	SCOP≈ 3.7 / SEER ≈ 4.5	45 °C / 7 °C
[106] Ozyurt & Ekinci	Vertical - GCHP (University)	SCOP≈ 2.7	47 °C
[107] Pulat *et al.*	Horizontal - GCHP	SCOP≈ 3.3	
[108] Ruiz-Calvo & Montagud	Vertical - GCHP	SCOP≈ 3.5 / SEER ≈ 3.5	45 °C / 10 °C

2. Change the "reference point" approach of classical design methods with a "simulation-based" approach. Indeed, there are no reference/nominal conditions for GSHPs as the energy exchanges between the ground and the heat pump alter the initial state of the source creating a reciprocal interference between heat source exploitation and system performances.
3. Establish an evaluation methodology for GSHP operative performances (back-ups included) to simulate the effects of different design alternatives. An accurate prediction of system behavior seems to be the necessary tool also for reliable energetic and economic analyses.
4. Overcome the current sequential and hierarchical logic of the design process with an interconnected approach aimed at optimizing both subsystems concurrently.

All the above-listed subjects will be discussed in the next sections of this Thesis.

3 GSHP systems modeling and performance evaluation

In the previous section 2.4.3, we introduced the achievable benefits of an alternative design approach based on the operative simulation of GSHPs. Here, we review some of the numerous GSHP models that are currently available in literature. In particular, we focus on those formulas that we consider particularly appropriate to be implemented within an optimization algorithm.

The following subsystems are discussed: ground source, ground heat exchangers, heat pump unit, and back-up generators. For each of them, a specific model will be proposed. These expressions will be coupled to a full set of equations to simulate the operative performances of the GSHP system. In this context, the assumptions and the validity range (in terms of length and time scales) of each model are analyzed in order to ensure sound results.

3.1 *Ground source*

In this section, we discuss the main mathematical models to simulate the ground thermal behavior when it is used as thermal source (or sink). More specifically, these models allow to evaluate the temperature field evolution around ground heat exchangers (GHEs). It this section, we do not deal with the heat transfer process within the exchangers (i.e. BHEs), but we refer to their geometry to define the boundary conditions of the problem.

Heat transfer process within the ground medium is influenced by several factors: e.g. the geometrical configuration of the GHE field, thermo-physical properties of the layers, soil moisture content, possible groundwater movement, possible freezing and thawing of the soil [111]. Some of these parameters are difficult to evaluate with a high level of confidence, therefore, for engineering practice, they are often estimated on the basis of simplifying assumptions.

Classical models refer to vertical borehole heat exchangers as linear, or cylindrical, heat sources with a constant heat transfer rate per unit depth; then, the transient energy equation

is solved within the ground domain according to the involved physical phenomena. With regard to the latter point, we can define two main categories: the *purely conductive medium* and the *saturated porous medium*. The former is used when the influence of groundwater movement on the heat transfer process is negligible.

Another classification criterion regards the technique employed to solve the energy equation. *Analytical models* have long been used: the first contribution comes from Lord Kelvin who developed the *line source* theory in 1882 [112]. The works of Carslaw and Jeager [84] and Ingersoll *et al.* [83], [113] applied Kelvin's solution to ground heat exchangers: their models are sill used in current design methodologies [42], [49] (see section 2.4.1). Indeed, despite the development of more accurate simulation methods (i.e. numerical simulations), the analytical approach is able to provide piratical and useful indications with an appropriate tradeoff between implementation efforts and solution accuracy [111], [114]. Indeed, analytical formulations are preferred in many practical applications because of their short computational time and flexibility in parametric designs. Consequently, they are particularly appropriate to be implemented both in technical standards and simulation algorithms [88], [111], [115]–[118]. On the other hand, their employment is limited to classical configurations, homogeneous media, appropriate length and time scales. Therefore, the applicability of any analytical formulation is subject to the verification of consistency between the model assumptions and the specific case study.

Different *numerical models* have been developed in the last decades for the analysis and the prediction of GHEs performances (see, among others, [119]–[125]). However, accordingly to the aims of this Thesis, we consider "models" only those empirical or semi-empirical correlations obtained through a regression analysis of the results of several numerical simulations. We do not refer to numerical simulations of a single particular configuration or test case as this kind of work is strongly connected to the specific case considered, without providing general indications applicable to other systems.

The so-called "*g-functions*" given by Eskilson [120] are the most famous numerical-based correlations. The g-functions give the relation between the heat extracted from the ground and the mean temperature at the borehole surface as a function of time and BHE field geometry. Eskilson obtained *g-functions* value by means of several finite-difference simulations. Other numerical models have been developed to analyze the heat transfer process within, or adjacent to, GHEs surface (see, among others, [118], [122], [123], [126]–[130]); in other words, these studies aim to investigate the effects of the thermal capacity of the heat exchangers and spatial inhomogeneity of the heat flux. The same subjects have been addressed analytically by other authors with particular reference to high-thermal capacity exchangers (i.e. energy piles) [64], [117]. "*Hybrid models*" have been developed, too: the latter combine a numerical modeling for the GHEs and an analytical approach fron the surrounding ground [131].

It is worth recalling that both numerical and analytical models are typically based on the same constitutive equations (i.e. Fourier and Darcy Law), therefore there are no deviation on simulated phenomena. The advantage of numerical approach, at least in theory, is the great variety of geometry, boundary conditions, length and time-scales that could be analyzed. However, results accuracy is nonetheless connected to the level of reliability of

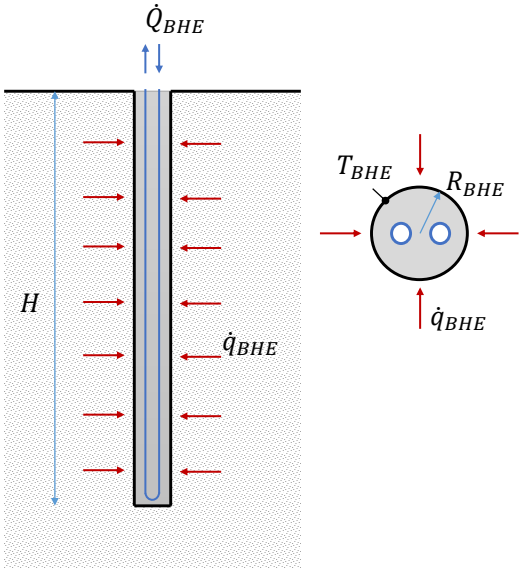

Figure 3.1. Schematic diagram of a typical borehole heat exchanger.

input parameters (i.e. boundary conditions, geometry, and thermo-physical properties): an elevate level of accuracy is typically unavailable at the initial stages of a design process, therefore, the use of complex and time-consuming numerical tools could result in the very same outcomes than simplified analytical models. For standard configurations, simplified approaches can be satisfactory. Similar considerations can be extended to the overall GSHP simulation process (see section 4.4.1).

3.1.1 Purely conductive ground media

The figure 3.1 shows a schematic diagram of a typical borehole heat exchanger. The *infinite line source solution* (ILS), the *infinite cylindrical source solution* (ICS), and the *finite line source solution* (FLS) are the classical analytical models to evaluate the ground temperature as a function of the heat flux at the BHE surface. Since the early works of Carslaw and Jeager [84] and Ingersoll *et al.* [83], [113], a large amount of papers have been published on these models (see, for instance, [36], [63], [86], [132], [133]). In recent years, Man *et al.* [63], [65] used the point heat source theory to develop the explicit solution of the *finite cylindrical heat source* (FCS) .

In the next sections, we will illustrate the main features of each model, paying a particular attention to their applicability within a global GSHP simulation model aimed at evaluating the operational performances of the overall system. We will discuss and

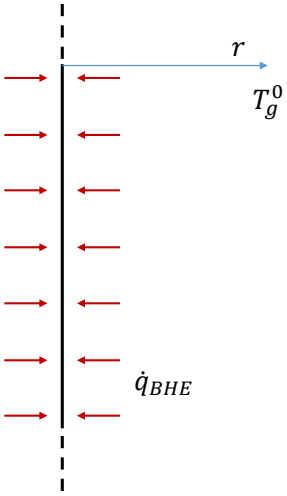

Figure 3.2. Schematic representation of the infinite line source model.

compare the above-mentioned models in terms of computational efforts, length, and time scales. In particular, we will refer only to those models that do not include the GHE domain as the modeling of the latter subsystem will be discussed in section 3.2.

In sections 3.1.1, 3.1.1, 3.1.1 and 3.1.1 we will illustrate an exhaustive analysis of ILS, FLS, ICS and FCS models in case of a purely conductive medium. The effects of groundwater movement will be analyzed in sections 3.1.2 3.1.2.

Infinite line source model - ILS

This model represents the borehole as an infinite line source embedded in a semi-infinite homogeneous medium with constant and isotropic properties (Fig. 3.2) . Thus, we have two main assumptions: first, the heat flux is applied at the center of the borehole; secondly, only radial dimension is considered. If groundwater movement is neglected, the energy equation is governed by heat conduction (i.e. Fourier's law). The latter reads:

$$\begin{cases} \alpha_g \left(\frac{\partial^2 T_g}{\partial r^2} + \frac{1}{r} \frac{\partial T_g}{\partial r} \right) = \frac{\partial T_g}{\partial t} \\ T_g \left(r \to \infty, t \right) = T_g^0 \\ T_g \left(r, t = 0 \right) = T_g^0 \\ \dot{q} \left(r \to 0, t \right) = - \left(2\pi r \right) \lambda_g \frac{\partial T_r}{\partial r} \Big|_{r \to 0} = \dot{q}_{BHE} \end{cases} \tag{3.1}$$

The dimensionless solution to the problem (3.1) is given in Eqs. (3.2) [83], [84].

$$\Theta_g(Fo_r) = \frac{1}{2\pi}\int_{r/2\sqrt{\alpha_g t}}^{\infty}\frac{\exp\left(-\beta^2\right)}{\beta}d\beta = \frac{1}{4\pi}Ei\left(\frac{1}{4Fo_r}\right) \tag{3.2a}$$

$$\Theta_g(z) = \frac{1}{4\pi}\left(-\ln(z) - \gamma + \sum_{k=1}^{\infty}\frac{z^k}{z!z}\right) \tag{3.2b}$$

where:

$$Fo_r = \frac{\alpha_g t}{r^2} \qquad z = \frac{1}{4Fo_r}$$

$$\Theta_g = \frac{\left(T_g^0 - T_g\right)\lambda_g}{\dot{q}_{BHE}} \qquad \gamma \approx 0.577216$$

We note that the dimensionless temperature, Θ_g, depends only on Fourier number. At small z the high-order terms in the series (3.2b) become successively smaller; therefore, we can neglect these terms obtaining the simplified expression (3.3) [35], [65], [120].

$$\Theta_g = \frac{1}{4\pi}\left(z - \ln(z) - \gamma\right) \tag{3.3}$$

Fig. 3.3 shows the deviation between Eq. (3.2b) and Eq. (3.3). As a matter of fact, the approximate expression (3.3) can be used when $Fo_r \geq 1$: for typical ground thermal diffusivities and GHEs radii, this condition corresponds to a time period of about $1-3$ hours.

Infinite cylindrical source model - ICS

This model represents the borehole as an infinite-long circular cylinder in a semi-infinite homogeneous medium with constant and isotropic properties (Fig. 3.4). The heat flux $\dot{q}_{BHE}$ is imposed at the hollow surface $(r = r_{BHE})$; as in the ILS model, only the radial dimension is taken into account. In this case, the energy equation reads:

$$\begin{cases} \alpha_g\left(\frac{\partial^2 T_g}{\partial r^2} + \frac{1}{r}\frac{\partial T_g}{\partial r}\right) = \frac{\partial T_g}{\partial t} \\ T_g\left(r\to\infty, t\right) = T_g^0 \\ T_g\left(r, t=0\right) = T_g^0 \\ \dot{q}\left(r_{BHE}, t\right) = -\lambda_g\frac{\partial T_g}{\partial r}\Big|_{r=r_{BHE}} = \frac{\dot{q}_{BHE}}{2\pi r_{BHE}} \end{cases} \tag{3.4}$$

The solution to the problem (3.4) is given in Eq. (3.5) [83], [84].

$$\Theta_g(Fo_{BHE}, R) = \frac{1}{\pi^2}\int_0^{\infty}\frac{\exp\left(-\beta^2 Fo_{BHE}\right) - 1}{J_1^2(\beta) + Y_1^2(\beta)}\left[J_0(R\beta)Y_1(\beta) + Y_0(R\beta)\right]\frac{d\beta}{\beta^2} \tag{3.5}$$

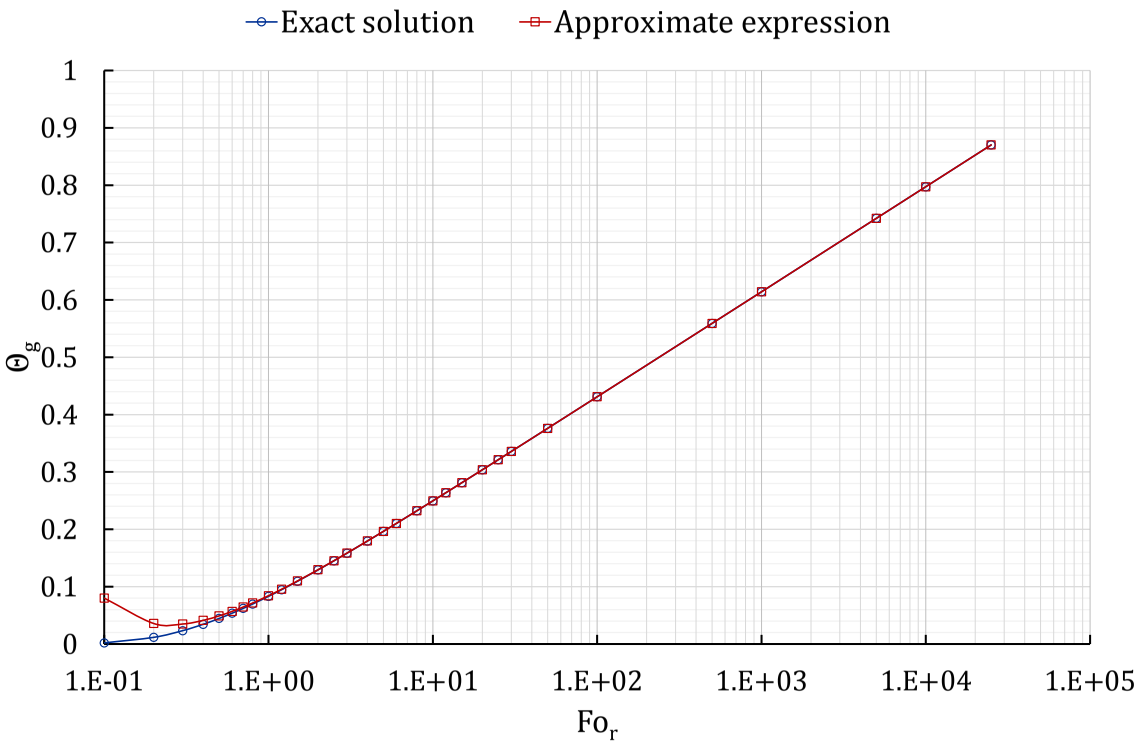

Figure 3.3. ILS solution: the dimensionless temperature, Θ_g, as a function of the Fourier number, Fo_r

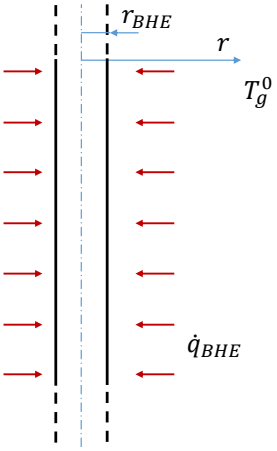

Figure 3.4. Schematic representation of the infinite cylindrical source model.

where J_0, J_1 are Bessel functions of the first kind of order 0 and 1, respectively, Y_0, Y_1 are Bessel functions of the second kind of order 0 and 1, respectively, $Fo_{BHE} = \alpha_g t / r_{BHE}^2$ is the Fourier number at the borehole radius, and R is a dimensionless radial distance ($R = r/r_{BHE}$). Eq. (3.5) can be evaluated numerically, though some computational difficulties [134]. The values of $\Theta_g(Fo_{BHE}, R)$ have been computed by Ingersoll *et al.* first [83]: the reader can refer to Table 3.1.

Philippe *et al.* [134] recall an interesting expression of the ICS solution proposed by Baudoin [135] that avoids the calculation of the integral in Eq. (3.5). The latter was obtained by means of the Laplace transform and direct numerical inversion, it reads:

$$\Theta(Fo_{BHE}, p) = \frac{1}{2\pi} \sum_{j=1}^{10} \left[\frac{V_j}{j} \frac{K_0(\omega_j p)}{\omega_j K_1(\omega_j)} \right] \tag{3.6}$$

with:

$$\omega_j(t) = \sqrt{\frac{j \ln(2)}{Fo_{BHE}}}$$

$$V_j = \sum_{k=Int\left(\frac{j+1}{2}\right)}^{min(j,5)} \frac{(-1)^{j-5} k^5 (2k)!}{(5-k)!(k-1)!k!(j-k)!(2k-j)!}$$

where K_0 and K_1 are modified Bessel functions of the second kind of order 0 and 1, respectively.

Table 3.1. Values of $\Theta_g(Fo_{BHE}, R)$ as used in Eq. (3.5) [83].

Fo_{BHE}	$\Theta_g(Fo_{BHE},1)$	$\Theta_g(Fo_{BHE},2)$	$\Theta_g(Fo_{BHE},5)$	$\Theta_g(Fo_{BHE},10)$
0.10	0.049	-	-	-
0.20	0.067	-	-	-
0.30	0.080	-	-	-
0.40	0.090	-	-	-
0.50	0.099	-	-	-
0.60	0.107	-	-	-
0.70	0.113	-	-	-
0.80	0.118	-	-	-
1.00	0.128	0.035	0.001	0
1.20	0.137	-	-	-
1.50	0.148	-	-	-
2.0	0.163	-	-	-
2.5	0.175	-	-	-
3.0	0.186	-	-	-
4.0	0.203	-	-	-
5	0.217	0.112	0.0153	0.0001
6	0.228	-	-	-
8	0.247	-	-	-
10	0.263	0.155	0.0388	0.0024
12	0.275	0.167	0.0470	0.0042
15	0.291	0.182	0.0580	0.0072
20	0.312	0.203	0.0736	0.0129
25	0.328	0.219	0.0866	0.188
30	0.342	0.232	0.0979	0.0246
50	0.380	0.271	0.132	0.0460
100	0.433	0.323	0.181	0.0842
500	0.560	0.449	0.304	0.197
1000	0.614	0.504	0.359	0.250
5000	0.742	0.632	0.486	0.376
10,000	0.797	0.687	0.541	0.431
25,000	0.870	0.760	0.614	0.504

At short time scales (i.e. low Fourier numbers), ICS model results more accurate than ILS [83], [120], [134]. Ingersoll *et al.* [83] and Eskilson [120] state that ILS model can be used only for $Fo_{BHE} \geq 20$ and $Fo_{BHE} \geq 5$, respectively. The Figs. 3.5 and 3.6 show the relative difference between the ILS and ICS solutions as a function of the Fourier number $Fo_r = Fo_{BHE}/R^2$. Based on these results, Ingersoll criterion corresponds to a relative difference of 2.6% and the Eskilson criterion to a relative difference of 9.4% [134].

For typical ground thermal diffusivities and GHEs radii, Ingersoll and Eskilson criteria correspond to a time period of about $0.5 \div 5$ day and $4 - 24$ h, respectively. Philippe *et. al* [134] considers the deviation between the two models less than 2 % after 1 d approximately.

Finite line source model - FLS

The finite line source FLS solution is considered the most accurate ground model among the traditional ones (i.e. ILS, ICS, FLS), as it is able to consider the axial effects of the heat transfer process that occurs at long time scales [134]. The original formulation by Ingersoll *et al.* [83], [84], [120] has been improved in the last decades by several authors (see, among others, [63], [136], [137]).

FLS model is based on the following assumptions: the borehole is represented by a linear heat source of length H_{BHE} with the top corresponding to the soil surface (see Fig. 3.7); the ground is a semi-infinite homogeneous medium with constant and isotropic properties, and soil surface is taken to be equal to T_g^0. According to Eskilson [120], the actual evolution of the surface temperature can be neglected below a depth of 10 m; therefore, since the typical BHEs depth is about 100 m, the temperature oscillation on the top of the borehole do not produce relevant effects on the global heat transfer process [120], [134]. Other authors refer to the FLS solution proposed by Eckert and Drake [136], [138]: the latter satisfies the problem of a finite line source in a semi-infinite medium with a thermally insulated boundary at the ground surface: in this Thesis, we do not use this formulation.

The basis of the finite line source model (FLS) is the solution to the problem of a point heat source of strength $\dot{q}_0$ (Eq. 3.7)[1] [83], [84], [134].

$$\Theta_g(Fo_r) = \frac{\dot{1}}{4\pi} erfc\left(\frac{1}{2\sqrt{Fo_r}}\right) \tag{3.7}$$

where $\Theta_g = \left(T_g^0 - T_g\right)\lambda_g/\dot{q}_0$ and $Fo_r = \alpha_g t/r^2$.

The solution of the FLS problem can be evaluated by integrating Eq. (3.7) over the length of the borehole (see, for instance, [63], [83], [84], [120], [134]). The mirror image technique is used to account for the ground surface boundary condition: a "'virtual"' heat source of length H_{BHE}, with an opposite strength $-\dot{q}_{BHE}$, is located symmetrically above

1 Also known as "*Green's function*","*fundamental solution*", or "*impulse response function*".

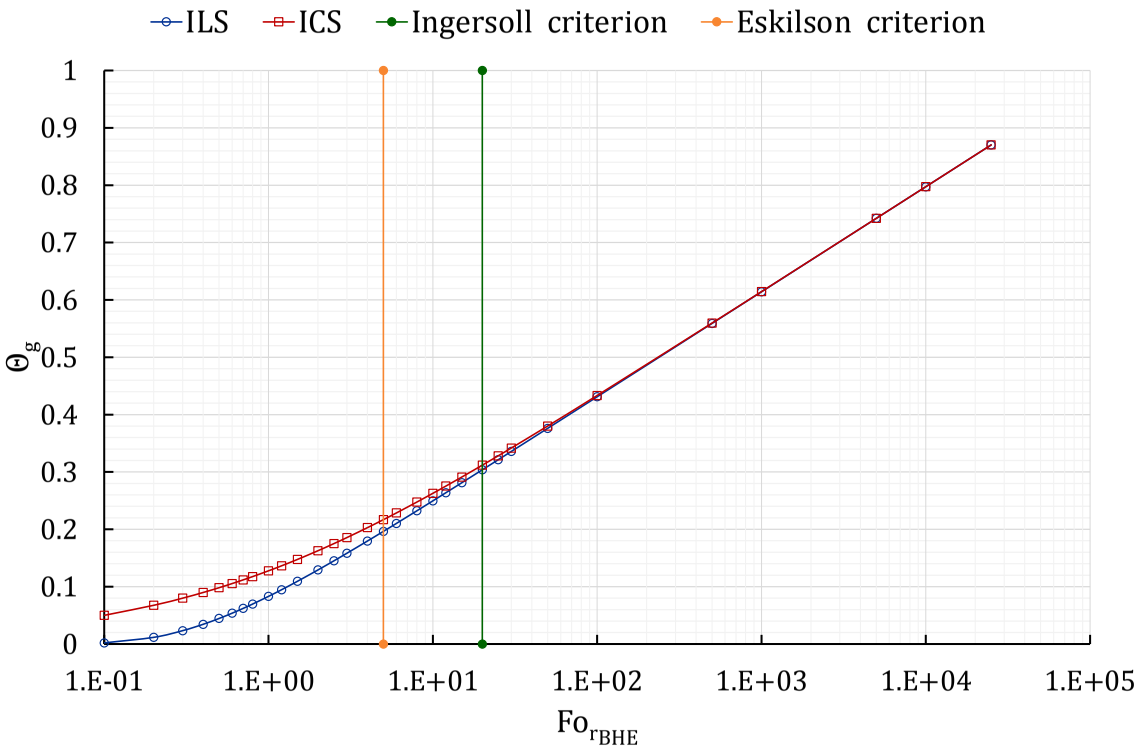

Figure 3.5. Dimensionless temperature, Θ_g, given by ILS and ICS models

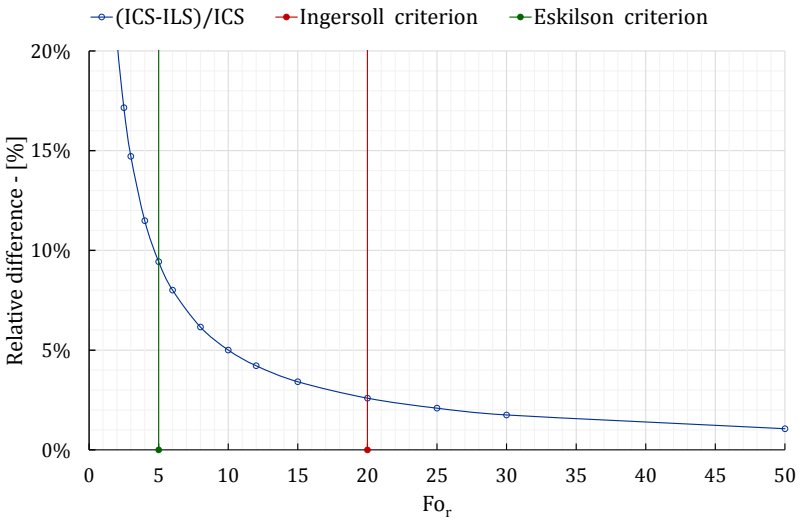

Figure 3.6. Relative difference between ILS and ICS solutions as a function of Fourier number.

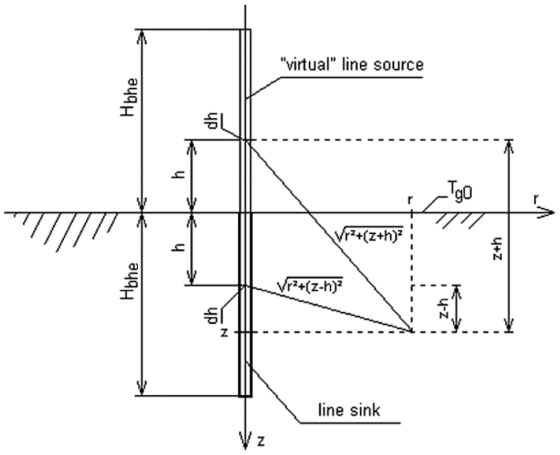

Figure 3.7. Schematic representation of the *mirror technique* for a line heat source of length H. We note the corresponding "virtual" line source [134].

the line sink (Fig. 3.7). In this way, the temperature variation at $z = 0$ remains null due to symmetry reasons. The dimensionless solution of the FLS problem is [63]:

$$\Theta_g(Fo_H, Z, R) = \frac{1}{4\pi}\int_0^1 \left[\frac{1}{d/H_{BHE}} erfc\left(\frac{d/H_{BHE}}{2\sqrt{Fo_H}}\right) - \frac{1}{d'/H_{BHE}} erfc\left(\frac{d'/H}{2\sqrt{Fo_H}}\right)\right] dZ' \tag{3.8}$$

where:

$$Fo_H = \alpha_g t/H_{BHE}^2 \quad Z = z/H_{BHE} \quad R = r/H_{BHE} \quad Z' = z'/H_{BHE}$$

$$d/H_{BHE} = \sqrt{R^2 + (Z - Z')^2} \qquad d'/H_{BHE} \quad = \sqrt{R^2 + (Z + Z')^2}$$

In engineering practice, it is convenient to have one only representative borehole wall temperature. Some authors take this reference value as the one at the middle point of the BHE ($z = H_{BHE}/2$); others prefer the integral average temperature along the borehole depth [114], [116], [136]. According to [114], at long time-scale, the former option overestimates the average temperature of the borehole surface; therefore, in this Thesis, we always refer to the second alternative (Eq. 3.9).

$$\overline{\Theta}_g = \int_0^1 \Theta_g dZ \tag{3.9}$$

Fig. 3.8 shows the average dimensionless temperature, $\overline{\Theta}_g$, as a function of Fourier number, Fo_H, and dimensionless radial distance $R = r/H_{BHE}$. The Figs. 3.9 and 3.10 show the difference between the ILS and FLS solutions; the dashed line named "Eskilson criterion" represents the limit for the applicability of the ILS solution as defined in [120] (i.e. $Fo_H < 1/90$). For typical ground thermal diffusivities and BHEs depths, Eskilson criterion corresponds to a large range of time of about $1 - 7$ years.

In contrast with the ILS model, FLS solution has a steady state value, *"... although it may take a long time to reach this state"* [83]. The asymptotic value of $\Theta_{g,s}$ is given by:

$$\Theta_{g,s}(R, Z) = \frac{1}{4\pi} \ln\left(\frac{\sqrt{R^2 + (Z-1)^2} - (Z-1)}{\sqrt{R^2 + (Z+1)^2} + (Z+1)} \frac{\sqrt{R^2 + Z^2} + Z}{\sqrt{R^2 + Z^2} - Z}\right) \tag{3.10}$$

In practical applications, we can consider our system at the steady state condition after the time taken to reach the 0.98 of the steady state value of $\overline{\Theta}_{g,s}$. The latter value and the corresponding Fourier number, $Fo_{H,s}$, can be evaluated by means of the Eq. (3.11). As above mentioned, we need a very long period of time to reach the steady condition: e.g for a typical BHE of 100 m depth and 0.05 m of radius, the resulting $Fo_{H,s}$ is about 0.3. This value corresponds even to 200 years depending on the soil thermal diffusivity.

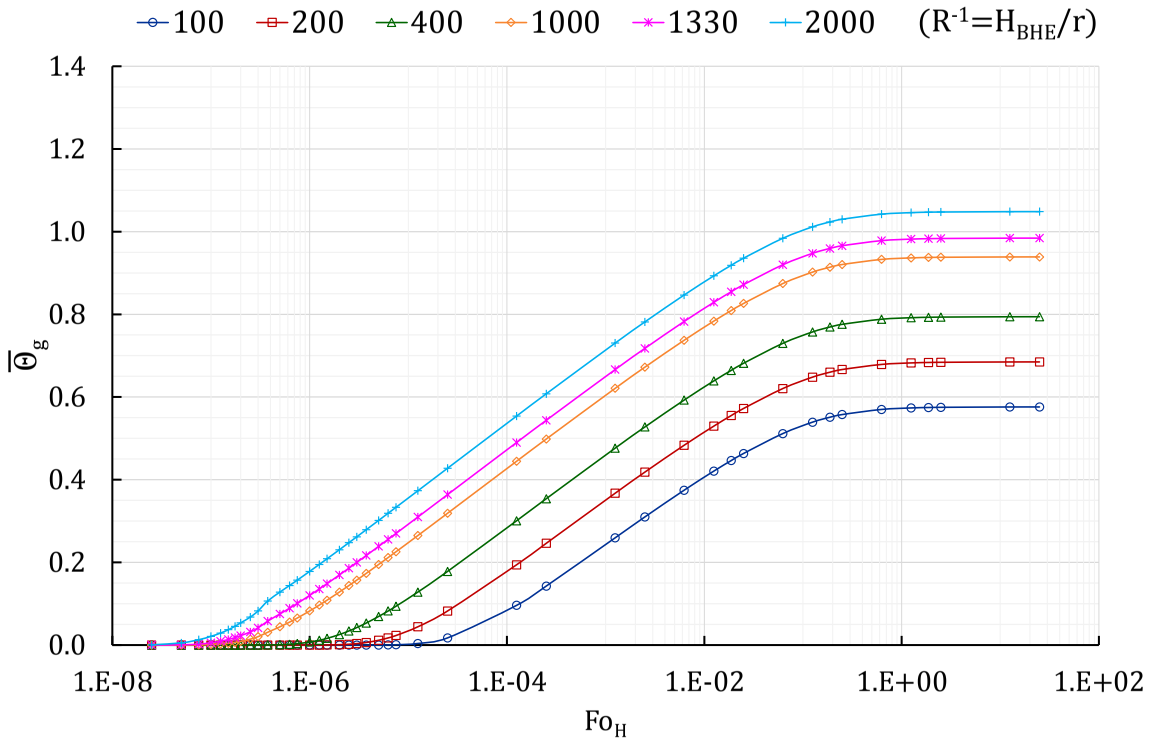

Figure 3.8. FLS solution: the average dimensionless temperature, $\overline{\Theta}_g$, as a function of Fourier number, Fo_H, and dimensionless radius, R.

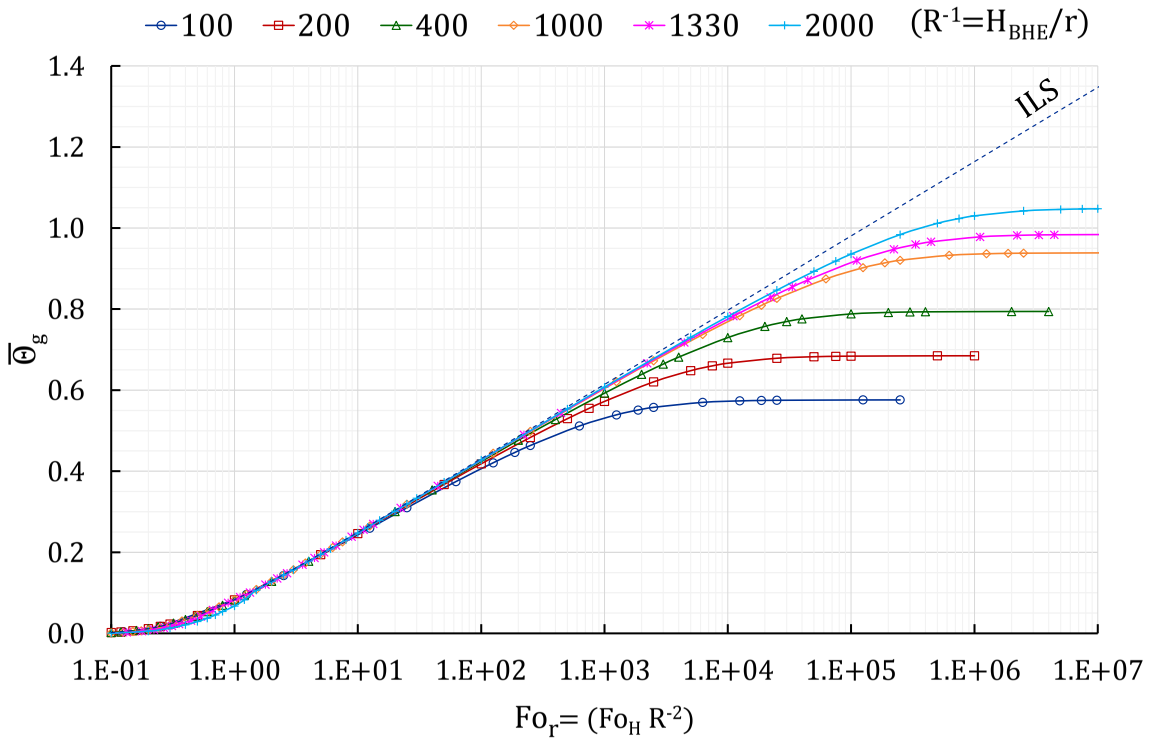

Figure 3.9. Average dimensionless temperature, $\overline{\Theta}_g$, given by ILS and FLS models.

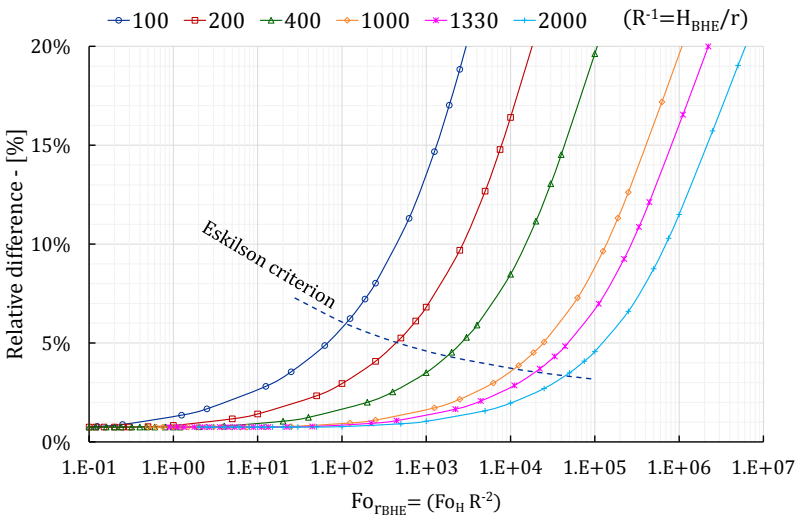

Figure 3.10. Relative difference between FLS and ILS models.

$$Fo_{H,s} = 30.427 R^{-1} + 0.266 \tag{3.11a}$$

$$\overline{\Theta}_{g,s} = -0.365 \log_{10} R + 0.154 \tag{3.11b}$$

An approximated expression of the exact solution (3.8) was derived in order to increase the computational speed of FLS. It reads:

$$\overline{\Theta}_g = \begin{cases} \frac{1}{4\pi} Ei\left(\frac{R}{4Fo_H}\right), & Fo_H < 1/90 \\ \overline{\Theta}_{g,s} - 0.173 \log_{10}\left(1 + \frac{0.086}{Fo_H}\right), & Fo_H \geq 1/90 \end{cases} \tag{3.12}$$

where the first formula is the ILS solution (Eq. 3.3), and $\overline{\Theta}_{g,s}$ is evaluated accordingly to Eq. (3.11b). As shown in Fig. 3.11, there is no significant difference between the approximate expression and the exact one. According to the aims of this Thesis, Eq. (3.12) is preferable as it can be used in long-term simulations with a reduced computational effort and the same results accuracy.

Claesson and Javed [137] extended the traditional FLS model considering a linear heat source that goes from a generic depth d to $d + H$. In this case, [137] gives the solution as:

$$\overline{\Theta}_g = \frac{1}{4\pi} \int_{1/2\sqrt{Fo_H}}^{\infty} \exp\left(-R^2\beta^2\right) \frac{\Upsilon(\beta, D\beta)}{\beta^2} d\beta \tag{3.13}$$

where:

$$Fo_H = \alpha_g t / H^2 \quad D = d/H$$

$$\Upsilon(x,y) = 2 \cdot ierf(x) + 2 \cdot ierf(x+2y) - ierf(2x+2y) - ierf(2y)$$

$$ierf(x) = x \cdot erf(x) - \frac{1}{\sqrt{\pi}}\left(1 - e^{-x^2}\right)$$

When $D = 0$ the Eqs. (3.8) and (3.13) coincide.

Finite cylindrical source model - FCS

The FCS solution does not belong to the group of traditional analytical models (i.e. ILS, ICS, and FLS). The reason could be ascribed to the hard evaluation procedure of the FCS solution, with respect to the additional accuracy provided. Indeed, as above-mentioned, the use of cylindrical models are justified only at short time scales when significant axial effects do not occur. As a consequence, the use of FCS model provides similar results to ICS and FLS solutions at short and long time scales, respectively.

To our knowledge, the only available expression of the FCS model was provided by Man *et. al* [63], [65]. We stress that the proposed solution is based on a different geometry with respect to ICS model. In particular, the heat source is not assumed as an hollow cavity,

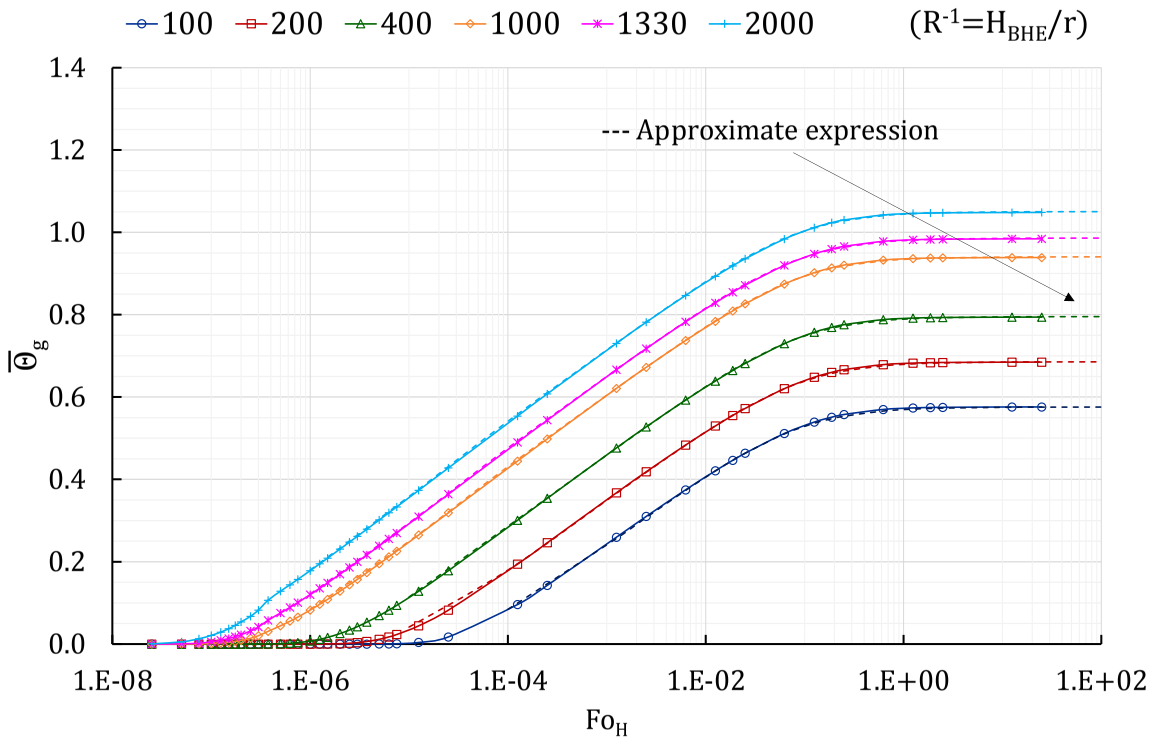

Figure 3.11. Comparison between approximate expression of the FLS solution (Eq. 3.12) and the real one (Eq. 3.8)

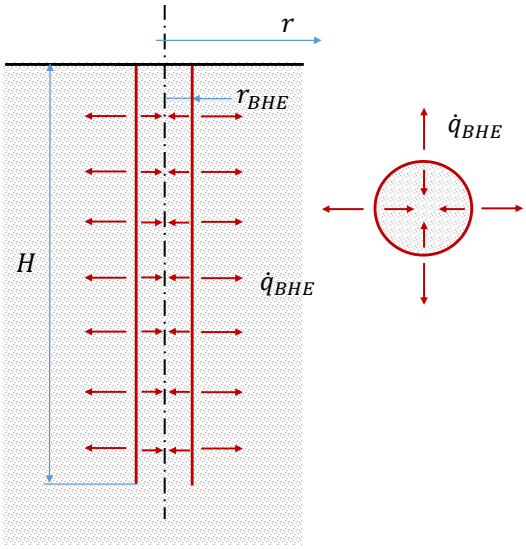

Figure 3.12. Schematic representation of the finite cylindrical sources model by Man *et. al* [63], [65].

but it consists in a cylindrical surface without the top and bottom areas (see Fig. 3.12); therefore, heat can diffuse also inward. The material within the borehole is considered to be homogeneous with the external ground.

As for FLS model, FCS solution is obtained through the mirror image technique (see section 3.1.1) ensuring a constant temperature T_g^0 at the ground surface. The analytical solution was obtained by Man *et al.* by means of the *Green's function method* [63], [65], [139]. Specifically, the cylindrical heat source was considered as a collection of numerous line sources of strength $\dot{q}_{BHE} d\phi / 2\pi$ each. The temperature rise at any location is obtained by superimposing all the individual temperature rises caused by the corresponding line sources. The dimensionless expression of the solution reads:

$$\Theta_g(Fo_H, Z, R, R_{BHE}) = \frac{1}{8\pi} \int_0^{Fo_H} \frac{1}{Fo_H - \beta} I_0 \left[\frac{R R_{BHE}}{2(Fo_H - \beta)} \right] \exp \left[-\frac{R^2 + R_{BHE}^2}{4(Fo_H - \beta)} \right] \left\{ 2 \cdot erf \left[\frac{Z}{2\sqrt{Fo_H - \beta}} \right] - erf \left[\frac{Z-1}{2\sqrt{Fo - \beta}} \right] - erf \left[\frac{Z+1}{2\sqrt{Fo - \beta}} \right] \right\} d\beta \quad (3.14)$$

where:

$$Fo_H = \alpha_g t / H_{BHE}^2 \quad Z = z / H_{BHE} \quad R = r / H_{BHE} \quad R_{BHE} = r_{BHE} / H_{BHE}$$

$I_0(z) = \frac{1}{\pi}\int_0^p i \exp(z\cos\phi)\, d\phi$ is the modified Bessel function of the first kind of order 0. For further details on calculation procedure, the reader can refer to [63], [65].

Eq. (3.14) shows that FCS solution depends on cylinder aspect ratio (R_{BHE}), together with radial and axial dimensionless coordinates (R and Z). As for FLS model, in GSHP applications, we are mainly interested in the average temperature at the BHE surface. The latter can be evaluated by imposing $R = R_{BHE}$ and integrating Eq. (3.14) over the borehole depth ($0 < Z < 1$).

Fig. 3.13 shows the dimensionless temperature , $\overline{\Theta}_g$, as a function of the Fourier number, Fo_H, and dimensionless BHE radius, R_{BHE}. We note that the application of FCS model do not provide significant improvements with respect to classical ICS and FCS models. At long time-scales, FCS provides the very similar results of FLS solution against remarkable additional computational efforts.The relative error between the two solution is lower than 2 % at $Fo_r \geq 1000$.

A small deviation with respect to ICS solution can be observed at $Fo_{BHE} \leq 10$. The latter can be ascribed to the presence of additional ground medium within the heat generation surface which slows the rise of temperature. Indeed, Man *et al.* developed this model also to investigate the effect of heat capacity of ground heat exchangers during the initial phases of the operation.

At high Fo_H, the ground in the proximity of the heat source reaches a steady-state condition, therefore, $\overline{\Theta}_g$ can be evaluated through both cylindrical and linear models.

3.1.2 Saturated porous media

The presence of groundwater movement modifies the heat transfer mechanism within the ground layers. The resulting ground temperature depends on heat conduction through the solid phases (soil and water) and heat advection given by moving groundwater. There are no actual *"streams"* in the underground (except in special geological situations): fluids move within voids and fractures in response to the hydraulic gradient. The so-called *"porous media theory"* is the reference subject for analyzing these cases.

The main parameter affecting energy and momentum equations are the *porosity*, ϕ, of the ground medium. The latter is defined as the ratio between the void volume contained in a medium sample and its total volume (eq 3.15) [140].

$$\phi = \frac{void\ volume}{total\ volume} \tag{3.15}$$

If the voids are totally filled by the fluid phase, we refer to *saturated medium*.

The momentum and energy balances in porous media are described in terms of volume-average quantities. Therefore, similarity to the "mechanical of continuous", the porous

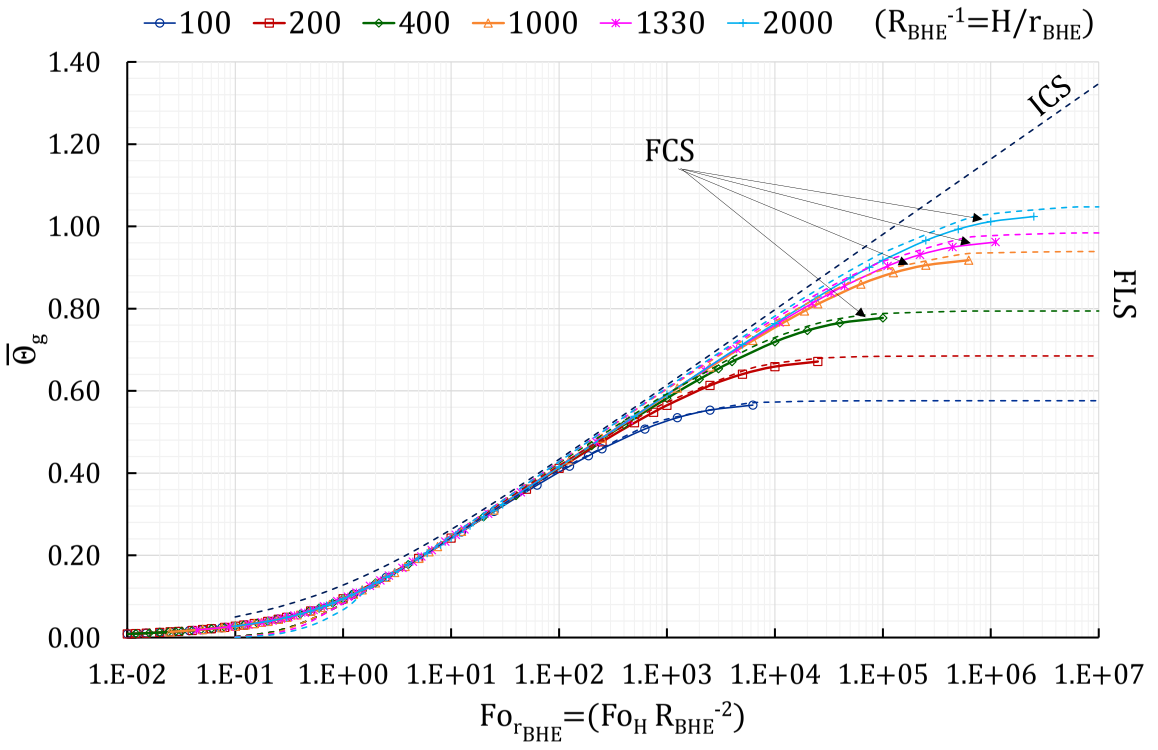

Figure 3.13. FCS solution: dimensionless temperature $\overline{\Theta}_g$ given by ICS and FCS models. The solid lines refer to FCS solutions.

media theory is based on the concept of a representative length scale, i.e. the so-called *representative elementary volume* (REV). The length scale of a single REV is much larger than a single pore size but considerably smaller than the length scale of the macroscopic flow. For further details on this subject, the reader can refer to [140]–[142]

In this Thesis we deal with the simplest situations of porous media analysis. We suppose that ground is a saturated and homogeneous medium, with an uniform distribution of the pores and without a directional preference for the fluid flow (i.e. isotropic medium). The latter assumption can be considered reasonable if the REV contains many pores, in other words, for sufficiently large length scales of analysis. Radiative effects, viscous dissipation, solid matrix deformations, and the work done by pressure changes are neglected. In addition, we assume that there is a local thermal equilibrium between the solid and the fluid phases, without a net heat transfer between them.

Under the above-mentioned assumptions, the flow is described by the *Darcy's law* (see, for instance, [111], [140]), it reads:

$$\mathbf{v} = \frac{\kappa}{\mu}\left(-\nabla p + \rho \mathbf{g}\right) \tag{3.16}$$

where:

- $\mathbf{v}$ is the volumetric flow rate per unit of cross-sectional area [2], $\mathrm{m\,s^{-1}}$ (i.e. seepage or Darcy velocity);
- κ is the permeability of the medium, $\mathrm{m^2}$;
- μ is the the dynamic viscosity of the fluid phase, $\mathrm{kg\,m^{-1}\,s^{-1}}$;
- ∇p is the pressure gradient, $\mathrm{Pa\,m^{-1}}$;
- $\mathbf{g}$ is the body acceleration vector, $\mathrm{m\,s^{-2}}$.

This Thesis refers only to homogeneous and isotropic media, thus thermo-pysical properties are always considered as scalar values. We note that the velocity field is the gradient of a scalar function, therefore the fluid movement can be analyzed as a potential flow. κ values are related to porosity; the latter can be evaluated by means of experimental tests or simplified models and correlations (see, for instance, [140]). In GSHPs analysis, Eq. (3.16) is typically presented in the following form assuming that gravitational effects are negligible in considered length scales (Eq. 3.17) [111].For alternative flow models in porous media, reference can be made to [140]–[142].

$$\mathbf{v} = -K\nabla h \tag{3.17}$$

where K is the hydraulic conductivity of the medium,$\mathrm{m\,s^{-1}}$, and h is the hydraulic head,$\mathrm{m\,m^{-1}}$.

2 The Darcy velocity $\mathbf{v}$ corresponds to the volumetric average of actual fluid velocity over a medium volume element including both solid and fluid phase [141]. The intrinsic average velocity $\mathbf{V}$ of the fluid phase is related to v by the Dupuit-Forchheimer relationship $\mathbf{v} = \phi\mathbf{V}$.

We note the perfect analogy between Darcy's and Fourier's laws (i.e. $\dot{\mathbf{q}} = -\lambda \nabla T$). The temperature T corresponds to the hydraulic load h, thermal conductivity λ corresponds to hydraulic conductivity K, and heat flux $\dot{\mathbf{q}}$ corresponds to velocity $\mathbf{v}$. The similarities between the subsurface behavior of water and heat diffusion has been exploited by hydrologists to derive the analytical expression of current groundwater models [31]. For instance, the so-called *Theis equation*, used to evaluate the productivity of a water well (see section 2.2), has the same form of the ILS solution (Eqs. 3.2b and (2.3)). Therefore, all the considerations hereafter exposed can be easily adapted to possible to GWHP systems.

By applying the local thermal equilibrium assumption, the energy law in a porous medium can be expressed as [140]:

$$\sigma \frac{\partial T_g}{\partial t} + \mathbf{v} \cdot \nabla T_g = \nabla \cdot (\alpha_{eff} \nabla T_g) \tag{3.18}$$

where σ is the heat capacity ratio (Eq. 3.19a), α_{eff} is the effective thermal diffusivity (Eq. 3.19b), and $\mathbf{v}$ is the seepage velocity (Eq. 3.17)

$$\sigma = \phi + (1 + \phi) \frac{(\rho c)_s}{(\rho c_p)_f} \tag{3.19a}$$

$$\alpha_m = \frac{k_m}{(\rho c)_f} \tag{3.19b}$$

$$\lambda_m = (1 - \phi)\lambda_s + \phi \lambda_f \tag{3.19c}$$

$$(\rho c)_m = \phi (\rho c)_f + (1 - \phi)(\rho c)_f \tag{3.19d}$$

Eq. 3.18 will be used in the next sections to derive the analytical expression of the thermal field around a heat source in presence of groundwater advection.

Table 1.1 in Appendix 1 shows the some reference values for typical ground media. We stress the illustrative purpose of those tables, as the actual values of soil materials vary in a very broad ranges depending on local conditions. For real projects, designers should always consider the possibility of using specific site-investigation techniques to obtain accurate values of local thermo-physical parameters.

Infinite line source problem with water advection - MILS

The transient solution of the infinite line source in a semi-infinite medium with groundwater advenction has been presented by several authors (see, among others, [88], [111], [120], [143], [144]). This model neglects the effects due to the ground surface and the finite length of the GHE. Furthermore, the following assumptions are applied:

- the ground is considered as an homogeneous and isotropic porous medium;
- the GHE is approximated by an infinite line source of constant strength, $\dot{q}_{BHE}$;

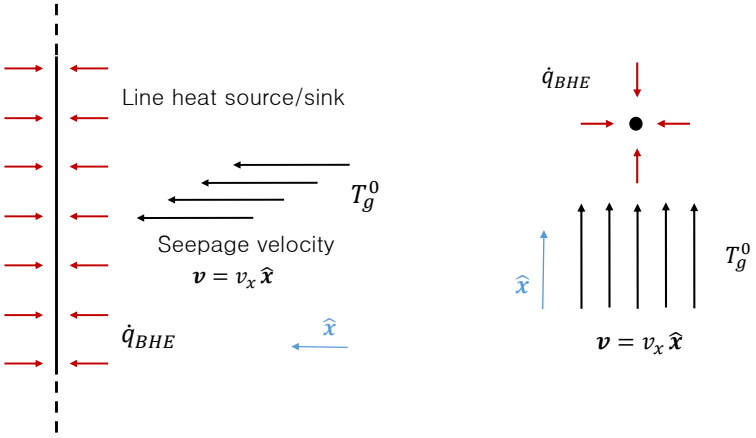

(a) *Side view.* (b) *Top view.*

Figure 3.14. Schematic representation of the infinite line source problem with groundwater flow.

- the initial temperature,T_g^0, is equal to the far-field one;
- the groundwater velocity is considered uniform, constant and parallel to the ground surface, $\mathbf{v} = \{v_x \hat{x}\}$,.

Under these assumptions,the infinite line source problem in presence of groundwater advection reads:

$$\begin{cases} \frac{\partial T_g}{\partial t} + v_{x,eff} \frac{\partial T_g}{\partial x} = \alpha_{eff} \left(\frac{\partial^2 T_g}{\partial x^2} + \frac{\partial^2 T}{\partial y^2} \right) \\ T_g \left(r \to \infty, t \right) = T_g^0 \\ T_g \left(r, t = 0 \right) = T_g^0 \\ \dot{q} \left(r \to 0, t \right) = - \left(2\pi r \right) \lambda_g \frac{\partial T_r}{\partial r} \Big|_{r \to 0} = \dot{q}_{BHE} \end{cases} \tag{3.20}$$

where:

$$v_{x,eff} = \frac{(\rho c)_f}{(\rho c)_m} v_x \quad \alpha_{eff} = \frac{k_m}{(\rho c)_m} \quad r = \sqrt{x^2 + y^2}$$

The schematic representation of the problem is shown in Fig. 3.14.

The problem (3.20) is known as the *moving infinite line source model* (MILS): its solution was given by Carslaw and Jaeger [84] and subsequently by other authors (see, for instance, [111], [143], [144]).

$$\Theta_g(\theta, Pe_r, Fo_r) = \frac{1}{4\pi} \exp\left(\frac{Pe_r}{2} \cos(\theta) \right) \int_{\frac{1}{4Fo_r}}^{\infty} \frac{1}{\beta} \exp\left(-\beta - \frac{Pe_r^2}{16\beta} \right) d\beta \tag{3.21}$$

where:

$$Pe_r = \frac{v_{x,eff} r}{\alpha_{eff}} \quad \Theta_g = \frac{\left(T_g^0 - T_g\right) \lambda_g}{\dot{q}_{BHE}} \quad Fo_r = \frac{\alpha_{eff} t}{r}$$

The integral in the Eq. 3.21 is named "*generalized incomplete gamma function*"[143]–[145], namely:

$$\Gamma(a, x, b) = \int_x^\infty \beta^{a-1} \exp\left(-\beta - \frac{b}{\beta}\right) d\beta \tag{3.22}$$

Therefore, the MILS solution (3.21) becomes:

$$\Theta_g(\theta, Pe_r, Fo_r) = \frac{1}{4\pi} \exp\left(\frac{Pe}{2}\cos(\theta)\right) \Gamma\left(0, \frac{1}{4Fo_r}, \frac{Pe_r^2}{16}\right) \tag{3.23}$$

The steady state expression of Eqs. 3.21 and 3.23 reads [144]:

$$\Theta_{g,s}(\theta, Pe_r) = \frac{1}{2\pi} \exp\left(\frac{Pe_r}{2}\cos(\theta)\right) K_0\left(\frac{Pe_r}{2}\right) \tag{3.24}$$

where K_0 is the modified Bessel function of the second kind of order 0. The average temperature at the BHE surface can be evaluated by integrating Eqs. 3.23 with respect to the angular coordinate Θ:

$$\begin{aligned} \overline{\Theta}_g\left(Pe_r, Fo_r\right) &= \left[\frac{1}{\pi}\int_0^\pi \exp\left(\frac{Pe_r}{2}\cos(\theta)\right) d\theta\right] \left[\frac{\Gamma\left(0, \frac{1}{4Fo_r}, \frac{Pe_r^2}{16}\right)}{4\pi}\right] \\ &= \frac{1}{4\pi} I_0\left(\frac{Pe_r}{2}\right) \Gamma\left(0, \frac{1}{4Fo_r}, \frac{Pe_r^2}{16}\right) \end{aligned} \tag{3.25}$$

where $I_0(z) = \frac{1}{\pi}\int_0^\pi \exp\left(z\cos\theta\right) d\theta$ is the modified Bessel function of the first kind of order 0. Eq. 3.25 is plotted in Fig. 3.15.

At the steady-state, Eq. (3.25) reads:

$$\overline{\Theta}_{g,s}\left(Pe_r\right) = \frac{1}{2\pi} I_0\left(\frac{Pe_r}{2}\right) K_0\left(\frac{Pe_r}{2}\right) \tag{3.26}$$

The Figs. 3.15 and 3.16 show the difference between ILS and MILS solutions. The deviation between the two models can be neglected for $Fo_r < Fo_c$, where Fo_c is named "*critical Fourier number*". At high Fo_r, the solution is no longer axisymmetric because of the presence of groundwater advection which generates a thermal plume downstream the heat source. Fo_c depends on on Pe_r (Fig. 3.17) according to the following expression:

$$Fo_c = 3.25 Pe_r^{-1.5} \tag{3.27}$$

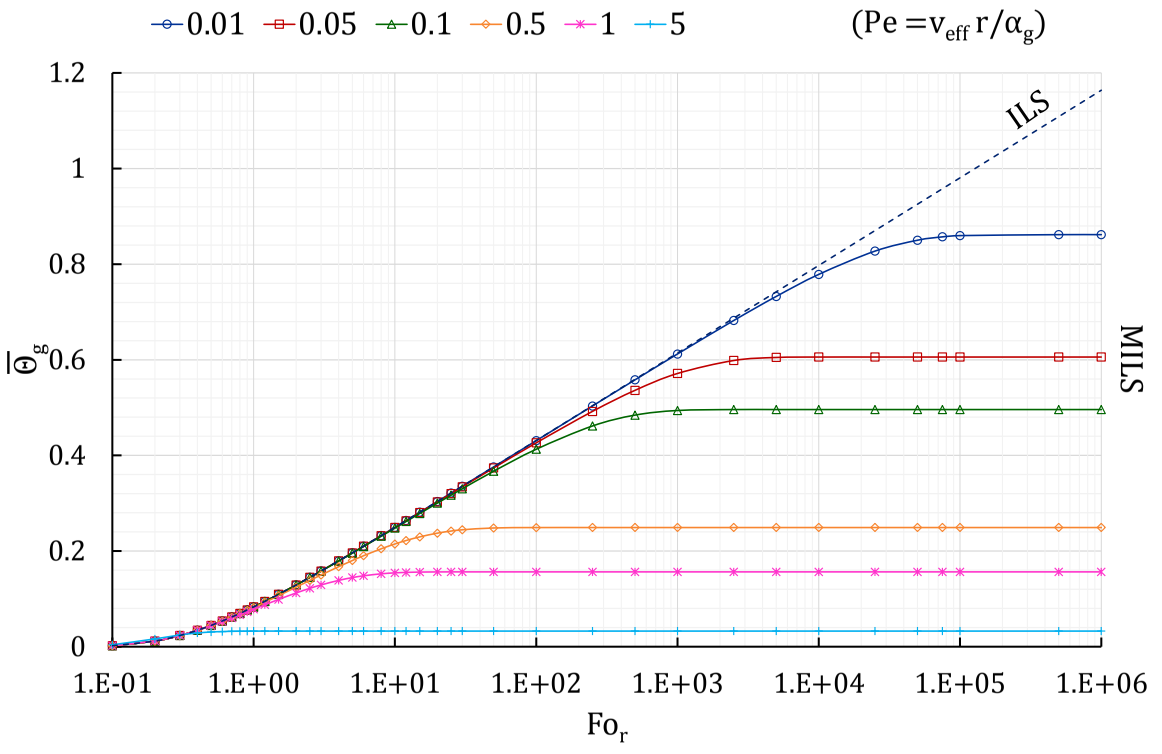

Figure 3.15. MILS solution: dimensionless temperature, $\overline{\Theta_g}$, as a function of Fourier number, Fo_r, and Péclet number, Pe_r.

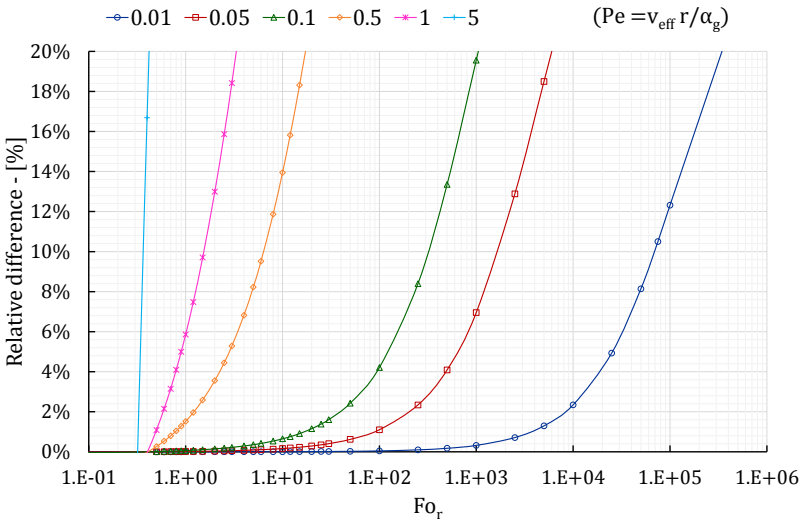

Figure 3.16. Relative difference between ILS and MILS model.

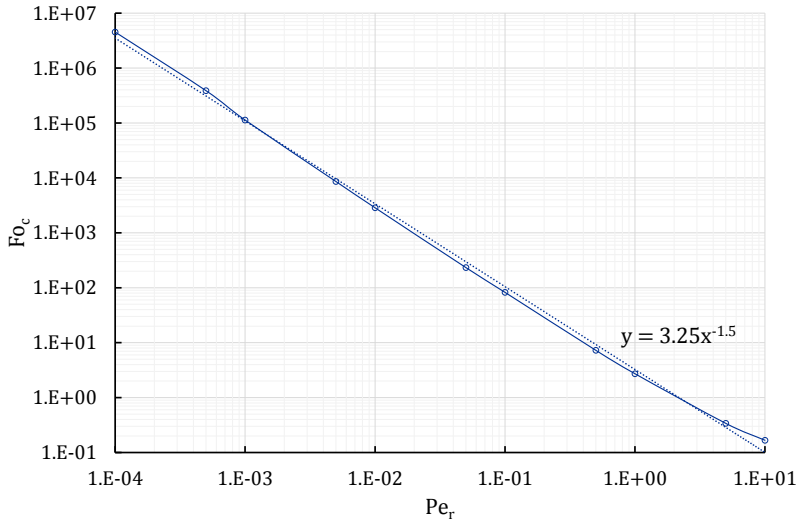

Figure 3.17. Critical Fourier number, Fo_c, depending on Pe_r. For $Fo_r \leq Fo_c$ the MILS solution is equivalent to the ILS one; in other words, advection effects are negligible.

We note that $\overline{\Theta}_g(Fo_c)$ corresponds to about 80 % of the steady-state value $\overline{\Theta}_{g,s}$ (see Fig. 3.15). We can define $Fo_{r,s}$ as the Fourier number at which the transient solution approaches 99 % of the steady state solution [144]. Fig. 3.16 shows $Fo_{r,s}$ and $\Theta_{g,s}$ as a function of Péclet number.

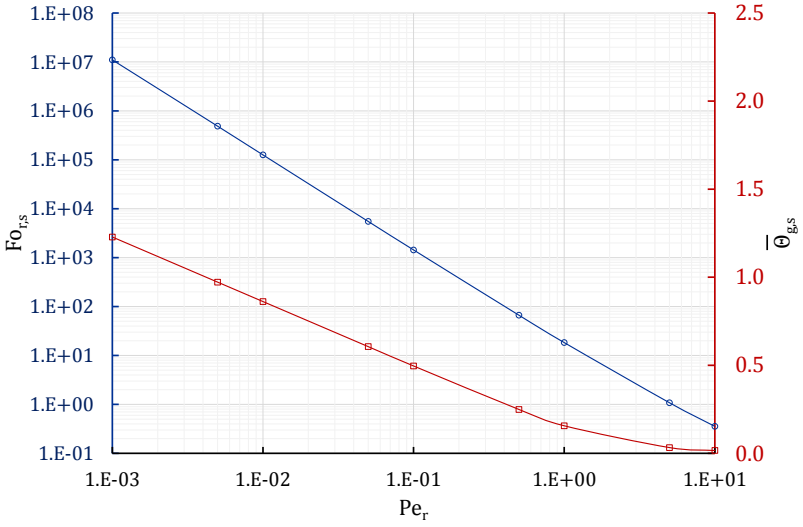

Figure 3.18. Critical Fourier number, $Fo_{r,s}$, and corresponding dimensionless temperature, $\Theta_{g,s}$, as a function of Péclet number,Pe_r.

We can use $L = \frac{\alpha_g}{v_{x,eff}}$ as the characteristic length of the problem, and $\tau = \frac{v_{eff}^2 t}{\alpha_{eff}} = Fo_r Pe_r^2$ as the characteristic time [111]. The dimensionless coordinates of the problem are given by $\overline{X} = \frac{x}{L}$ and $\overline{Y} = \frac{y}{L}$. We note that Pèclet number, Pe_r, corresponds also to the dimensionless radial coordinate. The Θ_g field as a function of the dimensionless lengths ($\overline{X}$, $\overline{Y}$) at different times (τ) is shown in Figs. 3.19 3.20 3.21 3.22 3.23.

In section 3.1.3 we will discuss the *superposition technique* to evaluate the thermal interference among different GHEs. The linearity of the problem (3.20) allows to calculate the temperature excess at any location by summing the contribution of each BHE. Here, we note that the Θ-average dimensionless temperature $\overline{\Theta_g}$ can be used to evaluate the temperature raise at a given distance, r, only if the corresponding Fo_r is lower than Fo_c. Indeed, as above-mentioned, the Fo_c is the limit beyond which the MILS solution equates the ILS one. In other words, at Fo_r grater than Fo_c the thermal field is no longer axisymmetric. Consequently, assuming that boreholes radii are smaller with respect to

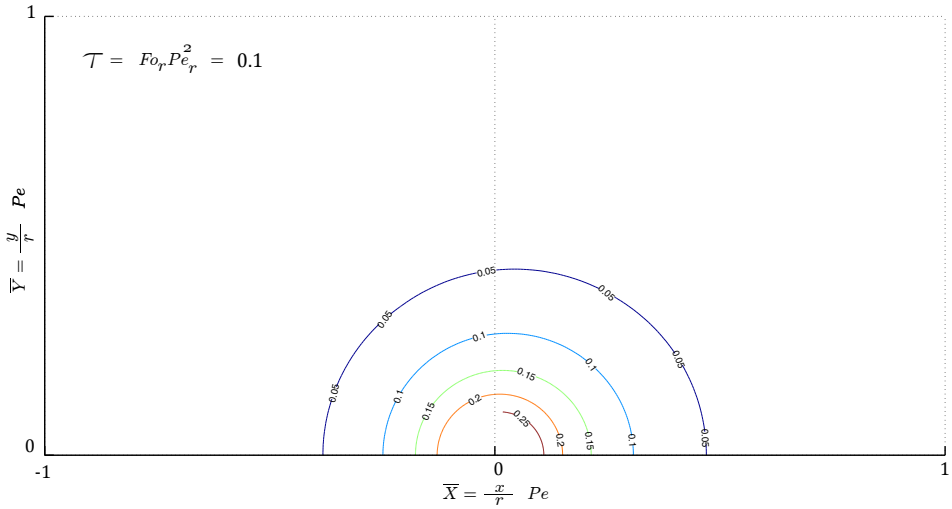

Figure 3.19. Isotherms of the MILS model at $\tau = 0.1$.

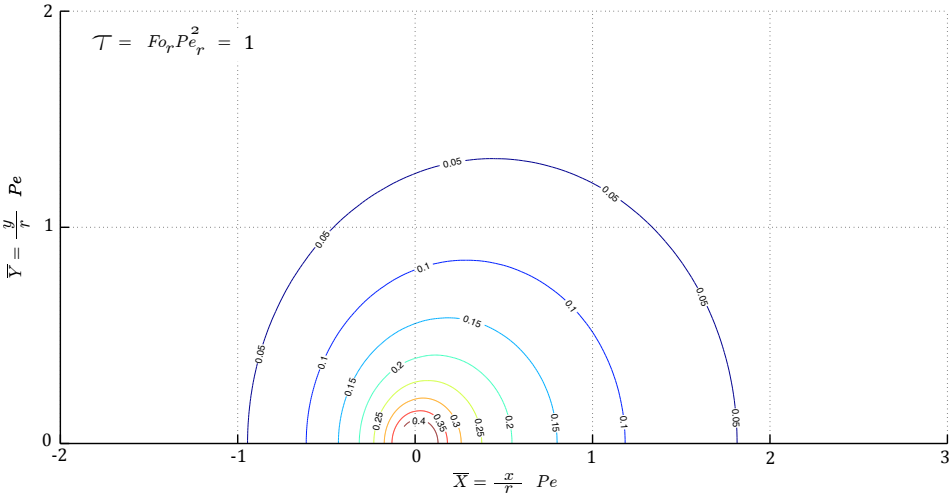

Figure 3.20. Isotherms of the MILS model at $\tau = 1$.

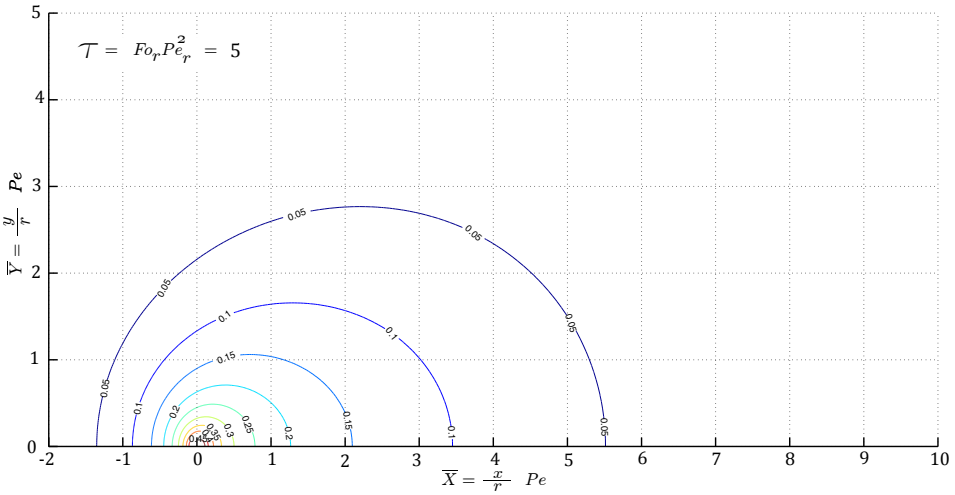

Figure 3.21. Isotherms of the MILS model at $\tau = 5$.

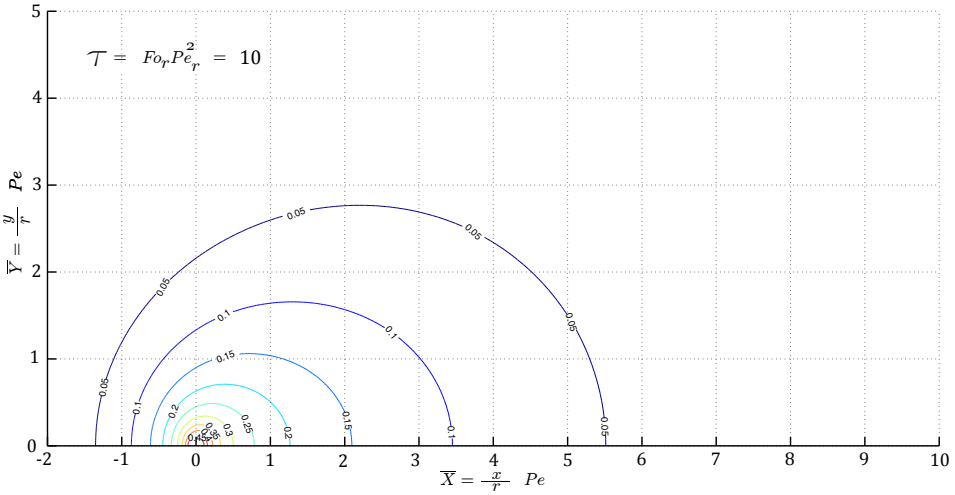

Figure 3.22. Isotherms of the MILS model at $\tau = 10$.

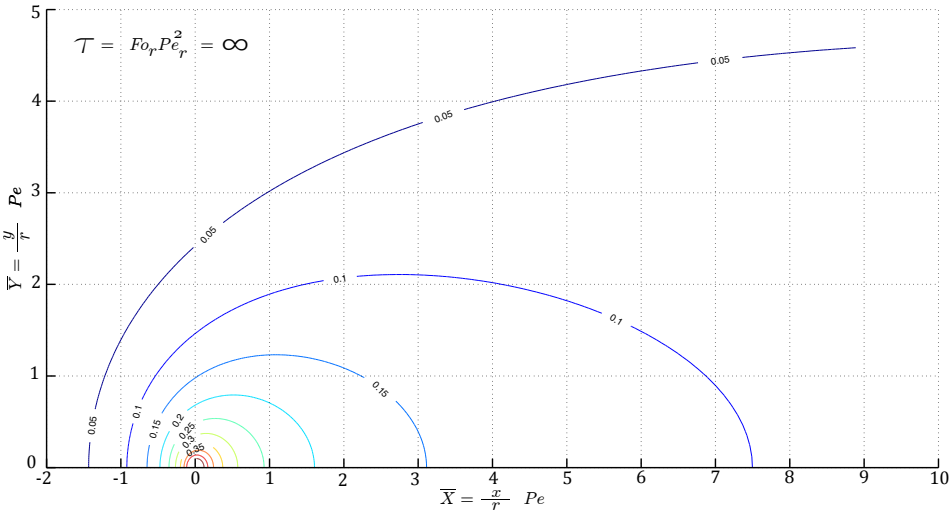

Figure 3.23. Isotherms of the MILS model at the steady-state.

BHE field dimension, the temperature alteration at distance r should be evaluated through the maps 3.19 3.20 3.21 3.22 3.23 or Eq. (3.21).

Finite line source problem with groundwater advection - MFLS

In section 3.1.1 we analyzed the impact of axial effects by comparing the ILS and FLS solution. Similarly to purely conductive models, also the MILS can be extended through the so-called *moving finite line source model* (MFLS), which considers both the finite length of the heat source and groundwater movement.

The analytical solution of the MFLS problem was developed by Molina-Giraldo *et al.* in recent times [114]. The following assumptions were applied:

- The underground is considered as a homogeneous semi-infinite porous medium, with fixed, homogeneous and isotropic thermo-physical properties;
- The ground surface has a fixed temperature equal to the undisturbed initial temperature;
- The groundwater velocity is considered uniform, constant and parallel to the ground surface, i.e. $\mathbf{v} = v_x\{\hat{\mathbf{x}}\}$;
- A constant heat flow rate per unit length, $\dot{q}_{BHE}$, is applied to a line source of finite length.

The geometry of the MFLS model is shown in Fig. 3.24.

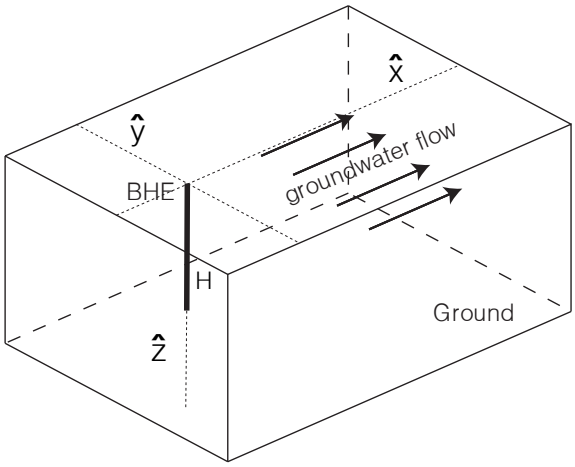

Figure 3.24. Geometry of the MFLS model. The BHE is represented by the bold line.

The formulation of the problem reads:

$$\begin{cases} \frac{\partial T_g}{\partial t} + v_{x_{eff}} \frac{\partial T_g}{\partial x} = \alpha_{eff} \left(\frac{\partial^2 T_g}{\partial x^2} + \frac{\partial^2 T}{\partial y^2} + \frac{\partial^2 T}{\partial z^2} \right) \\ T_g \left(r \to \infty, t \right) = T_g^0 \\ T_g \left(r, t = 0 \right) = T_g^0 \\ \dot{q} \left(r \to 0, t \right) = - \left(2\pi r \right) \lambda_g \frac{\partial T_r}{\partial r} \Big|_{r \to 0} = \dot{q}_{BHE}, \qquad 0 \leq z \leq H_{BHE} \end{cases} \tag{3.28}$$

Molina-Giraldo *et al.* obtained the solution of the problem (3.28) through the Green's function method [114], [139] and the mirror image technique (see section 3.1.1). The dimensionless form of the MFLS solution reads:

$$\Theta(R', Z, \phi, Fo_H, Pe_H) = \frac{1}{2\pi} \exp \left[\frac{Pe_H}{2} R' \cos(\theta) \right] \left[\int_0^1 f(R, Fo_H, Pe_H) dZ' - \int_{-1}^0 f(R, Fo_H, Pe_H) dZ' \right]$$

where:

$$f(R', Z, Fo, Pe) = \frac{1}{4R} \exp \left(-\frac{Pe_H}{2} R \right) erfc \left(\frac{R - Pe_H}{2\sqrt{Fo}} \right) + \frac{1}{4R} \exp \left(\frac{Pe_H}{2} R \right) erfc \left(\frac{R + Pe_H Fo_H}{2\sqrt{Fo}} \right) \tag{3.29}$$

$$Pe_H = \frac{v_{x_{eff}} H_{BHE}}{\alpha_{eff}} \qquad R' = \frac{r}{H_{BHE}} \qquad Z = \frac{z}{H_{BHE}}$$

$$\Theta_g = \frac{\left(T_g^0 - T_g\right)\lambda_g}{\dot{q}_{BHE}} \qquad Fo_H = \frac{\alpha_{eff} t}{H^2} \qquad R = \sqrt{R'^2 + (Z - Z')^2}$$

The analysis of the MFLS model is still ongoing. Therefore, in this section we shortly report some of the main conclusions of the work by Molina-Giraldo *et al.* [114]. In particular, the cited work investigated the influence of the finite length of the source on the ground temperature response by comparing the results of Eq. 3.29 with FLS and MILS models. They concluded that axial effects on the BHE wall temperature evolution can be neglected for high groundwater flow (i.e. high Péclet number). On the contrary, groundwater movement does not have effect al low Darcy velocities (i.e. low Péclet number). Molina-Giraldo *et al.* [114] *et al.* concluded that MFLS model should be used for $(0.2 \leq Pe_H \leq 10)$.

We note that the cited authors figured out their conclusions investigating a typical borehole geometry ($r_{BHE} = 0.1$ m, $H = 50$ m) at its middle depth (Figs. 3.25). More general conclusion could be obtained by a complete dimensionless analysis. As above-mentioned, this research activity is still ongoing, therefore, future works will be dedicated to this topic.

3.1.3 Superposition techniques

All the above-described analytical models refer to the ground response when a constant heat pulse is imposed at a single borehole surface. The operative conditions of real GSHPs are different: first, a typical BHE field is made of several boreholes any of which exchanges a time-variable thermal power. The actual evolution of the heat flux $\dot{q}_{BHE}$ depends on several factors: e.g. building thermal load profile, instantaneous COP/EER of the heat pump unit, heat transfer effectiveness of each borehole, supply temperature, and the instantaneous value of the ground temperature resulting from previous heat exchanges. Only a complete simulation model, taking into account the behavior of each GSHP subsystem, is able to evaluate the actual heat flux at each borehole surface. The latter topic will be discussed in section 4.4.

In this section, we describe the mathematical techniques to obtain the analytical expression of the ground temperature when more than one time-dependent heat source is considered, i.e. the *time superposition* and *space superposition* techniques.

Time superposition technique

The solution to heat transfer problems with time-dependent boundary conditions can be related to the solution of the same problem with constant boundary conditions by

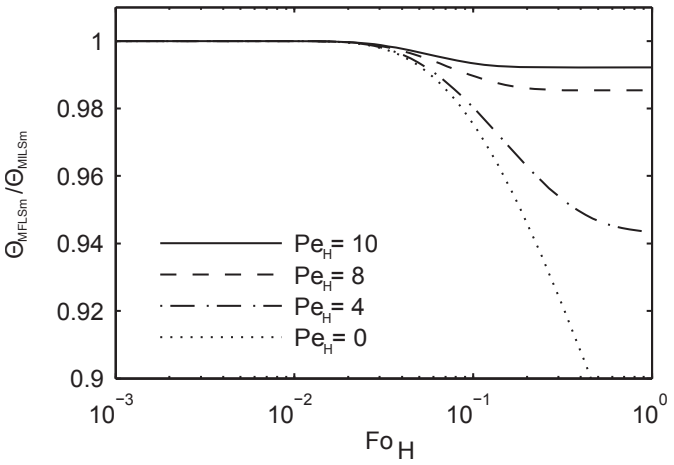

(a) *Ratio of the MFLS and MILS model (Axial effects).*

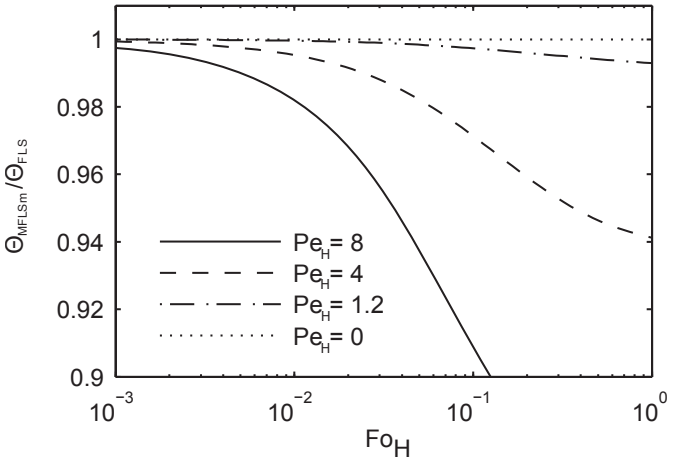

(b) *Ratio of the MFLS and FLS model (Groundwater effects).*

Figure 3.25. Temperature response of a circle around the heat source ($r = 0.1$ m, $H = 50$ m, $z = 0.5$ m) [114].

means of the *Duhamel's theorem* [3][139]. In other words, we evaluate the ground temperature response to an arbitrary time-dependent $\dot{q}_{BHE}(t)$ through the "fundamental solution" of the same problem to a single, constant, unitary heat pulse.

All the $\Theta_g(\mathbf{x}, t)$ expressions illustrated in the previous sections (i.e. ILS, FLS, ICS, FLS, MILS, MFLS) are *fundamental solutions*. Therefore, according to Duhamel's theorem, the ground response to a time-varying term $\dot{q}_{BHE}(t)$ reads:

$$\frac{T_g(\mathbf{x}, t) - T_g^0}{\lambda_g} = \left[\int_0^t \Theta_g(\mathbf{x}, t - \beta) \frac{\dot{q}_{BHE}}{dt}(\beta) \quad d\beta \right] + \Theta_g(\mathbf{x}, 0) \dot{q}_{BHE}(0) \tag{3.30}$$

where $\mathbf{x}$ is the generic spatial coordinate, β is the auxiliary time variable, and Θ_g corresponds to Eqs. (3.2), (3.5), (3.8), (3.14), (3.25), and (3.29) depending on the specific model employed.

As we will see in section 4.4.1, our simulation approach is based on a steady-state formulation: in other words, the actual evolution of the physical quantities (e.g. temperature and energy exchanges) are approximated by a series of constant average values (see Fig. 3.26-a). Thus, the general expression of the Duhamel's theorem (Eq. 3.30) can be rearranged as follows:

$$\frac{T_g(\mathbf{x}, t = n\Delta t)) - T_g^0}{\lambda_0} = \sum_{i=1}^{n} \left[\Theta_g(\mathbf{x}, t = i\Delta t) \left(\dot{q}_{BHE}^{n-i+1} - \dot{q}_{BHE}^{n-i} \right) \right] \tag{3.31}$$

where $T_g(\mathbf{x}, t = n\Delta t)$ corresponds to the ground temperature at the end of the n-th time step and $\dot{q}^0 = 0$.

The physical interpretation of Eq. 3.31 is shown in Fig. 3.26. The basic heat pulse $\dot{q}_{BHE}^1$ is applied for the entire duration of the analysis (in this case, four time step). Then, the subsequent effective pulses are superimposed: $\dot{q}*^2 = \dot{q}_{BHE}^2 - \dot{q}_{BHE}^1$ for three steps, $\dot{q}*^3 = \dot{q}_{BHE}^3 - \dot{q}_{BHE}^2$ for two steps and finally $\dot{q}*^4 = \dot{q}_{BHE}^4 - \dot{q}_{BHE}^3$ for the last step.

Space superposition technique

If we assume that the radial dimension of BHEs is negligible compared to the size of the field, the ground temperature at a given coordinate $\mathbf{x}$ is obtained by summing up all the individual temperature alteration caused by each borehole, namely:

$$T_g(\mathbf{x}, t) - T_g^0 = \sum_{b=1}^{N_{BHE}} T_g(|\mathbf{x} - \mathbf{x}_b|, t) \tag{3.32}$$

where N_{BHE} is the boreholes number, $\mathbf{x}_b$ is the position of the b-th borehole.

3 Rigorous math terminology refers to *homogeneous* and *non-homogeneous* boundary conditions [139].

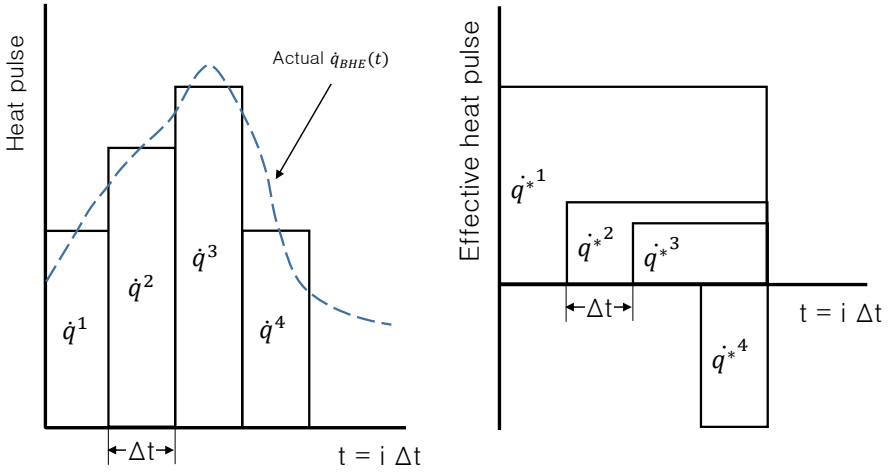

(a) *Actual thermal pulses.* (b) *Effective thermal pulses.*

Figure 3.26. Superposition of piecewise linear step heat inputs in time. The actual pulses $\dot{q}_1$,$\dot{q}_2$,$\dot{q}_3$,$\dot{q}_4$ are super- imposed in time as "effective pulses" $\dot{q}^*_1$,$\dot{q}^*_2$,$\dot{q}^*_3$,$\dot{q}^*_4$.

Considering both time and space superposition, the final expression of the ground thermal field reads:

$$T_g(\mathbf{x}, t = n\Delta t) = T_g^0 - \sum_{b=1}^{N_{BHE}} \sum_{i=1}^{n} \frac{\Theta_g\left(|\mathbf{x} - \mathbf{x}_b|, t = i\Delta t\right)}{\lambda_g} \left[\dot{q}_{BHE}^{n-i+1} - \dot{q}_{BHE}^{n-i}\right] \tag{3.33}$$

3.2 *Ground heat exchangers - GHEs*

As we pointed out in the previous section, we consider the ground source and ground heat exchangers as two different subsystems. Consequently, we evaluate their thermal behavior by means of two distinct models. The latter will be connected within the same overall set of equation in a second step (see section 4.4).

On the contrary, several works have investigated both systems concurrently (see, for instance, [63], [117], [123], [125], [127], [128], [130], [131], [146]–[148]). This approach, however, is typically employed to investigate the short-term unsteady behavior of GHEs under quick variations of the operative conditions (e.g. ON/OFF cycles, variation of flow rate and/or supply temperature). Generally, due to the reduced thermal mass and the high aspect ratio of a typical BHE, the internal energy variations are negligible with respect to the energy exchanges at the BHE surface and ground temperature dynamic. Thus, it is a common practice that the heat transfer within the BHEs is assumed as a steady-state process [149]. Such simplification will be discussed in section 3.2.4.

Our previous considerations about numerical and analytical approaches to ground-source modeling can be extended to BHEs analysis. Several works have dealt with the numerical simulation of the boreholes thermal performances (see, for instance, [123], [125], [130], [147], [148], [150]); however, as above mentioned, we believe that the potential of the numerical analysis can be totally exploited only if all input parameters are known with a sufficient accuracy. Therefore, during the design phase, analytical formulation are to be preferred as it represent a proper tradeoff among computational efforts, results accuracy, and flexibility for parametric designs.

Fig. 3.1 shows a schematic representation of a typical BHE: a proper model shall be able to predict the heat exchange between the circulating fluid and surrounding ground. Under the steady-state assumption, we propose to analyze boreholes behavior through the classical heat exchanger theory, i.e. the so-called $\epsilon - NTU$ *method* (see, for instance, [140], [151]).

The energy balance and the heat transfer equation for a generic borehole is given in Eqs. (3.34a) and (3.34a):

$$\dot{Q}_g = \dot{q}_{BHE} H_{BHE} = \dot{m}_w c_w \left(T_{w,in} - T_{w,out}\right) \tag{3.34a}$$

$$\dot{Q}_g = UA \left(\overline{T}_w - T_g\right) \tag{3.34b}$$

$$\tag{3.34c}$$

where:

- $\dot{Q}_g$ is the heat transfer rate, W;
- $\dot{q}_{BHE}$ is the linear heat flux per unit length, $\mathrm{W\,m^{-1}}$;
- H_{BHE} is the borehole depth, m;
- $\dot{m}_w$ is the total flow rate entering the BHEs, $\mathrm{kg\,s^{-1}}$;
- $T_{w_{in}}$ is the supply temperature of the circulating fluid, K or °C;
- $T_{w_{out}}$ is the return temperature from the BHE, K or °C;
- UA is the overall heat transfer coefficient,$\mathrm{W\,K^{-1}}$;
- $\overline{T}_w$ is the mean temperature of the circulating fluid, K or °C;
- T_g is the average ground temperature at the BHE surface, K or °C;

The use of the $\epsilon - NTU$ method ensures that the heat transferred at the BHE surface $\dot{Q}_g$ is coherent with the temperature variation of the fluid $\left(T_{w,i} - T_{w,out}\right)$; in other words, we impose that outlet fluid temperature, $T_{w,out}$, is greater/lower than T_g depending on heat flux direction (i.e. cooling/heating mode). On the contrary, the use of Eq. 3.34b alone could result in inconsistent evaluations because of the small temperature drop between the fluid and the ground.

The $\epsilon - NTU$ method can be easily coupled to another widely used concept of BHEs analysis: the *borehole thermal resistance* (R_b), defined as [152]:

$$Rb = \frac{\overline{T}_w - T_g}{\dot{q}_{BHE}} \tag{3.35}$$

Following this definition, R_b is a stationary parameter that relates the mean fluid temperature to the BHE wall temperature, T_g: dynamic and axial effects are thus neglected. Furthermore, we stress that R_b conventionally refers to the BHE depth (i.e. H) and not to the length of the ducts. Combining eq. (3.34) and (3.35), we obtain:

$$\frac{H}{R_b} = UA \tag{3.36}$$

Since the borehole surface temperature T_g is assumed uniform, we can write, for every BHE:

$$\epsilon_{BHE} = f\left(NTU\right) = f\left(\frac{1}{\dot{m}_w c_w}\frac{H}{R_b}\right) \tag{3.37a}$$

$$T_{w,out} = T_{w,in} + \epsilon_{BHE}\left(T_g - T_{w,in}\right) \tag{3.37b}$$

Suitable expressions and models for Eq. (3.37a) will be discussed hereafter.

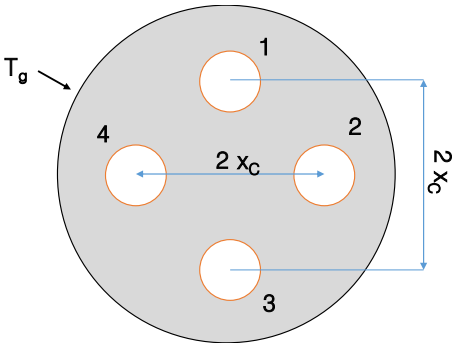

Figure 3.27. Cross section of a generic 2-U borehole.

The value of R_b is given by three contributions: the convective thermal resistance between the fluid and pipes wall,$\left(R_{b,conv}\right)$, the conductive thermal resistance across the pipes $\left(R_{b,duct}\right)$, and the conductive thermal resistance of the grout $\left(R'_b\right)$.

$$R_p = R_{b,conv} + R_{b,duct} + R'_b = R_p + R'_b \tag{3.38}$$

where:

$$R_{b,conv} = \frac{1}{2N_U}\frac{1}{\pi r_{p,i} h_{conv}} \qquad R_{b,duct} = \frac{1}{2N_U}\frac{\ln\left(r_{p,e}/r_{p,i}\right)}{\pi\lambda_p}$$

- N_U is the number of U-pipes within the same borehole;
- $r_{p,i}$ and $r_{p,o}$ are the inner and outer pipe radius, respectively, m;
- h_{conv} is the convective heat transfer coefficient within the ducts,$\mathrm{W\,m^{-2}\,K^{-1}}$;
- λ_p is the thermal conductivity of the pipe material, $\mathrm{W\,m^{-1}\,K^{-1}}$.

The main parameters influencing R_b are: thermal conductivity of the pipes and of the grout λ_{grout}, radius of the pipe and of the BHE, and shank spacing between U-legs, x_c (see Fig. 3.27). The convective resistance $\left(R_{b,conv}\right)$ can be neglected when the flow regime within BHE ducts is turbulent [6], [80]. Table 3.2 shows some reference value of the thermal conductivity of typical grout materials.

Table 3.2. Thermal conductivity of borehole filling materials (after [6], [57], [80]).

Grouts/Backfills Materials	Thermal conductivity $\mathrm{W\,m^{-1}\,K}$
Bentonite (20 − 30%)	0.73 − 0.75
Neat cement (not recommended)	0.69 − 0.78
20% Bentonite / 80% Quartzite sand (SiO_2)	1.47 − 1.64
15% Bentonite / 85% Quartzite sand (SiO_2)	1.00 − 1.10
10% Bentonite / 90% Quartzite sand (SiO_2)	2.08 − 2.42
30% Concrete / 70% Quartzite sand (SiO_2) , s. plasticizer	2.08 − 2.42

Several authors have proposed different analytical expressions to evaluate R_b, $\overline{T}_w$ and ϵ_{BHE} (see, for instance, [149], [152]–[158]). In all these works, the following assumptions are applied:

- Dynamic effects are considered negligible, therefore heat capacity of the materials is not taken into account;
- The heat conduction in the axial direction is negligible;
- The borehole wall temperature is uniform;
- Both the ground and the grout are homogeneous with temperature-independent thermophysical properties.

In the following sections, we will review the main models to evaluate R_b as a function of the borehole geometry, materials, and configuration. We can group available expressions in three main categories: the so-called *one-dimensional models*, *two-dimensional models* and *quasi-three-dimensional models* [36], [111].

3.2.1 One-dimensional models

The one-dimensional approach considers the U-pipes within the borehole as a single "equivalent pipe" (see 3.28) [109], [159], [160]. However this approach seem too simplified for many authors as R_b' value is not affected by actual ducts position [109], [159].

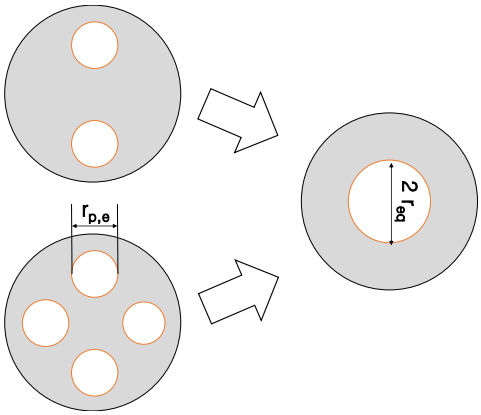

Figure 3.28. Equivalent geometry of R_b one-dimensional models.

Single U-pipe

For single U-pipe configuration, the R'_b expression reads:

$$R'_b = \frac{1}{2\pi\lambda_{grout}} \ln\left(\frac{r_{BHE}}{\sqrt{2}r_{p,e}}\right) \tag{3.39}$$

where $\sqrt{2}r_{p,e}$ is the equivalent pipe radius, and λ_{grout} is the thermal conductivity of the grout.

For the sake of completeness, we cite one of the most common expression for the evaluation of the 1-U borehole thermal resistance. It was proposed by Paul [156] and consists in an empirical correlation between R'_b,r_{BHE} and $r_{p,e}$: therefore, it can be considered as a one-dimensional model. It reads [152]:

$$R'_b = \frac{1}{\beta_0 \left(\frac{r_{BHE}}{r_{p,e}}\right)^{\beta_1} \lambda_g} \tag{3.40}$$

The values of β_0 and β_1 are given in Table 3.3 for three reference geometries in Fig. 3.29.

Double U-pipe

Similar to the single U-pipe configuration, also the double U-pipe arrangement is converted to an equivalent pipe (see Fig. 3.28). The expression of R'_b is very similar to Eq.

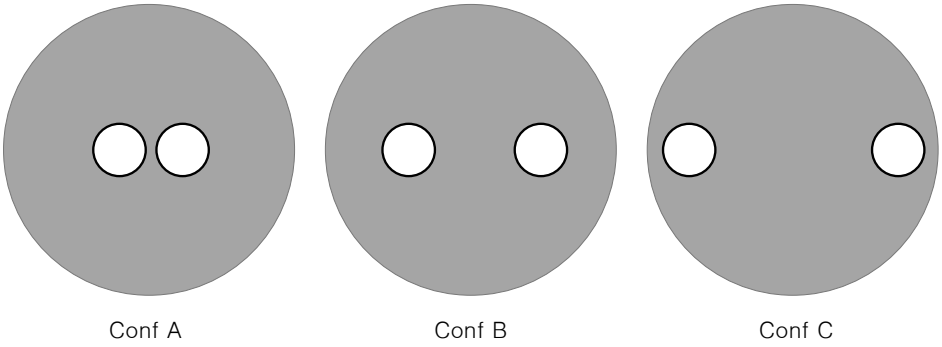

Figure 3.29. Paul test configurations [156].

Table 3.3. Parameters for Eq. (3.40)

Configuration	β_0	β_1
A	20.10	−0.9447
B	17.44	−0.6052
C	21.91	−0.3796

(3.39), except for the equivalent pipe radius value.

$$R'_b = \frac{1}{2\pi\lambda_{grout}} \ln\left(\frac{r_{BHE}}{2r_{p,e}}\right) \tag{3.41}$$

where $2r_{p,e}$ is the equivalent pipe radius.

3.2.2 Two-dimensional models

In two-dimensional models the heat exchange among the ducts and the surrounding ground are evaluated through the so-called *multipole method* [161], [162]. The latter solves the steady-state heat equation within a 2D BHE-soil cross-section imposing the temperature of the fluid within the ducts and the far-field one. There are no restrictions on the ducts number, size or position. The resulting 2-D temperature field is expressed in the form of an infinite series, or *"multipole expansion"*. For better details on the latter subject, the reader can refer to [161], [162].

For typical borehole geometries (see, for instance, Fig.3.27), the temperature difference among the mean temperature at the borehole surface, T_g, and the temperature of the fluid

within each ducts, $T_{w,i}$, can be evaluated through the set of equations (3.42).

$$\begin{cases} T_{w,1} - T_g = R_{1,1}\dot{q}_1 + R_{1,2}\dot{q}_2 + R_{1,3}\dot{q}_3 + R_{1,4}\dot{q}_4 \\ T_{w,2} - T_g = R_{2,1}\dot{q}_1 + R_{2,2}\dot{q}_2 + R_{2,3}\dot{q}_3 + R_{2,4}\dot{q}_4 \\ T_{w,3} - T_g = R_{3,1}\dot{q}_1 + R_{3,2}\dot{q}_2 + R_{3,3}\dot{q}_3 + R_{3,4}\dot{q}_4 \\ T_{w,4} - T_g = R_{4,1}\dot{q}_1 + R_{4,2}\dot{q}_2 + R_{4,3}\dot{q}_3 + R_{4,4}\dot{q}_4 \end{cases} \tag{3.42}$$

where

- q_i is the linear heat flux across the i-th duct wall, $\mathrm{W\,m^{-1}}$;
- $R_{i,j}$ are the first-order terms of the above-mentioned multipole expansion, $\mathrm{K\,W^{-1}}$. $R_{i,j}$ $(i \neq j)$ corresponds to the thermal resistance between the i-th and the j-th duct [149].

Generally, U-pipes are disposed in the borehole symmetrically (see Fig. 3.27), therefore $R_{i,j}$= $R_{j,i}$, $R_{i,i}$= $R_{j,j}$, $R_{1,4}$= $R_{1,2}$, $R_{2,1} = R_{2,3}$ and so on. The expressions of $R_{i,j}$ reads [149], [161], [163]:

$$R_{1,1} = \frac{1}{2\pi\lambda_{grout}} \left[\ln\left(\frac{r_{BHE}}{r_{p,e}}\right) - \sigma \ln\left(\frac{r_{BHE}^2 - x_c^2}{r_{BHE}^2}\right) \right] + R_p \tag{3.43a}$$

$$R_{1,2} = \frac{1}{2\pi\lambda_{grout}} \left[\ln\left(\frac{r_{BHE}}{\sqrt{2}x_c}\right) - \frac{1}{2}\sigma \ln\left(\frac{r_{BHE}^4 + x_c^4}{r_{BHE}^4}\right) \right] \tag{3.43b}$$

$$R_{1,3} = \frac{1}{2\pi\lambda_{grout}} \left[\ln\left(\frac{r_{BHE}}{2x_c}\right) - \sigma \ln\left(\frac{r_{BHE}^2 + x_c^2}{r_{BHE}^2}\right) \right] \tag{3.43c}$$

$$\tag{3.43d}$$

where:

$$\sigma = \frac{\lambda_{grout} - \lambda_g}{\lambda_{grout} + \lambda_g}$$

We note that the generic $R_{i,j}$ depends also on soil thermal conductivity, λ_g. This is due to the assumption of an uniform temperature at the borehole wall, which do not correspond to the real physical situation [152]. The actual angular variation of T_g at the BHE surface is affected by soil conductivity and it is considered through the σ value.

Theoretically, *two-dimensional models* are able to take into account the actual position and the thermal interaction among the pipes inside the borehole, improving the R_b evaluation. However, they are often employed assuming a single average-temperature within the ducts, i.e. $T_{f,1} = T_{f,2} = T_{f,3} = T_{f,4}$ and $q_1 = q_2 = q_3 = q_4$. Therefore, as a matter of fact, these models do not evaluate the thermal interference among the U-legs. However, the overall energy balance can be computed with sufficient accuracy.

The final expressions of 'two-dimensional R_b can be evaluated by means of Eqs. 3.43 and 3.42 [111], [120], [152], [163] depending on U-pipes number.

Single U-pipe

According to the above-mentioned hypothesis, we have $T_{f,1} = T_{f,2}$ and $\dot{q}_1 = \dot{q}_2 = \frac{\dot{q}_{BHE}}{2}$ (symmetry reasons). We obtain :

$$\begin{aligned} R_b &= \frac{\overline{T}_w - T_g}{\dot{q}_{BHE}} = \frac{R_{1,1} + R_{1,3}}{2} \\ &= \frac{1}{4\pi\lambda_{grout}} \left[\ln\left(\frac{r_{BHE}}{r_{p,e}}\right) + \ln\left(\frac{r_{BHE}}{2x_c}\right) + \sigma \ln\left(\frac{(r_{BHE}/x_c)^4}{(r_{BHE}/x_c)^4 - 1}\right) \right] + \frac{R_p}{2} \end{aligned} \tag{3.44}$$

Double U-pipe

In this configuration, under the assumptions of identical temperatures within all the pipes, we have $T_{f,1} = T_{f,2} = T_{f,3} = T_{f,4}$ and $\dot{q}_1 = \dot{q}_2 = \dot{q}_3 = \dot{q}_4 = \frac{\dot{q}_{BHE}}{4} =$ (symmetry reasons). The R_b value can be calculated similarity to single U-pipe:

$$\begin{aligned} R_b &= \frac{\overline{T}_w - T_g}{\dot{q}_{BHE}} = \frac{R_{1,1} + 2R_{1,2} + R_{1,3}}{4} \\ &= \frac{1}{8\pi\lambda_{grout}} \left[\ln\left(\frac{r_{BHE}}{r_{p,e}}\right) + 2\ln\left(\frac{r_{BHE}}{\sqrt{2}x_c}\right) + \ln\left(\frac{r_{BHE}}{2x_c}\right) - \sigma \ln\left(\frac{r_{BHE}^8 - x_c^8}{r_{BHE}^8}\right) \right] + \frac{R_p}{4} \end{aligned} \tag{3.45}$$

Eq. (3.45) is different from the one reported in Zeng *et al* and other similar works [57], [149], [163]. However, we are quite confident about its derivation procedure.

3.2.3 Quasi-three-dimensional models

As above-mentioned, two-dimensional models neglect the thermal interference between the U-legs as they are not able to evaluate the temperature profile of the fluid within the ducts. In some configurations (i.e. reduced shank space) or operative conditions (i.e. low flow rate) the deviation from actual R_b can be significant. In relation to the latter topic, Zeng *et al.* [149], [164] introduced the quasi-three-dimensional approach. This method aims to take into account the thermal interaction between the different legs of the U-pipe by considering the fluid temperature variation along the borehole depth. The term "'quasi-three-dimensional"' refers to the assumptions of a negligible axial heat conduction and a uniform borehole temperature.

Single U-pipe

A linear transformation of Eqs. (3.42), in case of a single U-pipe, leads to the following set of equations:

$$\begin{cases} \dot{q}_1 = \frac{T_{w,1}-T_g}{R_1^{\triangle}} + T_{w,1} - T_{w,2}R_{1,2}^{\triangle} \\ \dot{q}_2 = \frac{T_{w,2}-T_g}{R_2^{\triangle}} + T_{w,2} - T_{w,1}R_{1,2}^{\triangle} \end{cases} \tag{3.46}$$

where:

$$R_1^{\triangle} = \frac{R_{1,1}R_{2,2} - R_{1,2}^2}{R_{2,2} - R_{1,2}} \quad R_2^{\triangle} = \frac{R_{1,1} - R_{2,2} - R_{1,2}^2}{R_{1,1} - R_{1,2}} \quad R_{1,2}^{\triangle} = \frac{R_{1,1}R_{2,2} - R_{1,2}^2}{R_{1,2}}$$

Therefore, since the axial heat conduction is neglected, the 1D energy balance of the fluid can be written for upflow and downflow leg as [111]:

$$\begin{cases} \dot{q}_1(z) = -\dot{m}_w c_w \frac{dT_{w,1}}{dz}(z) & = \frac{T_{w,1}(z) - T_g}{R_1^{\triangle}} + \frac{T_{w,1}(z) - T_{w,2}(z)}{R_{1,2}^{\triangle}} \\ \dot{q}_2(z) = \dot{m}_w c_w \frac{dT_{w,2}}{dz}(z) & = \frac{T_{w,2}(z) - T_g}{R_2^{\triangle}} + \frac{T_{w,2}(z) - T_{w,1}(z)}{R_{1,2}^{\triangle}} \end{cases} \quad (0 \leq z \leq H_{BHE}) \tag{3.47}$$

The boundary conditions of the problem (3.47) are:

$$\begin{aligned} T_{w,1}(0) &= T_{w,in} \\ T_{w,1}(H) &= T_{w,2}(H_{BHE}) \end{aligned}$$

Due to the symmetric disposal of the U-pipe inside the borehole, the thermal resistances $R_1^{\triangle}$,$R_2^{\triangle}$.$R_{1,2}^{\triangle}$ can be simplified as follows:

$$\begin{aligned} R_1^{\triangle} &= R_2^{\triangle} = R_{1,1} + R_{1,2} \\ R_{1,2}^{\triangle} &= \left(R_{1,1}^2 - R_{1,2}^2\right) / R_{1,2} \end{aligned}$$

The solution of Eq. (3.47) can be derived by means of Laplace transformation. The detailed calculation procedure can be found in [165]. The expression of the temperature profile in the two pipes are shown in Eqs. 3.48.

$$\Theta_{w,1} = \cosh(\beta Z) - \frac{R_{1,1}}{\sqrt{R_{1,1}^2 - R_{1,2}^2}} \left[\frac{R_{1,2}}{R_{1,1}} \frac{\cosh(\beta) - \sqrt{\frac{R_{1,1}-R_{1,2}}{R_{1,1}+R_{1,2}}} \sinh(\beta)}{\cosh(\beta) + \sqrt{\frac{R_{1,1}-R_{1,2}}{R_{1,1}+R_{1,2}}} \sinh(\beta)} \right] \sinh(\beta Z) \tag{3.48a}$$

$$\Theta_{w,2} = \frac{\cosh(\beta) - \sqrt{\frac{R_{1,1}-R_{1,2}}{R_{1,1}+R_{1,2}}} \sinh(\beta)}{\cosh(\beta) + \sqrt{\frac{R_{1,1}-R_{1,2}}{R_{1,1}+R_{1,2}}} \sinh(\beta)} \cosh(\beta Z) + \frac{R_{1,1}}{\sqrt{R_{1,1}^2 - R_{1,2}^2}} \left[\frac{\cosh(\beta) - \sqrt{\frac{R_{1,1}-R_{1,2}}{R_{1,1}+R_{1,2}}} \sinh(\beta)}{\cosh(\beta) + \sqrt{\frac{R_{1,1}-R_{1,2}}{R_{1,1}+R_{1,2}}} \sinh(\beta)} - \frac{R_{1,2}}{R_{1,1}} \right] \sinh(\beta Z) \tag{3.48b}$$

where:

$$\Theta_w = \frac{T_w - T_g}{T_{w,in} - T_g} \quad Z = \frac{z}{H_{BHE}} \quad \beta = \frac{H}{\dot{m}_w c_w \sqrt{(R_{1,1} + R_{1,2})(R_{1,1} - R_{1,2})}}$$

We can write the overall heat transfer efficiency, ϵ_{BHE}, and borehole thermal resistance R_b as:

$$\epsilon_{BHE} = \frac{T_{w,out} - T_{w,in}}{T_g - T_{w,in}} = \frac{2\tanh(\beta)}{\sqrt{\frac{R_{1,1}+R_{1,2}}{R_{1,1}-R_{1,2}}} + \tanh(\beta)} \tag{3.49}$$

$$R_b = \frac{H_{BHE}}{\dot{m}_w c_w} \left(\frac{1}{\epsilon_{BHE}} - \frac{1}{2} \right) \tag{3.50}$$

The same results was obtained by Hellstrom [163] who proposed the "*corrected two-dimensional borehole thermal resistance*" R_b^* as:

$$R_b^* = R_b \eta \coth(\eta) \tag{3.51}$$

where:

$$\eta = \frac{H}{\dot{m}_w c_w \sqrt{R_a' R_b}}$$

$$R_a' = \frac{1}{\pi \lambda_{grout}} \ln \left\{ \frac{2x_c \left[\left(\frac{r_{BHE}}{x_c} \right)^2 + 1 \right]^\sigma}{r_{p,e} \left[\left(\frac{r_{BHE}}{x_c} \right)^2 - 1 \right]^\sigma} \right\}$$

It is possible to show that Eq. (3.51) and Eq. (3.50) are identical [152].

The relative error between two-dimensional and quasi-three-dimensional R_b depends on β value [111] (see Eq. 3.52 and Fig. 3.30):

$$\delta = \frac{R_b^{3D} - R_b^{2D}}{R_b^{3D}} \tag{3.52}$$

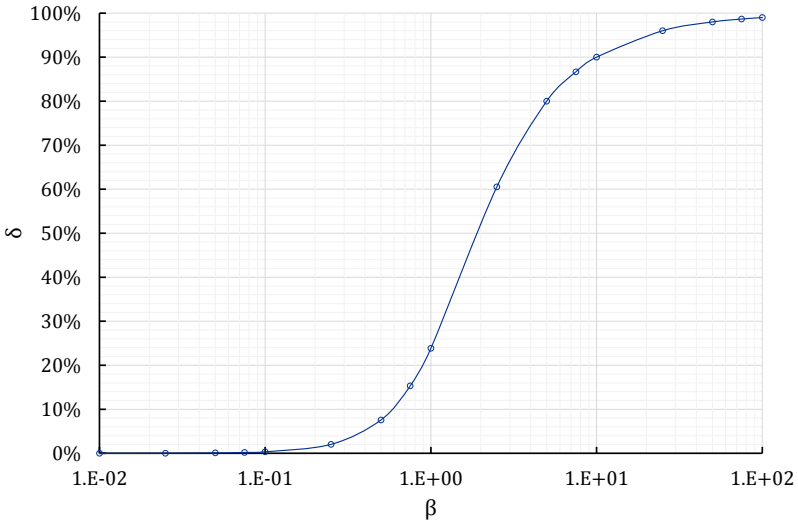

Figure 3.30. Relative error between two-dimensional and quasi-three-dimensional models for single-U R_b evaluation.

We note that δ increases at high β, e.g. high borehole depth, H_{BHE}, or low flow rates $\dot{m}_w$. In general, the relative error increases proportionally to the temperature drop between the inlet and outlet section ($T_{w,in} - T_{w,out}$) due to the greater temperature difference among the U-legs. The latter considerations are coherent with the hypothesis of "two-dimensional models" which assume an unique fluid temperature within all ducts.

Double U-pipe

The quasi-three-dimensional approach for double U-pipe configuration has been firstly developed by Zeng *et al.* [149]. Similarly to the single U-pipe configuration, the axial heat conduction is neglected and the temperature at the borehole wall is assumed uniform: therefore, the 1D energy balance of the fluid within the ducts can be written as:

$$\begin{cases} \dot{q}_1(z) = \pm\dot{m}_w c_w \dfrac{dT_{w,1}}{dz}(z) \\ \qquad = \dfrac{T_{w,1}(z) - T_g}{R_1^{\triangle}} + \dfrac{T_{w,1}(z) - T_{w,2}(z)}{R_{1,2}^{\triangle}} + \dfrac{T_{w,1}(z) - T_{w,3}(z)}{R_{1,3}^{\triangle}} + \dfrac{T_{w,1}(z) - T_{w,4}(z)}{R_{1,4}^{\triangle}} \\ \dot{q}_2(z) = \pm\dot{m}_w c_w \dfrac{dT_{w,2}}{dz}(z) \\ \qquad = \dfrac{T_{w,2}(z) - T_{w,1}(z)}{R_{2,1}^{\triangle}} + \dfrac{T_{w,2}(z) - T_g}{R_2^{\triangle}} + \dfrac{T_{w,2}(z) - T_{w,3}(z)}{R_{2,3}^{\triangle}} + \dfrac{T_{w,2}(z) - T_{w,4}(z)}{R_{2,4}^{\triangle}} \\ \dot{q}_3(z) = \pm\dot{m}_w c_w \dfrac{dT_{w,3}}{dz}(z) \\ \qquad = \dfrac{T_{w,3}(z) - T_{w,1}(z)}{R_{3,1}^{\triangle}} + \dfrac{T_{w,3}(z) - T_{w,2}(z)}{R_{3,2}^{\triangle}} + \dfrac{T_{w,3}(z) - T_g}{R_3^{\triangle}} + \dfrac{T_{w,3}(z) - T_{w,4}(z)}{R_{3,4}^{\triangle}} \\ \dot{q}_4(z) = \pm\dot{m}_w c_w \dfrac{dT_{w,4}}{dz}(z) \\ \qquad = \dfrac{T_{w,4}(z) - T_{w,1}(z)}{R_{4,1}^{\triangle}} + \dfrac{T_{w,4}(z) - T_{w,2}(z)}{R_{4,2}^{\triangle}} + \dfrac{T_{w,4}(z) - T_{w,3}(z)}{R_{4,3}^{\triangle}} + \dfrac{T_{w,4}(z) - T_g}{R_3^{\triangle}} \end{cases} \tag{3.53}$$

where:

$$R_1^{\triangle} = R_{1,1} + R_{1,3} + 2R_{1,2}$$

$$R_{1,2}^{\triangle} = R\frac{R_{1,1}^2 + R_{1,3}^2 + 2R_{1,1}R_{1,3} - 4R_{1,2}^2}{R_{1,2}}$$

$$R_{1,3}^{\triangle} = \frac{(R_{1,1} - R_{1,3})\left(R_{1,1}^2 + R_{1,3}^2 + 2R_{1,1}R_{1,3} - 4R_{1,2}^2\right)}{R_{1,3}^2 + R_{1,1}R_{1,3} - 2R1,2^2}$$

It is worth recalling that due to symmetry reasons, we have: $R_{i,i}^{\triangle} = R_{j,j}^{\triangle}$, $R_{i,j}^{\triangle} = R_{j,i}^{\triangle}$, $R_{1,2}^{\triangle} = R_{1,4}^{\triangle}$, $R_{2,1}^{\triangle} = R_{2,3}^{\triangle}$, and so on.

The sign $\pm$ in Eqs. (3.53) depends on the condition whether the fluid flows in the same direction as the z-coordinate: when the fluid moves downwards along the channel the sign is positive, and vice versa. Different flow circuit arrangements will lead to different flow directions, however, in this Thesis we refer only to the configuration in Fig. 3.31 (i.e.1-2,3-4).

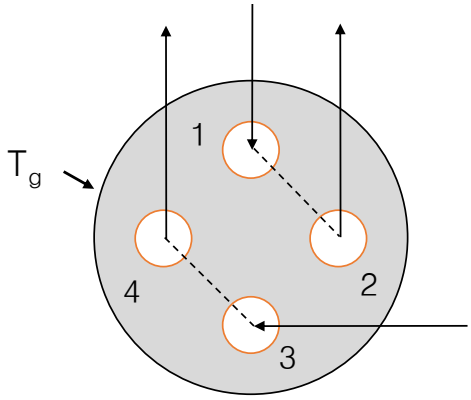

Figure 3.31. Considered double U-loops configuration (*1-2,3-4*)

Zeng *et al.* solved the set of equations (3.53) by means of Laplace transforms [149], [166]. Unfortunately, their final formulas are affected by some calculation errors [152]; therefore, we do not report the analytical expressions proposed by Chinese researchers.

The same approach was adopted by Eslami-nejad and Bernier [166] to develop the analytical model of the heat transfer process within a double U-pipe with two independent loops, i.e. when the two U-loops have different supply temperatures and/or flow rates. Although the different boundary conditions, we can rearrange the final expression proposed by Eslami-nejad and Bernier to obtain the analytical expressions of ϵ_{BHE} and R_b in the 1-2,3-4 parallel configuration (see Fig. 3.31).

According to the above-cited work, the expression of the temperature profile in the four

pipes are shown in Eqs. 3.54.

$$\Theta_{w,1} = \Theta_b - \Theta_b \cosh(\beta Z) + \frac{2\Theta_b S_{1,2} + S_1 [\Theta_{w,2}(0) + \Theta_{w,4}(0)]}{2\beta S_1 S_{1,2}} \sinh(\beta Z) + \exp(-\eta Z) \tag{3.54a}$$

$$\Theta_{w,2} = \Theta_b - \Theta_b \cosh(\beta Z) + \frac{\Theta_{w,2}(0) + \Theta_{w,4}(0)}{2} \cosh(\beta Z) + \frac{(S_{1,2} + S_1)[\Theta_{w,2}(0) + \Theta_{w,4}(0)] - 2\Theta_b S_{1,2}}{2\beta S_1 S_{1,2}} \sinh(\beta Z) + \frac{\Theta_{w,2}(0) - \Theta_{w,4}(0)}{2} \exp(\eta Z) \tag{3.54b}$$

$$\Theta_{w,3} = \Theta_b - \Theta_b \cosh(\beta Z) + \frac{2\Theta_b S_{1,2} + S_1 [\Theta_{w,2}(0) + \Theta_{w,4}(0)]}{2\beta S_1 S_{1,2}} \sinh(\beta Z) - \exp(-\eta Z) \tag{3.54c}$$

$$\Theta_{w,4} = \Theta_b - \Theta_b \cosh(\beta Z) + \frac{\Theta_{w,2}(0) + \Theta_{w,4}(0)}{2} \cosh(\beta Z) + \frac{(S_{1,2} + S_1)[\Theta_{w,2}(0) + \Theta_{w,4}(0)] - 2\Theta_b S_{1,2}}{2\beta S_1 S_{1,2}} \sinh(\beta Z) - \frac{\Theta_{w,2}(0) - \Theta_{w,4}(0)}{2} \exp(\eta Z) \tag{3.54d}$$

where:

$$S_1 = R_1^* \qquad S_{1,2} = \frac{R_{1,2}^*}{2} \qquad S_{1,3} = \frac{R_{1,3}^*}{2}$$

$$R_1^* = \frac{\dot{m}_{w,duct} c_w R_1^{\triangle}}{H_{BHE}} \qquad R_{1,2}^* = \frac{\dot{m}_{w,duct} c_w R_{1,2}^{\triangle}}{H_{BHE}} \qquad R_{1,3}^* = \frac{\dot{m}_{w,duct} c_w R_{1,3}^{\triangle}}{H_{BHE}}$$

$$\beta = \sqrt{\frac{1}{S_1^2} + \frac{2}{S_1 S_{1,2}}} \qquad \eta = \frac{1}{S_1} + \frac{1}{S_{1,2}} + \frac{1}{S_{1,3}}$$

The dimensionless fluid temperature at the outlet section #2, $\Theta_{w,2}(0)$, and #4, $\Theta_{w,4}(0)$, read [166]:

$$\Theta_{w,2}(0) = \exp(-2\eta) + \frac{\frac{2\Theta_b \sinh(\beta)}{S_1 \beta}}{\cosh(\beta) + \frac{\sinh(\beta)}{S_1 \beta}} \tag{3.55a}$$

$$\Theta_{w,4}(0) = -\exp(-2\eta) + \frac{\frac{2\Theta_b \sinh(\beta)}{S_1 \beta}}{\cosh(\beta) + \frac{\sinh(\beta)}{S_1 \beta}} \tag{3.55b}$$

The dimensionless variables Θ_i and Θ_b read:

$$\Theta_i = \frac{\left(T_{w,i}(Z) - T_{1,in}\right) + \left(T_{w,i}(Z) - T_{3,in}\right)}{T_{1,in} - T_{3,in}} \tag{3.56a}$$

$$\Theta_b = \frac{\left(T_g - T_{1,in}\right) + \left(T_g - T_{3,in}\right)}{T_{1,in} - T_{3,in}} \tag{3.56b}$$

where:

- $T_{w,i}$(Z) is the fluid temperature within the i-th duct at the dimensionless depth Z, °C or K;
- $T_{1,in}$ is the fluid temperature at the inlet section #1 , °C or K;
- $T_{3,in}$ is the fluid temperature at the inlet section #3, °C or K;
- $Z = \frac{z}{H_{BHE}}$ is the dimensionless depth.

We note that the the dimensionless variable Θ do not have meaning for $T_{1,in} = T_{3,in}$. In fact, the work by Eslami-nejad and Bernier does not consider this case. However, we can analyze the behavior of Eqs. (3.54), (3.55) and (3.56) when $T_{1,in}$ tends to $T_{3,in}$.

In particular, we note that supposing $T_{1,in} \approx T_{3,in}$ we obtain $\Theta_b >> 1$,$\Theta_{w,1}(Z) = \Theta_{w,3}(Z)$ and $\Theta_{w,2}(Z) = \Theta_{w,4}(Z)$ due to symmetry reasons. Consequently, also the outlet temperature from the two U-pipes are identical, namely $\Theta_{w,2}(0) = \Theta_{w,4}(0)$. Under these conditions, the ratio between the two sub-equations (3.56a) and (3.56b) correspond to the heat transfer effectiveness of the borehole, namely:

$$\epsilon_{BHE} = \frac{\dot{Q}_{1-2} + \dot{Q}_{3-4}}{\dot{Q}_{1-2,max} + \dot{Q}_{3-4,max}} = \frac{T_{w,2}(0) - T_{1,in}}{T_g - T_{1,in}} = \frac{\Theta_1(0)}{\Theta_b} \tag{3.57}$$

Therefore, dividing Eq. (3.55a) by Θ_b we obtain:

$$\epsilon_{BHE} = \frac{\frac{2\sinh(\beta)}{S_1\beta}}{\cosh(\beta) + \frac{\sinh(\beta)}{S_1\beta}} \tag{3.58}$$

The R_b expression can be derived as follows:

$$R_b = \frac{H_{BHE}}{\dot{m_{w,BHE}} c_w} \left(\frac{1}{\epsilon_{BHE}} - \frac{1}{2}\right) \tag{3.59}$$

3.2.4 Numerical models - BHE dynamics

Boreholes thermal behavior can be analyzed also through numerical simulations. Several works have dealt with this subject by employing commercial FEM software or "hand-made" codes [123], [125], [130], [147], [148], [150].

Early models were limited to a 2-D description because of the high number of elements required and to the extreme geometrical aspect ratio of typical boreholes (i.e. *"extreme slenderness"*) [159]. Recently, thanks to the increased availability of computational power, several authors have run full transient 3-D simulations of BHEs behavior [115], [148], [150], [152], [154]. As above-mentioned, in this Thesis we do not deal with numerical simulations as they are are not suitable to be implemented in a straightforward optimization procedure. However, in this section, we want to illustrate the main results of some numerical analysis as they are related to the applicability of the above-mentioned analytical models.

In previous sections, we presented the borehole thermal resistance, R_b, as a steady-state parameter. Consequently, it should be be used only when the BHE internal energy variation rate is almost null, in other words, when BHE operative conditions vary slowly or remain constant for a sufficient-long period of time. A preliminary study by Eskilson and Claesson [167] found that R_b steady-state models should be applied for time-scales longer than:

$$t_b \geq \frac{10 r_{BHE}^2}{4\alpha_g} \tag{3.60}$$

In this section, we discuss the validity of Eq. (3.60) analyzing the results of Bauer *et al.*[148], [159]. This author dealt with a particular technique for the numerical simulation of BHEs thermal performance: the so-called *thermal resistance and capacity model* (TRCM). Despite of traditional numerical methods (i.e. finite differences, finite volume, finite elements), TRCM uses a limited number of nodes: boreholes are modeled with an equivalent circuit of resistances and capacities (see Figs. 3.32 and 3.33).

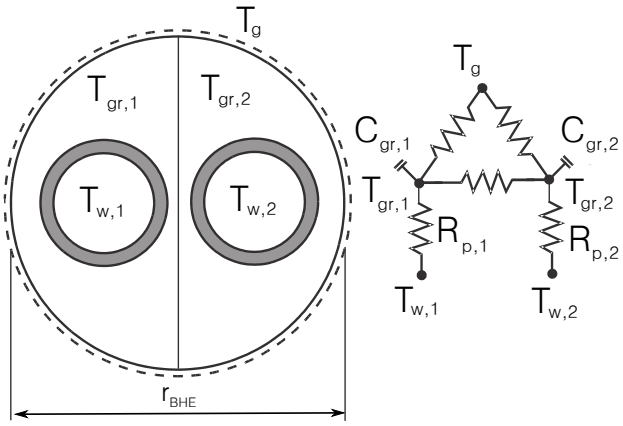

Figure 3.32. Horizontal cross-section and corresponding TRCM for single U-pipe configurations.

Bauer et al. [159] compared the results obtained by TRCMs with a full discredited 2-D finite elements method. A typical double U-loops BHE was simulated ($r_{BHE} = 0.065$

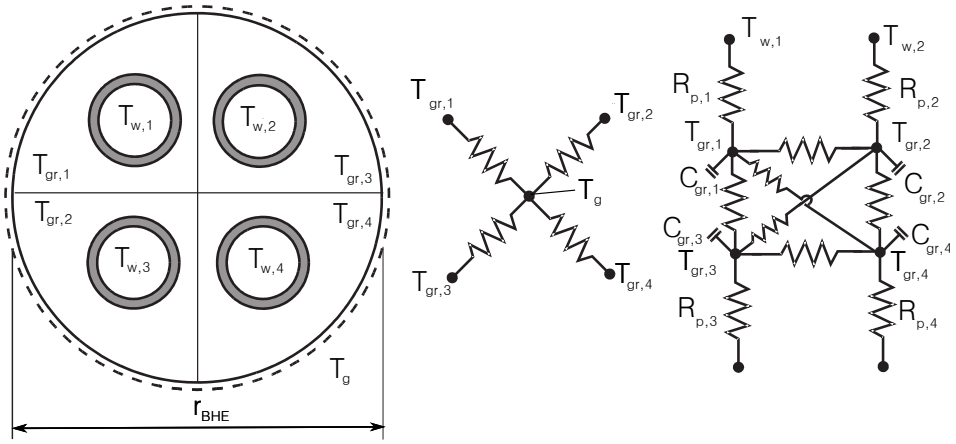

Figure 3.33. Horizontal cross-section and corresponding TRCM for double U-pipe configurations.

m, $\lambda_{grout} = 0.8\ \mathrm{W\,m^{-1}\,K^{-1}}$, and $\alpha_g = 4E-7\ \mathrm{m^2\,s^{-1}}$) setting different fluid temperature within the two U-legs. They found that the two heat fluxes evolution at the BHE wall evaluated through the TRCM and a complete FEM analysis, respectively, differ less than 5 % after 5 minutes of simulated time. Furthermore, the same work showed that steady-state methods (i.e. two dimensional method, section 3.2.2) give the same results of transient models after 10 h of operation. This result is coherent with Eq. 3.60, which indicates, for the same BHE, a t_b value of about 15 h.

The TRCM method can be extended in order to evaluate the axial effects due to heat conduction and fluid circulation. An exhaustive presentation of this method was proposed by Bauer *et. al* [148]. The whole 3-D domain is converted to a 3-D equivalent circuit (see Fig. 3.34); in other words, the original transient 3-D numerical simulation is reduced to a linear system with notable computational savings.

Both BHE and ground domains are fully discredited by means of an equivalent circuit of thermal resistances and capacities. Fig. 3.34 shows how the nodes of one layer (layer i) are connected to the others. Similar lumped-capacitance approaches have been adopted in other works (see for instance [123], [147])

In another work, Bauer *et. al* [148] presented the following test case: they compared the TRCM results with a complete transient 3D analysis of a borehole and a steady-state approach. Through a test case, they showed that the analyzed BHE reaches a steady-state condition after 3 h of operation. Again, this result is coherent with Eq. (3.60) that provides a t_b value of 5 h. Similar results were obtained by [147].

For the purposes of this Thesis, we refer to a time-scale of days or weeks (see section 4.4.1). Therefore, accordingly to the results of the cited BHE transient simulations, we can

conclude that steady-state models and R_b concept are totally appropriate. Our assumption is confirmed by Yang *et al.* [36] who stated that dynamics BHE models are required only to deal with simulation shorter than few hours.

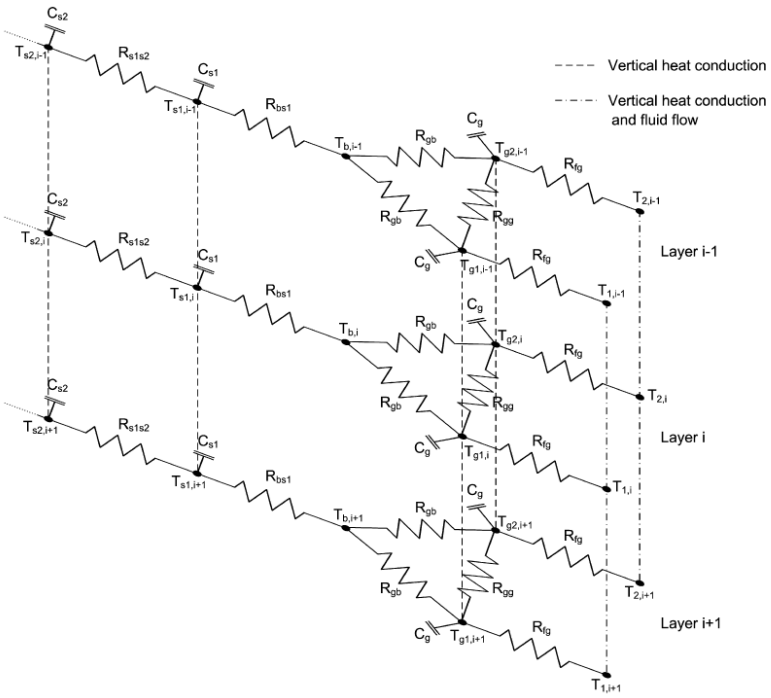

Figure 3.34. Equivalent 3-D TRCM for BHEs transient simulation (after [148]).

3.3 *Ground-coupled heat pump units - GHPs*

The ground-coupled heat pump unit is one of the hardest subsystem to model because of its complex technological structure, the wide range of operative conditions, and the variety of physical phenomena involved (e.g. compression, evaporation, condensation, controls...). Therefore, as for any other GSHP component, we need to find a proper tradeoff between model accuracy and implementation efforts. In other words, we aim to reproduce the behavior of the real system with satisfying accuracy, avoiding an excessive level of detail.

Different approaches have been proposed to simulate heat pumps performances as a function of actual operative conditions. We classify them into two main groups: *cycle-simulation* based models and *black-box* based models. In the former case, the inverse thermodynamic cycle undergone by the operative fluid is reproduced, combining specific

models of each component; in the latter case, instead, the overall performance of the heat pump unit is predicted by an appropriate interpolation of the data provided by HP manufacturers or through empirical correlations.

Cycle-simulation based models

The purpose of this approach is to simulate the evolution of the thermodynamic cycle states (in terms of pressure, temperature, entropy, enthalpy) depending on actual operative conditions. Each component (e.g. evaporator, condenser, compressor) is modeled through semi-empirical correlations (curve-fit approximation) or through energy and mass balances. The single sub-models are then coupled to each other, reproducing the physical assembly of the heat pump unit. For instance, [168]–[174] present some mathematical models for each component, together with brief reviews regarding refrigeration cycle simulations.

Generally, cycle-simulation based models requires numerous and detailed input parameters related to the specific simulated unit. Some of these (e.g. the geometry of the evaporator/condenser, compressor efficiency maps...) are very hard to evaluate, therefore, a tuning phase is often required to match the performance-data provided by manufactures. An high level of accuracy is required also for boundary conditions (e.g source temperatures). It follows that cycle-simulation approach may result impractical during the design phase because of the disproportion among implementation efforts and results accuracy. They seem more appropriate for energy audits and related cost benefit analysis as these kind of analysis require an accurate prediction of the energy fluxes of the specific case study analyzed [173], [175].

Black-box based models

The so-called "black box" principle is generally adopted by technical standards concerning HP performance evaluation. These methods cannot predict the working conditions of the unit components, but they merely calculate the overall energy inputs and outputs of the HP, as a function of the operative parameters, namely operating temperatures and capacity ratios. The reference European and Italian Standards for the calculation of HP energy requirements and efficiencies are the EN $15316-4-2:2008$ [176] and the UNI $11300-4:2012$ [90], respectively. Both of them are based on the interpolation of the data provided by manufacturers and some empirical penalization factors, which depend on actual operative conditions (i.e temperature of the secondary fluids entering the HP device). The software TRNSYS also uses a similar approach [177]. Further empirical black-box models and empirical formulas can be found in literature [146], [178]–[185].

The main parameters influencing HPs performance are the temperatures of the thermal sources and the so called "*capacity ratio*" (CR). Figs. 3.35 shows the declared performances (i.e. $CR = 1$) of a typical current water-to-water heat pump unit as a function of the outlet temperatures from evaporator ($T_{eva,out}$) and condenser ($T_{cond,out}$). We note that in a typical heating operative range ($0 \leq T_{eva,out} \leq 10$ °C) both output capacity and COP vary more

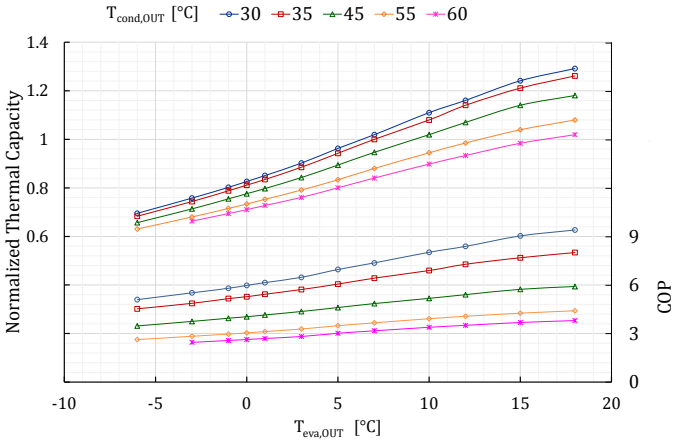

(a) *Heating mode.*

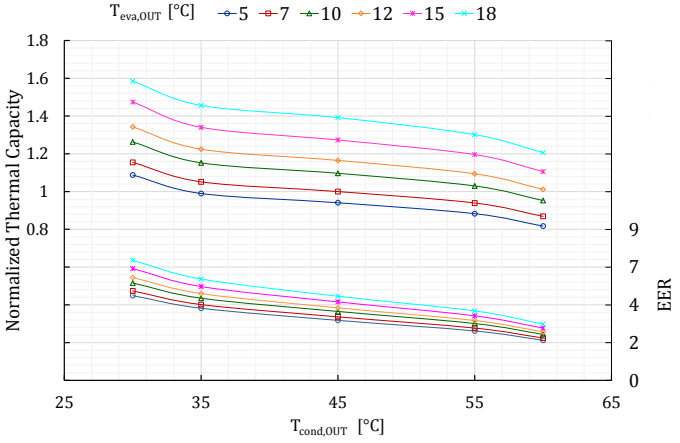

(b) *Cooling mode.*

Figure 3.35. Declared thermal capacity and COP values of a real heat pump, depending on outlet temperature from evaporator and condenser. Thermal output vales were normalized according to its nominal value at rating conditions [12].

than 20 %. In cooling mode, smaller variations occur ($\leq$ 10 %).

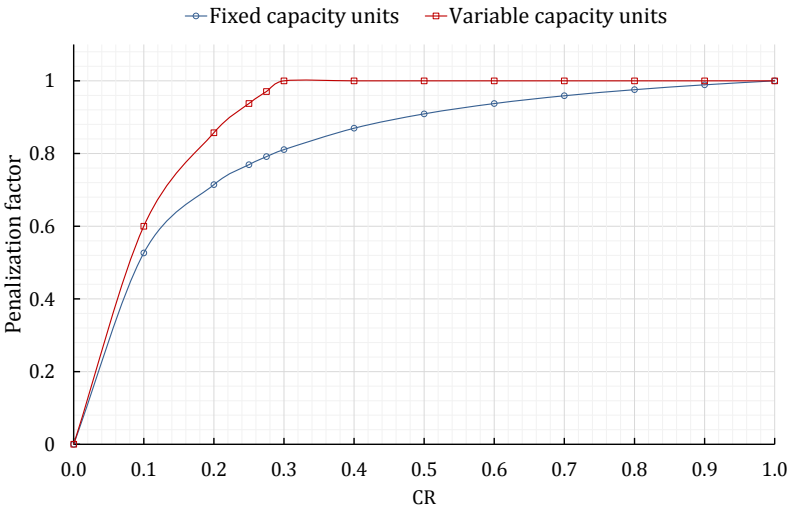

Figure 3.36. COP/EER penalization factor as a function of CR and modulation capability (after [13]).

In the present work, we refer to CR according to the definition given in Eq. (3.61). This formulation is based on the CR definition proposed by EN 14825:2012 [13].

$$CR = \frac{Q_l}{\dot{Q}_{DC}\tau} \tag{3.61}$$

where:

- τ is the duration of the reference time period, h;
- Q_l is the useful thermal energy delivered by the HP during the time τ, kWh;
- Q_{DC} is the maximum capacity of the HP unit, when operating at the temperatures of the thermal sources, averaged in the time τ, kW.

The effect of CR on COP value depends on the choice of the HP unit size and on its modulation capability in response to the evolution of the thermal load. Current technical standards (see, for instance, [13], [90]) evaluate a penalization factor for COP_{DC} and EER_{DC} as a function of CR and implemented control of power output. This factor can be

neglected for variable capacity control units[4], at least until CR is greater than the lower limit of the control range (see Fig. 3.36).

The typical form of the most common expression used to evaluate the HP performances at different operating conditions reads [13], [90], [146], [179], [181], [183]:

$$\dot{Q}_{E/C} = \dot{Q}_{E/C,nom} \quad f_T \quad CR \tag{3.62a}$$

$$COP = COP_{nom} \quad f_T \quad f_{CR} \tag{3.62b}$$

$$f_{CR} = a_0 + a_1 CR + a_2 CR^2 + \ldots + a_n CR^n \tag{3.62c}$$

$$f_T = b_0 + b_1 T_{cond,out} + b_2 T_{eva,out} + b_3 T_{cond,out}^2 + b_4 T_{eva,out}^2 + b_5 T_{eva,out} T_{con,out} \tag{3.62d}$$

where:

- $\dot{W}$ is the actual power use, W;
- $\dot{Q}_{E/C,nom}$ is the nominal thermal output, W;
- COP_{nom} is the nominal coefficient of performance (or EER in cooling mode);
- f_{CR} is the penalization factor due to the actual capacity ratio (see Fig. 3.36). Here, we reported a polynomial expression of f_{CR}, however, any other fitting equation can be used;
- f_T is the penalization factor due to the actual operating temperatures, °C or K.Here, we reported a quadratic approssimation of f_T, however, any other fitting equation can be used;
- $T_{cond,out}$ is the leaving temperature from HP condenser;
- $T_{eva,out}$ is the leaving temperature from HP evaporator;
- $a_0, a_1, a_2, b_0, b_1, b_2, b_3, b_4, b_5$ are parameters that can be obtained from the manufacturers data-sheets;

Madani *et al.* [169] discussed the required GSHP model complexity on the basis of the performed analysis: they concluded suggesting the use of cycle-based models, however, they recognized that black-box approach results in satisfactory results in GSHP performance evaluation. Carbonell *et al.* [186] consider black-box models as a proper approach when the operative conditions are close to the rating conditions reported in the manufacturer's data-sheets; on the other hand, the cycle-simulation approach, being based on a physical description of the system, should be used to reproduce off-design performance conditions.

According to the aims of this work, we consider *cycle-based* methods too complex to be applied at the earliest stages of a design process. These kind of methods need accurate models of each HP component and all parameters and boundary conditions should be available with sufficient accuracy. Moreover, according to aims of this work, we need to avoid complex formulations that would be impractical within the following optimization procedure (see Chapter 4).

4 Variable capacity control units are those devices able to change the output thermal power by modulating the compressor speed.

4 Proposed methodology for optimal design of ground-source heat pump systems

The design of every HVAC system aims to figure out the best technological solution to match building needs, both in terms of thermal power and energy. An universal straightforward design procedure does not exist as any specific project has particular characteristics and objectives [187]. Many different subsystems and physical phenomena are involved (e.g. building envelope, heat gains, emission systems, ductwork, control and generation technologies, pumps, fans...). Moreover, designers must face numerous technical, legal and economic specifications and constraints (e.g. energy and economic savings, comfort conditions, indoor air quality (IAQ), environmental restrictions*dot*) which often lead to conflicting objectives [187], [188]. For instance, the reduction of ventilation losses results in significant energy savings, but comfort conditions would be inadequate. Again, the installation of high performance equipment reduces overall energy use (if properly designed), but the related investment could be unfeasible. HVAC designers are always required to investigate optimal tradeoffs among different design and operational alternatives according to the specific context of the project.

The traditional approach to optimal design is know as "*parametric simulation method*" [189]: it consists on a standard sensitivity analysis, in which one or more variables are varied to see the effect on the design objectives while all other variables are kept unchanged. This procedure is repeated iteratively with other variables. This method is often time-consuming because of complex and non-linear interactions of input variables on simulated results.

Regarding GSHP systems, a proper design approach is based on two main compromises:

- Depending on local ground source characteristics, the operation of the GSHP system alters the initial state of the heat source. In other words, the heat exchange between the soil and GHEs decreases/increases the source temperature. We stress the connection among a sustainable exploitation of the ground source and the efficient operation of the GHP, indeed, the ground temperature alteration reduces the heat pump efficiency and several environmental issues (e.g. ground freezing) may occur. Similarly, in groundwater systems,

pumping operation may result in an excessive drawdown[1], increasing pumping energy needs and risking the aquifer depletion.

- Installing large size components (e.g. large GHEs surfaces) limits the alteration of the heat source, as we are reducing the "density" of exploitation. However, this strategy notably increases the investment costs and the resulting economic savings could not be sufficient to repay the initial expenditure. We note that the capacity ratio of the GHP unit (see section 3.3) is an important indicator also for economic evaluations: low CR values generally imply limited economic savings (i.e. operational costs) with respect to large installation costs (i.e. large size equipment). This issue has prompted the development of the so-called *hybrid systems* (see section 2.2), which share the thermal load among the ground source and back-up generators.

It follows that GSHP design can be seen as an optimization process, in which design variables have to be calculated according to their impact on final system performances. In the next sections, we will discuss the formulation and a suitable solution strategy to the optimization problem.

4.1 *Thermodynamic features of GSHPs operation: an illustrative analytical example*

The existence of an optimal level of exploitation of the geothermal source, corresponding to the best synergy among GSHP unit and back-up generators, can be shown by means of a simple test case. In this section, we will investigate the electrical energy use of a vertical GCHP system, depending on the BHEs size and the share of the building thermal load due to the ground source (control strategy). For the sake of simplicity, we do not consider all the necessary elements of a real design, but we deal with a plain analytical model, in order to highlight the main thermodynamic mechanisms that determine a minimum value of energy consumption. Details on evaluation methodology and system modeling are reported in Appendix 3. Here, we just show the main results of this simplified analysis.

The total electric energy consumption after 20 years of operational life is shown in Fig. 4.1, as a function of the fraction of the building heating load delivered by the ground-coupled heat pump (p_l) and BHEs number. In particular, we used a dimensionless efficiency parameter (ϵ) to normalize and compare the electric energy consumption of the different cases. In the present work, ϵ reads:

$$\epsilon = \frac{E^*_{in}}{E_{in}} \tag{4.1}$$

where E_{in} is the actual electric energy use and E^*_{el} is the electric energy use of an ideal case, in which the only GSHP unit is used (i.e., $p_l = 1$) and the ground temperature remains always constant (i.e., N_{BHE} tends to infinity). In other words, ϵ evaluates the gap between the actual performance and the theoretical minimum energy consumption (i.e.

1 The *drawdown* is the lowering of the fluid level when the well pump(s) operate(s) (see Fig 2.5).

$\epsilon = 1$). This latter concept, also known as "task efficiency", has already been discussed and applied in a previous work [11] and will be further discussed in section 5.2.

The results in Fig. 4.1 show how the ground source is not always convenient with respect to air. Nonetheless, an optimal share of the building load between the two sources can be found. For a given BHEs total depth, the minimum use of electric energy is the result of an optimal compromise between two impairing effects:

- at high p_l, the soil temperature at the borehole surface decreases and can even become lower than air temperature, e.g. when p_l is greater than 0.55 and 4 BHEs are used;
- at low p_l, we are not fully exploiting the ground thermal storage.

We note also that points of maximum efficiency are quite insensitive to a small change in p_l value, which makes the implementation of the control system easier.

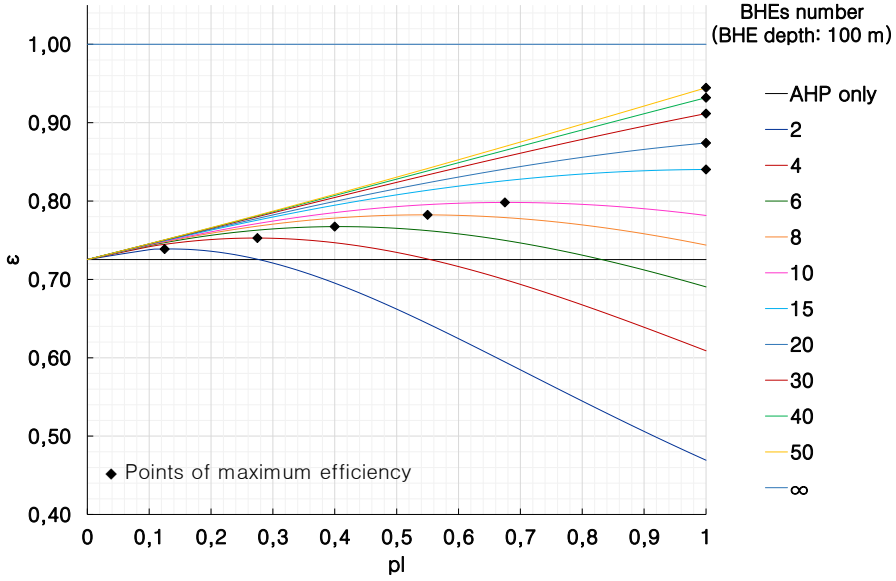

Figure 4.1. Dimensionless efficiency parameter (ϵ) as a function of the building load share provided by the GSHP unit (p_l) and BHEs number.

Regarding BHEs size, we can observe how maximum ϵ points monotonically increases with borehole number, as a consequence of a reduced alteration of the ground temperature; however, energy savings show a saturation trend, hinting that an oversized system is not going to be cost effective.

The conclusions of this small example provide useful thermodynamic indications for

a proper design of GSHP systems. In particular, the results confirm the existence of an optimal synergy between ground and back-up technologies that cand be found according to the local external climate, building thermal load, BHEs depth, and soil thermo-physical properties. Besides, boreholes number and depth have to be chosen as the optimal tradeoff between savings in operative costs and installation investment.

4.2 *The design process as a simulation-based optimization procedure*

The employment of a GSHP system is convenient only when an advantageous values of a selected performance index is obtained. The latter is affected by both design variables and control strategy: indeed, GSHP systems should operate only when working conditions allow them to reach efficiencies higher than back-up technologies. In particular, the ground-coupled system should be sized and managed to work in synergy with other generators: in other words, we need to find the optimal shares of the building thermal load among the available technologies (i.e. p_l value in section 4.1). Consequently, the GSHP design process is not a mere calculation of the size of every component, but is a comprehensive procedure based on the evaluation of the overall performance of the system during its operational life and cost-benefit considerations.

As discussed in section 2.4.3, design methodologies based on matching a reference thermal power demand under nominal conditions are not applicable for a ground-coupled system. First, the thermal power capacity of a heat pump is not defined *a priori*, but depends on the temperatures of the thermal sources (see section 3.3), one of them being the ground. Both the size of the components and the control strategy of the GHP are involved, because the ground temperature is the result of the entire history of heat exchanges (see section 3.1.3). Secondly, the final goal of the design process is not to guarantee that a certain reference thermal power is delivered by the GHP unit, but that the energetic and economic operative performances of the overall system (back-up generators included) are maximized. However, in order to ensure appropriate comfort conditions within the building, the thermal load must be met by the combined effort of GSHP and back-up units (project constraints).

In ground-coupled installations, it is a common practice either to employ different external thermal sources for the heat pumps (i.e. *hybrid systems*) [6], [9], [30], [36], [38], [40], [42], [65], [177], [190] or include back-up generation systems [6], [23], [91], [93], [181], [191]. This notwithstanding, current design methodologies do not provide an explicit focus on the optimal share of load delivered by the GSHP with respect to the total thermal need of the building and neglect the interaction between GSHP and back-up generators performances [91]. Furthermore, the criteria for selecting the GHP capacity is not clearly established: consequently, oversizing often occurs, with the associated energetic and economic disadvantages. Indeed, the main drawback of a GSHP system is its high installation cost, especially due to the execution of the necessary drillings. Hence, optimization of GHP capacity and GHEs dimension is a key-step for maximizing energetic and economic savings.

The design process can be structured as a typical optimization problem subject to project specifications and feasibility constraints. All possible configurations of GSHP components have to be evaluated comparatively, in terms of their impact on the operative performance of the overall system. With the proposed approach, feasibility study, sizing process, performance analysis, and design optimization are hence to be considered as the very same activity. Suitable objective functions refer to both energetic and economic parameters (see section 4.5.1); a multi-objective formulation can be adopted, too.

Several works have dealt with GSHPs optimization; we can group them into three main categories:

1. *optimal design of global system*, where the final goal consists in finding the optimal design parameters (e.g. BHEs number and depth, GHP units number and capacity) with given equipment characteristics [82], [192], [193]. This kind of studies can be classified as "*decision-making problems*" since they do not address any technological issues or development.
2. *optimization of components*, where authors investigate the optimal design and operative parameters of one or more GSHP components (e.g. heat pump cycle parameters such as saturated temperature/pressure of condenser and evaporator, ground loop temperatures and flow rates) [194]–[202];
3. *optimization of control strategy*, where only operative strategy is discussed; control variables, such as temperature set points, speed of compressor, pumps and fans are investigated [177], [203]–[205]

Typical objective functions concern thermodynamic, energetic and economic indexes: entropy generation (exergy destruction) [194], [197], [200], [202], energy savings [177], [195], [196], [201], [203], [204], total costs (initial and operative) [82], [193], [198], [202], [205], and thermoeconomic parameters [192], [199].

Among the mentioned approaches, (1) seems the most appropriate to be implemented in a design methodology for professionals. In particular, we are interested in those formulations aimed at investigating the operative performance of the project through the set-up of a physical-based model [2]. This optimization approach is named "*simulation-based optimization procedure*" as we are dealing with an optimization problem based on the simulation of the operative behavior of the analyzed system [172], [189]. This technique has been largely applied in building energetic studies in recent decades [187], [189], [208].

Fig. 4.2 shows the conceptual scheme of the just-mentioned approach. We note the strict coupling between optimization and simulation procedures: the former calls the latter to evaluate the value of the selected performance index at each iteration. Final optimal values of design variables, are obtained when a proper stopping criteria is met. As in any optimization problem, we need to define:

- the *mathematical formulation* of the optimization problem;

2 Several studies prefer employing data mining approaches to build predictive models (e.g. neural networks) [206], [207] instead of using complex, nonlinear, interconnected formulations to reproduce the numerous physical phenomena occurring during HVAC operation.

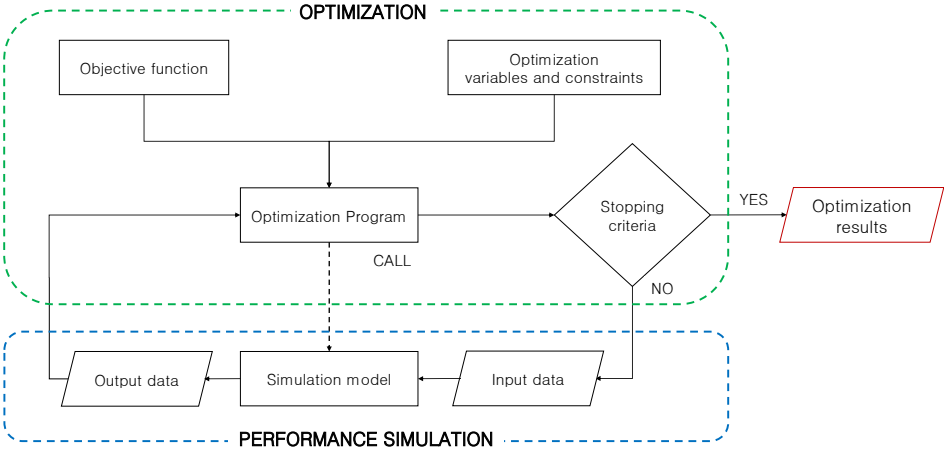

Figure 4.2. The coupling loop between the optimization and simulation routines applied in *simulation-based optimization* studies.

- the *objective function*, i.e. minimizing or maximizing a proper *performance index*;
- *design and/or control variables*, i.e. those parameters that we can actually handle in the specific system analyzed;
- *constraints*, i.e. those unmanageable elements that limit the choice of design variables and system evolution. These restrictions must be satisfied to produce acceptable design solutions according to specified functional and other requirements [209].

In the next sections, we will discuss the above-listed points.

4.3 *General statement of the optimization problem*

Every optimization (or mathematical programming) problem can be stated as follows [209]:

$$\text{Find} \quad \mathbf{X} = \{x_1, x_2, x_3 \dots x_n\} \quad \text{which minimizes } f(\mathbf{X}) \tag{4.2}$$

subject to:

$$g_k(\mathbf{X}) \leq 0, \qquad k = 1, 2, \dots, m \tag{4.3a}$$

$$h_j(\mathbf{X}) = 0, \qquad j = 1, 2, \dots, l \tag{4.3b}$$

$$x_{n,min} \leq x_n \leq x_{n,max} \tag{4.3c}$$

where:

- $\mathbf{X}$ is an n-dimensional vector called *design vector*;

- $f(\mathbf{X})$ is the *objective function*, its image is named *performance index*;
- $g_k(\mathbf{X})$ and $h_j(\mathbf{X})$ are known as *inequality* and *equality constraints*, respectively;
- $x_{n,min}$ and $x_{n,max}$ are the lower and upper bounds of each design variable x_n.

The number of variables and the number of constraints do not need to be related in any way.

As above mentioned, our optimization problem involves two types of design variables: the ones related to the sizing of the system (e.g. GHEs size and number, GHP capacity, ductwork diameters, flow rates within the loops ...) and the ones related to the control strategy (load share among GSHP and back-up generators). We suggest readers pay attention to the terminology used in these sections as it can result ambiguous: the terms "design" and "control" are often interchangeable in the optimization vocabulary as they both refer to those variables that are investigated to maximize/minimize the objective function. The same terms are used in engineering practice to indicate two distinct phases of the the project: the former refers to the system assembly, the latter to the system management. We will try to be as clear as possible.

The basic *optimal control problem* can be stated as follows [209]:

$$\text{find the } \textit{control vector} \quad \mathbf{u}(t) = \{u_1(t), u_2(t), u_3(t) \dots u_k(t)\} \tag{4.4}$$

that minimizes the functional:

$$J = \int_0^\tau R\left(\mathbf{x}(t), \mathbf{u}(t), t\right) dt \tag{4.5}$$

where $\mathbf{x}(t) = \{x_1(t), x_2(t), x_3(t), \dots, x_n(t)\}$ is called *state vector*, t is the time, τ the terminal time of the analysis, R is the objective/cost function. The state variables, $\mathbf{x}$, the control variables, $\mathbf{u}$, and time t are related as:

$$\frac{d\mathbf{x}}{dt} = \mathbf{f}(\mathbf{x}, \mathbf{u}, t) = \begin{cases} \dot{x}_1 = f_1(\mathbf{x}, \mathbf{u}, t) \\ \dot{x}_2 = f_2(\mathbf{x}, \mathbf{u}, t) \\ \dots \\ \dot{x}_n = f_n(\mathbf{x}, \mathbf{u}, t) \end{cases} \tag{4.6}$$

We note that in Eq. (4.4) the $\mathbf{u}$ vector includes also the design variables (engineering speaking), but they are not time dependent.

The optimization problem (4.4),(4.5), (4.6) can be rewritten as follows:

$$\begin{cases} -\frac{\partial \mathbf{H}}{\partial x_i} = p_i & i = 1, 2, \dots, n \\ -\frac{\partial \mathbf{H}}{\partial u_j} = 0 & j = 1, 2, \dots, k \end{cases} \tag{4.7}$$

where

- $\mathbf{H} = \mathbf{f}_0 + \sum_{i=1}^{n} p_i f_i$ is the *Hamiltonian functional*;

- p_i are the *Lagrange multipliers*, also known as the *adjoint variables*.

The optimum solutions for $\mathbf{x}(t)$, $\mathbf{u}(t)$, and $\mathbf{p}(t)$ can be obtained by solving Eqs. (4.6) and (4.7). If we know the initial conditions $x_i = 0$ ($i = 1, 2, 3, \dots n$) and l terminal conditions $x_j(\tau)$ ($j = 0, 1, 2, 3, \dots l$), with $l \leq n$, we have to introduce $n - l$ free-end conditions $p_j(\tau) = 0$ ($j = l + 1, l + 2, l + 3 \dots n$). The latter are named *transversality conditions*.

Solving the set of equations (4.7) is a very hard task, especially for complex, non-linear, constrained, and multi-variable problems. Therefore, in next sections, we will illustrate how the general form (4.4),(4.5), (4.6) can be adapted to find the optimal design and control of GSHP systems. Besides, as in every simulation-based optimization problem, we need to introduce some simplify assumptions in order to keep the problem manageable [206].

4.4 *Simulation strategy*

Each *simulation-based optimization problem* is based on the simulation of the operative life of the analyzed system. In Chapter 3, we reviewed several models for GSHP subsystems. Now, we built an overall model by coupling the above-mentioned sub-models in a unique set of equations. The latter will be used to simulate the behavior of GSHPs during their operational life within the proposed optimization procedure. In other words, in this section we provide a suitable expression of the general function $\mathbf{f}(\mathbf{x}, \mathbf{u}, t)$ in Eq. (4.6).

4.4.1 Preliminary considerations for GSHPs modeling: the quasi-steady-state approach

The following subsystems are considered in GSHP models: ground source, ground heat exchangers (GHEs), ground-coupled loop, ground-coupled heat pump unit, back-up generators, and building end-user loop (Fig. 4.3).

Rigorous dynamic simulation methods would need dynamic models of each component at the shortest simulation time scale. For instance, all the above-cited works based on the uses of building dynamic simulation software (e.g. TRNSYS ©) are based on hourly time-scales. For the sake of coherence, these simulations are (or should be) based on models able to reproduce the short-time response of every GSHP components. A lot of works on GSHP modeling have dealt with this subject (see section 3.2.4 or, for instance, [108], [117], [184], [210]), however, their use at the earliest stages of a design process may not be necessary.

Indeed, during the design phase, we do not need too accurate simulations (in terms of numerical results) as we are not interested in the actual evaluation of the energy requirements of the real system (i.e. energy audits). Such type of analysis would require that all parameters and boundary conditions (e.g. thermo-physical properties of the ground source, thermal load profile, generation units performances) are available with a sufficient level of accuracy. This level of detail is often not available, especially at the

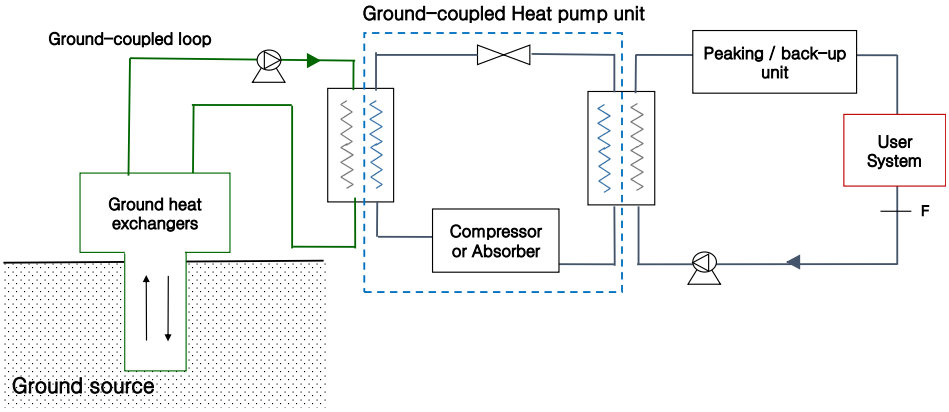

Figure 4.3. Scheme of the model subsystems.

earliest stages of a design process. Furthermore, according to aims of this work, we need to avoid complex formulations that would be impractical within the above-mentioned optimization procedure.

Consequently, we decided to adopt a quasi-steady-state method, calculating energy balances over a sufficiently long time which allows us to neglect internal energy variations (except for the ground) and to employ simpler models.

All the time-dependent inputs and unknown variables of the system have to be considered as constant for the entire duration of the time step, assuming average values. A weekly/monthly time scale ($\approx$ 300-700 h) seems appropriate for our aims, being neither too long to miss significant variations of the ground source temperature, nor too short to require a detailed building and systems usage schedules (generally unavailable during the design phase). Besides, in section 3.2.4, we observed that BHEs steady-state models can be applied for time steps longer than few hour tens. The choice of a monthly-time scale seems appropriate also for building load evaluation as it corresponds to current reference period employed in the main technical standards for building energy analysis (see for instance [94], [97]),

Eqs. (4.8a)-(4.8h) represent the proposed full set of equations for GSHP modeling. The entire system has to be solved at each time step, as common practice in quasi-steady-state approaches. Besides, all the variables are time-averaged values, thought as constant.

The two coefficients, f_H and f_C, were introduced to represent the control strategy of the system. They are defined as the heat delivered/removed to/from the end-user loop divided by the total energy load during a given time step. In other words, selecting a $f_{H/C}$ value corresponds to change the thermal load at the ground source. Such a control can be achieved, for instance, by varying the CR value of the heat pump unit through its capacity control system.

$$
f(\mathbf{x},\mathbf{u},t) = \begin{cases}
Q_{E/C} = Q_g & \text{(4.8a)}\\
Q_{E/C} = \dot{m}_w c_w |T_{w,in} - T_{w,out}| & \text{(4.8b)}\\
Q_{E/C} = F\left(T_{w,out}, T_l, CR\right) & \text{(4.8c)}\\
Q_g = H\left(\dot{m}_w, T_{w,in}, T_g, R_b, H_{BHE}, r_{BHE}, Z\right) & \text{(4.8d)}\\
T_g = S\left(T_g^0; Fo_g, Pe_g, Q_g, H_{BHE}, N_{BHE}\right) & \text{(4.8e)}\\
f_H = \dfrac{Q_E}{Q_l}\left(\dfrac{\langle COP\rangle}{\langle COP\rangle - 1}\right) \quad f_C = \dfrac{Q_C}{Q_l}\left(\dfrac{\langle EER\rangle}{\langle EER\rangle + 1}\right) & \text{(4.8f)}\\
Q_{bk} = B\left(T_l, CR_{bk}\right) & \text{(4.8g)}\\
Q_{bk} = (1 - f_{H/C}) & \text{(4.8h)}
\end{cases}
$$

The set of equations includes:

- Eq. (4.8a), which imposes that the total heat exchanged between the GHEs and the ground, Q_g, is equal to the heat transferred in the evaporator/condenser, $Q_{E/C}$;
- Eq. (4.8b), which is the energy balance for the fluid of the ground-loop at the evaporator/-condenser section;
- Eq. (4.8c), which represents the heat pump unit; the function $F()$ correlates the HP performance to the operative conditions;
- Eq. (4.8d), which represents the GHEs; the function $H()$ correlates Q_g to ground temperature at borehole surface, T_g, GHEs characteristics, and ground-coupled loop operative parameters (flow rate and temperature);
- Eq. (4.8e), which represents the ground source; the function $S()$ correlates T_g to heat fluxes, thermo-physical properties, and groundwater seepage;
- Eq. (4.8f), which introduces the two coefficients, (f_H) and (f_C), which represent the ratio of the heat delivered/removed by the GSHP system and the energy building load during a heating/cooling time step;
- Eq. (4.8g), which represents the back-up system; similarly to the heat pump unit, the performances of the back-up generator depend on its capacity ratio,CR_{bk}, and the supply temperature at the end-user loop, T_l. The function $B()$ characterizes the employed back-up technology;
- Eq. (4.8h), which imposes that the building thermal load (Q_l), up to the end-user distribution system, is given by the sum of the thermal energies delivered/removed in heating/cooling mode by GSHP and back-up generators.

Several works have already simulated the GSHP operative life interconnecting different models of the system components [38], [177], [179]–[181], [211], [212]; simulation software (e.g. TRNSYS ©) are widely used, too [40], [194], [213]–[218]. Therefore, many possible expressions for functions $F()$, $H()$, and $S()$, $B()$ can be found in literature; however, in this Thesis, we refer to the ones reviewed in Chapter 3.

4.5 *Explicit formulation of the optimal design problem*

The choice of a quasi-steady-state approach changes also the general formulation of the optimization problem (4.4)-(4.6). The decisions about the management of the system (optimal f_H and f_C values) have to be made at each stage of the simulation (i.e., at each time step). This kind of optimization problems are called *multistage decision problems* [209].

The general problem 4.4 can be rewritten as follow:

$$J(\mathbf{U}) = \min_{\mathbf{U}} \sum_{n=1}^{N} R\left(\mathbf{u}^n, \mathbf{x}^n\right) \tag{4.9}$$

subject to:

$$\begin{aligned} \mathbf{x}^{n+1} &= f\left(\mathbf{u}^n, \mathbf{x}^n\right) \\ h_j\left(\mathbf{x}^n\right) &= 0 \qquad\qquad j = 1, 2, \dots \\ g_k\left(\mathbf{x}^n\right) &= 0 \qquad\qquad k = 1, 2, \dots \\ u_{m_{min}} &=\leq u_m \leq u_{mmax} \end{aligned}$$

where:

- $\mathbf{u}^n = \left(u_1^n, u_2^n, \dots\right)$ is the vector of control variables at the n^{th} stage[3];
- $\mathbf{x}^n = \left(x_1^n, x_2^n, \dots\right)$ is the vector of state variables at the n^{th} stage;
- $J\left(\mathbf{U}\right)$ is the objective function (also know as the *performance index*);
- $\mathbf{U}$ is the set containing all the $\mathbf{u}^n$;
- $R\left(\mathbf{u}^n, \mathbf{x}^n\right)$ is also called *return function*; it represents the contribution of the n-th stage to the total objective function;
- $f\left(\mathbf{u}^n, \mathbf{x}^n\right)$ is the mathematical model of the system relating the state variables of a stage to the control variables and the state variables of the previous stage (set of Eqs. 4.8a-4.8h);
- $h_j(\mathbf{x})$ is the j^{th} equality constraint;
- $g_k(\mathbf{x})$ is the k^{th} inequality constraint.

4.5.1 Objective functions and performance indexes

As above-mentioned, the overall system performances is the evaluation criteria to figure out the best GSHP desing solution. Therefore, we need a proper return/cost function to quantify these performances.

3 The vector of control variables includes the GHEs depth, BHEs number, GHP capacity and the other time-independent design variables.

Energetic criteria

Primary energy consumption is the main energetic performance index. The use of any technology is energetically convenient when it delivers useful thermal energy with a primary energy utilization lower than alternative solutions. In this case, our performance index is simply given by the total energy use at the end of the project operative life. Different design solutions or components alternatives can be compared according to their impact on final J value.

The expressions of $R(\mathbf{u}^n, \mathbf{x}^n)$ to be used in Eq. (4.9) are:

$$R\left(\mathbf{u}^n, \mathbf{x}^n\right) = \frac{Q_E}{\langle COP \rangle} f_{ep,GHP} + \frac{Q_{bk}}{\eta_{bk}} f_{ep,bk} \qquad \text{(heating mode)} \tag{4.10a}$$

$$R\left(\mathbf{u}^n, \mathbf{x}^n\right) = \frac{Q_C}{\langle EER \rangle} f_{ep,GHP} + \frac{Q_{bk}}{EER_{bk}} f_{ep,bk} \qquad \text{(cooling mode)} \tag{4.10b}$$

$$\tag{4.10c}$$

where f_{ep} is the primary energy conversion factor.

Economic criteria

We can compare economic viability of different GSHP configurations according to their impact on investment profitability. Traditional methods for investment evaluation are applicable. Widely used indicators are net present value (NPV) and related indexes, namely payback period (simple or discounted), internal rate of return (IRR), and profitability index (PI).

All these indexes refer to the so-called "'*total cost*" (TC) [82], [198], [219] calculated by summing investment (including installation), operating, maintenance, and disposal costs. TC is evaluated according to the following equation:

$$TC = C^0 + C_{disp} + C_m + \sum_{n=1}^{N} R\left(\mathbf{u}^n, \mathbf{x}^n\right) \tag{4.11}$$

where:

- C^0 is the initial investment, €;
- C_m is the maintenance cost, €;
- C_{disp} is the disposal cost, €.
- $R\left(\mathbf{u}^n, \mathbf{x}^n\right)$ is associated to the operative costs during the n-th time step.

The expressions of the operative costs to be used in Eqs. (4.11) and (4.9) are:

$$R\left(\mathbf{u}^n, \mathbf{x}^n\right) = \frac{Q_E}{\langle COP \rangle} c_{GHP} + \frac{Q_{bk}}{\eta_{bk}} c_{bk} \qquad \text{heating mode} \tag{4.12a}$$

$$R\left(\mathbf{u}^n, \mathbf{x}^n\right) = \frac{Q_C}{\langle EER \rangle} c_{GHP} + \frac{Q_{bk}}{EER, bk} c_{bk} \qquad \text{cooling mode} \tag{4.12b}$$

$$\tag{4.12c}$$

where c_{GHP} and c_{bk} are the unitary cost (€ kWh^{-1}) of the energy carrier supplying the ground-coupled heat pump and back-up generators, respectively. The ratio between $f_{ep,GHP}$ and $f_{ep,bk}$ is generally different from the ratio between c_{GHE} and c_{bk}, meaning that the optimal sequence of $\mathbf{u}^n$ depends on the choice between the energetic and the economic goal.

We note that economic indexes are inevitably based on energy fluxes during operational life of the system (see Eq. 4.11). Therefore, an accurate simulation of system behavior seems to be the necessary tool also for effective economic evaluations. Other key non-energetic parameters for the economic evaluation are: fares of electric energy and fossil fuels, retail price of the equipment, drilling costs, and availability of convenient financial incentives. We stress that depending on the particular economic context, the same system and the same energy performances can lead to opposite conclusions on economic viability of the project.

Multi-objective optimization

Actually, a real design process needs to investigate energetic and economic criteria simultaneously. This subject could be refereed to the *multi-objective optimization* theory. Several works dealt with multi-criteria optimization strategies in HVAC and HP design (see, for instance, [189], [199], [202], [209], [219]–[221]). We cite three of the most widespread methods for multi-objective optimization applicable to GSHP systems: *Pareto criterion*, *utility function method*, *bounded objective function method*, and *goal programming method*. Details about this topic can be found in [209]. In short, all these multi-objective techniques are based on proper "'weights" or priority lists among considered objective functions. In other words, according to the specific context, designers are asked to define a new objective function on the basis of a given priority level among energy, economic, and other performance criteria.

4.5.2 Design variables and constraints

Table 4.1 shows an overview of the main parameters and variables of each subsystem. We note that some variables affect the behavior of more than a single subsystem, creating a reciprocal influence between the GSHP components. For instance, the evolution of

Table 4.1. List of notable parameters and variables influencing the performance of GSHP subsystems.

Ground source	Ground Heat Exchangers	Ground-coupled loop
Thermophysical properties:	Number, N_{BHE}	Flow rate, $\dot{m}_w$
- undisturbed temperature, T_g^0	Depth, H_{BHE}	Fluid supply temperature, $T_{w,in}$
- thermal conductivity, λ_g	Radius, r_{BHE}	Head losses
- thermal diffusivity, α_g	Arrangement	Pump efficiency, η_{pump}
- porosity, ϕ	Number of U	Pump speed control
- hydraulic conductivity, K	Thermal conductivity of the ducts, λ_p	
- groundwater velocity, v	Thermal diffusivity of grout, α_{gr}	

GHP unit	Back-up generators	End-user loop
Type:	*Type*:	Thermal needs (power and energy)
- electrically-driven	- boiler	Demand evolution
- absorption	- air-source heat pump	Puffer capacity
- endothermic engine-driven	- electric resistance	Load ratio [1]
Nominal capacity, $\dot{Q}_{DC}$	- solar collectors	Delivery Temperature, T_l
Control system:	- cooling tower(s)	
- fixed capacity units (on/off)	Capacity	
- power steps units	Control system	
- variable capacity units	Manufacturer data-sheets	
Manufacturer data-sheets		

[1] Load ratio is the ratio between building peak load and seasonal energy demand. It should not be confused with CR which refers to HP unit (see Eq. 3.61).

end-user energy needs influences the performance of the GSHP unit and, subsequently, the amount of heat exchanged with the ground. The latter – together with BHEs and soil characteristics – influences the temperature evolution of the ground source and, hence, the average temperature of the ground-coupled loop. In conclusion, to simulate a given GSHP system, we have to "solve" all the subsystems concurrently. Ignoring the aforementioned interconnections can lead to significant errors in the evaluation of the actual operating conditions of the system; thus, even detailed sub-models may produce incorrect results.

As above-mentioned, the overall optimization problem involves two types of control variables: the variables related to the sizing of the system (design variables) and the ones related to the control strategy. It is worth recalling to pay attention to the terminology: the terms "design" and "control" should not to be confused with their engineering meanings. Both design (e.g GHEs depth, BHEs number, GHP capacity) and control variables (e.g. CR, temperature and/or flow rates set-points) are referred as "control variables" in optimal multistage decision problem (i.e. the $\mathbf{U}$ set).

The main *control strategy variable* is the capacity ratio (CR) of the heat pump unit. At each time step, we can change the thermal output of the GSHP unit and, consequently, the share of the building load delivered by the GSHP system (i.e. $f_{H/C}$). At some stages, we can also decide to turn off the heat pump and match the thermal load only with the back-up generators.

The *design variables* are not time dependent. This notwithstanding, they have to be evaluated within the optimization process. In addition, the design variables can be divided into two sub-groups: the *continuous variables* and the *discrete variables* (also called design parameters). The continuous variables can assume every value within the allowed range. The discrete variables are instead limited to certain discrete values, such as integer numbers; therefore, different and specific optimization techniques have to be applied.

GSHPs design process includes sources selection, equipment sizing (back-ups included), and apparatus arrangement. The possible GSHP system layouts and the size of the components have to be considered as discrete parameters for the optimization process, even if they cannot be associated to a numerical variable. Indeed, different design alternatives correspond to different $F()$, $H()$, $S()$, $B()$ functions.

Examples of the main variables, parameters and constraints for the optimization of vertical GCHP systems are summarized in Table 4.2. However, we stress that any design process requires a specific formulation of the set of equations (4.8a)-(4.8h) together with the definition of optimized variables and constraints.

4.6 *Proposal of a resolution strategy*

In this work, we propose a methodology for selecting the best design option among a set of possible alternatives. In other words, we are not interested in the technological development of the single GSHP component, but we aim to find the best configuration among current available devices.

Table 4.2. Examples of some notable control variables for the optimization of vertical GSHPs.

	Symbol	Name and comments	Lower and upper bounds
Control-strategy variables			
	CR	Capacity Ratio	*Min*: Minimum value specified by manufacturer *Max*: 1
Design variables			
Continuous variables	H	Borehole depth	*Min*:: 0 *Max*: 100−120 m (suggested values)
	$\dot{m}_w$	Mass flow rate of ground-coupled loop	*Min*:: the flow rate must be large enough to guarantee a Reynolds number of at least 6000 and a fluid velocity within the ducts higher than 0.3 m/s
	$T_{w,in}$	Supply temperature of ground-coupled loop	*Min*:: If pure water flows in the ground-coupled loop, the supply temperature should be a few degrees higher than 0 °C (about 5 °C). This constraint can be removed if a mixture of water and glycol is used
	L	BHEs spacing	Depend on land aviability
Discrete variable or parameters	N_{BHE}	Number of BHEs	Integer value
	$F()$	Function describing GHP capacity and performance (Eq. 4.8c)	
	$H()$	Function describing BHEs design (Eq. 4.8d)	
	$B()$	Function describing back-up generators (Eq. 4.8g)	

In the previous section, we have proposed a suitable formulation for the optimal GSHP design problem (Eq. 4.9). Our approach refers to two classical subjects of optimization theory: *simulation-based optimization methods* and *multistage decision process*. We aim to investigate both design and control variables concurrently according to their impact on the operative performance of the GSHP system.

Although the mathematical formulation of the problem was given in Eq. (4.9), we cannot solve it analytically or through classical optimization techniques: several simplify assumptions and tailored resolution strategies are needed because of the high number of dissimilar and heterogeneous variables (e.g. continuous and discrete variables, design parameters, control strategy, system components) and the high number of time steps (the so-called "'*curse of dimensionality*").

Several reviews have been published on optimization methods applied to building and HVAC design and simulation-based optimization methods [187], [189], [222], [223]. *Genetic algorithms* (GAs) and other direct search methods (e.g. *simulated annealing* and *probabilistic global search lausanne*) are the most used techniques for physics-based models [188], [209], [224], [225]. These methods use the concept of black box optimization in which the objective function does not need to have an explicit mathematical representation. The model of the system is treated as a black-box (see Fig. 4.2), therefore, unlike traditional optimization methods, mathematical characteristics of the problems including convexity or the expression of the gradient [188], [189]. This feature allows to separate optimization and simulation algorithms: all the design variables are concurrently investigated through different iterative methods, which approach the optimal solution progressively.

It is worth recalling that the term "optimization" does not necessarily mean that the globally optimal design is found. Due to the complexity of the problem, the inaccuracy of input an thermo-physical parameters, the necessary approximations of the simulation model and algorithm, the heuristic nature of typical optimization techniques we should refer to "*satisfactory sub-optimal solutions*". In this context, a physical insight of the problem is a fundamental tool to guide the optimization process and outcomes evaluation.

With regards to GSHPs design, we suggest to follow the algorithm described in Fig. 4.4. The optimization problem is split into subsequent phases, fixing a hierarchy among the investigated variables:

1. The proposed optimization methodology starts *creating a set of possible design alternatives* (indicated in Fig. 4.4 as "'*conf*"). Each *conf* element refers to those elements that cannot be quantified with a numerical value (e.g. generators models, equipment arrangement, ductwork layout ...) and to a single possible value of discrete variables. For instance, in each vertical GCHP design we have to decide the GHP model (i.e. a non-numerical design variable) and the BHEs number (i.e. discrete design variable).

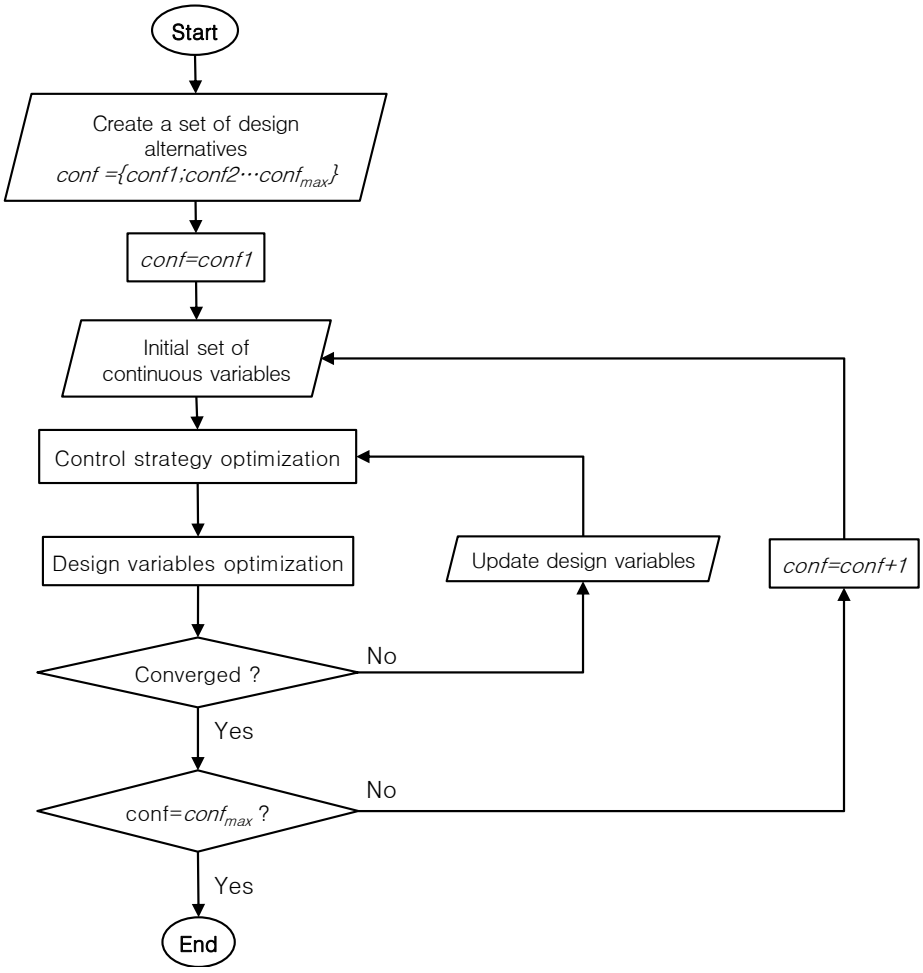

Figure 4.4. Suggested algorithm for the resolution of the optimal GSHP design problem.

The corresponding *conf* set reads:

$$conf = \left\{ \begin{array}{ccc} GHP_1 & - & N_{BHE,1} \\ GHP_1 & - & N_{BHE,2} \\ & \vdots & \\ GHP_1 & - & N_{BHE,max} \\ GHP_2 & - & N_{BHE,1} \\ & \vdots & \\ GHP_2 & - & N_{BHE,max} \\ GHP_3 & - & N_{BHE,1} \\ & \vdots & \\ GHP_{max} & - & N_{BHE,max} \end{array} \right\}$$

As above-mentioned, a physical insight of the problem can significantly reduce the number of tests, saving computational time and efforts. Best *conf* is investigated through an "'*exhaustive enumeration method*"; in other words, we evaluate the performance index value, J for each configuration to find the optimal one;

2. Continuous design variables and control strategy for each *conf* element are investigated in two different steps by an iterative procedure. In this first step we set an initial guesses of continuous design variables;
3. Control strategy is optimized;
4. Continuous variables are optimized according to the previously-found control strategy;
5. The previous two steps are iterated, till a convergence criterion is satisfied;
6. Steps from #2 to #5 are repeated for each *conf* element;
7. The $conf$ element with the best performance index, J, is chosen together with the associated optimal control strategy and continuous design variables value[4].

4.6.1 Design variables optimization

As above mentioned, we adopt different methods for discrete and continue design variables optimization. The former are investigated through an *exhaustive enumeration method* (i.e. "brutal-force" approach) within the $conf$ set. The latter can be investigated by means of any derivative-free methods (e.g. pattern search methods, simplex algorithm) without particular critical issues to be discussed.

4 We can base our choice on the same criterion used during the previous optimization steps or, alternatively, we can adopt a new one. The latter issue will be discuss in section 5.1.

4.6.2 Control strategy optimization

Theoretically, the optimal control in multistage decision problems can be solved by direct application of the classical optimization techniques. However, this requires the number of variables to be small, the functions involved to be quite simple, without strong discontinuities, and with a limited number of local minima. Specific approaches can be found in literature regarding optimal control analysis (i.e. "*mathematical programming*"): three of the most popular multistage programming technique are briefly illustrated hereafter. In particular, we discuss their applicability to GSHPs design.

Dynamic programming

Dynamic programming (DP) is the reference mathematical technique for solving *multistage decision problems* [209], [226]. When applicable, DP reduces the dimension of the solution space, decomposing the original problem in a sequence of N single decision problems. In other words, we do not need to solve a N-dimensional problem, but N one-dimensional problems. Indeed, DP solves problem stages sequentially including one stage at time and solving one-stage problems until the overall optimum has been found. This procedure can be based on a *backward* or *forward induction* process, where the first stage to be analyzed is the final/first stage of the problem and problems, moving back/forward one stage at time until all stages are included [226]. In other words, the dynamic programming solution is obtained by using an iterative functional equation that determines the optimal design/control at any stage [227] (see Eq. 4.13) [5].

The basis of this recursive optimization is the so-called "*Bellman's principle of optimality*", which states that *"...an optimal policy has the property that, whatever the current state and decision, the remaining decisions must constitute an optimal policy with regard to the state resulting from the current decision"* [209], [226], [227]. Therefore, final objective function (Eq. 4.9) can be rewritten in an iterative forms as follows:

$$J^n\left(\mathbf{x}^n\right) = \min_{\mathbf{u}^n}\left[R\left(\mathbf{u}^n, \mathbf{x}^n, t\right) + \beta J^{n+1}\left(f\left(\mathbf{u}^n, \mathbf{x}^n\right)\right)\right] \tag{4.13}$$

where β is a arbitrary discount factor.

Eq. (4.13) states that the minimum cost at stage n is found by choosing the control vector $\mathbf{u}^n$ that minimize the sum of the cost to be paid at the present stage, $R\left(\mathbf{u}^n, \mathbf{x}^n, t\right)$, and the optimal cost in going to the end from the state $n+1$ that results from applying this control [227].

The resolution of Eq. (4.13) requires the discretization of the state variables $\mathbf{x}$: at each stage, we need to investigate the best control policy for all admissible values of vector $\mathbf{x}$. The number of state variables (i.e. the length of $\mathbf{x}$ vector) should be small, since the

5 Stages do not necessary have time implications. A typical example is the one that relates stages at any intersection among possible route alternatives to go from a point to an other.

computational effort associated with the dynamic-programming approach could result unfeasible (*curse of dimensionality*) [209], [226].

In our GSHP model, we can refer to T_g as the only state variable. To apply DP we need to define a set of admissible values of T_g, say $\mathbf{T}_g = \{3, 3.5, 4, 4.5, \ldots, 34.5, 35\}$°C. Starting from last time step, we investigate the optimal u_N value (i.e. $f^N_{H/C}$) for each element in $\mathbf{T}_g$. Optimal control values $u^{N,*}$ and corresponding return/cost function value $R(\mathbf{u}^*, \mathbf{x})$ are obtained for the last time step depending on T_g^{n-1}. Now, we move backwards investigating the best $f_{H/C}$ value (i.e. $u^{N-1,*}$) for any possible value of T_g^{N-2} according to Eq. (4.13). This procedure is shown in Fig. 4.5

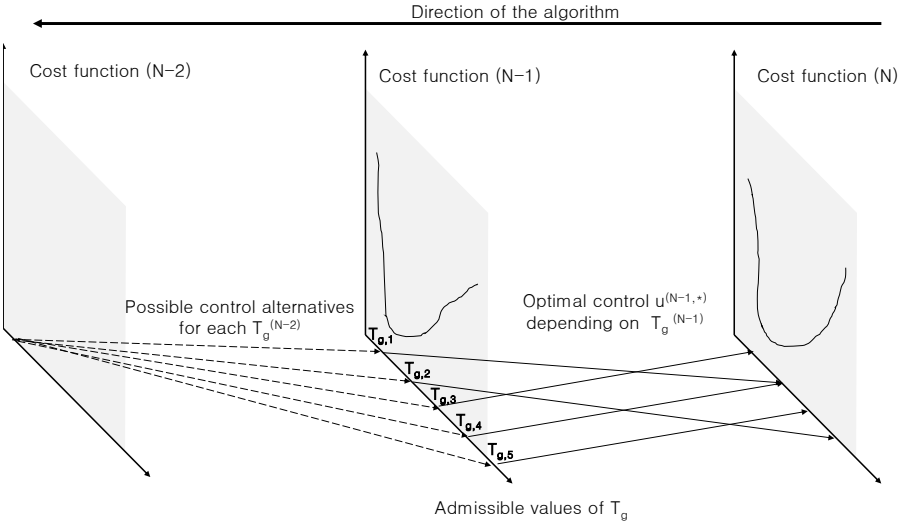

Figure 4.5. Dynamic programming alorithm.

Unfortunately, as shown in Fig. 4.5, a necessary condition for the applicability of the DP technique is that the state vector at the n-th stage depends only on the previous one, i.e $\mathbf{x}^{n+1} = f(\mathbf{x}^n, \mathbf{u}^n)$. In ground source applications, the value of the ground temperature is the result of the entire history of heat exchanges (see section 3.1.3); consequently, DP cannot be applied as both next state vector, $\mathbf{x}^{n+1}$, and return function, $R(\mathbf{u}^n, \mathbf{x}^n)$) depend on all previous steps. De Ridder *et al.* [205] appliey dynamic programming technique to a GSHP optimal control problem, but they used a lumped capacitance model for the ground: i.e. $\frac{dT_g}{dt} = f(T_g, \dot{q}_{BHE}, Fo_g)$. However, this approach does not seems totally appropriate as it neglect the impact of the heat exchange history.

We note that our considerations are not a break of the Bellman's principle of optimality: the discussed limit of applicability regards the evaluation of the state variable (T_g) and cost function without the knowledge of previous time steps. DP is still applicable theoretically,

but ,in these conditions, it equals to an exhaustive enumeration technique.

Genetic algorithms

The most widely-used optimization algorithms in all physics-based models are the so-called *"genetic algorithms"* [187]. GAs are not a pure programming technique, but as above-mentioned, any multistage decision problem can be seen as a N-dimensional optimization problem where each stage n is considered as a design variables. Therefore, GAa can be applied as their notable potential in handling large multidimensional optimization problems.

GAs are based on the principles of natural genetics and natural selection [209]. According to Rao [209], GAs were first presented systematically by Holland [228], but the basic ideas of analysis and design based on the concepts of biological evolution can be found in Rechenberg [229]. Shortly, GAs consist in a stochastic method that can find the global minimum with a high probability. They are well suited for solving problems with mixed continuous-discrete variables, discontinuous and non-convex design spaces; in other words, they are appropriate in all those problems in which standard optimization techniques are inefficient, computationally expensive, and attracted by local optimum points close to the starting point. Genetic algorithms are based on the following features [209]:

- The procedure starts from a set of trial design vectors in the space of solutions, i.e. $\hat{\mathbf{U}} = \{\hat{\mathbf{u}}_1; \hat{\mathbf{u}}_2; \hat{\mathbf{u}}_3, \dots\}$ instead of a single initial vector. The set $\mathbf{U}$ is named *population*, each $\mathbf{u}_i$ vector represents one *individual* characterized by its *chromosomes* (design/control variables) $\mathbf{u}_i = \{u_{i,1}; u_{i,2}; \dots, u_{i,K}\}$. Here, the subscript i refers to individual (design vectors) and the subscript j refers to the single chromosome (single design variable).
  If the number of design variables is K, usually the size of the initial population, $\hat{\mathbf{U}}$, is taken as $2K$ to $4K$ [209]. Trial design vectors are chosen randomly within a range of suitable values, therefore , since many points are used as candidate solutions, GAs are less likely to get trapped at a local optimum.
- GAs use only the values of the objective function (i.e. the *fitness function*) to seek the optimal solution. They do not need any particular elaboration of the optimization problem. The latter is considered as a black box that provides the value of the fitness function corresponding to any design vectors.
- Design vectors are ranked according to their corresponding "fitness function value". Individuals with higher fitness value are selected to "generate" new possible candidates. To draw a comparison with the evolution theory, the individuals with best fitness have a better chance of producing offspring.
- In every new generation, a new set of individuals is produced by selecting randomized parents chromosomes and crossover from the old generation (old population). Although randomized, GAs are not simple random search techniques. They select the best individuals in order to find a new generation with better fitness (objective) function value.

The basic operations of GAs are the *reproduction*, *crossover*, *mutation*, and *immigration*.

Reproduction is a process in which the individuals are selected based on their fitness values. In this process, each individual string (design vector) is assigned a probability of being selected, typically:

$$p_i = \frac{J_i}{\sum_1^P J_i}$$

where J_i is the fitness or objective function value of the i-th individual (the design vector $\mathbf{u}_i$) and P is the size of population $\mathbf{U}$. Thus individuals with higher fitness values have a greater chance of being selected for reproducing. Consequently, highly fit individuals "live and reproduce", and less fit individuals "die". Besides, the individuals in the current generation with the best fitness values automatically survive to the next generation (i.e. "*elite children*").

After reproduction, the **crossover** operation is implemented in two steps. First, two individual (two strings of chromosomes) are selected at random from the mating pool generated by the reproduction operator. Next, a crossover site is selected at random along the string length, and the chromosomes (the single optimization variable value, $u_{i,j}$) are swapped between the two strings following the crossover site. For example, for two design vectors (parents)

$$\mathbf{u}_1 = \{u_{1,1}, u_{1,2}, u_{1,3}, u_{1,4}, u_{1,5}\}$$
$$\mathbf{u}_2 = \{u_{2,1}, u_{2,2}, u_{2,3}, u_{2,4}, u_{2,5}\}$$

If the crossover site is 3, the offspring generation is given by

$$\mathbf{u}_3 = \{u_{1,1}, u_{1,2}, u_{1,3}, u_{2,4}, u_{2,5}\}$$
$$\mathbf{u}_4 = \{u_{2,1}, u_{2,2}, u_{2,3}, u_{1,4}, u_{1,5}\}$$

The new individuals obtained from crossover (offspring) are placed in the new population and the process continues.

Finally, the **mutation** operator is applied to the new strings with a specified mutation probability. A mutation is the occasional random alteration of a chromosome. Thus, in mutation one randomly-selected chromosome changes randomly within a set of possible values. The mutation inserts random individuals within the population trying to escape from local maximum of the fitness value.

Before the selection of the "parents" for the next generation, a set of randomly generated individuals can be added to the population set. Typically, crossover and mutation narrow the search to an area of the design space based on the characteristics of the current population: e.g. they are related to *local minimum*. To keep the search oper for the global minimum, other areas of the solutions space must be explored. This is achieved by bringing in unbiased individuals in the population set, i.e. **immigration** [224].

Many *reproduction*, *crossover*, *mutation*, and *immigration* algorithms are currently applied. Indeed, except some general features, genetic algorithms have always to be "tuned" on the specific optimization problem. For each operation there are more sophisticated models

and methods that are being researched ad developed. More details on GAs can be easily found in literature.

Here, we only stress the probabilistic/stochastic nature of the algorithm. Similarity to other heuristic methods (e.g. simulated annealing) GAs are based on several probability functions that lead to the best individual. As above-mentioned, there is not guarantee that the selected design vector is the global optimum, but it is the most likely according to our initial population, reproduction crossover, mutation, and migration strategies. However, satisfactory results are generally achieved.

We will discuss this topic again in section 4.7 where we will propose an evaluation methodology for optimization results.

The greedy algorithm

With reference to our specific problem (Eq. 4.9), genetic algorithms should be able to find the optimal control sequence $\{f^1_{H/C}, f^2_{H/C}, f^3_{H/C}, \dots, f^N_{H/C}\}$ where N is the time steps number. A above-mentioned, control sequence involves several hundred of design steps (we proposed one $f_{H/C}$ for each month of simulation) with corresponding high computational efforts.

A *greedy algorithm* is a rapid and straightforward alternative in programming problems: this resolution strategy finds the optimal choice at each individual time step "*..in the hope that this choice will lead to a globally optimal solution*" [230]. In other words, in each step we decide for the best solution at the moment, without considering the future evolution of the system (Eq. 4.14).

$$J(\mathbf{U}) = \min_{\mathbf{u}^1}\left[R\left(\mathbf{u}^1, \mathbf{x}^1\right)\right] + \min_{\mathbf{u}^2}\left[R\left(\mathbf{u}^2, \mathbf{x}^2\right)\right] + \ldots + \min_{\mathbf{u}^N}\left[R\left(\mathbf{u}^N, \mathbf{x}^N\right)\right] \tag{4.14}$$

This approach may seem somewhat contradictory with the previous stressed consideration about the importance of the heat exchanges history. Therefore, the effectiveness and the limits of this algorithm in GSHP control problems have been analyzed with respect to genetic algorithms. The outcomes of this analysis will be discussed in sections 4.7 and 5.1. Research activity is still ongoing on this subject.

4.7 *Evaluation methodology for optimization algorithms*

In section 4.6, we pointed out as current wide-spread algorithms for large-dimensional, mixed continuous-discrete variables, and non-convex problems are characterized by a probabilistic approach and high computational efforts (e.g. genetic algorithms). The greedy algorithm may seem a rough strategy as it does not take into account the effects of the current choice on the future evolution of the system. However, its computational savings are very attractive, therefore, in this Thesis, we propose an evaluation methodology to

compare the results of the greedy approach with respect to more complex algorithms. More generally, the proposed methodology can be used to analyze the soundness of the results of any heuristic optimization procedure.

Suppose that the employed optimization algorithm (e.g. GAs or greedy) has found an optimal control/design vector $\mathbf{u}^* = u_1^*; u_2^*; u_3^3, \ldots, u_N^2$ and its corresponding performance index J^*. The basic concept of the proposed evaluation methodology is the following: what are the chances of finding a better solution with respect to the current J^*? We propose to investigate the latter question through the following steps:

1. Define a set of possible control/design vectors, say $\overline{\mathbf{u}}_i = \overline{u}_1; \overline{u}_2; \overline{u}_3 \ldots \overline{u}_K$. In multistage decision problems each u_i correspond to the control strategy in the i-th time step: therefore, we aim to find the best u_i sequence that minimizes/maximizes the selected objective function. We have K^N possible alternatives, with N the length of the sequence. K^N is generally a huge value that makes "brutal-force" (*exhaustive enumeration* [209], [224]) techniques unfeasible even for modern calculators;
2. Start investigating objective function values by testing different random sequences of $\overline{u}_i$. In this way, we obtain a large number of performance indexes J_i, each of one corresponds to the tested sequence $\overline{\mathbf{u}}_i$;
3. Group J_i elements into a proper number of equally spaced containers (bins) and calculate the number of elements in each container. By increasing the number of tests, the frequency distribution tends to a given profile (see Figs. 4.6). When statistics converge (e.g. mean μ and standard deviation σ), we can stop testing further random combinations (see Fig. 4.7);
4. Compare the performance index obtained through our optimization algorithm J^* with μ and σ values: for instance, if we want to minimize a given PI (e.g. primary energy consumption), the $\overline{\mathbf{u}}_i$ sequence associated to the black value in Figs. 4.8 cannot be accepted because there are many better sequences. On the contrary, the $\overline{u}_i$ sequence associated to the green value can be considered a satisfactory result.

Our approach allows also to investigate the probability of finding better $\overline{u}_i$ vectors/sequences than current $\mathbf{u}^*$, hinting the cost-benefits ratio of implementing a more complex and time-consuming algorithm.

The so-called "*statistical interference*" theory consists in those methods used to make decisions or to draw conclusions about a population (i.e. the total solution space of control sequences) using the information contained in a random sample (i.e. the above-mentioned random tests) [231]. In other words, we can associate a probability distribution function (PDF) (e.g. Normal, Log-normal, Beta, Gamma, Student's t, Weibull ...) to the control sequences population. The parameters of interest of the selected distribution can be obtained through the analysis of sample results: e.g. mean, variance and standard deviation of the population can be considered equal to the sample ones [231].

In this work, the decision about the best PDF is taken according to a semi-quantitative method. As above-mentioned, random testing is stopped when the mean and the standard deviation converge (see again Fig. 4.7); at that point, we look for the best PDFfunction depending on the profile of the sample distribution. For instance, in Figs. 4.9, a normal

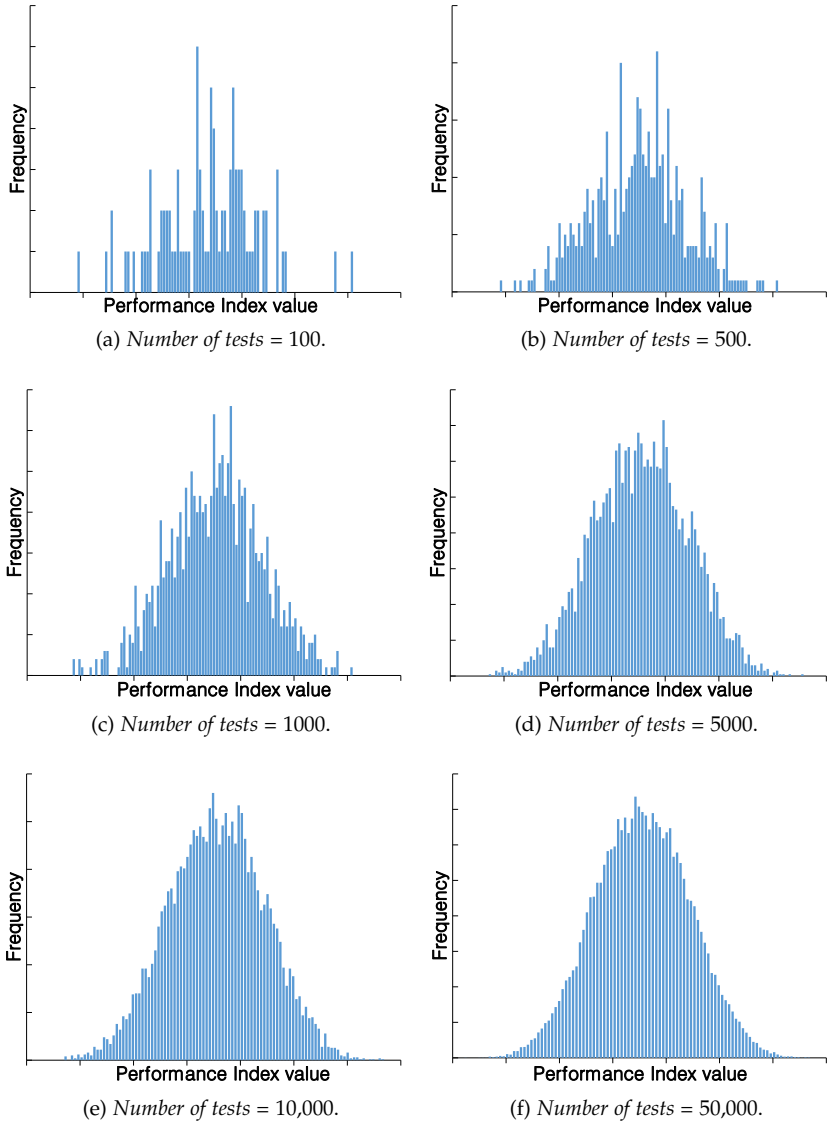

(a) *Number of tests* = 100.

(b) *Number of tests* = 500.

(c) *Number of tests* = 1000.

(d) *Number of tests* = 5000.

(e) *Number of tests* = 10,000.

(f) *Number of tests* = 50,000.

Figure 4.6. Qualitative example of the frequency distribution obtained through 50,000 random test.

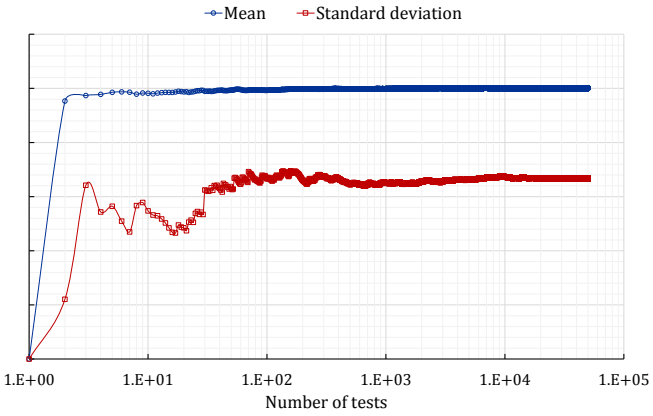

Figure 4.7. Mean and standard deviation value as a function of tests number.

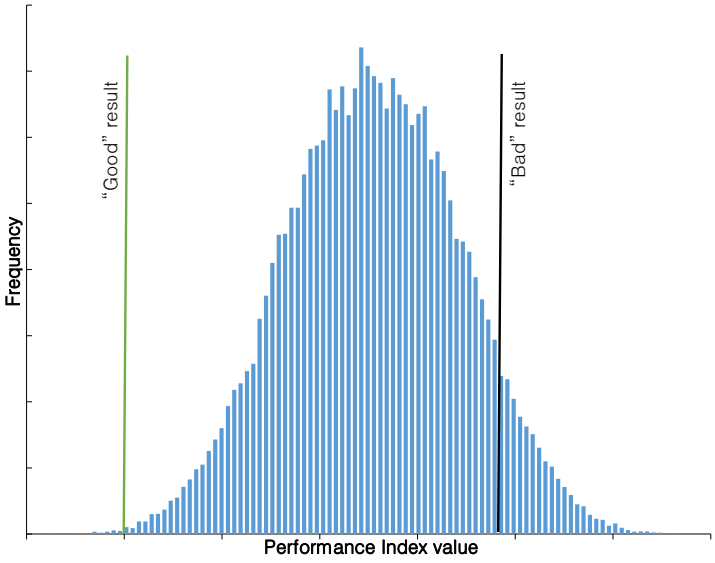

Figure 4.8. Qualitative evaluation of two different optimization results.

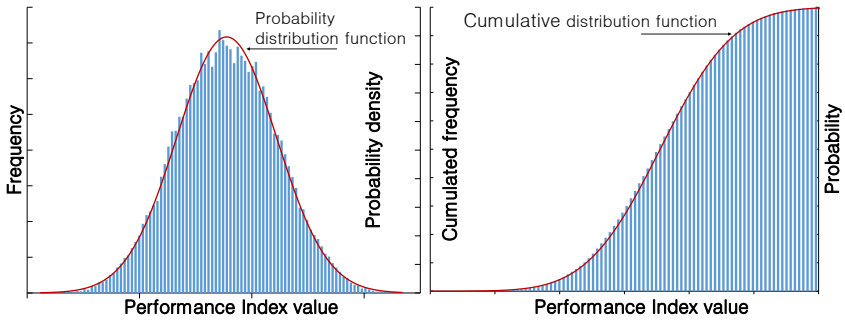

(a) *PDF*. (b) *CDF*.

Figure 4.9. Qualitative examples of PDF and CDF obtained through 50,000 random tests.

(or Gaussian) PDF was chosen. The rigorous procedure leading to the acceptation or the rejection about our hypothesis of the correspondence between the sample profile and the selected PDF is called "*hypothesis testing*". The latter is based on several statistical test methods (e.g. the "*Chi-squared test*"), however, in this Thesis, we do not deal with this subject, leaving its application to future works.

According to the classical theory of probability distributions, the probability of a random variable falling within a particular range of values by the integral (4.15), corresponding to the evaluation of the selected cumulative distribution function (CDF):

$$P\left(a \leq J \leq b\right) = F_J(b) - F_J(a) = \int_a^b f_J\left(\beta\right) d\beta \tag{4.15}$$

where J is the performance index, a is the lower limit of acceptability, b is the upper limit of acceptability , f_J is the selected continuous probability distribution, F_J is the corresponding cumulative distribution function, and β is the auxiliary variable.

In our case, we are seeking the minimum value of J, therefore a is imposed equal to $-\infty$. In other words, the final decision on the acceptance of the control sequence associated to J^* depends on the corresponding $F_J\left(J^*\right)$ value.

In section 5.1 we will apply the proposed methodology to evaluate the applicability of the greedy algorithm to a test case. In particular, we will compare the results obtained by a greedy approach with the results of a GA. Besides, we will investigate the probability of finding a better control strategies.

5 Case studies

The previously illustrated approach to the optimal design and management of GSHPs and all the involved subsystems can be conveniently applied in several contexts: designers can be supported during their professional activity of HVAC systems design, political authorities can investigate proper assessments and criteria for specific incentives, energy efficiency operators (e.g. energy service companies) can investigate the investment profitability of any specific GSHP project, industrial operators (e.g. drilling companies and GHP manufacturers) can analyze of the best economic operative savings to properly decide drilling and equipment prices, researcher can investigate current GSHP systems to seek technological developments and room for improvement. In short, possible applications regards numerous professional, political, economical, and research activities.

This section provides two examples of applying the proposed simulation-based optimization methodology. We aim to show some achievable benefits of the proposed approach without, obviously, claiming to complete the discussion on the GSHPs.

The first case refers to a typical design issue: the heating and cooling loads of a reference building is given and we have to select the best design among a set of four possible alternatives. We will show how the proposed methodology allows to identify the best solution resulting in remarkable energy and economic benefits with respect to traditional methodologies. Besides, we will compare the results of the greedy and generic algorithm in seeking the best control strategy. The evaluation methodology described in section 4.7 applies.

The second case refers to an alternative use of the simulation/optimization routines. In particular, we will investigate the maximum benefits that can be achieved improving the technological level of each component. In other words, we will quantify the impact of the ground source, ground heat exchangers, ground-coupled heat pump unit, and pumping devices on overall GSHPs performances. According to the respective room for improvement, we can figure out the subsystem on which technological development should be focused, the expected benefits and some hints about a possible strategy for technological developments.

5.1 *Case study #1*

In this test case, we illustrate how the proposed optimization methodology can be used for GSHPs design. The results of traditional design methods are compared with the present approach in terms of final energy consumption. Furthermore, concerning optimal control strategies, we apply the evaluation methodology proposed in section 4.7 to compare the results of the greedy approach with respect to a genetic algorithm. Finally, a rough economic analysis was performed parametrically in in order analyze the impact of drilling cost on the investment profitability.

In Chapter 4, we illustrated a conceptual holistic design approach based on a simulation-based optimization procedure. The latter focuses on two main aspects: an interconnected analysis of every subsystem (viz. ground source, borehole heat exchangers (BHEs), ground-coupled loop, heat pump (HP) unit, back-up generators, and end-user loop) and a design aimed at maximizing a proper performance index. In addition, we identified the geothermal heat pump control strategy as one of the main design variables: the share of building thermal load delivered by the GSHP becomes a key parameter to obtain an effective synergy between the geothermal system and the back-up technologies. In conclusion, we formulated an optimization problem based on the global set of equations (4.8a)-(4.8h) (shown again below), which we will now apply to a specific case study.

$$
f(\mathbf{x},\mathbf{u},t) = \begin{cases}
Q_{E/C} = Q_g & \text{(5.1a)}\\
Q_{E/C} = \dot{m}_w c_w |T_{w,in} - T_{w,out}| & \text{(5.1b)}\\
Q_{E/C} = F\left(T_{w,out}, T_l, CR\right) & \text{(5.1c)}\\
Q_g = H\left(\dot{m}_w, T_{w,in}, T_g, R_b, H_{BHE}, r_{BHE}, Z\right) & \text{(5.1d)}\\
T_g = S\left(T_g^0; Fo_g, Pe_g, Qg, N_{BHE}\right) & \text{(5.1e)}\\
f_H = \dfrac{Q_E}{Q_l}\left(\dfrac{\langle COP\rangle}{\langle COP\rangle - 1}\right) \quad f_C = \dfrac{Q_C}{Q_l}\left(\dfrac{\langle EER\rangle}{\langle EER\rangle + 1}\right) & \text{(5.1f)}\\
Q_{bk} = B\left(T_l, CR_{bk}\right) & \text{(5.1g)}\\
Q_{bk} = (1 - f_{H/C}) & \text{(5.1h)}
\end{cases}
$$

5.1.1 Definition of the case study

The present test case concerns a ground-coupled vertical heat exchanger heat pump system (GCHP). We simulated 20 years of operational life by means of the methodology described in section 4.4. The chosen duration of the simulation time step is one month, according to current technical standards (e.g. EN 15316-4-2:2008 [13], UNI/TS 11300-4:2012 [90], and UNI 11466:2012 [57]) on building energy assessment.

Primary energy consumption is the selected performance index. The primary energy factor for electric energy is assumed to be 2.5, in agreement with the European Directive

2012/27/EU on energy efficiency [232].

The optimized variables are: generators configuration (GHP and back-ups), BHEs number and depth (N_{BHE}, H_{BHE}), flow rate within ground-coupled loop ($\dot{m}_w$), and control strategy (monthly values of f_H and f_C). In this work, dealing with a limited number of BHEs (< 10), we decided not to include BHEs spacing among the optimization variables; a typical distance of 8 m was imposed (Table 3), so to avoid heat transfer impairing effects due to interference among the boreholes.

The following subsystems is considered: ground source, ground heat exchangers (BHEs), ground-coupled loop, heat pump unit, back-up generators, and building thermal load. The physical models implemented for each subsystem will be described in the following sections.

Reference building

We chose an ideal office building located in Southern Europe. We did not include the building energy balance in the model, but the monthly profiles of heating and cooling loads are based on a numerical example given in [57], [193]. The global seasonal energy demands almost balance each other, as shown in Table 5.1.

Table 5.1. Monthly heating and cooling loads of the tested office building.

Month	Heating demand[1] kWh	Cooling demand[1] kWh
January	8056	0
February	5834	0
March	3472	0
April	694	0
May	0	3750
June	0	7222
July	0	8611
August	0	8611
September	0	3472
October	694	0
November	4166	0
December	6944	0
Total	29,860	31,670
Peak load	30 kW	40 kW

[1] Delivery temperature of the building end-user loop: 45 °C (heating) and 7 °C (cooling).

Ground reservoir

We assumed the ground as a purely conductive medium with homogeneous, constant, and isotropic properties (Table 5.2). The general Eq. (5.1e) is explained by Eq. (5.2a):

the finite line source (FLS) model was used to calculate the average temperature at the borehole surface (see section 3.1.1). Furthermore, space and time superposition techniques were applied to evaluate the evolution of the BHE field temperature (see section 3.1.3). In this test case, we assumed that all the boreholes have the same radius and depth. The wall temperature of the $\overline{b}$-th borehole reads:

$$T^{n}_{g,\overline{b}}\left(r_{BHE}, n\cdot\Delta t\right) = T^{0}_{g} - \sum_{b=1}^{N_{BHE}}\sum_{i=1}^{n}\frac{\overline{\Theta}_{g}\left(\left|\mathbf{x}_{\overline{b}}-\mathbf{x}_{b}\right|, n\cdot\Delta t, H_{BHE}\right)}{\lambda_{g}}\left[\dot{q}_{b}^{n-i+1}-\dot{q}_{b}^{n-i}\right] \tag{5.2a}$$

where $\dot{q}_{b}^{i}$ is the heat flow per unit length at the i-th time step for the b-th BHE, $\overline{\Theta}_{g}$ is evaluated through Eq. (3.12), and $\left|\mathbf{x}_{\overline{b}}-\mathbf{x}_{b}\right| = r_{BHE}$ when $\overline{b} = b$.

Ground-coupled heat exchangers (vertical BHEs)

We simulated the heat transfer between the boreholes and the surrounding ground (Eq. 5.1d) through the effectiveness method for heat exchanger analysis (see section 3.2). Table 5.2 shows the geometrical and thermal characteristics of the BHEs for a double "U-tube" configuration. As above-mentioned, the borehole thermal resistance (R_b) includes both conductive (pipes and grout) and convective contributions. The latter was evaluated through the Gnielinski formula [233], employing the Petukhov correlation [234] for the friction factor. The conductive contribution of the grout matirial R'_b was evaluated through the Eq. 3.45.

The ground-coupled loop contains pure water, without antifreeze additives: we considered the temperature dependence of its thermo-physical properties, in order to analyze possible differences in heat transfer effectiveness and pumping power between heating and cooling mode.

Table 5.2. Ground thermal properties and BHEs characteristics.

Property	Value	Unit
Ground thermal conductivity	1.7	$\mathrm{W\,m^{-1}\,K^{-1}}$
Ground thermal diffusivity	0.68	$\mathrm{mm^2\,s^{-1}}$
BHE diameter	15	cm
BHE configuration	Double U	
Spacing between boreholes	8	m
Grouting thermal conductivity	1.7	$\mathrm{W\,m^{-1}\,K^{-1}}$
BHE pipe diameter (inner – outer)	2.62 – 3.2	cm
U-legs shank spacing	9.4	cm
Pipe thermal conductivity	0.35	$\mathrm{W\,m^{-1}\,K^{-1}}$
BHE thermal resistance R_b	0.062	$\mathrm{m\,K\,W^{-1}}$

Ground-coupled heat pump unit

We considered electrically-driven HPs with variable capacity control units, namely units able to change the output thermal power by modulating the compressor speed. The heat pump performance (Eq. 5.1c) is evaluated by interpolation of manufacturers' data at the sources temperatures. A penalization factor for the Coefficient of Performance, COP, in heating mode or the Energy Efficiency Ratio, EER, in cooling mode depending on the capacity ratio, CR, is also considered. Specifically, Eq. (5.3) is used: in analogy to [13]:

$$\frac{COP}{COP_{DC}} = \begin{cases} 1, & CR > CR_{min} \\ CR/\left(0.1CR + 0.225\right), & CR \leq CR_{min}. \end{cases} \tag{5.3}$$

where $CR_{min} = 0.25$.

In the present paper, we compared three strategies for the sizing of the ground-coupled heat pump unit. The first approach is based on the building peak thermal load, the second one considers the average power demands of the design months (January and July), and the third strategy considers the average load of the entire heating/cooling season. The characteristics of the selected GHPs are reported in Table 5.3.

Table 5.3. Declared capacities (DC) of the generators [12].

	Ground-coupled unit		**Condensing boiler**	**Air/water unit**
	Heating DC	Cooling DC	Heating DC	Cooling DC
Conf. #1	35.0 kW	40.5 kW	-	-
Conf. #2	10.7 kW	12.1 kW	23.9 kW	29.1 kW
Conf. #3	12.1 kW	8.88 kW	23.9 kW	32.9 kW
Conf. #4	-	-	33.5 kW	44.2 kW

1 - Heat pump sized on the peak load.
2 - Heat pump sized on the average power demand of the cooling month.
3 - Heat pump sized on the average power demand of the cooling season.
4 - "NO-GSHP" solution.

Back-up generator for heating: condensing boiler

As back-ups for the heating seasons, we considered natural gas condensing boilers able to control the output thermal power by means of modulating burners. The boiler performance (Eq. 5.1h) is evaluated by means of manufacturers' data, interpolating at the user-loop temperature and unit capacity ratio (CR_{bk}). Monthly delivered useful thermal energies (Q_{bk}) and boiler efficiencies (η_{bk}) are calculated. The boiler capacity was chosen in accordance with the size of the ground-coupled heat pump unit: the sum of the declared capacity of the two generators must match the peak load of the building. The characteristics of the selected boilers are also reported in Table 5.3.

Back-up generator for cooling: air-cooled water chiller

We considered air/water refrigeration units with variable capacity control units. Energetic performances are evaluated with a similar procedure to the one employed for the ground-coupled unit. In fact, also this method interpolates manufacturers' data at the sources temperatures and considers a penalization factor depending on the unit capacity ratio.

The air units were supposed to operate 10 hours per day (from 9 a.m. to 7 p.m.), corresponding to the office working time. For each month of the cooling season, we calculated the average temperature of the external air during the working time, using the reference hourly temperature distribution proposed by [90].

Hydraulics of the ground-coupled loop

In this test case, both the U-ducts and the BHEs are arranged in parallel. A constant flow rate is imposed in the ground-coupled loop. As a common rule, the electric energy supplied for pumping was included in the evaluation of the overall system COP/EER. We included two main contributions for the head loss: the distributed losses in the BHE ducts and the lumped loss in the HP evaporator/condenser. The former was evaluated through the classical Darcy-Weisbach equation [151], the latter was considered proportional to the square of the flow rate through a constant lumped loss coefficient, resulting from manufacturers' data. A single circulation pump was considered for each simulated configuration. The global efficiency of the circulation pump was obtained by manufacturers' catalogs, at the actual flow rate and hydraulic losses of the ground-coupled loop. The efficiency values span from 35 % to 66 %.

5.1.2 Application of the proposed design methodology

For our case study, we followed the general optimization approach described in Chapter 4, with the specifications illustrated hereafter.

A first guess of BHEs number and depth using traditional design methods (i.e. ASHRAE method) resulted in a total length of about 700 m (7 x 100 m). As above-mentioned (see section 2.4.3), classical methodologies tend to overestimate the boreholes size; therefore, in this test case, the possible BHEs number ranges from 1 to 7.

According to our methodology, possible design alternatives (the *conf* set introduced in section 4.6) are investigated through a sensitivity analysis on the selected performance index, i.e. primary energy consumption. In this test case, we have a *conf* set made of 22 elements given by all the possible combinations of heat generators alternatives (Table 5.3) and N_{BHE} values (i.e. $3 \times 7 + 1$)[1].

1 The "NO-GSHP" solution' was obviously tested once without considering any ground-coupled system

Following the proposed methodology (Fig. 4.4), the optimization of the control strategy (monthly values of f_H and f_C) and continue design variables ($\dot{m}_w$ and H_{BHE}) occurs into two subsequent phases. The proposed routine starts setting the initial value of $\dot{m}_w$ and H_{BHE} and continues iterating control strategy and design variables optimization.

The following assumptions and constraints on design/control variable apply:

- Since pure water is used within the ground-coupled loop, we imposed upper and lower bounds for the supply temperature of the ground-coupled loop, in order to avoid, respectively, overheating of the ground and water freezing in the pipes. Design variables are optimized such that $3\ ^\circ\text{C} \leq T_{w,in} \leq 35\ ^\circ\text{C}$;
- $\dot{m}_w$ has to be large enough to guarantees a fully turbulent regime ($Re_D \geq 6000$) and/or a fluid velocity of at least $0.3\ \text{m}\,\text{s}^{-1}$ within the U-ducts;
- H_{BHE} cannot exceed 100 m to avoid excessive drilling costs.
- $f_{H/C}$ is assumed as a discrete variable. In each time-step it can take one of the following values: $f_{H/C} = \{0, 0.1, 0.2, \ldots 0.9, 1\}$;

Initial set of design parameters

As above-mentioned, a proper physical insight of the phenomena involved in GSHP operation can significantly speed-up the optimization procedure. Fig. 5.1-a displays the various contributions to R_b value at different Reynolds numbers for typical heating and cooling working temperatures. As illustrated, the conductive contribution is the main term, while the convective resistance has a small relevance, especially when the flow is turbulent. Fig. 5.1-b shows the hydraulic pumping power needed to keep a given Reynolds number in the BHEs ducts. As illustrated, the greatest contribution is due to the lumped head loss in the evaporator/condenser of the HP unit. ASHRAE [6] suggest that pumping power does not exceed 3-5 % of the nominal thermal capacity of the ground-coupled heat pump unit. For GHP #3 this limit corresponds to about 500 W. There is not a clear advantage in increasing the fluid velocity in the ground-coupled loop, because the benefits of a lower R_b are small, compared to the corresponding augmentation of pumping energy. Thus, we decided to use the lowest allowable flow rate as the initial value of the optimization procedure.

As for depth of the boreholes (H_{BHE}), Fig. 5.2 shows the heat transfer effectiveness (ϵ_{BHE}) as a function of H_{BHE} at $\dot{m}_w = 0.3\ \text{kg}\,\text{s}^{-1}$ in the U-ducts. The latter flow rate corresponds to a reasonable lower bound for the fluid velocity within the ducts, i.e. $0.3\ \text{m}\,\text{s}^{-1}$. Considering the small relevance of the distributed hydraulic losses to the total pumping energy (see again Fig. 5.1), a deeper BHE is supposed to be always convenient, thanks to the increase of the ϵ_{BHE} value. However, the actual feasibility limit for H_{BHE} is due to the high installation costs; in other words, the additional amount of energy exchanged with the ground does not compensate the higher investment costs. For this reason, in our test case, we set the initial H_{BHE} value for the optimization procedure equal to its upper bound (i.e. 100 m), expecting this to be also the optimal depth.

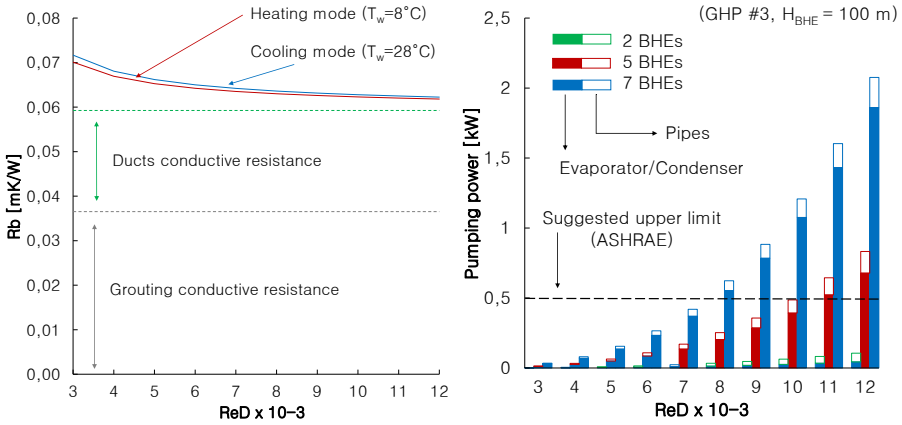

(a) *Borehole thermal resistance.* (b) *Pumping power of the ground-coupled loop.*

Figure 5.1. Borehole thermal resistance (R_b) and pumping power of ground-coupled loop for HP #2 as a function of the Reynolds number in the U-ducts and the number of BHEs ($2-5-7$). The full background of the bars refers to the contribution of the lumped head loss at the evaporator/condenser.

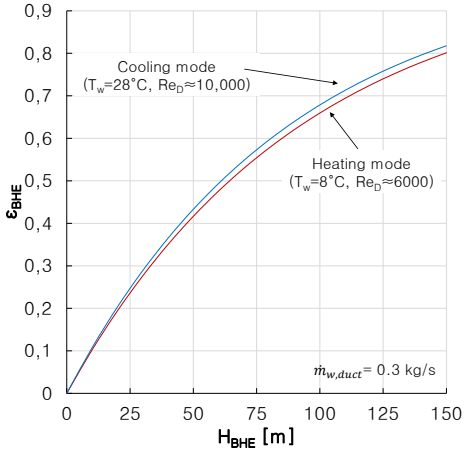

Figure 5.2. Heat transfer effectiveness, ϵ_{BHE}, as a function of the BHE length.

Control policy optimization

As above-mentioned, the control policy optimization problem has a typical structure of a *multistage decision problem* [209]. Nevertheless, two main drawbacks restrict the application of classical optimization techniques to our case: the non-linearity of the physical model (Eqs. (4.8a)-(4.8h)) and the high number of variables corresponding to the number of time steps ("'*curse of dimensionality*"'). Consequently, our preliminary optimization attempt was to apply a *greedy algorithm*, investigating the local optimal choice at each individual time step (see section4.6.2). This technique was then used for all the possible combinations of $conf$ and N_{BHE}. In any case, the resulting optimal control strategies have shown an annual periodicity, indicating that the undesirable effects due to the alteration of the ground temperature are less significant than other technological factors (e.g. CR, bounds on supply temperature at the ground-coupled-loop, head lossess). The latter consideration hints us that the "*greedy algorithm*"' can be considered adequate for the present case study, because of the limited relevance of the ground thermal capacity on the optimal $f_{H/C}$ values. However, as above mentioned, we applied also a *genetic algorithm* to find the best control strategy. In section 5.1.4, we will compare the results of the two different methods through the evaluation methodology proposed in section 4.7.

Design variables optimization

For calculating the optimal values of $\dot{m}_w$ and H_{BHE}, we utilized the "*fmincon*" command of MATLAB© Optimization Toolbox™. The chosen method is the "*interior-point algorithm*", based on [235]–[237]. This problem is a standard optimization of a multivariable function within a fixed interval and does not present critical issues to be discussed. Any derivative-free methods (e.g. pattern search methods) can be applied.

5.1.3 Results and discussion

Optimal design variables and control strategy were found and the corresponding primary energy consumptions were calculated for all configurations as a function of BHEs number (Fig. 5.3). Primary energy consumption in the absence of a GSHP system (i.e., only with back-up generators) is 1183 MWh after 20 years of operation. The latter energy value was used to normalize the other values.

Conf. # 1 needs 5 boreholes to cover the building thermal load alone; with respect to the ASHRAE method based on peak loads, we saved 2 BHEs, even without considering a synergy between GSHP system and back-ups. This result highlights the benefits of simulation-based methods, which provide a better estimation of real GSHP performances. However, the energy savings with respect to the No-GSHP solution are negligible, emphasizing again the issue of GHP oversizing. Moreover, it is worth recalling that our simulation is based on a quasi-steady-state approach: more BHEs could be necessary to match peak needs.

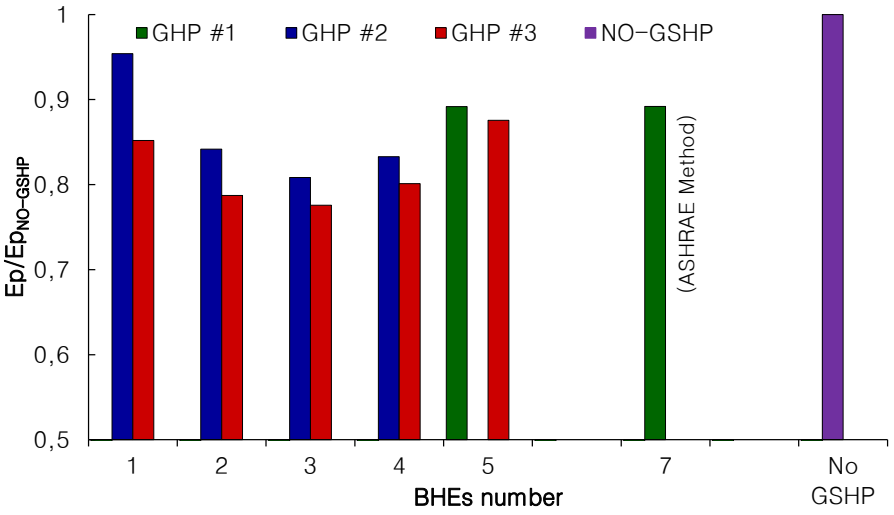

Figure 5.3. Normalized primary energy consumption after 20 years of operation for different numbers of BHEs. All values were normalized on the basis of the energy conspumtion of the "No-GSHP" solution, i.e. 1.183 MWh.

Primary energy consumptions of Conf. # 2 and Conf. # 3 are always lower than the ones of Conf. # 1 and Conf. # 4 (No-GSHP), showing the benefit of an appropriate synergy between geothermal source and back-up technologies. Both GHP2 and GHP3 perform better up to 3 boreholes with an energy consumption of 956 MWh and 917 MWh, respectively. The best configuration (HP3) saves about 22.5% of primary energy with respect to the No-GSHP solution or to the use of the sole geothermal system. Conf. # 2 and Conf. # 3 cannot operate with a BHEs number grater than 4 and 5, respectively, because of the excessive heat losses due to the large flow rate within the U-ducts (i.e $Re_D \geq 6000$ or fluid velocity greater than 0.3 $\mathrm{m\,s^{-1}}$).

The results also provide useful indications for optimal values of BHEs length and flow rate within a geothermal loop. In every configuration, as expected, the optimal flow rate ($\dot{m}_w$) corresponds to its lower bound value, while the optimal borehole depth (H_{BHE}) is its upper bound value.

The configuration of minimum energy consumption corresponds to the best compromise between heat transfer effectiveness and pumping energy consumption. In fact, increasing the number of boreholes and the heat transfer surface, ϵ_{BHE} is augmented: consequently, the ground-coupled loop temperature stays closer to the ground temperature, with corresponding enhancement of <COP*> and <EER*> values. On the other hand, with an increasing number of BHEs, the total flow rate and the hydraulic losses are also increased, with drawbacks on performance due to the additional pumping energy consumption. This trade-off is clearly illustrated in Fig. 5.4, which shows – for configuration #3 – the different

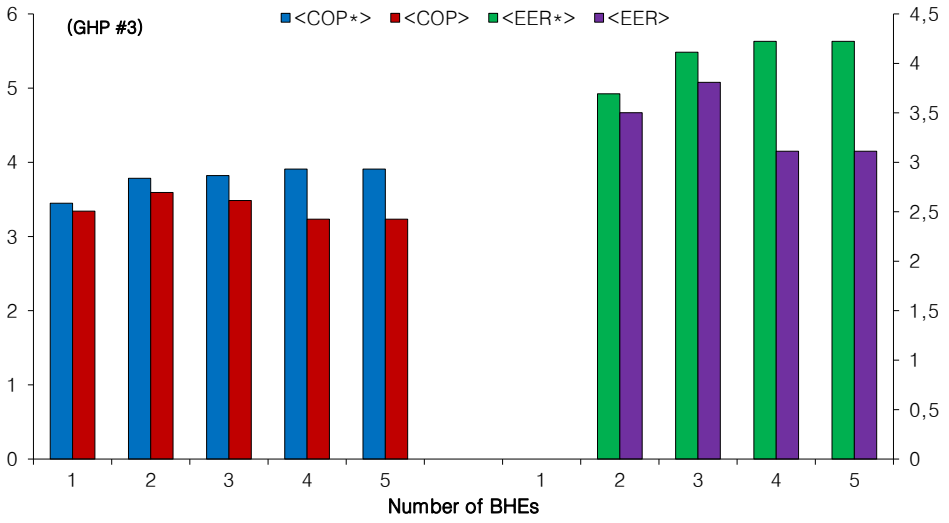

Figure 5.4. Average $< COP^* >$, $< EER^* >$ (only considering the energy required by the compressor), $< COP >$, $< EER >$ (considering the energy required by the compressor and the circulation pump) for 20 years of operation, as a function of the number of BHEs. Cooling service is not provided with a single BHE.

trends of COP and EER values, with and without taking into account the electric energy consumption requested for the fluid circulation.

Besides, Fig. 5.4 shows how, in this test case, the above-discussed technological issues (i.e. CR penalization factor, evaporator/condenser head losses, bounds on $T_{w,in}$ value) are predominant in determining the optimal HP size and BHEs number with respect to the pure-thermodynamics considerations (see section 4.1). The minimum of energy consumptions does not correspond to the limit of exploitation of the ground source, indeed, without the drawback of the head losses in the ground-coupled loop, we could install more BHEs increasing GHP performances and overall system efficiency. Presumably, a different design of the HP ground-side heat exchanger is needed to obtain lower head losses, however, as above-declared, in this Thesis, we do not deal with the development of system equipment. The latter consideration stresses the importance of a proper verification of the compatibility of all GSHP components in order to avoid negative coupling effects.

Further insights on the energy performance and preliminary economic results are given in Figs. 5.5-5.9. Particularly, Fig. 5.5 shows the 20-year evolution of <COP> and <EER> for the best case. The trends are almost periodic, with no significant penalization of the heat pump performance year after year. The contributions of GHP #3 and back-up generators to satisfy the monthly building energy demands are illustrated in Fig. 5.6. We can observe that the geothermal heat pump is supposed to be off during the months of April, May,

June, September, and October, since it would work at an energy efficiency lower than back-ups. Also, GHP #3 is not capable of delivering the entire energy need during the other cooling months, due to its limited capacity; this notwithstanding, the simulations show that this GHP, together with the corresponding back-up generators, is indeed the optimal solution in terms of overall energy performance.

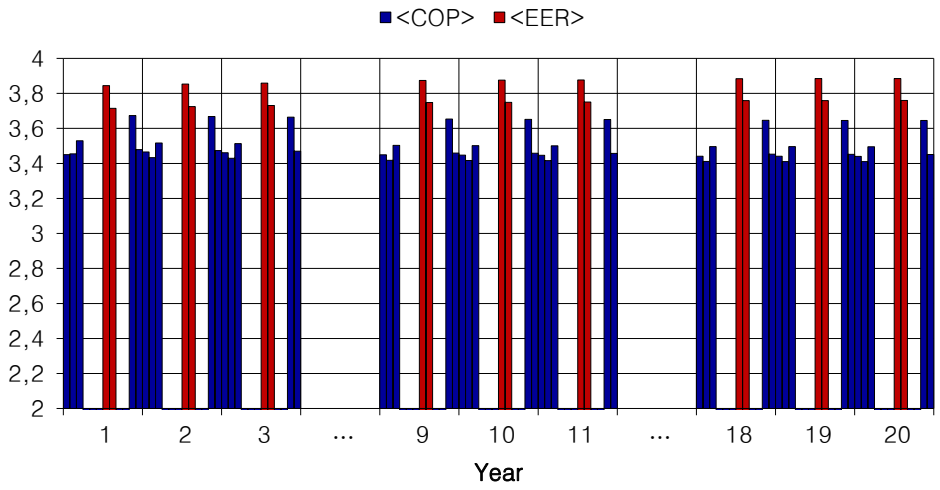

Figure 5.5. COP and EER evolution during 20 years of operation (GHP # 3, 3 BHEs).

Table 5.4 shows the main results of the optimization procedure for the three best configurations and the one resulting from the application of the ASHRAE method.

5.1.4 Application of the proposed evaluation methodology

Table 5.5 shows the optimal control policy obtained through a greedy approach for the best energetic configuration (GHP # 3, 3 BHEs). As above-mentioned, the $f_{H/C}$ sequence shows an annual periodicity, therefore, we can refer to a single year.

The proposed evaluation methodology involves the evaluation of a proper probability distribution function (PDF) to evaluate our chances of finding better controls. 20,000 random control sequences were tested obtaining the normal PDF in Fig. 5.7. The mean value μ is 1.157 MWh and the standard deviation σ is 50 MWh. We note the relative "slenderness" of the distribution as the σ value is two order of magnitude lower than μ. This implies that most of the possible control sequences result in an energy consumption of about μ; according to Eq. 4.15, the probability of finding control sequences with corresponding energy consumptions of $\mu - \sigma$, $\mu - 2\sigma$, $\mu - 3\sigma$, and $\mu - 4\sigma$ is about 0.16, 0.02, 0.001, and 3.17×10^{-5}, respectively.

Table 5.4. Main results of the optimization procedure.

	GHP #2 – 3 BHEs	GHP #3 – 3 BHEs	GHP #3 – 2BHEs	GHP #1 – 7BHEs (ASHRAE)
Total length of BHEs, m	100×3	100×3	100×2	100×7
Total flow rate, kg s^{-1}	1.02	1.02	0.68	2.38
f_H	0.94	0.85	0.65	1.00
f_C	0.84	0.36	0.23	1.00
$< COP >$	3.42	3.48	3.59	2.53
$< EER >$	3.52	3.81	3.50	3.40
Boiler efficiency	1.09	1.09	1.09	-
$< EER >$ air unit	1.88	3.94	3.33	-
CR (heating/cooling)	0.39 / 0.65	0.61 / 0.56	0.47 / 0.56	0.14 / 0.24
CR air unit (heating/cooling)				
Heat flow per unit length (heating/cooling), W m^{-1}	19.4 / 34.5	17.21 / 20.6	19.7 / 31.6	7.3 / 10.3
Primary energy consumption (after 20 years), MWh	956	917	931	1060
Energy savings with respect to the "NO-GSHP" solution	-19.2%	-22.5%	-21.3%	-10.8%

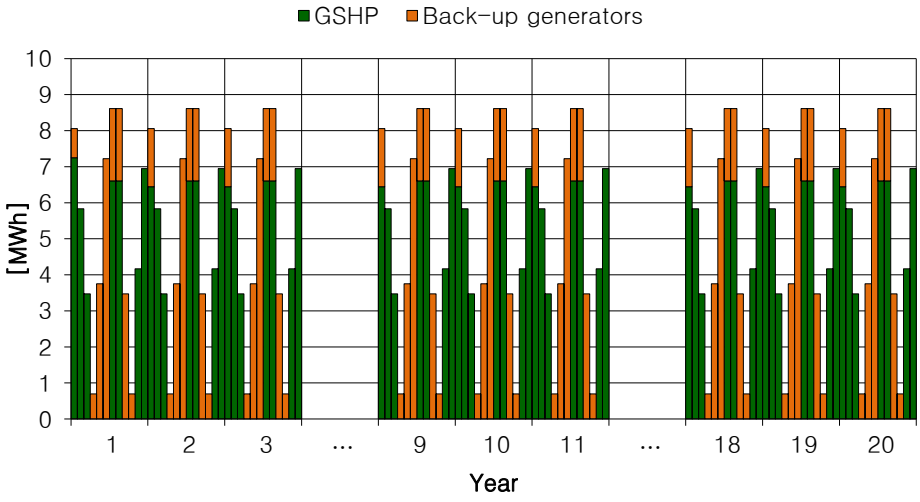

Figure 5.6. Thermal energy delivered to the building during 20 years of operation (GHP # 3, 3 BHEs).

Table 5.5. Optimal control strategy for GHP # 3 and 3 BHEs obtained by means of the greedy algorithm.

	JAN	FEB	MAR	APR	MAY	JUN	JUL	AUG	SEP	OCT	NOV	DEC
$f_{H/C}$	0.8	1.0	1.0	0	0	0	0.8	0.8	0	0	1.0	1.0

Table 5.6. Best control strategy for GHP # 3 and 3 BHEs obtained by means of GAs.

	JAN	FEB	MAR	APR	MAY	JUN	JUL	AUG	SEP	OCT	NOV	DEC
$f_{H/C}$	0.8	1.0	1.0	0	1.0	0	0.6	0.8	1.0	0	1.0	0.9

The energy consumption obtained through the greedy algorithm (917 MWh), which is about 4σ lower than mean value. The probability of finding better sequences, could be estimated in 7.9×10^{-7} approximately. As a matter of fact, the chances of finding better control sequences through a probably-based heuristics method are practically nil. Therefore, we can consider the greedy result more than satisfactory.

Anyway, in this test case, we tested also a genetic algorithm to further demonstrate the soundness of the greedy algorithm. We used the default initial population, reproduction, crossover, mutation and the other options suggested by MATLAB© Optimization Toolbox™. As supposed, the heuristic nature of the algorithm does not allows to find better results: on the contrary, after several trials with different initial populations, the

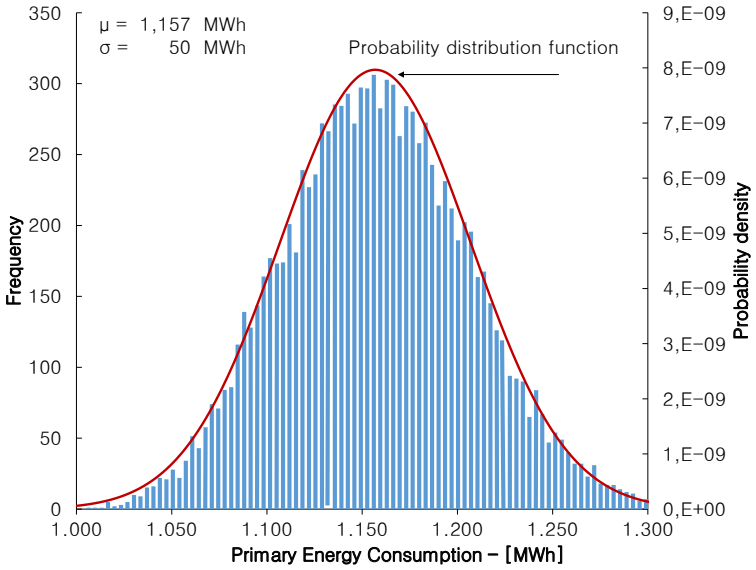

Figure 5.7. Normal PDF resulting from 20.000 random control sequences (μ is 1.157 MWh, σ is 50 MWh).

better result obtained through the GAs employment (1013 MWh) is the one showed in Fig. 5.8, which corresponds to the control sequence illustrated in Table 5.6.

The reasons for the successful results of the greedy algorithm is an ongoing research topic. Indeed, as above-mentioned, the greedy approach seems to contradict the relevance of the history of the heat exchanges. In this test case, heating and cooling loads are quite similar, therefore, we can suppose that the thermal alteration of the ground source is limited. Furthermore, we stress again that an optimal and efficient GSHP design ensures the sustainability of the heat source exploitation, avoiding temperature drifts and reducing the impact of previous operation on remaining working period. However, the latter considerations are not sufficient to fully explain the good results provided by the greedy algorithm. As above mentioned, further research activities are currently ongoing.

5.1.5 Preliminary economic considerations

Fig. 5.9 reports, on a monthly basis, the expenses for natural gas (used by the back-up boiler) and electric energy and the economic savings obtained by means of the GSHP. A rough economic analysis was performed parametrically, in terms of BHEs installation costs, going from 20 to 100 euros per meter of drilling. Other economic parameters are shown in Table 5.8. Investment metrics are calculated neglecting the discount rate and any inflation of prices. Economic savings are evaluated with respect to "NO-GSHP" configuration.

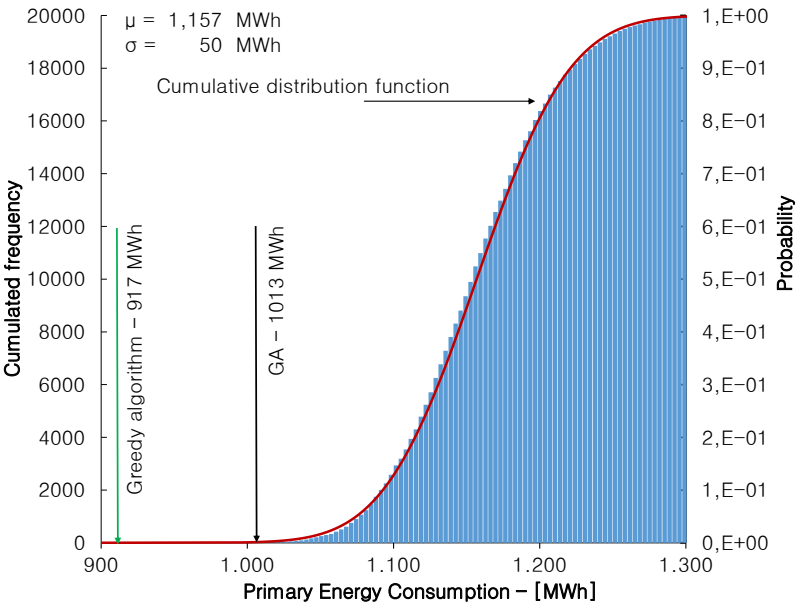

Figure 5.8. Normal CDF resulting from 20,000 random control sequences. The green and black lines indicate the results obtained through the greedy and the genetic algorithm, respectively.

Estimates of simple payback periods (SPP) as a function of BHEs installation costs for the two best energetic configurations (GHP #3 - 3 BHEs and GHP # 2 - 3 BHEs) are presented in Fig. 5.10 and Table 5.7. Furthermore, we included a specific focus on the (GHP # 3 - 2 BHEs) configuration as its final energy consumption is very close to the best one (931 MWh vs. 918 MWh), but one less BHE is drilled.

We note that the highest unitary costs €m^{-1} allowing to obtain a SPP shorter than 20 years are 38 €m^{-1}, 46* €m^{-1}, and 51 €m^{-1}, respectively. Simple net values and profitability indexes at the end of the considered operative life (20 years) are shown in Table 5.8.

5.1.6 Final Remarks

In the present work, we applied the proposed holistic GSHP design methodology described in Chapter 4 to a design case: an office building with both heating and cooling demands. The performed simulations showed that an optimized GSHP system can save remarkable amounts of primary energy, if compared either to conventional technologies (-22.5 %) or to GSHP designs based on covering the peak thermal load, without back-ups (- 11 %).

Table 5.7. Parameters of the economic analysis.

Energy fees	
Assumed unit price of electric energy	0.20 € kWh^{-1}
Assumed unit price of natural gas	0.08 € kWh^{-1}
Retail prices of generators*	
GHPs	
#1	18,500 €
#2	5200 €
#3	4600 €
Boiler	
#2	4000 €
#3	4000 €
#4	5000 €
Air unit	
#2	8500 €
#3	10,000 €
#4	14,000 €

*Prices are purely indicative (not confirmed by the manufacturer).

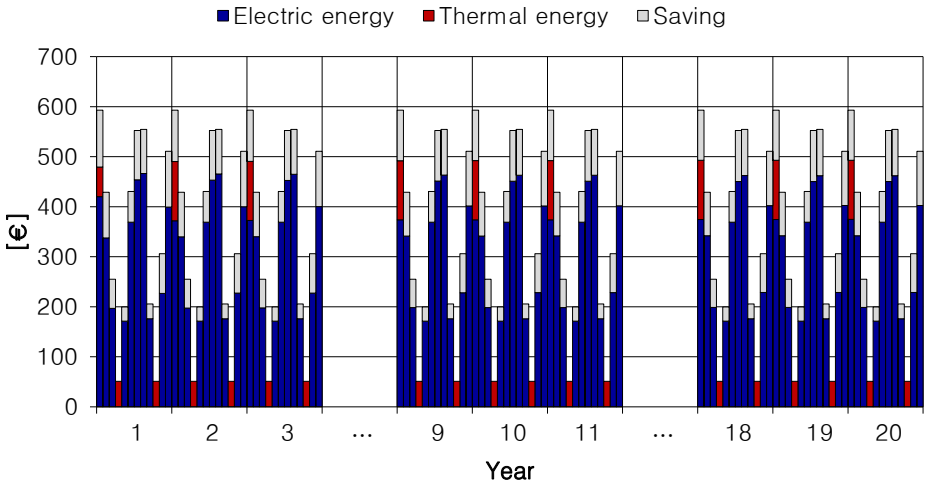

Figure 5.9. Breakdown of expenses for gas and electrical energy and economic savings obtained by the GSHP during 20 years of operation (GHP # 3, 3 BHEs).

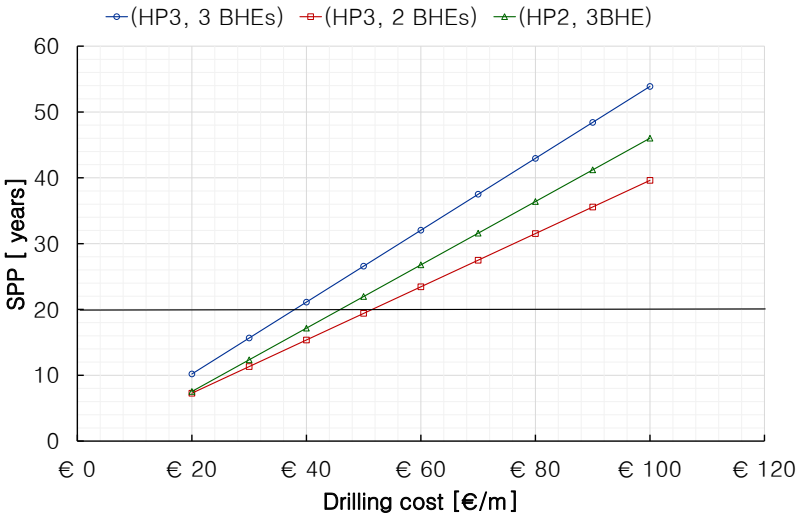

Figure 5.10. SPPs as a function of the drilling costs. The highest unitary costs €m^{-1} allowing to obtain a SPP shorter than 20 years are 38 €m^{-1}, 46* €m^{-1}, and 51 €m^{-1}, respectively.

Table 5.8. Estimated SPPs, simple net values (SNV), and profitability indices (PI) for the optimal configurations.

	GHP #2 – 3 BHEs			GHP #3 – 3 BHEs			GHP #3 – 2 BHEs			GHP #1 – 7 BHEs (ASHRAE)		
Drilling costs	SPP	SNV [k€]	PI	SPP	SNV [k€]	PI	SPP	SNV [k€]	PI	SPP	SNV [k€]	PI
20 € m^{-1}	8	7.8	0.33	10	5.4	0.22	7	6.3	0.28	< 0	< 0	< 0
40 € m^{-1}	17	1.8	0.06	21	< 0	<0	15	2.3	0.09	< 0	< 0	< 0
60 € m^{-1}	27	< 0	< 0	32	<0	<0	23	< 0	< 0	< 0	< 0	<0
80 € m^{-1}	36	< 0	< 0	43	<0	< 0	32	< 0	< 0.45	< 0	< 0	< 0
100 € m^{-1}	46	< 0	< 0	54	< 0	< 0	40	< 0	< 0.45	< 0	< 0	< 0

This case study – besides proving the high potential for energy efficiency enhancement of the system – hinted that initial installation costs can be greatly reduced by the limited number of boreholes associated to the optimal design solutions. However, we pointed out that installation costs remain the main drawback of this technology, possibly limiting its diffusion, especially for small-medium buildings. The simple net value after 20 years resulted positive only for drilling costs lower than ≈ 50 € m^{-1}. At given retail prices of the heat generators (see Table 5.7), the best solution in terms of energy savings (GHP #3 - 3 BHEs) needs lower drilling cost to be advantageous (max. 38 € m^{-1}) with respect to GHP #3 - 2 BHEs configuration. The latter one results in a similar energy consumption (931 MWh vs. 917 MWh), but allows a maximum drilling expenditure of about 51 € m^{-1}, higher profitability indexes, higher net present value and shorter payback periods.

We stress the illustrative purposes of the presented economic evaluations. The actual economic feasibility and GSHPs diffusion depend on several extrinsic factors, such as inflation of energy fees, equipment prices evolution, operators fees, possible financial incentives, and others. Any specific design case have to be analyzed according to the specific technical and economical contexts. Here, we showed only an illustrative application of the proposed design methodology, together with related energetic and economic benefits.

5.2 *Case study # 2*

In this case study, we show an alternative application of the proposed optimal-design methodology. The present work aims to identify the relative influence of GSHP subsystems (viz. ground source, earth heat exchangers, heat pump unit, pumping devices) on the overall efficiency and the limits to which technological improvements should be pushed to obtain proper advantageous. Indeed, beyond these limits, only minor benefits may be achieved with respect to corresponding development offers. To this end, an analysis of thermodynamic losses is conducted for a case study, followed by a sensitivity analysis on the heat pump unit thermal performance. However, to obtain sound results, we need to separate the inefficiencies due to a wrong design and/or coupling of GSHP equipment to actual intrinsic efficiencies of the components. In the present analysis, we are interested only in the latter ones, therefore, an optimal design methodology represents the key-tool to our aims: indeed, when an optimal design is employed, we can consider the final performance of the system as a function of the technological level of the equipment only (say, the second law efficiencies of the components).

5.2.1 Proposed second-law analysis method

This work aims to find which component mainly affects the overall performance, in order to evaluate the corresponding room for improvement and – through a sensitivity analysis on technological performances – identify appropriate strategies for GSHP development.

Thermal inefficiencies are typically investigated by means of the “second-law analysis”

or "exergy analysis" (see, for instance, [17]). Exergy efficiency (ψ) is the corresponding index of performance: its value, given by the ratio of the desired exergy output to the exergy used, is generally associated with a measure of the relative deviation between a real system and the corresponding ideal one.

Several works have involved exergy analyses of ground heat pumps (see, for instance, [19], [20], [22], [27], [238]). However, it is worth recalling that the results of this type of analysis are strongly dependent on the choice of the reference state, especially when the operative temperatures of the system are close to it [238], [239]. Heat pump applications are usually investigated using external air as reference state [20], [22], [26], therefore, this choice is pivotal.

In the present work, an alternative approach has been followed: instead of analyzing exergy fluxes, ideal subsystems are simulated, comparing primary energy consumptions. The GSHP system comprises four subsystems, viz. ground source, borehole heat exchangers (BHEs), ground-coupled heat pump unit (GHP), and pumping devices; each of them has an ideal reference configuration. Combining ideal and real subsystems, nine different configurations, listed in Table 5.9, are obtained.

Table 5.9. Analyzed configurations in terms of real and ideal subsystems.

Configuration	Ground source	BHEs	GHP	Hydraulic losses
# 1 (Benchmark)	Real	Real	Real	Real
# 2	Ideal	Real	Real	Real
# 3	Real	Ideal	Real	Real
# 4	Real	Real	Ideal	Real
# 5	Real	Real	Real	Ideal
# 6 = # 2 + # 4	Ideal	Real	Ideal	Real
# 7 = # 3 + # 4	Real	Ideal	Ideal	Real
# 8 = # 4 + # 5	Real	Real	Ideal	Ideal
# 9 = # 2 + # 3 + # 4 + # 5	Ideal	Ideal	Ideal	Ideal

Global design and control strategy have been optimized in every configuration, thus, final energy consumptions depend only on the performance of the various subsystems. Considering an ideal subsystem, it is possible to quantify the maximum benefits that can be achieved improving the technological level of each component. The employed optimization procedure is the one introduced in Chapter 4.

A dimensionless efficiency parameter (ϵ) is used to normalize and compare the energetic performances of the different simulated configurations. ϵ is based on the "task efficiency" definition provided by Moran [17]. In the present case, it reads:

$$\epsilon = \frac{En_p^*}{En_p} \tag{5.4}$$

Where En_p^* is the theoretical minimum primary energy consumption, obtained by a

loss-free system (Configuration #9), and En_p is the actual primary energy consumption of the system.

5.2.2 Description of the analyzed configurations

- *Configuration #1.*
  The benchmark configuration is based on the case study illustrated in 5.1. A ground-coupled vertical heat exchanger heat pump system has been simulated during 10 years of operational life, a convenient period for evaluating the effects of possible long-term ground temperature drifts. The back-up generators are a condensing boiler and an air/water cooler. Heating and cooling loads are imposed, as shown in Table 5.10, according to a numerical example given in [57], referring to a typical medium-scale office in the Mediterranean climate. The characteristics of ground, BHEs and generators employed in the simulation are reported in tables 5.11 and 5.12.
- *Configuration #2.*
  This configuration considers an *ideal ground source* with an infinite thermal capacity. In this way, BHEs surface temperatures remain always constant.
- *Configuration #3.*
  In this case, *ideal BHEs* are employed: borehole thermal resistance (R_b) is considered null and heat exchanger effectiveness is set equal to 1. This condition represents the maximum theoretical performance of any ground heat exchanger as the return temperature of the fluid concedes with the ground one.
- *Configuration #4.*
  The real GHP unit is replaced by an totally reversible thermodynamic cycle. All the *HP components are considered ideal*: operating and secondary fluids can exchange heat without temperature difference (no external irreversibilities) and compression and expansion processes are isentropic (no internal irreversibilities). This ideal device can deliver any thermal load without power limitations and with no penalization due to low capacity ratios.
- *Configuration #5.*
  In this configuration, no distributed or lumped losses are present; thus, *pumping energy is null*.

5.2.3 Results and discussion

Optimal control strategies and design variables, together with the main performance indices, are reported for each configuration in Tables 5.13 and 5.14. We shortly recall that f_H and f_C coefficients represent the share of the building thermal load that is delivered by the GSHP unit in heating and cooling mode, respectively. Their value is optimized within the proposed optimization procedure (see section 4.6.2).

In Configuration #1, the $f_{H/C}$ sequence (control strategy) is given by the optimal synergy among GHP unit and back-up generators (condensing boiler and air/water heat pump).

Table 5.10. Monthly heating and cooling loads of the tested office building.

Month	Heating demand[1] MWh	Cooling demand[1] MWh
January	16.1	0
February	11.7	0
March	6.9	0
April	1.4	0
May	0	7.5
June	0	14.4
July	0	17.2
August	0	17.2
September	0	6.9
October	1.4	0
November	8.3	0
December	13.9	0
Total	59.7	63.3
Peak load	30 kW	60 kW

[1] Delivery temperature of the building end-user loop: 45 °C (heating) and 7 °C (cooling)

Table 5.11. Ground thermal properties and BHE characteristics.

Property	Value	Unit
Ground thermal conductivity	1.7	$W\,m^{-1}\,K^{-1}$
Ground thermal diffusivity	0.68	$mm^2\,s^{-1}$
BHE diameter	15	cm
BHE configuration	Double U	
Spacing between boreholes	10	m
Grouting thermal conductivity	1.7	$W\,m^{-1}\,K^{-1}$
BHE pipe diameter (inner – outer)	2.62 – 3.2	cm
U-legs shank spacing	9.4	cm
Pipe thermal conductivity	0.35	$W\,m^{-1}\,K^{-1}$
BHE thermal resistance R_b	0.062	$m\,K\,W^{-1}$

Table 5.12. Declared capacity (DC) of the ground heat pump and back-up generators [12].

Ground-coupled (water/water) unit		**Condensing boiler**	**Air/water unit**
Heating DC	Cooling DC	Heating DC	Cooling DC
24.7 kW	22.9 kW	33.5	59.2

In heating mode, the geothermal solution performs better than the boiler, except during the transitional months (April and October), when the building load is below the control range of the GHP unit. $f_H = 0.9$ in January is due to the constraint imposed on the supply temperature of the ground-coupled loop ($T_{w,in} \geq 3$ °C): indeed, the optimal BHEs number and depth (7×100 m) resulting from the best trade-off between heat transfer performance and pumping energy, is not sufficient to exchange all the heat required to match the building heating load. For the same reasons, during the cooling season, the BHEs field is not able to match the total cooling load, therefore, the air unit integration is always required. Nevertheless, the optimal solution does not split the cooling load between air and ground sources, but it finds more convenient operating the sole air unit during the hottest months (July and August) and the sole GHP during the others (June and September).

In Configuration #2, the ground temperature remains constant; hence, a reduced number of BHEs is sufficient to meet the total heating load. The ideal properties of the ground allow to operate the GHP also during the hottest months: $f_C = 0.7$ corresponds to the optimal capacity ratios for the actual air and ground temperatures. Energy consumption is slightly reduced and the corresponding ϵ value increases from 0.19 to 0.22.

In Configuration #3, the heating load is fully delivered by the GSHP, thanks to the enhanced heat transfer performance of the BHEs. However, in cooling mode, we deal with the same situation illustrated for Configuration #1; therefore, E_p value does not decrease significantly.

In Configuration #4, the high performances of the ideal GHP allow to match the total building load. As in Configuration #1, $f_H = 0.9$ in January is due to the heat transfer effectiveness of the BHEs and to the constraints on $T_{w,in}$. The ϵ value reaches 0.42 and the primary energy consumption is notably reduced.

In Configuration #5, hydraulic head losses are neglected. Both N_{BHE} and $\dot{m}_w$ tend to infinity; thus, temperature alteration of the ground results negligible. The behavior is very similar to the one of Configuration #2: the small difference between the two E_p^{tot} values is due to the pumping energy.

In summary, for the first five configurations, where only the effect of single subsystems is investigated, the greatest improvement of the system performance is obtained by replacing the GHP unit with an ideal one (Configuration #4); on the contrary, the other components slightly affect the overall performance, even when loss-free.

The results of Configurations #6, #7, and #8 show that, when an ideal heat pump is present, it canbe advantageous to improve the other subsystems, too. In Configurations #6 and #8, when an ideal heat pump is coupled with an ideal ground and with a system free of head losses, ϵ reaches, respectively, 0.74 and 0.75.

In conclusion, a technological development of GSHP components does not produce adequate benefits unless the efficiency of the heat pump unit is concurrently augmented. Conversely, the equivalence of ϵ values in Configurations #6 and #8 suggests that reducing

both thermal and hydraulic losses of the heat pump is a possible way of obtaining high performances, even in the presence of a soil with unfavorable thermal properties.

5.2.4 Sensitivity analysis

In the previous section, it has been shown that the GHP is the key element for the improvement of the whole GSHP system. Here, a sensitivity analysis is carried out on system performances, increasing the GHP second-law efficiencies in heating and cooling modes ($\eta^{II}_{H/C}$) [2]. The aim is to find a preferable path and practical upper limits for technological development of the heat pump device. . Their values are given by he ratio of actual COP/ EER of the unit and the coefficient of performance of a theoretical loss-free heat pump, operating at the same temperatures of the sources (COP' / EER').

Optimal design and control strategies for minimum primary energy consumption are evaluated for different combinations of $\eta^{II}_{H,nom}$ and $\eta^{II}_{C,nom}$ values, starting from the nominal values and moving towards the ideal ones (see table 5.15). The subscript "nom" indicates that $\eta_{H/C}$ value is evaluated at standard rating conditions [12].

In every case, minimum energy consumptions are obtained with 7 BHEs. The relative energy savings (percentage savings with respect to the benchmark value) are depicted in the contour plot of figure 1, as a function of second-law efficiencies in heating and cooling modes. A saturation trend can be observed for the system performance, which reaches its maximum (37 % savings) for unitary values of $\eta^{II}_{H_nom}$ and $\eta^{II}_{C_nom}$.

The continuous red line represents the shortest path from the benchmark to the maximum, but its practical meaning is poor, as it is impossible to eliminate all the inefficiencies with a single technological leap. The dotted blue line, instead, is obtained by following the shortest paths between each consecutive iso-line (with steps of 5 % savings) and shows a more realistic technological development strategy, based on step-by-step evolutions. A practical indication that can be derived from the graph is that heating and cooling efficiencies should increase concurrently, but with a small, though significant, preference for heating mode improvement. This can be explained by the higher values of f_H with respect to f_C , with a greater weight associated to the heating performance.

It is worth recalling that – although the suggested development path and the outlined conclusions, strictly speaking, are valid only for the analyzed case study – the proposed method is generally applicable to any other building system, even selecting different objective functions.

2 Heat pumps $\eta^{II}_{H/C}$ have been defined in Eqs. (2.4)- It corresponds to the actual coefficients of performance of a given HP unit divided by the theoretical Carnot efficiencies under the same sources temperature.

Table 5.13. Optimal control strategies.

Configuration	JAN	FEB	MAR	APR	MAY	JUN	JUL	AUG	SEP	OCT	NOV	DEC
#1	0.9	1	1	0	1	1	0	0	1	0	1	1
#2	1	1	1	0	1	1	0.7	0.7	1	0	1	1
#3	1	1	1	0	1	1	0	0	1	0	1	1
#4	0.9	1	1	1	1	1	1	1	1	1	1	1
#5	1	1	1	0	1	1	0.7	0.7	1	0	1	1
#6 = #2 + #4	1	1	1	1	1	1	1	1	1	1	1	1
#7 = #3 + #4	0.9	1	1	1	1	1	1	1	1	1	1	1
#8 = #4 + #5	1	1	1	1	1	1	1	1	1	1	1	1
#9 = #2 + #3 + #4 + #5	1	1	1	1	1	1	1	1	1	1	1	1

Table 5.14. Optimal design variables and performance indices.

Configuration	En_p^{tot}	ϵ	N_{BHE}	H	$\dot{m}_w$	f_H	f_C	COP	EER	CR_H	CR_C	η_{bh}	EER_{air}	CR_{air}
#1	856	0.19	7	100	2.39	0.93	0.46	3.94	3.75	0.98	1	1.09	3.18	0.94
#2	721	0.22	4	100	1.36	0.95	0.84	4.83	4.70	1	0.84	1.09	2.18	0.28
#3	843	0.19	7	100	2.39	0.95	0.46	3.98	3.84	1	1	1.09	3.18	0.94
#4	375	0.42	7	100	2.39	0.97	1	6.41	12.0	0.98	1	1.09	-	-
#5	713	0.22	n.a. (∞)	100	n.a. (∞)	0.95	0.84	5.00	4.67	1	0.84	1.09	2.18	0.28
#6 = #2 + #4	214	0.74	4	100	1.36	1	1	9.08	31.9	1	1		-	-
#7 = #3 + #4	358	0.44	7	100	2.39	0.99	1	6.50	12.7	1	1	1.09	-	-
#8 = #4 + #5	214	0.75	n.a. (∞)	100	n.a. (∞)	1	1	9.49	28.7	0.98	1	1.09	-	-
#9 = #2 + #3 + #4 + #5	159	1	n.a	n.a	n.a	1	1	10.8	77.5	1	1		-	-

Table 5.15. Nominal second-law efficiencies of GHP unit used for the sensitivity analysis (in parentheses, the efficiency increase with respect to the benchmark configuration).

$\eta^{II}_{H,nom}$	0.55[a]	0.6 (+ 8 %)	0.7 (+ 26 %)	0.8 (+ 44 %)	0.9 (+ 62 %)	1 (+ 80%)	
$\eta^{II}_{C,nom}$	0.40[a]	0.5 (+ 26 %)	0.6 (+ 51 %)	0.7 (+ 76 %)	0.8 (+ 102 %)	0.9 (+ 127 %)	1 (+ 152 %)

[a] Current value (benchmark configuration) in rating conditions [12].

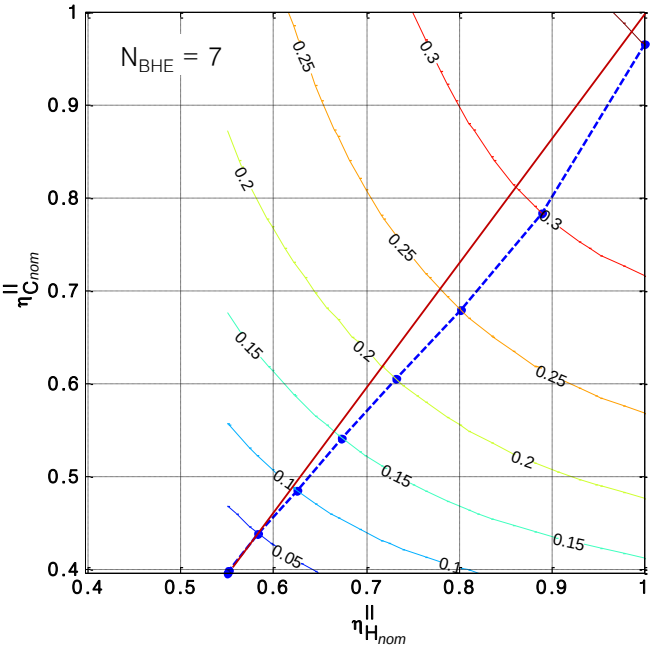

Figure 5.11. Relative energy savings as a function of second-law efficiencies in heating and cooling modes; the blue line follows the shortest path between two consecutive iso-lines.

5.2.5 Conclusions

In this case study, the thermodynamic losses of a GSHP case study have been analyzed. Primary energy consumptions of nine configurations with different combinations of real and ideal subsystems have been compared, identifying their relative influence on the overall performance of the system. Furthermore, the use of theoretical loss-free components, together with optimized sizing and control strategies, allows to calculate the maximum energy savings achievable through the development of each subsystem. The results reveal the possibility of an inherent hierarchical approach to the development of the subsystems. Specifically, the ground-coupled heat pump unit is the key element on which technological development should be focused. Increasing GHP performances also allows to enhance the positive effects given by other components: e.g. the task efficiency is 42 % in Configuration # 4 (ideal heat pump unit) and 22% in Configuration #5 (no head losses); combining the two ideal subsystems (Configuration #8), ϵ reaches 0.75.

Focusing on the heat pump device, a sensitivity analysis is performed on its heating and cooling efficiencies, aimed at finding the best path of technological development. The results show a saturation trend of the system performance, but with different behaviors in heating and cooling modes, suggesting a small but significant preference for the promotion of the heating efficiency. It has to be stressed that these conclusions do not have a general value, but depend on the particular case under exam. This notwithstanding, the proposed methodological approach can be applied to any other GSHP system (e.g. in other climatic conditions or on larger or smaller scale buildings). As for future developments, they are mainly required for the hydraulic design of the evaporator/condenser and control capacity of the heat pump unit. The head losses in the evaporator/condenser have to be lowered through an optimized hydraulic design or with a proper layout of the ground-coupled loop. Besides, the penalization effects due to low capacity ratios should be reduced. To do this, the control range of the GHP unit should be as wide as possible or smaller capacity units should be installed, compatibly with the available economic budget.

This case study deals only with energy savings. Economic and thermoeconomic aspects will be included in future works, in order to appropriately take into account in the optimization procedure also installation and technological development costs. In this way, a graph similar to the one of figure 1, but with iso-lines of thermoeconomic savings, should show a maximum, and the optimal way to reach it.

5.3 *Further applications and case studies*

The above-described case studies showed two of the numerous possible applications of the proposed methodology: a design case and a thermodynamic analysis of GSHP equipment. In addition, the proposed approach is being applied to other different case studies. For instance, in [193], we investigated the optimal BHEs number and the investment profitability as a function of BHEs drilling fees. We showed how an accurate evaluation of maximal GSHPs performances, covering a proper set of benchmark buildings and

loads, may help authorities to assess amounts and access criteria for financial incentives, encouraging GSHPs diffusion, but avoiding market distortions or speculations.

Another application of the proposed method is described in [240], [241][3]. The latter work analyzed a real case study (a primary school located in the north of Italy) characterized by high heating loads. A ground-source gas absorption heat pump (GS-GAHP) is currently installed in the building (nominal capacity 40 kW, together with a monitoring systems. The collected data were compared with the performances predicted by our model resulting in a satisfactory accordance. In addition, we investigated the achievable benefits of possible design alternatives (GS-GAHP and condensing boiler) and different control strategies (lower supply temperature to the end-user loop). In this case, the simulation model proved to be an effective prediction-tools also for energy savings actions and related cost-benefit analysis.

The latter case study was also adopted to test the applicability of the greedy algorithm to a heating-dominated load. We expected that in a unbalanced load condition the relevance of the history of heat exchanges leads to the algorithm failure. On the contrary, the proposed statistical-evaluation method shows that greedy approach provides good results also for the present case study. Further details can be found in [241].

The analysis of the applicability of the greedy algorithm in GSHPs design is currently undergoing a research activity. Future works will be dedicated to this subject.

3 We gratefully acknowledge Mr. Giulio Pellegrini, with regard to his work on modeling and analyzing the cited case study during his Master Degree Thesis.

6 Conclusions

The ever-increasing demand of high-efficiency, low-cost and environmental-friendly energy solutions has prompted modern design processes to deal with interconnected systems, in which different technologies (each of one with its own characteristics) seek concurrent objectives in increasingly strict economic and regulatory contexts.

In this framework, the Thesis illustrated an innovative design approach for ground source heat pump systems. The proposed design method refers to the so-called *simulation-based optimization algorithms* (see section 4.4) that concurrently investigate the best design and control strategies, trying to maximize/minimize a selected operative performance index (see section 4.5.1).

In the second chapter of the Thesis (2) we illustrated the current status of GSHP technology. In particular, we discussed the main pros and cons of possible heat source alternatives and traditional design methodologies. The latter ones, despite their practical usefulness, show several room of improvement in terms of operative performances and cost-benefit analyses. Indeed, as it has been emphasized several times in this work, the uncertainty of the operative performances and the high installation cost remain the main drawbacks of this technology.

Chapter 3 was dedicated to GSHPs simulation methods. We focused on those expressions which present the following characteristics: they have to be practically manageable within an optimization algorithm, they have to result in a proper tradeoff between accuracy and implementation efforts (also considering the typical availability of data and input parameters at the early-stages of every design process), and they have to be able to provide some general indications on the physical mechanisms governing the energy exchanges, in order to simplify the interpretation of the results. Therefore, analytical formulations were preferred. Besides, assumptions, simplifications, length and time scales of applicability of each model were illustrated and discussed. All GSHPs subsystems are modeled by a proper mathematical expression (see Chapter 3) that is coupled to the others within a full set of equations (Eqs. 4.8a -4.8h). Similarly, the simulation algorithm is based on a quasi-steady-state approach, as rigorous dynamic methods require that all boundary conditions (e.g. the actual behavior of the user system) are known at the shortest simulation time scale. It is worth recalling that our goal is not to reproduce the actual performances

of an existing system, but to provide useful indications about the optimal design and management of a specific project.

The rigorous mathematical formulation of the optimization problem is provided in Chapter 4 together with a dedicated resolution method. With regards to control strategy optimization, we discussed the applicability of three different algorithms (i.e. dynamic programming, genetic algorithms, and greedy algorithm). Due to the large number of variables and the non-convex nature of the problem, a heuristic approach is practically mandatory; consequently, we elaborated an evaluation methodology to rate and compare the results of different optimization algorithms according to the chances of finding even better solutions (see section 4.7).

Finally, in Chapter 5 we presented two examples of application of the proposed methodology. The first one refers to a classical GSHP design issue: i.e. the selection of the best heat generators configuration to meet a given heating and cooling load. We showed how the proposed methodology allows to achieve remarkable energy and economic benefits with respect to the traditional ASHRAE method. The second case refers to an alternative use of the simulation/optimization routines. We aimed at analyzing the thermodynamic losses of a GSHP case study, followed by a sensitivity analysis on the heat pump unit thermal performance. In this analysis, we were interested only in the actual intrinsic efficiencies of the components, therefore we needed to nullify all those inefficiencies due to a wrong design and/or coupling of GSHP equipment.

The proposed approach suits many other applications and analyses that are currently undergoing a research activity. Here, we want to shortly summarize the main steps of the proposed methodology, leaving the discussion on future developments to the next section.

1. *Calculate heating and cooling needs of the building*. An accurate evaluation of building thermal load is the basis for any design methodology: in our method, building load profile is the main input to evaluate the evolution of the system during its operative lifetime.
2. *Analyze technical, economic, environmental, legal contexts of the specific design case*. All these non-energetic parameters result in necessary inputs or constraints for a cost-benefit assessment of the project. The same energy savings can lead to opposite conclusions on project viability according to the specific technical, economic, and environmental context.
3. *Characterize the initial state of the ground source*. Initial temperature and thermo-physical properties of the ground source are required input for the optimization algorithm. The simulated energy performances are strongly affected by these parameters, therefore they have to be estimated as accurately as possible (see Appendix 2).
4. *Create a set of possible GSHP configurations, BHEs type and number, GHP units and back-up alternatives*. The overall procedure finds the best GSHP configuration (e.g. GHP type and capacity, boreholes number, depth and spacing, operative temperature and flow rate, back-up technology) comparing the performance of each element of the set of alternatives. A proper insight on HVAC design is a fundamental tool to guide the optimization process, limiting the number of configurations to be tested.
5. *Simulate and optimize each possible GSHP configuration* through the proposed algorithm (see Chapter 4) according to a proper objective function .

6. *Select the best configuration* among the set of optimized solutions obtained in the previous step. We can base our choice on the same performance index of the previous step or, alternatively, we can adopt a new one. For instance, in the first case study of this Thesis (section 5.1), first we minimized the energy consumption of each combination of BHEs number and GHP, then we chose the final design solution according to some economic considerations on the previously-obtained optimized configurations.

With regards to the latter point, we stress that it is quite complex to provide general indications on economic features, as the actual viability of any project depends on the very specific context of the project itself. Indeed, the final decision on the best design solution is always up to designers. In this context, the proposed methodology represents a very useful tool as it provides a proper estimation of the maximum performance of a small set of GSHP configuration alternatives. Therefore, designers are supported in their investigation of the actual applicability of GSHP technology, avoiding disproportions between expected benefits and actual performances.

6.1 *Future developments*

During last decades, GSHP systems have aroused a great interest among heating & cooling operators and have undergone a notable increase in the number of installations [48]. However, at least in Mediterranean countries (e.g. Italy), this technology has not yet achieved the expected attractiveness with respect to other high-efficiency solutions. This is probably due to the particular energetic and economic context (e.g. temperate climate, reduction of buildings needs, energy fees, installation costs, absence of specific incentives) and to the application of a design methodology based on the "peak-load" approach. The latter one results in oversized systems which are often economically unfeasible. Consequently, an optimization-based approach, based on a cost-benefit analysis, seems to be a proper strategy for further developments. In this context, the proposed design methodology may represent a useful tool to face the mentioned drawbacks, however, its development and the general research activity on GSHP systems need many other subjects to be investigated.

The proposed design methodology refers to the so-called *simulation-based optimization methods*, therefore, the soundness of its results is affected by the characteristics of the simulation and resolution algorithms. Consequently, the development of simulation models, methods and optimization routines is one of the main development activities. With particular reference to GSHP design, future researches will be addressed to the development of the following subjects[1]:

1 Some of the listed activities have already started and the analysis of some preliminary results is currently ongoing.

- *GSHP subsystem modeling.*
  This Thesis dealt with vertical ground-coupled heat pump systems employing several analytical models to simulate overall system performances (see Chapter 3). The same methodological approach can be applied to other GSHP configurations, such as shallow heat exchangers (e.g. energy piles and geothermal baskets) and groundwater heat pump systems. To do that, we need proper modeling correlations giving the thermal performance of the ground heat exchangers as a function of time, geometric variables (e.g. coil length, depth of installation, aspect ratio), and other operative parameters (e.g. flow rate, supply temperature, thermo-physical properties of the ground, undisturbed ground temperature, possible interference of surface phenomena). These correlations are currently undergoing a research activity through a regression analysis of the results of several transient FEM simulations, in order to identify the most relevant parameters, characteristic lengths and time scales. Regarding HPs technology, as mentioned in section 5.3, the proposed methods have already been applied to ground-source gas absorption heat pumps [240], [241]. Endothermic engine-driven HPs can be analyzed, too, provided that a proper performance-evaluation model is implemented.
- *Integration with other back-up technologies.*
  The proposed approach can be used to investigate optimal coupling strategies among GSHPs and other HVAC technologies (e.g. solar systems) and other equipment layouts. Technical and economical limits could be analyzed in a similar fashion to the presented case study # 1 in order to find advantageous design solutions. Furthermore, specific technological development strategies could be investigated in a similar fashion to the case study # 2.
- *Development of simulation methods and algorithms.*
  Each simulation-based optimization process relies on the sound prediction of equipment energetic performances during the operative period. In this Thesis, we used a quasi-steady-state approach over a sufficiently long time step (i.e. a month), which allows us to neglect internal energy variations (except for the ground) and employ simpler models. However, shorter time-scales are needed to simulate the effects of actual GHEs control strategies: the latter are generally based on an ON/OFF control criterion in which heat is injected/extracted to/from the ground in short heat pulses with a duration of some tens of minutes (i.e. stopping/activating ground-coupled loop circulation pumps). Therefore, significant dynamic phenomena can affect the actual evolution of the fluid temperature returning from GHEs, with related impact on GHP performances. More accurate simulation methods could be implemented also for ground-coupled heat pump unit (i.e. cycle-simulation based models) and back-up generators, together with a dynamic simulation of the end-user loop and building thermal loads. The latter simulation approach has already been applied in another work concerning a full transient model for radiant systems coupled to a modulating air-source heat pump [242]. The applicability to ground-source systems depends on the development of the above-described short-time-scale models and proper simulation routines.
- *Development of optimization methods and algorithms.*
  Currently, alternative optimization algorithms, with respect to the one proposed in Chapter 4, are undergoing a notable research activity. In particular, statistical and stochastic approaches seem particularly attractive for investigating optimal control strategies due to

the large dimension, the non-linearity, and the non-convex nature of the solution space. Predictive non-physical models (e.g. dynamic neural networks) for HVAC optimization have been proposed in literature, too [189], [206]–[208]. With regards to the applicability of the greedy algorithm, as mentioned in section 5.1, it has already been successfully employed in a heating-dominated test case [240], [241]. The latter result seems to contradict the relevance of the history of the heat exchanges on the sustainable exploitation of the ground source. However, as we already pointed out in section 4.1, an efficient and favorable operation of the GSHPs implies a limited alteration of the soil temperature. Therefore, also the greedy approach, applied to a sufficiently-long time step (i.e. a month), tends to limit the temperature drift of the soil.

- *Development of simplified and straightforward guidelines for professional designers*.
Although an optimal design requires a detailed analysis of the specific case under consideration, it is possible to provide some general indications on the proper sizing of GSHP components to support designers in their professional activity. We are currently investigating the possibility of building some reference performance maps relating some significant parameters (e.g. ground-source thermal characteristics, GHEs number and size, heat load profile, nominal efficiency of the heat pump unit and back-up generators) to the GSHP performances. These maps could be drawn on the basis of a large number of sensitivity analyses that calculate the energy performance of the overall system through the proposed simulation and optimization methodology.

Future works will be dedicated to the discussion of the above-listed topics.

A Thermo-pysical properties of common soils and rocks

Table 1.1. Typical values of hydraulic properties of soils and rocks [111], [243].

Medium	K		ϕ		v
	Range	Average	Range	Average	
Soils					
Gravel	$3.0 \times 10^{-4} - 3.0 \times 10^{-2}$	3.0×10^{-3}	$0.2 - 0.4$	0.3	3.0×10^{3}
Sand (coarse)	$9.0 \times 10^{-7} - 6.0 \times 10^{-3}$	7.3×10^{-5}	$0.3 - 0.5$	0.4	6.0×10^{1}
Sand (fine)	$2.0 \times 10^{-7} - 2.0 \times 10^{-4}$	6.3×10^{-6}	$0.3 - 0.5$	0.4	5.0
Silt	$1.0 \times 10^{-9} - 2.0 \times 10^{-5}$	1.4×10^{-7}	$0.3 - 0.6$	0.5	9.4×10^{-2}
Clay	$1.0 \times 10^{-11} - 4.7 \times 10^{-9}$	2.2×10^{-10}	$0.3 - 0.6$	0.5	1.5×10^{-4}
Ground					
Limestone, dolomite	$1.0 \times 10^{-9} - 6.0 \times 10^{-6}$	7.7×10^{-8}	$0.0 \times 10^{1} - 2.0 \times 10^{-1}$	1.0×10^{-1}	2.4×10^{-10}
Karst limestone	$1.0 \times 10^{-6} - 1.0 \times 10^{-2}$	1.0×10^{-4}	$5.0 \times 10^{-2} - 5 \times 10^{-1}$	3.0×10^{-1}	1.1×10^{2}
Sandstone	$3.0 \times 10^{-10} - 6.0 \times 10^{-6}$	4.2×10^{-8}	$5.0 \times 10^{-2} - 3 \times 10^{-1}$	2.0×10^{-1}	7.6×10^{-2}
Shale	$1.0 \times 10^{-13} - 2.0 \times 10^{-9}$	1.4×10^{-11}	$0.0 \times 10^{1} - 1 \times 10^{-1}$	5.0×10^{-2}	8.5×10^{-5}
Fractured igneous and metamorphic	$8.0 \times 10^{-9} - 3.0 \times 10^{-4}$	1.5×10^{-6}	$0.0 \times 10^{1} - 1.0 \times 10^{-1}$	5×10^{-2}	9.78
Unfractured igneous and metamorphic	$3.0 \times 10^{-13} - 2.0 \times 10^{-10}$	2.3×10^{-12}	$0.0 \times 10^{1} - 5.0 \times 10^{-1}$	2.0×10^{-2}	3.09×10^{-5}

Table 1.2. Typical values of thermal properties of soils and rocks [111], [243].

Medium	λ		ρc		α
	Range	Average	Range	Average	
Soils					
Gravel	$0.7 - 0.9$	0.8	–	1.4×10^6	5.7×10^{-7}
Sand (coarse)	$0.7 - 0.9$	0.8	–	1.4×10^6	5.7×10^{-7}
Sand (fine)	$0.7 - 0.9$	0.8	–	1.4×10^6	5.7×10^{-7}
Silt	$1.2 - 2.4$	1.8	$2.4 \times 10^6 - 3.3 \times 10^6$	2.8×10^6	6.3×10^{-7}
Clay	$0.8 - 1.1$	1.0	$3.0 \times 10^6 - 3.6 \times 10^6$	3.3×10^6	3.0×10^{-7}
Rocks					
Limestone, dolomite	$1.5 - 3.3$	2.4	$2.1 \times 10^7 - 5.5 \times 10^6$	1.3×10^7	1.8×10^{-7}
Karst limestone	$2.5 - 4.3$	3.4	$2.1 \times 10^7 - 5.5 \times 10^6$	1.3×10^7	2.5×10^{-7}
Sandstone	$2.3 - 6.5$	4.4	$2.1 \times 10^6 - 5.0 \times 10^6$	3.6×10^6	1.2×10^{-6}
Shale	$1.5 - 3.5$	2.5	$2.4 \times 10^6 - 5.5 \times 10^6$	4.0×10^6	6.3×10^{-7}
Fractured igneous and metamorphic	$2.5 - 6.6$	4.6	–	2.2×10^6	2.1×10^{-6}
Unfractured igneous and metamorphic	$2.5 - 6.6$	4.6	–	2.2×10^6	2.1×10^{-6}

B Site-investigation methods

Ground thermo-physical properties affect both the thermal performance and the sustainable level of exploitation of the source. Therefore, an accurate knowledge of the local values of these properties is a key-factor of the design process. For a preliminary feasibility study, one can use reference values or data from previous nearby projects; however, *in-situ* test procedures should always be performed [80]. Different methodologies and techniques for TRT and pumping test have been presented in literature (see for instance [6], [9], [244]–[249]. In the following paragraphs, we describe the basis concepts of these two widespread procedures, highlighting their analogies.

2.1 *Thermal response test - TRT*

Reference standards, procedures and recommendations for TRTs have been published by IGSHPA [79] and ASHRAE [6]. Here, we provide a short overview of the main steps:

- The test starts installing a pilot borehole in the construction site. The test BHE dimensions should approximate the size and depth of the actual heat exchangers planned for the project. The experimental apparatus is shown in Fig. 2.1.
- The initial/undisturbed average temperature of the ground along BHE depth, T_g^0, is evaluated. This can be achieved either by "dipping" the borehole with a temperature gauge (e.g. thermocouple [6]) on a graduated tape, and taking an average of the readings at every, say, 2 m. Alternatively, a carrier fluid can be circulated throughout the borehole loop (without any heat input): the average return fluid temperature over this duration will approximate the T_g^0 value.
- Heat is added in a water loop at a constant rate (by means of an electrical resistance), and data are collected.

After the heaters are switched on at time $t = 0$, the mean fluid temperature evolves quickly at first and then ever slower with increasing time. If we plot average fluid temperature ($\overline{T}_w$) against t, we obtain a curve similar to the one shown in Fig. 2.2. At large values of t (typically $t > 10$ h) [80], the temperature displacement evolves with a logarithmic profile (see Fig 2.3).

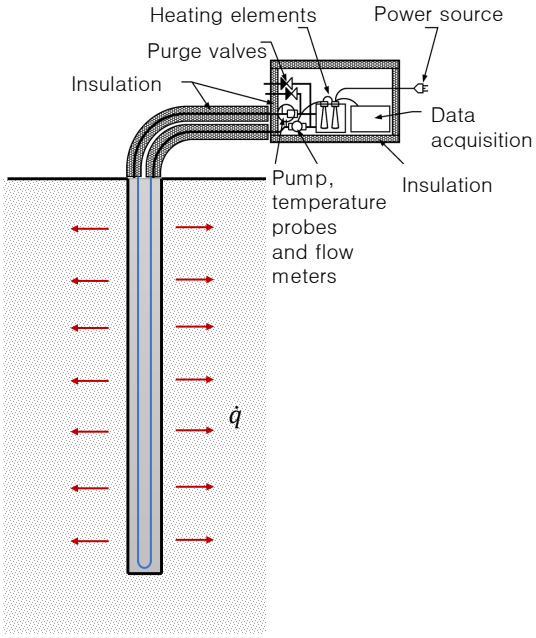

Figure 2.1. Experimental apparatus for thermal response test.

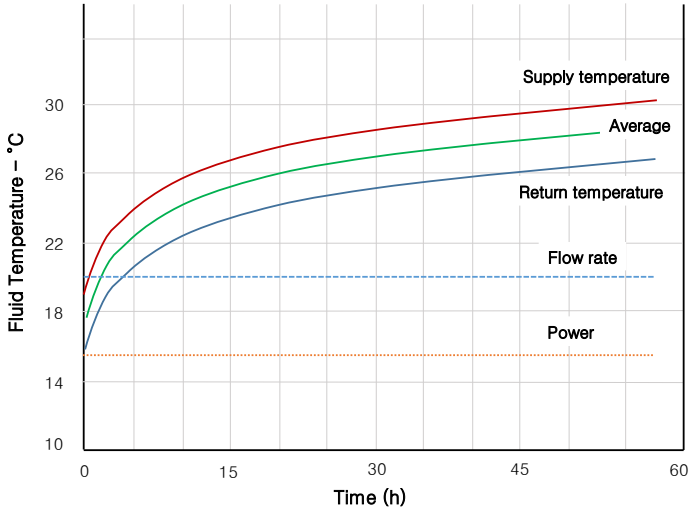

Figure 2.2. Typical evolution of fluid temperatures in a thermal response test (after [80]).

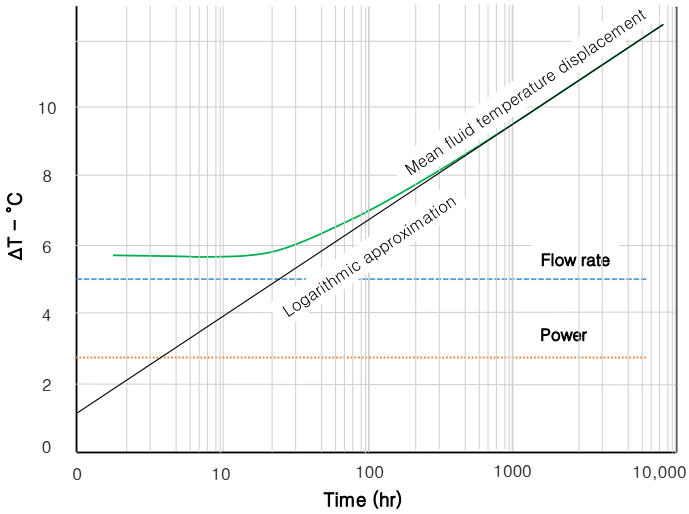

Figure 2.3. Typical evolution of fluid temperatures in a thermal response test, plotted on a semi-log graph (after [57], [80]).

Inverse methods are applied to find thermo-physical properties (i.e. thermal conductivity, λ_g, and diffusivity, α_g). These methods are based on various analytical models for conductive heat transfer in a semi-infinite body (i.e ILS,ICS,FLS).

Thermal response test is based on the concept of two effective thermal resistances among the circulating fluid and the far-field ground (see Fig. 2.4). The infinite line source model (ILS) is the most simple and common model to evaluate the ground thermal resistance (section 3.1.1), the *borehole thermal resistance* is used to evaluate the heat transfer within the borehole. At sufficient long time, $Fo_g > 1$, the temperature displacement of the circulating fluid reads [31], [80], [83], [84]:

$$\overline{T}_w - T_g^0 = \frac{\dot{q}_{BHE}}{4\pi\lambda_g}\left[\ln\left(\frac{4\alpha_g t}{r_{BHE}^2}\right) - 0.5772\right] + \dot{q}_{BHE} R_b \tag{2.1}$$

where:

- $\dot{q}_{BHE}$ is the total heat input divided by the BHE depth, $\mathrm{W\,m^{-1}}$;
- λ_g is the effective thermal conductivity of the ground, $\mathrm{W\,m^{-1}\,K^{-1}}$;
- α_g is the effective thermal diffusivity of the ground, $\mathrm{m^2\,s^{-1}}$;
- r_{BHE} is the BHE radius, m;
- R_b is the *borehole thermal resistance* (see section 3.2), $\mathrm{m\,K\,W^{-1}}$.

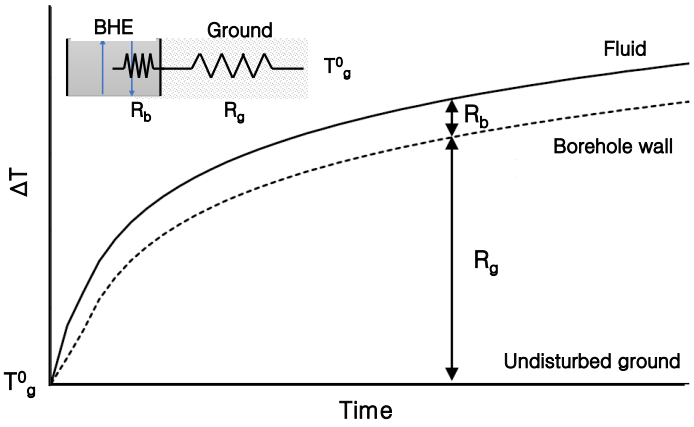

Figure 2.4. Borehole resistance analogy.

The plot of the temperature displacement $\Delta\overline{T}_w = \overline{T}_w - T_g^0$ against the natural logarithm of time (t) has a slope equal to $\frac{\dot{q}_{BHE}}{4\pi\lambda_g}$, while the intercept is proportional to R_b and α_g values. Since the volumetric heat capacity of the ground does not vary greatly for saturated strata (typically 2 to 2.5 MJ m^{-3} K^{-1}) [80], we can estimate α_g and use the intercept of the graph to calculate the borehole thermal resistance (R_b). Otherwise, R_b can be obtained through the BHEs models described in section 3.2. In this case, the curve intercept can be used to calculate α_g value.

We report some of the recommended test specifications by ASHRAE [6]:

- TRT should be performed for 36 to 48 h.
- TRT $\dot{q}_{BHE}$ should be 50 to 80 W/m, which are the expected peak loads on the U-tubes for an actual heat pump system;
- resulting temperature variation should be less than $\pm$ 0.3 K from a straight trend line of a log (time) versus average loop temperature;
- accuracy of temperature measurement and recording devices should be $\pm$ 0.3 K;
- A waiting period of five days is suggested for low-conductivity soils (i.e. $\lambda_g = 1.7$ W/m/K)) after the ground loop has been installed and grouted (or filled) before the TRT is initiated. A delay of three days is recommended for higher conductivity formations (i.e. $\lambda_g \geq 1.7$ W m^{-1} K^{-1})). This period of time is needed to dissipate the heat released during the installation phase (i.e. drilling friction and grouting consolidation);
- The initial ground temperature measurement should be made at the end of the waiting period;
- Data collection should be at least once every 10 min;

2.2 *Pumping test*

This procedure is very familiar to hydrogeologists and water wells operators: an introduction on principles and methodologies can be found, for instance, in [6], [80], [247], [248]. The pumping test is the reference *in-situ* investigation technique for open-loop systems. The following list provides a short overview of some common terms of water well technology. Reference is made to ASHRAE handbook [6]. Figure 2.5 illustrates some of the more important well terms.

- An *aquifer* is a geologic unit that is capable of yielding groundwater to a well in sufficient quantities to be of practical use;
- *Static water level* (SWL) is the level that exists under static (nonpumping) conditions.
- *Pumping water level* (PWL) is the level that exists under specific pumping conditions. It depends on pumping flow rates (higher pumping rates mean lower pumping levels), well, and aquifer characteristics. The difference between the SWL and the PWL is the *drawdown* (s_w);
- The *pumping rate* is the volumetric flow rate pumped out from the well;
- The *specific capacity* of a well is given by the pumping rate per meter of drawdown, $\mathrm{l\,s^{-1}\,m^{-1}}$;
- *Water entrance velocity* (through the screen or perforated casing) can be an important design consideration. Velocity should be limited to a maximum of 0.03 m/s (0.015 m/s for injection wells) to avoid incrustation of the entrance openings [6];
- *Total pump head* is composed of four primary components: lift, column friction, surface requirements, and injection head (pressure). *Lift* is the vertical distance to reach the surface. *Column friction* evaluates the friction loss in the pump column between the bowl assembly and the surface. *Surface pressure requirements* account for friction losses through piping, heat exchangers, and controls: typical values are between 8 and 11 m [6]. *Injection pressure requirements* are a function of well design, aquifer conditions, and water quality. Depending on water quality, sand production, and drilling methods injection pressure may be 10 to 40 % higher than production one.

Flow testing can be divided into three different types of tests: rig, short-term, and long-term [6]. Rig tests are accomplished while the drilling rig is on site: the primary purpose is to purge the well of remaining drilling fluids and cuttings. The duration of the test is generally governed by the time required for the water to run clean.

The most usual pumping test for HP applications is the *short-term test*. It takes from 4 to 24 h to collect information about well flow rate, temperature, drawdown, and recovery (i.e productivity curve). This normally comprises a sequence of four or five short 100 - 120 minute tests at increasing pumping rates $Q_1 \dots Q_5$ (Fig. 2.6). Generally, the large flow rate coincides with the nominal capacity of the well. Water level and pumping rate should be stabilized at each point before flow is increased.

Similarity to the fluid temperature during the TRT, the drawdown evolves quickly at first and then ever slower with increasing time (see Fig 2.6). When water level becomes

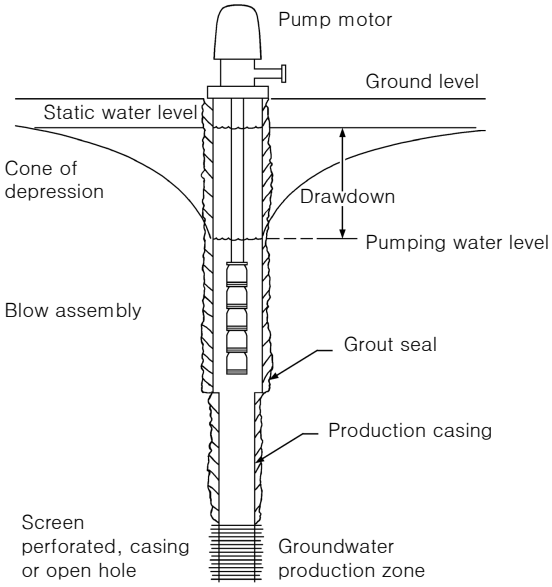

Figure 2.5. Water well scheme and terminology.

almost constant, we can measure the s_w value that corresponds to the given flow rate.

By plotting the collected data, we can draw the the so-called "well productivity curve" (Fig. 2.7). The latter can be used to calculate the necessary pumping power to obtain the desired flow rate. This correlation is a key-tool for GWHPs design as it allows to evaluate the maximum flow rate that could be extracted with a reasonable/feasible energy consumption. The simplest model for well behavior reads [31], [80]:

$$s_w = B\dot{Q} + C\dot{Q}^2 \tag{2.2}$$

where B and C can be considered constant for short time-scales. The former coefficient, B, depends on the aquifer's hydraulic resistance, the latter, C, is related to the hydraulic resistance of the well structure and several fluid dynamics mechanisms (e.g. turbulence) [31].

As above-mentioned, the Eq. (2.2) is not appropriate for long period of time due to the actual variation of B coefficient. For continuous long time operations, aquifer characteristics becomes predominant on well productivity. The latter can be evaluated by means of the *Theis's equation* and *constant rate test*.

Long-term tests of up to 30 days providing information on the hydraulic transmissivity, storage coefficient, reservoir boundaries, and recharge areas of the aquifer. Normally these tests involve monitoring nearby wells to evaluate interference effects (see Fig. 2.8).

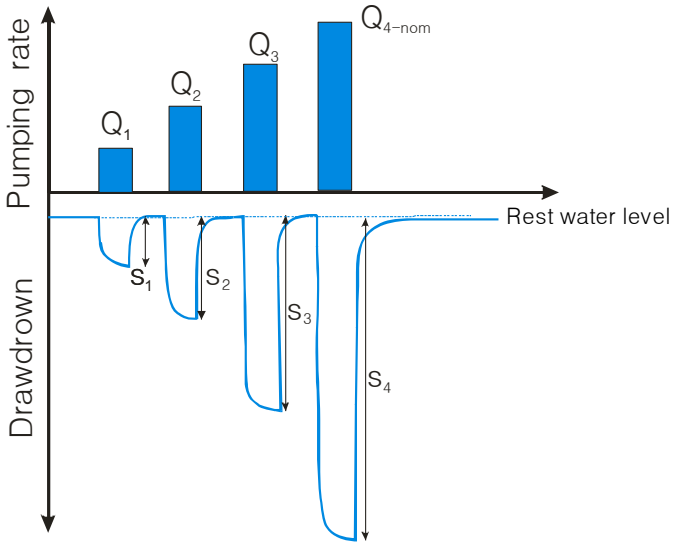

Figure 2.6. A schematic diagram showing the phases of step-testing.

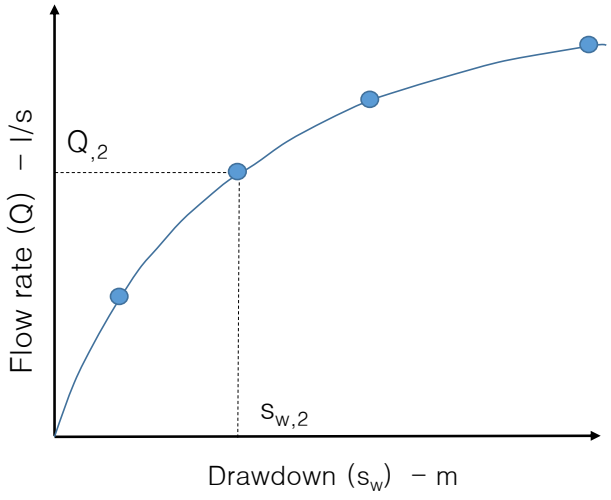

Figure 2.7. Example of a well productivity curve.

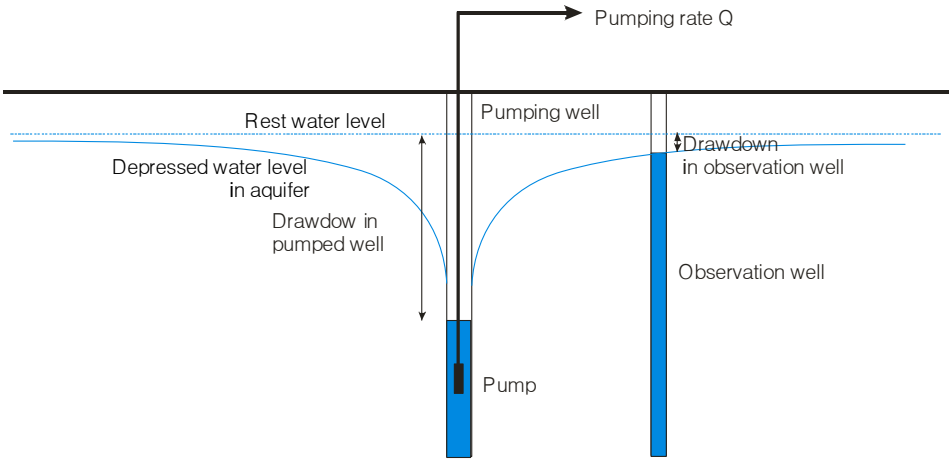

Figure 2.8. Schematic set-up for a hydraulic pumping test (after [80]).

Similarity to the TRT test, where a constant thermal power is injected into the ground, a pumping test extract a constant flow rate (Q) from the aquifer. If we plot s_w against the natural logarithm of the time t , we obtain the curve shown in Fig. 2.10.

The mathematical model describing the drawdown evolution is the the so-called *Theis's equation*. At large time ($t \geq 15$ h [31]), it can be approximate by the so-called *Cooper-Jacob equation*: the latter reads [31], [80]:

$$s_w \approx \frac{Q}{4\pi T}\left[ln\left(\frac{4Tt}{r_{well}^2 S}\right) - 0.5772\right] \tag{2.3}$$

where:

- Q is the water discharge rate, m^3/s;
- T is the effective hydraulic trasmissivity of the ground, $m^2\,s^{-1}$;
- S is the storativity of the aquifer;
- r_{well} is the well radius, m;

As for TRT, the trasmittivity (T) can be calculated evaluating the slope of the black line in Fig. 2.10. Storativity value, S, can be derived from the intercept. Theoretically, one pumping well is sufficient to derive reasonable values of T and S. However, if we wish to increase the evaluation accuracy, we need more observation wells (Fig. 2.8) [80]. As above-mentioned, s_w curve can be used to evaluate the pumping energy required to supply water to HP system.

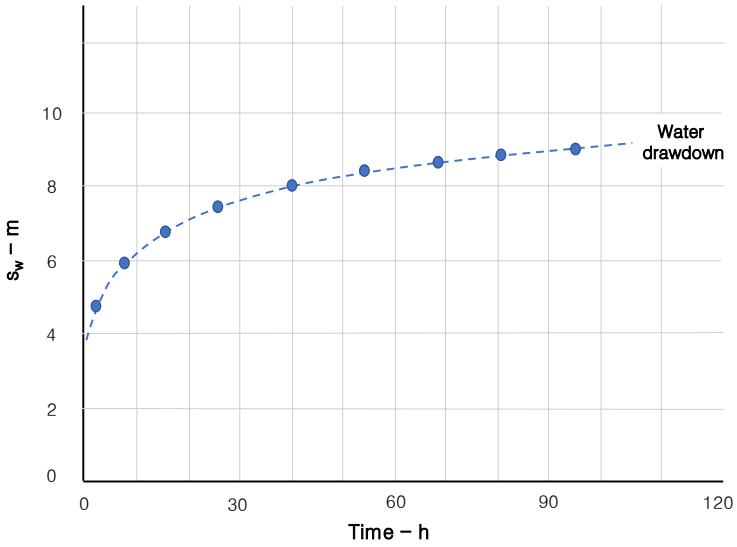

Figure 2.9. Typical curve from a constant rate pumping test (after [80]).

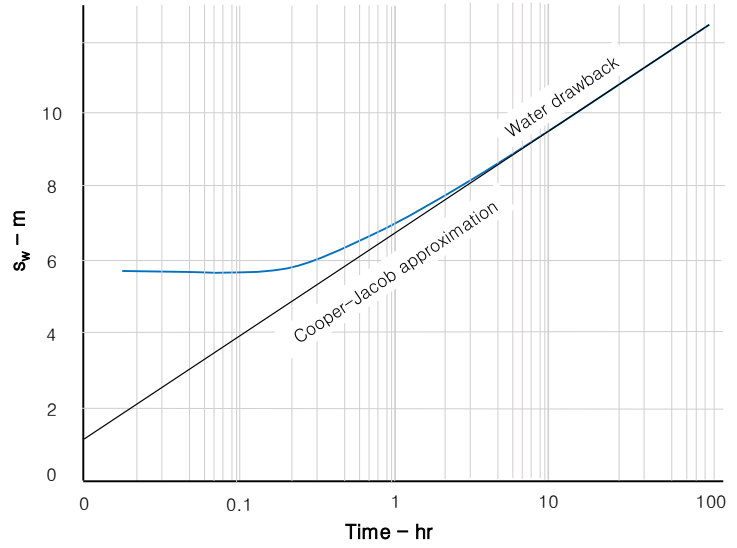

Figure 2.10. Typical curve from a constant rate pumping test, plotted on semi-log graph (after [80]).

C Modeling and simulation procedures of the illustrative analytical example in section 4.1

In this appendix, we illustrate the evaluation methodology and system modeling of the illustrative analytical example introduced in section 4.1. We suggest the reader to deal with this section afterward the reading of section 4.4.

As mentioned in section 4.1, the existence of an optimal level of exploitation of the geothermal source, corresponding to the best synergy among GSHP unit and back-up generators, can be shown by means of a simple test case. In this example, we will investigate the electrical energy use of a vertical GCHP system, depending on the BHEs size and the share of the building thermal load due to the ground source (control strategy). For the sake of simplicity, we do not consider all the necessary elements of a real design, but we deal with a plain analytical model, in order to highlight the main thermodynamic mechanisms that determine a minimum value of energy consumption.

As already mentioned, GSHPs involve different subsystems, viz. ground reservoir, ground heat exchangers (i.e. vertical BHEs), ground-coupled loop and connecting duct-work, GHP unit, back-up generators, and building end-user loop or destination thermal source (see Fig. 3.1). Each of them operate in strict connection with the others, creating a reciprocal influence on their own performance. Therefore, to apply the proposed design methodology, based on performance simulation, we have to employ a comprehensive set of equations, including at least the physical models of each element involved in the energy conversion process, namely: GSHP unit and back-ups, BHE field, and ground source.

In this example, we considered a heating system with a GSHP unit and an air heat pump (ASHP) as back-up. Thermal performances of the two generators were calculated assuming two constant second-law efficiency values, η^{II}, for each generators (see Table 2.2): in other words, we took into account only the effects of the different temperature evolution of the two sources assuming standard efficiency values for equipment. The ground temperature was evaluated by means of the infinite-line source model (see section 3.1.1) and the time-superposition technique (i.e. Duhamel's principle , see section 3.1.3). Both external air temperature and building load profiles were assumed sinusoidal.

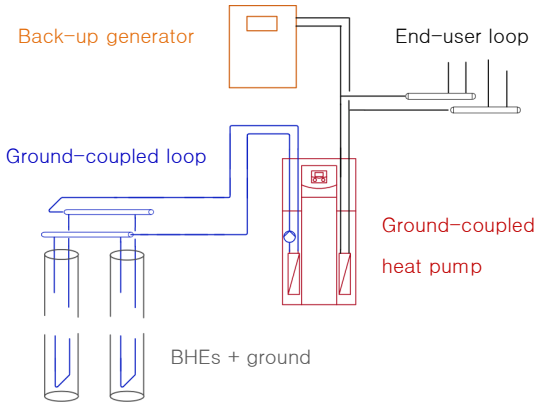

Figure 3.1. Scheme of the model subsystems.

Similarly to [239], we used a coefficient p_l to represent the fraction of the building heating load delivered by the geothermal heat pump. As above-mentioned, we aim to analyze the overall system performance depending on the different load share between air and ground systems: to do that, we performed a sensibility analysis of the overall system energy use at various p_l values. In this simple example, p_l was assumed as constant over the system lifetime, leaving a more accurate treatment of the problem to next sections. All the input parameters, including the thermo-physical properties of the soil, are reported in Table 3.1.

The total electrical energy use, E_{el} kWh, of the two heat pumps after a period of time τ was calculated as:

$$E_{el} = \int_0^\tau L(t) \left(\frac{p_l}{COP_{GHP}(t)} + \frac{1 - p_l}{COP_{ASHP}} \right) dt \tag{3.1}$$

where:

$$\begin{cases} COP_{GHP} = \dfrac{T_l}{T_l - T_g(t)} \eta^{II}_{GHP} & (3.2a) \\ COP_{ASHP} = \dfrac{T_l}{T_l - T_a(t)} \eta^{II}_{ASHP} & (3.2b) \\ L(t) = \max\left[A_l \cos\left(2\pi / \omega_l t \right) \right] & (3.2c) \\ T_a(t) = \overline{T}_a - A_a \cos\left(2\pi / \omega_a t \right) & (3.2d) \\ T_g(t) = T_g^0 + \displaystyle\int_0^t W\left(t - \beta \right) \frac{d\dot{q}_{BHE}}{dt} \left(\beta \right) d\beta & (3.2e) \\ W(t) = \dfrac{1}{2\pi\lambda_g} \displaystyle\int_{\frac{r_{BHE}}{2\sqrt{\alpha_g t}}}^{+\infty} \frac{\exp\left(-\beta^2 \right)}{\beta} d\beta & (3.2f) \\ \dot{q}_{BHE}(t) = \dfrac{p_l L(t)}{N_{BHE} H_{BHE}} \left(\dfrac{COP_{GHP} - 1}{COP_{GHP}} \right) & (3.2g) \end{cases}$$

Table 3.1. Input parameters.

Property	Value	Unit
Ground thermal conductivity	1.7	$\mathrm{W\,m^{-1}\,K^{-1}}$
Ground thermal diffusivity	0.68	$\mathrm{mm^2\,s^{-1}}$
BHEs radius	7.5	cm
BHEs depth	100	m
$\overline{T}_a$	15	°C
A_a	15	°C
$2\pi/\omega_a$	1	yr
A_l	20	kW
$2\pi/\omega_l$	1	yr
η^{II}_{GHP}	0.55	
η^{II}_{ASHP}	0.4	
τ	20	yr
T_l	45	°C
T^0_g	15	°C

The set of Eqs. (3.2a) and (3.2g) was solved numerically adopting a time-step of 700 h. The latter value was investigated through a convergence analysis on final E_{el} value: it was seen that a shorter time step provides the very same results in the face of higher computational costs. We can conclude that, for the selected α_g and r_{BHE}, monthly-average values of simulation variables (e.g. T_g and COP_{GHP}) do not differ significantly from an actual integration of the instantaneous values. The results of the simulation are illustrated and discussed in section 4.1.

Bibliography

[1] M. Preene and W. Powrie, "Ground energy systems: from analysis to geotechnical design", *Géotechnique*, vol. 59, no. 3, pp. 261–271, 2009.

[2] J. Spitler and M. Bernier, "Ground-source heat pump systems: the first century and beyond", *HVAC&R Research*, no. December 2014, pp. 37–41, 2011.

[3] A. Cavallini and L. Mattarolo, *Termodinamica Applicata*. Padova (IT): CLEUP, 1990.

[4] "Applied heat pump and heat recovery systems", in *ASHRAE Handbook - HVAC Systems and Equipment*, Atlanta (GA): American Society of Heating, Refrigerating and Air-Conditioning Engineers (ASHRAE), 2008, ch. 8, pp. 8.1 –8.21.

[5] "Unitary air conditioners and heat pumps", in *ASHRAE Handbook - HVAC Systems and Equipment*, Atlanta (GA): American Society of Heating, Refrigerating and Air-Conditioning Engineers (ASHRAE), 2008, pp. 48.1–48.14.

[6] "Geothermal energy", in *ASHRAE Handbook - HVAC Applications*, Atlanta (GA): American Society of Heating, Refrigerating and Air-Conditioning Engineers (ASHRAE), 2011, ch. 34, pp. 34.1 –34.4.

[7] K. Chua, S. Chou, and W. Yang, "Advances in heat pump systems: a review", *Applied Energy*, vol. 87, no. 12, pp. 3611–3624, Dec. 2010.

[8] A. Hepbasli and Y. Kalinci, "A review of heat pump water heating systems", *Renewable and Sustainable Energy Reviews*, vol. 13, no. 6-7, pp. 1211–1229, Aug. 2009.

[9] I. Sarbu and C. Sebarchievici, "General review of ground-source heat pump systems for heating and cooling of buildings", *Energy and Buildings*, vol. 70, pp. 441–454, Feb. 2014.

[10] EU, *Directive 2009/28/ec of the european parliament and of the council of 23 april 2009 on the promotion of the use of energy from renewable sources and amending and subsequently repealing directives 2001/77/ec and 2003/39*, Brussels, 2009.

[11] P. Conti and W. Grassi, "How heat pumps work: criteria for heat sources evaluation", in *Proceedings of XIV International Conference ECSAC: Geothermal Energy, status and future in the Peri-Adriatic Area*, Lošinj (HR), 2014, p. 10.

[12] UNI, *Uni en 14511-2. air conditioners, liquid chilling packages and heat pumps with electrically driven compressors for space heating and cooling. part 2: test conditions.* Milan, 2013.

[13] CEN, *Uni en 14825. air conditioners, liquid chilling packages and heat pumps, with electrically driven compressors, for space heating and cooling. testing and rating at part load conditions and calculation of seasonal performance*, Brussels, 2012.

[14] ANSI/AHRI, *Ansi/ahri 210/240. performance rating of unitary air-conditioning and air-source heat pump equipment,* Washington, DC, 2012.

[15] ISO, *Iso 13256-1. water-source heat pumps – testing and rating for performance - part 1: water-to air and brine-to-air heat pumps*, Geneva (CH), 2012.

[16] ——, *Iso 13256-2. water-source heat pumps – testing and rating for performance - part 2: water-to water and brine-to-water heat pumps*, Geneva (CH), 2012.

[17] M. J. Moran, *Availability Analysis - A guide to efficient energy use (Corrected Edition)*, ASME Press, Ed. New York: ASME Press, 1989, p. 260.

[18] M. Alalaimi, S. Lorente, R. Anderson, and A. Bejan, "Effect of size on ground-coupled heat pump performance", *International Journal of Heat and Mass Transfer*, vol. 64, pp. 115–121, 2013.

[19] M. R. Ally, J. D. Munk, V. D. Baxter, and A. C. Gehl, "Exergy and energy analysis of a ground-source heat pump for domestic water heating under simulated occupancy conditions", *International Journal of Refrigeration*, vol. 36, no. 5, pp. 1417–1430, Aug. 2013.

[20] Y. Bi, X. Wang, Y. Liu, H. Zhang, and L. Chen, "Comprehensive exergy analysis of a ground-source heat pump system for both building heating and cooling modes", *Applied Energy*, vol. 86, no. 12, pp. 2560–2565, Dec. 2009.

[21] U. Çakır, K. Çomaklı, O. Çomaklı, and S. Karslı, "An experimental exergetic comparison of four different heat pump systems working at same conditions: as air to air, air to water, water to water and water to air", *Energy*, vol. 58, pp. 210–219, Sep. 2013.

[22] R. Li, R. Ooka, and M. Shukuya, "Theoretical analysis on ground source heat pump and air source heat pump systems by the concepts of cool and warm exergy", *Energy and Buildings*, vol. 75, pp. 447–455, Jun. 2014.

[23] J. Urchueguía, M. Zacarés, J. Corberán, A. Montero, J. Martos, and H. Witte, "Comparison between the energy performance of a ground coupled water to water heat pump system and an air to water heat pump system for heating and cooling in typical conditions of the european mediterranean coast", *Energy Conversion and Management*, vol. 49, no. 10, pp. 2917–2923, Oct. 2008.

[24] C. A. De Swardt and J. P. Meyer, "A performance comparison between an air-source and a ground-source reversible heat pump", *International Journal of Energy Research*, vol. 25, no. 10, pp. 899–910, 2001.

[25] S. Ito and N. Miura, "Studies of a heat pump using water and air heat sources in parallel", *Heat Transfer - Asian Research*, vol. 29, no. 6, pp. 473–490, 2000.

[26] S. Lohani and D. Schmidt, "Comparison of energy and exergy analysis of fossil plant, ground and air source heat pump building heating system", *Renewable Energy*, vol. 35, no. 6, pp. 1275–1282, Jun. 2010.

[27] A. Hepbasli and O. Akdemir, "Energy and exergy analysis of a ground source (geothermal) heat pump system", *Energy Conversion and Management*, vol. 45, no. 5, pp. 737–753, Mar. 2004.

[28] E. K. Akpinar and A. Hepbasli, "A comparative study on exergetic assessment of two ground-source (geothermal) heat pump systems for residential applications", *Building and Environment*, vol. 42, no. 5, pp. 2004–2013, May 2007.

[29] A. Hepbasli and M. Tolga Balta, "A study on modeling and performance assessment of a heat pump system for utilizing low temperature geothermal resources in buildings", *Building and Environment*, vol. 42, no. 10, pp. 3747–3756, Oct. 2007.

[30] O. Ozgener and A. Hepbasli, "Modeling and performance evaluation of ground source (geothermal) heat pump systems", *Energy and Buildings*, vol. 39, no. 1, pp. 66–75, Jan. 2007.

[31] D. Banks, H. Scott, and C. Ogata, "From fourier to darcy , from carslaw to theis : the analogies between the subsurface behaviour of water and heat", *Acque Sotterranee*, pp. 9–18, 2012.

[32] R. H. D. Rawlings and J. Sykulski, "Ground source heat pumps: a technology review", *Building Services Engineering Research and Technology*, vol. 20, pp. 119–129, 1999.

[33] W. Leong, V. Tarnawski, and A Aittomäki, "Effect of soil type and moisture content on ground heat pump performance", *International Journal of Refrigeration*, vol. 21, no. 8, pp. 595–606, Dec. 1998.

[34] A. Zarrella and P. Pasquier, "Effect of axial heat transfer and atmospheric conditions on the energy performance of gshp systems: a simulation-based analysis", *Applied Thermal Engineering*, vol. 78, pp. 591–604, Mar. 2015.

[35] T. V. Bandos, A. Montero, E. Fernández, J. L. G. Santander, J. M. Isidro, J. Pérez, P. J. F. de Córdoba, and J. F. Urchueguía, "Finite line-source model for borehole heat exchangers: effect of vertical temperature variations", *Geothermics*, vol. 38, pp. 263–270, 2009.

[36] H. Yang, P. Cui, and Z. Fang, "Vertical-borehole ground-coupled heat pumps: a review of models and systems", *Applied Energy*, vol. 87, no. 1, pp. 16–27, Jan. 2010.

[37] S. P. Kavanaugh, "Design method for hybrid ground-source heat pumps", in *ASHRAE Transactions*, vol. 104, ASHRAE, 1998, pp. 691–698.

[38] M. Yi, Y. Hongxing, and F. Zhaohong, "Study on hybrid ground-coupled heat pump systems", *Energy and Buildings*, vol. 40, no. 11, pp. 2028–2036, Jan. 2008.

[39] C. Yavuzturk and J. D. Spitler, "Comparative study of operating and control strategies for hybrid ground-source heat pump systems using a short time step simulation model", *ASHRAE Transactions*, vol. 106, 2000.

[40] E. Kjellsson, G. Hellström, and B. Perers, "Optimization of systems with the combination of ground-source heat pump and solar collectors in dwellings", *Energy*, vol. 35, no. 6, pp. 2667–2673, Jun. 2010.

[41] K. Klein, K. Huchtemann, and D. Müller, "Numerical study on hybrid heat pump systems in existing buildings", *Energy and Buildings*, vol. 69, pp. 193–201, Feb. 2014.

[42] S. P. Kavanaugh and K Rafferty, *Design of geothermal systems for commercial and institutional buildings*, Atlanta (GA): American Society of Heating, Refrigerating and Air-Conditioning Engineers (ASHRAE), 1997, p. 167.

[43] Observ'ER, "Heat pumps barometer", EurObserv'ER Project, Tech. Rep., 2013, p. 18.

[44] R. M. Lazzarin, F. Buscato, and M. Noro, "Heat pumps in refurbishment of existing buildings", *REHVA Journal*, vol. 49, no. 6, pp. 45–49, 2012.

[45] G. Bagarella, R. M. Lazzarin, and B. Lamanna, "Cycling losses in refrigeration equipment: an experimental evaluation", *International Journal of Refrigeration*, vol. 36, no. 8, pp. 2111–2118, Dec. 2013.

[46] C. Naldi, G. L. Morini, and E. Zanchini, "A method for the choice of the optimal balance-point temperature of air-to-water heat pumps for heating", *Sustainable Cities and Society*, vol. 12, pp. 85–91, Jul. 2014.

[47] J. D. Spitler, *Editorial: ground-source heat pump system research—past, present, and future*, 2005.

[48] J. W. Lund and T. Boyd, "Direct utilization of geothermal energy 2015 worldwide review", in *Proceedings of the World Geothermal Congress*, Melbourne, AU, 2015.

[49] *The ashrae handbook 2011: hvac applications*, Atlanta (GA): American Society of Heating, Refrigerating and Air-Conditioning Engineers (ASHRAE), 2011, pp. 34.1–34.34.

[50] G. Florides and S. Kalogirou, "Ground heat exchangers—a review of systems, models and applications", *Renewable Energy*, vol. 32, no. 15, pp. 2461–2478, Dec. 2007.

[51] RETScreen® International, *Ground-source heat pump project analysis*, 2012.

[52] A. Mustafa Omer, "Ground-source heat pumps systems and applications", *Renewable and Sustainable Energy Reviews*, vol. 12, no. 2, pp. 344–371, Feb. 2008.

[53] CEN, *En 15450. heating systems in buildings – design of heat pump heating systems*, Brussels, 2007.

[54] VDI, *Vdi 4640-2:thermal use of the underground. ground source heat pump systems*, Düsseldorf, 2001.

[55] K. Kupiec, B. Larwa, and M. Gwadera, "Heat transfer in horizontal ground heat exchangers", *Applied Thermal Engineering*, vol. 75, pp. 270–276, Jan. 2015.

[56] *Manuale d'ausilio alla progettazione termotecnica*, Milan (IT): Associazione Italiana Condizionamento dell'Aria Riscaldamento e Refrigerazione, 2009, Q–2.1–Q–2.33.

[57] UNI, *Uni 11466. heat pump geothermal systems - design and sizing requirements*, Milan, 2012.

[58] H. Brandl, "Energy foundations and other thermo-active ground structures", *Géotechnique*, vol. 56, no. 2, pp. 81–122, Jan. 2006.

[59] J. Gao, X. Zhang, J. Liu, K. Li, and J. Yang, "Numerical and experimental assessment of thermal performance of vertical energy piles: an application", *Applied Energy*, vol. 85, no. 10, pp. 901–910, Oct. 2008.

[60] Y. Hamada, H. Saitoh, M. Nakamura, H. Kubota, and K. Ochifuji, "Field performance of an energy pile system for space heating", *Energy and Buildings*, vol. 39, no. 5, pp. 517–524, May 2007.

[61] M. de Moel, P. M. Bach, A. Bouazza, R. M. Singh, and J. O. Sun, "Technological advances and applications of geothermal energy pile foundations and their feasibility in australia", *Renewable and Sustainable Energy Reviews*, vol. 14, no. 9, pp. 2683–2696, Dec. 2010.

[62] D. Pahud and M. Hubbuch, "Measured thermal performances of the energy pile system of the dock midfield at zurich airport", in *European Geothermal Congress 2007*, Unterhaching , D, 2007.

[63] M. Li and A. C. Lai, "Heat-source solutions to heat conduction in anisotropic media with application to pile and borehole ground heat exchangers", *Applied Energy*, vol. 96, pp. 451–458, Aug. 2012.

[64] ——, "New temperature response functions (g functions) for pile and borehole ground heat exchangers based on composite-medium line-source theory", *Energy*, vol. 38, no. 1, pp. 255–263, Feb. 2012.

[65] Y. Man, H. Yang, N. Diao, J. Liu, and Z. Fang, "A new model and analytical solutions for borehole and pile ground heat exchangers", *International Journal of Heat and Mass Transfer*, vol. 53, no. 13-14, pp. 2593–2601, Jun. 2010.

[66] W. Zhang, H. Yang, L. Lu, and Z. Fang, "Investigation on heat transfer around buried coils of pile foundation heat exchangers for ground-coupled heat pump applications", *International Journal of Heat and Mass Transfer*, vol. 55, no. 21-22, pp. 6023–6031, Oct. 2012.

[67] P. Cui, X. Li, Y. Man, and Z. Fang, "Heat transfer analysis of pile geothermal heat exchangers with spiral coils", *Applied Energy*, vol. 88, no. 11, pp. 4113–4119, Nov. 2011.

[68] D. Bozis, K. Papakostas, and N. Kyriakis, "On the evaluation of design parameters effects on the heat transfer efficiency of energy piles", *Energy and Buildings*, vol. 43, no. 4, pp. 1020–1029, Apr. 2011.

[69] Y. Rabin and E. Korin, "Thermal analysis of a helical heat exchanger for ground thermal energy storage in arid zones", *International Journal of Heat and Mass Transfer*, vol. 39, no. 5, pp. 1051–1065, Mar. 1996.

[70] C. Knellwolf, H. Peron, and L. Laloui, "Geotechnical analysis of heat exchanger piles", *Journal of Geotechnical and . . .*, no. October, pp. 890–902, 2011.

[71] L. Laloui and A. Di Donna, Eds., *Energy Geostructures: Innovation in Underground Engineering*. Hoboken (NJ): John Wiley & Sons, Inc., 2013, p. 320.

[72] T. Amis, "Energy piles and other thermal foundations for gshp – developments in uk practice and research", *REHVA Journal*, no. January, pp. 32–35, 2014.

[73] M. Suryatriyastuti, H. Mroueh, and S. Burlon, "Understanding the temperature-induced mechanical behaviour of energy pile foundations", *Renewable and Sustainable Energy Reviews*, vol. 16, no. 5, pp. 3344–3354, Jun. 2012.

[74] L. E. Almanza Huerta and M. Krarti, "Foundation heat transfer analysis for buildings with thermal piles", *Energy Conversion and Management*, vol. 89, pp. 449–457, Jan. 2015.

[75] D. Banks, "Thermogeological assessment of open-loop well-doublet schemes: a review and synthesis of analytical approaches", *Hydrogeology Journal*, vol. 17, no. 5, pp. 1149–1155, 2009.

[76] D Banks, "The application of analytical solutions to the thermal cooling scheme", *Quarterly Journal of Engineering Geology and Hydrogeology*, vol. 44, pp. 191–197, 2011.

[77] E. Milnes and P. Perrochet, "Assessing the impact of thermal feedback and recycling in open-loop groundwater heat pump (gwhp) systems: a complementary design tool", *Hydrogeology Journal*, vol. 21, no. 2, pp. 505–514, 2013.

[78] A. Casasso and R. Sethi, "Modelling thermal recycling occurring in groundwater heat pumps (gwhps)", *Renewable Energy*, vol. 77, pp. 86–93, May 2015.

[79] *Closed-loop/geothermal heat pump systems: design and installation standards*, Stillwater (OK): International Ground Source Heat Pump Association (IGSHPA), 2007.

[80] *Geotrainet training manual for designers of shallow geothermal systems*, Brussels: EFG, 2011.

[81] W. Grattieri, "Il centro di competenza sulle pompe di calore", in *La Ricerca di Sistema e le linee-guida per la progettazione dei campi geotermici per pompe di calore a terreno*, Padova (IT), 2012.

[82] F. Robert and L. Gosselin, "New methodology to design ground coupled heat pump systems based on total cost minimization", *Applied Thermal Engineering*, vol. 62, no. 2, pp. 481–491, Jan. 2014.

[83] L. R. Ingersoll, O. J. Zobel, and A. C. Ingersoll, *Heat conduction with engineering, geological and other applications*. New York: McGraw-Hill, 1954.

[84] H. S. Carslaw and J. C. Jeager, *Conduction of heat in solids*, Second Edi, C. Press, Ed. Clarendon Press, 1959.

[85] M. Bernier, A Chahala, and P Pinel, "Long-term ground-temperature changes in geo-exchange systems", *ASHRAE Transactions*, vol. 114, no. 2, pp. 342–350, 2008.

[86] A. Capozza, M. De Carli, and A. Zarrella, "Design of borehole heat exchangers for ground-source heat pumps: a literature review, methodology comparison and analysis on the penalty temperature", *Energy and Buildings*, vol. 55, pp. 369–379, Dec. 2012.

[87] M. Fossa, "The temperature penalty approach to the design of borehole heat exchangers for heat pump applications", *Energy and Buildings*, vol. 43, no. 6, pp. 1473–1479, Jun. 2011.

[88] M. Tye-Gingras and L. Gosselin, "Generic ground response functions for ground exchangers in the presence of groundwater flow", *Renewable Energy*, vol. 72, pp. 354–366, Dec. 2014.

[89] S. Kavanaugh, "A 12-step method for closed-loop ground heat-pump design source", *ASHRAE transactions*, vol. 114, pp. 328–327, 2008.

[90] UNI, *Uni/ts 11300-4:2012. energy performance of buildings - part 4: renewable energy and other generation systems for space heating and domestic hot water production*, Milan, 2012.

[91] M. Alavy, H. V. Nguyen, W. H. Leong, and S. B. Dworkin, "A methodology and computerized approach for optimizing hybrid ground source heat pump system design", *Renewable Energy*, vol. 57, pp. 404–412, Sep. 2013.

[92] CAN/CSA, *Can/csa-c448 series-13 - design and installation of earth energy systems*, 2013.

[93] L. Ni, W. Song, F. Zeng, and Y. Yao, "Energy saving and economic analyses of design heating load ratio of ground source heat pump with gas boiler as auxiliary heat source", in *2011 International Conference on Electric Technology and Civil Engineering (ICETCE)*, IEEE, Apr. 2011, pp. 1197–1200.

[94] UNI, *Uni/ts 11300-1. energy performance of buildings - part 1: evaluation of energy need for space heating and cooling.* Milan, 2014.

[95] ——, *Uni en 12831:2006. heating systems in buildings - method for calculation of the design heat load*, Milan, 2006.

[96] CEN, *En 12831. heating systems in buildings - method for calculation of the design heat load*, Brussels, 2012.

[97] ——, *En iso 13790. energy performance of buildings - calculation of energy use for space heating and cooling.* Brussels, 2008.

[98] ASHRAE, *ASHRAE Handbook - Fundamentals*. Atlanta (GA): American Society of Heating, Refrigerating and Air-Conditioning Engineers (ASHRAE), 2009.

[99] K. Bakirci, "Evaluation of the performance of a ground-source heat-pump system with series ghe (ground heat exchanger) in the cold climate region", *Energy*, vol. 35, no. 7, pp. 3088–3096, Jul. 2010.

[100] A. Capozza, M. De Carli, A. Galgaro, and A. Zarrella, "Linee guida per la progettazione dei campi geotermici per pompe di calore", Ricerca sul Sistema Energetico – RSE S.p.A., Milan (IT), Tech. Rep., 2012, p. 150.

[101] A. Hepbasli, O. Akdemir, and E. Hancioglu, "Experimental study of a closed loop vertical ground source heat pump system", *Energy Conversion and Management*, vol. 44, no. 4, pp. 527–548, Mar. 2003.

[102] Y. Hwang, J.-K. Lee, Y.-M. Jeong, K.-M. Koo, D.-H. Lee, I.-K. Kim, S.-W. Jin, and S. H. Kim, "Cooling performance of a vertical ground-coupled heat pump system installed in a school building", *Renewable Energy*, vol. 34, no. 3, pp. 578–582, Mar. 2009.

[103] R. Karabacak, e. Güven Acar, H. Kumsar, A. Gökgöz, M. Kaya, and Y. Tülek, "Experimental investigation of the cooling performance of a ground source heat pump system in denizli, turkey", *International Journal of Refrigeration*, vol. 34, no. 2, pp. 454–465, Mar. 2011.

[104] a. Michopoulos, T. Zachariadis, and N. Kyriakis, "Operation characteristics and experience of a ground source heat pump system with a vertical ground heat exchanger", *Energy*, vol. 51, pp. 349–357, Mar. 2013.

[105] C. Montagud, J. Corberán, A. Montero, and J. Urchueguía, "Analysis of the energy performance of a ground source heat pump system after five years of operation", *Energy and Buildings*, vol. 43, no. 12, pp. 3618–3626, Dec. 2011.

[106] O. Ozyurt and D. A. Ekinci, "Experimental study of vertical ground-source heat pump performance evaluation for cold climate in turkey", *Applied Energy*, vol. 88, no. 4, pp. 1257–1265, Apr. 2011.

[107] E. Pulat, S. Coskun, K. Unlu, and N. Yamankaradeniz, "Experimental study of horizontal ground source heat pump performance for mild climate in turkey", *Energy*, vol. 34, no. 9, pp. 1284–1295, Sep. 2009.

[108] F. Ruiz-Calvo and C. Montagud, "Reference data sets for validating gshp system models and analyzing performance parameters based on a five-year operation period", *Geothermics*, vol. 51, pp. 417–428, Jul. 2014.

[109] W. Yang, "Experimental performance analysis of a direct-expansion ground source heat pump in xiangtan, china", *Energy*, vol. 59, pp. 334–339, Sep. 2013.

[110] A. Franco, F. Fantozzi, and E. Ciulli, "Experimental analysis on synergy of pv and heat pumps for residential building", in *Proceedings of 32nd UIT (Italian Union of Thermo–fluid-dynamics) Heat Transfer Conference*, Pisa, IT: Italian Union of Thermo–fluid-dynamics, 2014.

[111] N. Diao, Q. Li, and Z. Fang, "Heat transfer in ground heat exchangers with groundwater advection", *International Journal of Thermal Sciences*, vol. 43, no. 12, pp. 1203–1211, Dec. 2004.

[112] T. W. Kelvin, *Mathematical and physical papers*. London: Cambridge University Press, 1882.

[113] L. Ingersoll and H. Plass, "Theory of the ground pipe heat source for the heat pump", *Heating, Piping and Air conditioning*, vol. 20, pp. 119–122, 1948.

[114] N. Molina-Giraldo, P. Blum, K. Zhu, P. Bayer, and Z. Fang, "A moving finite line source model to simulate borehole heat exchangers with groundwater advection", *International Journal of Thermal Sciences*, vol. 50, no. 12, pp. 2506–2513, Dec. 2011.

[115] G. a. Florides, P. Christodoulides, and P. Pouloupatis, "Single and double u-tube ground heat exchangers in multiple-layer substrates", *Applied Energy*, vol. 102, pp. 364–373, Feb. 2013.

[116] L. Lamarche and B. Beauchamp, "A new contribution to the finite line-source model for geothermal boreholes", *Energy and Buildings*, vol. 39, no. 2, pp. 188–198, Feb. 2007.

[117] L. Lamarche, "Short-term behavior of classical analytic solutions for the design of ground-source heat pumps", *Renewable Energy*, vol. 57, pp. 171–180, Sep. 2013.

[118] A. Zarrella, A. Capozza, and M. De Carli, "Analysis of short helical and double u-tube borehole heat exchangers: a simulation-based comparison", *Applied Energy*, vol. 112, pp. 358–370, 2013.

[119] S. P. Rottmayer, W. A. Beckman, and J. W. Mitchell, "Simulation of a single vertical u-tube ground heat exchanger in an infinite medium", in *ASHRAE Transactions*, vol. 103, ASHRAE, 1997, pp. 651–659.

[120] P. Eskilson, "Thermal analysis of heat extraction boreholes", Doctoral Thesis, University of Lund (S), 1987.

[121] Y. Nam, R. Ooka, and S. Hwang, "Development of a numerical model to predict heat exchange rates for a ground-source heat pump system", *Energy and Buildings*, vol. 40, no. 12, pp. 2133–2140, Jan. 2008.

[122] C. Lee and H. Lam, "Computer simulation of borehole ground heat exchangers for geothermal heat pump systems", *Renewable Energy*, vol. 33, no. 6, pp. 1286–1296, Jun. 2008.

[123] M. De Carli, M. Tonon, A. Zarrella, and R. Zecchin, "A computational capacity resistance model (carm) for vertical ground-coupled heat exchangers", *Renewable Energy*, vol. 35, no. 7, pp. 1537–1550, Jul. 2010.

[124] Z. Li and M. Zheng, "Development of a numerical model for the simulation of vertical u-tube ground heat exchangers", *Applied Thermal Engineering*, vol. 29, no. 5-6, pp. 920–924, Apr. 2009.

[125] E. J. Kim, J. J. Roux, M. A. Bernier, and O. Cauret, "Three-dimensional numerical modeling of vertical ground heat exchangers: domain decomposition and state model reduction", *HVAC and R Research*, vol. 17, no. 6, pp. 912–927, 2011.

[126] A. Zarrella, M. Scarpa, and M. D. Carli, "Short time-step performances of coaxial and double u-tube borehole heat exchangers: modeling and measurements", *HVAC&R Research*, vol. 17, no. 6, pp. 959–976, 2011.

[127] C. Yavuzturk, J. Spitler, and S. Rees, "A transient two-dimensional finite volume model for the simulation of vertical u-tube ground heat exchangers", *ASHRAE Transactions*, vol. 105, no. 2, pp. 465–474, 1999.

[128] C. Yavuzturk and J. Spitler, "A short time step response factor model for vertical ground loop heat exchangers", *Ashrae Transactions*, vol. 105, no. 2, pp. 475–485, 1999.

[129] I. R. Maestre, F. J. González Gallero, P. Álvarez Gómez, and J. D. Mena Baladés, "Performance assessment of a simplified hybrid model for a vertical ground heat exchanger", *Energy and Buildings*, vol. 66, pp. 437–444, Nov. 2013.

[130] H. Esen, M. Inalli, and Y. Esen, "Temperature distributions in boreholes of a vertical ground-coupled heat pump system", *Renewable Energy*, vol. 34, no. 12, pp. 2672–2679, Dec. 2009.

[131] E.-J. Kim, M. Bernier, O. Cauret, and J.-J. Roux, "A hybrid reduced model for borehole heat exchangers over different time-scales and regions", *Energy*, vol. 77, pp. 318–326, Dec. 2014.

[132] M. Cimmino, M. Bernier, and F. Adams, "A contribution towards the determination of g-functions using the finite line source", *Applied Thermal Engineering*, vol. 51, no. 1-2, pp. 401–412, Mar. 2013.

[133] S. Javed, P. Fhalén, and J. Claesson, "Vertical ground heat exchangers: a review of heat flow models", in *Effstick*, 2009.

[134] M. Philippe, M. Bernier, and D. Marchio, "Validity ranges of three analytical solutions to heat transfer in the vicinity of single boreholes", *Geothermics*, vol. 38, no. 4, pp. 407–413, Dec. 2009.

[135] A Baudoin, "Stockage intersaisonnier de chaleur dans le sol par batterie d'échangeurs baionnette verticaux: modèle de prédimensionnement", Ph.D. Thesis, Université de Reims Champagne-Ardenne (F), 1988.

[136] H. Y. Zeng, N. R. Diao, and Z. H. Fang, "A finite line-source model for boreholes in geothermal heat exchangers", *Heat Transfer - Asian Research*, vol. 31, no. 7, pp. 558–567, Nov. 2002.

[137] J. Claesson and S. Javed, "An analytical method to calculate borehole fluid temperatures for time-scales from minutes to decades", *ASHRAE Transactions*, vol. 117, no. 2, pp. 279–288, 2011.

[138] E. R. G. Eckert and R. M. Drake, *Analysis of heat and mass transfer*. New York (NY): McGraw-Hill, 1972, p. 832.

[139] M. N. Ozisik, *Heat conduction*. John Wiley & Sons, 1993.

[140] A. Bejan and A. D. Kraus, Eds., *Heat Tranfer Handbook*. Hoboken (NJ): John Wiley & Sons, Inc., 2003, p. 1496.

[141] D. A. Nield and A Bejan, *Convection in Porous Media*. New York (NY): Springer Science+Business Media, Inc, 2006, vol. 165, p. 640.

[142] J. Bear, *Dynamics of Fluids in Porous Media*, 2. New York (NY): American Elsevier Publishing Company, Inc., Aug. 1972, vol. 120, p. 764.

[143] A. Capozza, M. De Carli, and A. Zarrella, "Investigations on the influence of aquifers on the ground temperature in ground-source heat pump operation", *Applied Energy*, vol. 107, pp. 350–363, Jul. 2013.

[144] M. G. Sutton, D. W. Nutter, and R. J. Couvillion, "A ground resistance for vertical bore heat exchangers with groundwater flow", *Journal of Energy Resources Technology*, vol. 125, no. 3, p. 183, 2003.

[145] M. Chaudhry and S. Zubair, "Generalized incomplete gamma functions with applications", *Journal of Computational and Applied Mathematics*, vol. 55, no. 1, pp. 99–123, Oct. 1994.

[146] M. He, S. Rees, and L. Shao, "Simulation of a domestic ground source heat pump system using a three-dimensional numerical borehole heat exchanger model", *Journal of Building Performance Simulation*, vol. 4, no. 2, pp. 141–155, Jun. 2011.

[147] F. Ruiz-Calvo, M. De Rosa, J. Acuña, J. Corberán, and C. Montagud, "Experimental validation of a short-term borehole-to-ground (b2g) dynamic model", *Applied Energy*, vol. 140, pp. 210–223, Feb. 2015.

[148] D. Bauer, W. Heidemann, and H.-J. Diersch, "Transient 3d analysis of borehole heat exchanger modeling", *Geothermics*, vol. 40, no. 4, pp. 250–260, Dec. 2011.

[149] H. Zeng, N. Diao, and Z. Fang, "Heat transfer analysis of boreholes in vertical ground heat exchangers", *International Journal of Heat and Mass Transfer*, vol. 46, no. 23, pp. 4467–4481, Nov. 2003.

[150] R. Al-Khoury, P. G. Bonnier, and R. B. J. Brinkgreve, "Efficient finite element formulation for geothermal heating systems. part i: steady state", *International Journal for Numerical Methods in Engineering*, vol. 63, no. 7, pp. 988–1013, 2005.

[151] A. S. Lavine, D. P. DeWitt, T. L. Bergman, and F. P. Incropera, *Fundamentals of Heat and Mass Transfer*, 7th. Hoboken (NJ): John Wiley & Sons, Inc., 2011, p. 1080.

[152] L. Lamarche, S. Kajl, and B. Beauchamp, "A review of methods to evaluate borehole thermal resistances in geothermal heat-pump systems", *Geothermics*, vol. 39, no. 2, pp. 187–200, Jun. 2010.

[153] M. H. Sharqawy, E. M. Mokheimer, and H. M. Badr, "Effective pipe-to-borehole thermal resistance for vertical ground heat exchangers", *Geothermics*, vol. 38, no. 2, pp. 271–277, Jun. 2009.

[154] D. Marcotte and P. Pasquier, "On the estimation of thermal resistance in borehole thermal conductivity test", *Renewable Energy*, vol. 33, no. 11, pp. 2407–2415, Nov. 2008.

[155] N. R. Diao, H. Y. Zeng, and Z. H. Fang, *Improvement in modeling of heat transfer in vertical ground heat exchangers*, 2004.

[156] N. Paul, "The effect of grout thermal conductivity on vertical geothermal heat exchanger design and performance", M.Sc. Thesis, South Dakota University, 1996.

[157] C. Zhang, P. Chen, Y. Liu, S. Sun, and D. Peng, "An improved evaluation method for thermal performance of borehole heat exchanger", *Renewable Energy*, vol. 77, pp. 142–151, May 2015.

[158] S. Yoon, S.-R. Lee, and G.-H. Go, "A numerical and experimental approach to the estimation of borehole thermal resistance in ground heat exchangers", *Energy*, vol. 71, pp. 547–555, Jul. 2014.

[159] D Bauer, W. Heidemann, H. Müller-Steinhagen, and H.-J. G. Diersch, "Thermal resistance and capacity models for borehole heat exchangers", *International Journal of Energy Research*, vol. 35, no. 4, pp. 312–320, Mar. 2011.

[160] Y Gu and D O'Neal, "Development of an equivalent diameter expression for vertical u-tubes used in ground-coupled heat pumps", *ASHRAE Transactions*, vol. 104, no. 2, pp. 347–355, 1998.

[161] J Bennet, J. Claesson, and G. Hellström, *Multipole method to compute the conductive heat transfer to and between pipes in a composite cylinder*, Lund (S), 1987.

[162] J. Claesson and G. Hellström, "Multipole method to calculate borehole thermal resistances in a borehole heat exchanger", *HVAC and R Research*, vol. 17, no. 6, pp. 895–911, 2011.

[163] G Hellstrom, "Ground heat storage; thermal analysis ofduct storage systems", Doctorial Thesis, University of Lund, 1991.

[164] H. Zeng, N. Diao, and Z. Fang, "Efficiency of vertical geothermal heat exchangers in the ground source heat pump system", *Journal of Thermal Science*, vol. 12, no. 1, pp. 77–81, 2003.

[165] H. Zeng and Z. Fang, "A heat transfer model for double u-tube geothermal heat exchangers", *Journal of Shandong Institute of Architecture and Engineering*, vol. 17, no. 1, pp. 7–11, 2002.

[166] P. Eslami-nejad and M. Bernier, "Heat transfer in double u-tube boreholes with two independent circuits", *Journal of Heat Transfer*, vol. 133, no. 8, pp. 1–12, 2011.

[167] P. Eskilson and J. Claesson, "Simulation model for thermally interacting heat extraction boreholes", *Numerical Heat Tranfer*, vol. 13, no. 2, pp. 149–165, 1988.

[168] M. Scarpa, G. Emmi, and M. De Carli, "Validation of a numerical model aimed at the estimation of performance of vapor compression based heat pumps", *Energy and Buildings*, vol. 47, pp. 411–420, Apr. 2012.

[169] H. Madani, J. Claesson, and P. Lundqvist, "Capacity control in ground source heat pump systems", *International Journal of Refrigeration*, vol. 34, no. 6, pp. 1338–1347, Sep. 2011.

[170] D. L. Blanco, K. Nagano, and M. Morimoto, "Steady state vapor compression refrigeration cycle simulation for a monovalent inverter-driven water-to-water heat pump with a desuperheater for low energy houses", *International Journal of Refrigeration*, vol. 35, no. 7, pp. 1833–1847, Nov. 2012.

[171] T Zakula, "Heat pump simulation model and optimal variable-speed control for a wide range of cooling conditions", Master Thesis, Massachusetts Institute of Technology, 2010.

[172] A. Afram and F. Janabi-Sharifi, "Review of modeling methods for hvac systems", *Applied Thermal Engineering*, vol. 67, no. 1-2, pp. 507–519, Jun. 2014.

[173] E. Schito, "Modellazione dinamica di un sistema pompa di calore - edificio", Master Degree Thesis in Energy Engineering, University of Pisa, 2013.

[174] E. Tiberi, "Sviluppo e validazione di un modello dinamico per pompe di calore elettriche di piccola taglia: simulazione di un impianto di riscaldamento a pannelli radianti", Master Degree Thesis in Energy Engineering, University of Pisa, 2015.

[175] D. Testi, E. Schito, E. Menchetti, and W. Grassi, "Dynamic simulation of a heat pump serving a historical building: seasonal performance and economic evaluation", in *Historical and existing buildings: Designing the retrofit*, Rome: Associazione Italiana Condizionamento dell'Aria Riscaldamento e Refrigerazione (AiCARR), 2014.

[176] CEN, *En 15316-4-2. heating systems in buildings – method for calculation of system energy requirements and system efficiencies – part 4-2: space heating generation systems, heat pump systems.* Brussels, 2008.

[177] N. Pardo, A. Montero, A. Sala, J. Martos, and J. F. Urchueguía, "Efficiency improvement of a ground coupled heat pump system from energy management", *Applied Thermal Engineering*, vol. 31, no. 2-3, pp. 391–398, Feb. 2011.

[178] Y. Man, H. Yang, and J. Wang, "Study on hybrid ground-coupled heat pump system for air-conditioning in hot-weather areas like hong kong", *Applied Energy*, vol. 87, no. 9, pp. 2826–2833, Sep. 2010.

[179] W. B. Yang, M. H. Shi, and H. Dong, "Numerical simulation of the performance of a solar-earth source heat pump system", *Applied Thermal Engineering*, vol. 26, no. 17-18, pp. 2367–2376, Dec. 2006.

[180] K. Nagano, T. Katsura, and S. Takeda, "Development of a design and performance prediction tool for the ground source heat pump system", *Applied Thermal Engineering*, vol. 26, no. 14-15, pp. 1578–1592, Oct. 2006.

[181] P. Cui, H. Yang, J. D. Spitler, and Z. Fang, "Simulation of hybrid ground-coupled heat pump with domestic hot water heating systems using hvacsim+", *Energy and Buildings*, vol. 40, no. 9, pp. 1731–1736, Jan. 2008.

[182] H. Wang, Q. Wang, and G. Chen, "Experimental performance analysis of an improved multifunctional heat pump system", *Energy and Buildings*, vol. 62, pp. 581–589, Jul. 2013.

[183] L. Lu, W. Cai, Y. S. Chai, and L. Xie, "Global optimization for overall hvac systems—part i problem formulation and analysis", *Energy Conversion and Management*, vol. 46, no. 7-8, pp. 999–1014, May 2005.

[184] V. Partenay, P. Riederer, T. Salque, and E. Wurtz, "The influence of the borehole short-time response on ground source heat pump system efficiency", *Energy and Buildings*, vol. 43, no. 6, pp. 1280–1287, Jun. 2011.

[185] F. Li, G. Zheng, and Z. Tian, "Optimal operation strategy of the hybrid heating system composed of centrifugal heat pumps and gas boilers", *Energy and Buildings*, vol. 58, pp. 27–36, Mar. 2013.

[186] D Carbonell, J Cadafalch, P Pärisch, and R Consul, "Numerical analysis of heat pumps models: comparative study between equation-fit and refrigerant cycle based models", in *Solar Energy for a Brighter Future: Book of Proceedings: EuroSun 2012*, Rijeka (HR), 2012.

[187] R. Evins, "A review of computational optimisation methods applied to sustainable building design", *Renewable and Sustainable Energy Reviews*, vol. 22, pp. 230–245, Jun. 2013.

[188] J. Pantelic, B. Raphael, and K. W. Tham, "A preference driven multi-criteria optimization tool for hvac design and operation", *Energy and Buildings*, vol. 55, pp. 118–126, Dec. 2012.

[189] A.-T. Nguyen, S. Reiter, and P. Rigo, "A review on simulation-based optimization methods applied to building performance analysis", *Applied Energy*, vol. 113, pp. 1043–1058, Jan. 2014.

[190] S. Hackel, G. Nellis, and S. Klein, "Optimization of cooling-dominated hybrid ground-coupled heat pump systems", in *ASHRAE Transactions*, vol. 115 PART 1, 2009, pp. 565–580.

[191] A. Michopoulos, D. Bozis, P. Kikidis, K. Papakostas, and N. A. Kyriakis, "Three-years operation experience of a ground source heat pump system in northern greece", *Energy and Buildings*, vol. 39, no. 3, pp. 328–334, 2007.

[192] W. Retkowski and J. Thöming, "Thermoeconomic optimization of vertical ground-source heat pump systems through nonlinear integer programming", *Applied Energy*, vol. 114, pp. 492–503, Feb. 2014.

[193] P. Conti, W. Grassi, and D. Testi, "Proposal of a holistic design procedure for ground source heat pump systems", in *European Geothermal Congress 2013*, Pisa, IT, 2013.

[194] M. Li and A. C. K. Lai, "Thermodynamic optimization of ground heat exchangers with single u-tube by entropy generation minimization method", *Energy Conversion and Management*, vol. 65, pp. 133–139, Jan. 2013.

[195] T. Sivasakthivel, K. Murugesan, and H. R. Thomas, "Optimization of operating parameters of ground source heat pump system for space heating and cooling by taguchi method and utility concept", *Applied Energy*, vol. 116, pp. 76–85, Mar. 2014.

[196] M. Beck, P. Bayer, M. de Paly, J. Hecht-Méndez, and A. Zell, "Geometric arrangement and operation mode adjustment in low-enthalpy geothermal borehole fields for heating", *Energy*, vol. 49, no. 1, pp. 434–443, Jan. 2013.

[197] J. Marzbanrad, A. Sharifzadegan, and A. Kahrobaeian, "Thermodynamic optimization of gshps heat exchangers", *International Journal of Thermodynamics*, vol. 10, no. 3, pp. 107–112, 2007.

[198] S. Sanaye and B. Niroomand, "Thermal-economic modeling and optimization of vertical ground-coupled heat pump", *Energy Conversion and Management*, vol. 50, no. 4, pp. 1136–1147, Apr. 2009.

[199] H. Sayyaadi, E. H. Amlashi, and M. Amidpour, "Multi-objective optimization of a vertical ground source heat pump using evolutionary algorithm", *Energy Conversion and Management*, vol. 50, no. 8, pp. 2035–2046, Aug. 2009.

[200] S. Huang, Z. Ma, and P. Cooper, "Optimal design of vertical ground heat exchangers by using entropy generation minimization method and genetic algorithms", *Energy Conversion and Management*, vol. 87, pp. 128–137, Nov. 2014.

[201] P. Bayer, M. de Paly, and M. Beck, "Strategic optimization of borehole heat exchanger field for seasonal geothermal heating and cooling", *Applied Energy*, vol. 136, pp. 445–453, Dec. 2014.

[202] S. Huang, Z. Ma, and F. Wang, "A multi-objective design optimization strategy for vertical ground heat exchangers", *Energy and Buildings*, Nov. 2014.

[203] X. Q. Zhai, X. L. Wang, H. T. Pei, Y. Yang, and R. Z. Wang, "Experimental investigation and optimization of a ground source heat pump system under different indoor set temperatures", *Applied Thermal Engineering*, vol. 48, pp. 105–116, Dec. 2012.

[204] J. M. Corberan, D. P. Finn, C. M. Montagud, F. T. Murphy, and K. C. Edwards, "A quasi-steady state mathematical model of an integrated ground source heat pump for building space control", *Energy and Buildings*, vol. 43, no. 1, pp. 82–92, Jan. 2011.

[205] F. De Ridder, M. Diehl, G. Mulder, J. Desmedt, and J. Van Bael, "An optimal control algorithm for borehole thermal energy storage systems", *Energy and Buildings*, vol. 43, no. 10, pp. 2918–2925, Oct. 2011.

[206] A. Kusiak and G. Xu, "Modeling and optimization of hvac systems using a dynamic neural network", *Energy*, vol. 42, no. 1, pp. 241–250, Jun. 2012.

[207] A. Kusiak, G. Xu, and F. Tang, "Optimization of an hvac system with a strength multi-objective particle-swarm algorithm", *Energy*, vol. 36, no. 10, pp. 5935–5943, Oct. 2011.

[208] J. Seo, R. Ooka, J. T. Kim, and Y. Nam, "Optimization of the hvac system design to minimize primary energy demand", *Energy and Buildings*, vol. 76, pp. 102–108, Jun. 2014.

[209] S. S. Rao, *Engineering Optimization: Theory and Practice*, 3rd, ser. A Wiley Interscience publication. Hoboken (NJ): John Wiley & Sons, Inc., 1996.

[210] J. R. Cullin and J. D. Spitler, "A computationally efficient hybrid time step methodology for simulation of ground heat exchangers", *Geothermics*, vol. 40, no. 2, pp. 144–156, Jun. 2011.

[211] C. Lee, "Dynamic performance of ground-source heat pumps fitted with frequency inverters for part-load control", *Applied Energy*, vol. 87, no. 11, pp. 3507–3513, Nov. 2010.

[212] A. Michopoulos and N. Kyriakis, "A new energy analysis tool for ground source heat pump systems", *Energy and Buildings*, vol. 41, no. 9, pp. 937–941, Sep. 2009.

[213] A. Arteconi, C. Brandoni, G. Rossi, and F. Polonara, "Experimental evaluation and dynamic simulation of a ground coupled heat pump for a commercial building", *International Journal of Energy Research*, vol. 37, no. 14, pp. 1971–1980, Jul. 2013.

[214] C. Montagud, J. M. Corberán, and F. Ruiz-Calvo, "Experimental and modeling analysis of a ground source heat pump system", *Applied Energy*, vol. 109, pp. 328–336, Sep. 2013.

[215] O. Zogou and A. Stamatelos, "Optimization of thermal performance of a building with ground source heat pump system", *Energy Conversion and Management*, vol. 48, no. 11, pp. 2853–2863, Nov. 2007.

[216] E. Entchev, L. Yang, M. Ghorab, and E. Lee, "Simulation of hybrid renewable microgeneration systems in load sharing applications", *Energy*, vol. 50, pp. 252–261, Feb. 2013.

[217] J Hoogmartens and L Helsen, "Influence of control parameters on the system performance of ground coupled heat pump systems: a simulation study", in *12th Conference of International Building Performance Simulation Association*, Sydney, 2011.

[218] L Lamarche, G Dupré, and S Kajl, "A new design approach for ground source heat pumps based on hourly load simulations", in *Proceedings of the ICREPQ Conference*, Santander (E), 2008, pp. 1–5.

[219] A. Avgelis and A. Papadopoulos, "Application of multicriteria analysis in designing hvac systems", *Energy and Buildings*, vol. 41, no. 7, pp. 774–780, Jul. 2009.

[220] M. Hamdy, A. Hasan, and K. Siren, "Applying a multi-objective optimization approach for design of low-emission cost-effective dwellings", *Building and Environment*, vol. 46, no. 1, pp. 109–123, Jan. 2011.

[221] F. Ascione, N. Bianco, C. De Stasio, G. M. Mauro, and G. P. Vanoli, "A new methodology for cost-optimal analysis by means of the multi-objective optimization of building energy performance", *Energy and Buildings*, vol. 88, pp. 78–90, Dec. 2014.

[222] V. Machairas, A. Tsangrassoulis, and K. Axarli, "Algorithms for optimization of building design: a review", *Renewable and Sustainable Energy Reviews*, vol. 31, pp. 101–112, Mar. 2014.

[223] W. Wang, R. Zmeureanu, and H. Rivard, "Applying multi-objective genetic algorithms in green building design optimization", *Building and Environment*, vol. 40, no. 11, pp. 1512–1525, Nov. 2005.

[224] P Venkataraman, *Applied Optimization with MATLAB Programming*. Hoboken (NJ): John Wiley & Sons, Inc., 2002, p. 416.

[225] B Raphael and I. Smith, "A direct stochastic algorithm for global search", *Applied Mathematics and Computation*, vol. 146, no. 2-3, pp. 729–758, Dec. 2003.

[226] S. P. Bradley, A. C. Hax, and T. L. Magnanti, *Applied Mathematical Programming*. Boston (MA): Addison Wesley, 1977.

[227] P. Wong and R. Larson, "Optimization of natural-gas pipeline systems via dynamic programming", *IEEE Transactions on Automatic Control*, vol. 13, no. 5, 1968.

[228] J. H. Holland, *Adaptation in natural and artificial systems: An introductory analysis with applications to biology, control, and artificial intelligence.* U Michigan Press, 1975.

[229] I. Rechenberg, "Cybernetic solution path of an experimental problem", 1965.

[230] T. H. Cormen, C. E. Leiserson, R. L. Rivest, and C. Stein, *Introduction to Algorithms*, 3rd. Cambridge (MA): The MIT press, Sep. 2009, p. 816.

[231] D. C. Montgomery, G. C. Runger, and N. F. Hubele, *Engineering Statistics*. Hoboken (NJ): John Wiley & Sons, Inc., 2006, p. 490.

[232] EU, *Directive 2012/27/eu on energy efficiency*, Brussels, 2009.

[233] V. Gnielinski, "New equations for heat and mass transfer in turbulent pipe and channel flow", *International Journal of Chemical Engineering*, vol. 16, no. 2, pp. 359–368, 1976.

[234] B. Petukhov, "Heat transfer and friction in turbulent pipe flow with variable physical properties", *Advances in Heat Transfer*, vol. 6, pp. 503–564, 1970.

[235] R. H. Byrd, M. E. Hribar, and J. Nocedal, *An interior point algorithm for large-scale nonlinear programming*, 1999.

[236] R. H. Byrd, J. C. Gilbert, and J. Nocedal, "A trust region method based on interior point techniques for nonlinear programming", *Mathematical Programming, Series B*, vol. 89, pp. 149–185, 2000.

[237] R. A. Waltz, J. L. Morales, J. Nocedal, and D. Orban, "An interior algorithm for nonlinear optimization that combines line search and trust region steps", *Mathematical Programming*, vol. 107, pp. 391–408, 2006.

[238] S. Lohani, "Energy and exergy analysis of fossil plant and heat pump building heating system at two different dead-state temperatures", *Energy*, vol. 35, no. 8, pp. 3323–3331, Aug. 2010.

[239] M. A. Rosen and I. Dincer, "Effect of varying dead-state properties on energy and exergy analyses of thermal systems", *International Journal of Thermal Sciences*, vol. 43, no. 2, pp. 121–133, Feb. 2004.

[240] M. Ghisleni, G. Pellegrini, P. Conti, D. Testi, and W. Grassi, "Analysis of monitoring data and simulation of seasonal energy performance of the gs-gahp system installed in the kindergarten building of oulx, turin", in *L'impiantistica per i climi estremi: Tecnologie per i nuovi mercati della climatizzazione*, Padova (IT): Associazione Italiana Condizionamento dell'Aria Riscaldamento e Refrigerazione (AiCARR), 2015.

[241] G. Pellegrini, "Simulazione delle prestazioni energetiche stagionali di un sistema gs-gahp e analisi dei dati di monitoraggio della scuola dell'infanzia di oulx (to)", Master Degree Thesis in Energy Engineering, University of Pisa, 2015.

[242] D. Testi, E. Schito, E. Tiberi, P. Conti, and W. Grassi, "Building energy simulation by an in-house full transient model for radiant systems coupled to a modulating heat pump", in *6th International Building Physics Conference (IBPC 2015)*, Turin, 2015.

[243] A. D. Chiasson, S. J. Rees, and J. D. Spitler, "Preliminary assessment of the effects of groundwater flow on closed-loop ground-source heat pump systems", *ASHRAE Transactions*, vol. 106, no. 1, pp. 380–393, 2000.

[244] W Austin, C. Yavuzturk, and J. D. Spitler, "Development of an in-situ system for measuring ground thermal properties", *ASHRAE Transactions*, vol. 106, no. 1, pp. 365–370, 2000.

[245] S. Gehlin, "Thermal response test: method development and evaluation", PhD thesis, LuleåUniversity of Technology (S), 2002.

[246] C. Zhang, Z. Guo, Y. Liu, X. Cong, and D. Peng, "A review on thermal response test of ground-coupled heat pump systems", *Renewable and Sustainable Energy Reviews*, vol. 40, pp. 851–867, Dec. 2014.

[247] P. S. Osborne, "Suggested operating procedures for aquifer pumping tests", EPA Environmental Assessment Sourcebook, Tech. Rep., 1996, p. 191.

[248] G. P. Kruseman and N. A. Ridder, "Analysis and evaluation of pumping test data", *ILRI publication*, no. 47, p. 377, 1990.

[249] J. Raymond, R. Therrien, L. Gosselin, and R. Lefebvre, "A review of thermal response test analysis using pumping test concepts", *Ground Water*, vol. 49, no. 6, pp. 932–945, 2011.

Ringraziamenti

Chi mi conosce sa bene che non mi sono mai dedicato troppo ai ringraziamenti. Consapevole dei limiti della mia efficacia espressiva, ho sempre preferito lasciar posto alle azioni più che alle parole. Sono quindi sicuro che qualunque frase io riesca a scrivere, non sarà mai in grado di rendere giustizia al contributo di tutte quelle persone che mi hanno accompagnato in questi anni di attività di ricerca. Il mio debito verso di loro non riguarda unicamente la mia crescita formativa e professionale, ma è legato soprattutto ad un processo di maturazione umana e sociale.

Il primo ringraziamento va ai miei due relatori, i Proff. Walter Grassi e Daniele Testi. Il primo per avermi guidato e consigliato ben oltre i contenuti accademici, insegnandomi ad affrontare i problemi (lavorativi e non) con criterio, in maniera organica, sulla base di poche e solide considerazioni di contenuto e di metodo, senza mai sostituirsi o imponendosi sulla mia libera scelta. Il secondo, non solo per la sua amicizia, ma per la costanza e la professionalità con cui mi ha sempre seguito nel lavoro, in qualsiasi momento, senza limiti di orari o di argomenti, correggendo pazientemente i miei errori e fornendomi continuamente spunti e stimoli di miglioramento. Entrambi, per le proprie capacità, conoscenze e competenze, rappresentano i riferimenti a cui mi ispiro costantemente.

Grazie a Davide, Elena, Eva, Roberto e agli ultimi arrivati Emidio, Giulio e Marco. L'enorme supporto fornito durante le attività lavorative, insieme all'immensa amicizia dimostrata nella vita di tutti i giorni, hanno fatto si che io possa considerarmi una di quelle persone con la fortuna di recarsi al proprio posto di lavoro con entusiasmo, fiducia e passione, senza alcun peso o disagio. Grazie anche a tutti quei colleghi, ai professori e ai tesisti che hanno contribuito alle attività di questi anni, anche se per un breve periodo di tempo o con brevi suggerimenti. In particolare, grazie al mio "sempai" Maurizio, il quale mi ha educato alla vita del dottorando, aiutandomi fino all'ultimo anche per l'impaginazione di questa tesi. Un grazie va anche agli amici e ai colleghi dell'UGI, i quali, dimostrando un'eccessiva fiducia nei confronti, mi stanno introducendo e guidando in contesti che mai avrei pensato adatti a me.

Grazie alla mia Avenale, la mia terra, e a tutti gli amici di Genga, Sassoferrato, Arcevia e dintorni: vorrei citarvi tutti, ringraziandovi uno ad uno per tutto quello che mi avete sempre dato, ma non basterebbe un intero libro. Durante questi anni ho avuto la fortuna

di viaggiare in diverse parti d'Italia e del mondo, incontrando persone di diverse culture e mentalità, scoprendo situazioni e contesti sempre nuovi e stimolanti. Ritengo che la conoscenza ed il confronto con gli altri costituiscano un grande e necessario percorso di crescita che ogni persona dovrebbe intraprendere. Tuttavia, per quanto il viaggio possa essere bello, c'è sempre un solo ed un unico luogo a cui sempre ritornerò e che sempre chiamerò "casa". Grazie anche agli amici ed alle amiche di Roma, che con la loro simpatia e spensieratezza rendono ogni serata nella Capitale imprevedibile ed esilarante.

Grazie a mio padre, a mia madre, a mio fratello e a tutta la mia famiglia per avermi concesso la libertà ed il sostegno necessario per intraprendere questo percorso iniziato da quasi dieci anni. A loro devo la mia educazione e i miei valori. Un pensiero speciale va a mio nonno Luigi, il quale più di tutti mi ha insegnato l'importanza e la dignità del duro lavoro e della morale. Quando sarà il momento spero solo di riuscire a trasmettere il più possibile di quanto ho ricevuto. Grazie ad Antonina e Costantino, i quali mi hanno subito accolto e fatto sentire un membro della loro famiglia.

Grazie soprattutto a Margherita. A lei dedico questa tesi e l'intero triennio di lavoro. Grazie per la sua pazienza, l'affetto ed il sostegno ricevuto durante la stesura di questo elaborato. La bontà, la spontaneità, la trasparenza d'animo, la pura ingenuità, la passione e l'impegno con cui affronta ogni dettaglio della sua vita costituiscono il mio più grande stimolo nel non cedere alle piccole e grandi difficoltà di ogni giorno. A lei ricorderò sempre le proprie capacità e potenzialità, cercando di trasmetterle fiducia in se stessa ed il coraggio di non arrendersi. La vita e la felicità che stiamo costruendo insieme rappresentano senza ombra di dubbio il mio più grande successo.

A tutti voi, a tutti quelli che ho dimenticato o citato troppo velocemente, va il mio più sincero e sentito ringraziamento.

Paolo Conti